GROUND-WATER AGE AND ATMOSPHERIC TRACERS: SIMULATION STUDIES AND ANALYSIS OF FIELD DATA FROM THE MIRROR LAKE SITE, NEW HAMPSHIRE

Daniel James Goode

A DISSERTATION
PRESENTED TO THE FACULTY
OF PRINCETON UNIVERSITY
IN CANDIDACY FOR THE DEGREE
OF DOCTOR OF PHILOSOPHY

RECOMMENDED FOR ACCEPTANCE
BY THE DEPARTMENT OF
CIVIL ENGINEERING AND OPERATIONS RESEARCH
PROGRAM IN ENVIRONMENTAL ENGINEERING AND
WATER RESOURCES

June 1998

© Daniel James Goode, 1998. All rights reserved.

Abstract

The use of environmental tracers in characterization of ground-water systems is investigated through mathematical modeling of ground-water age and atmospheric tracer transport, and by a field study at the Mirror Lake site, New Hampshire. Theory is presented for modeling ground-water age using the advective-dispersive transport equation. The transport equation includes a zero-order source of unit strength, corresponding to the rate of aging, and can accommodate matrix diffusion and other exchange processes. The effect of temperature fluctuations and layered soils on transport of atmospheric gases to the water table is investigated using a one-dimensional numerical model of chlorofluorocarbon (CFC-11) transport. The nonlinear relation between temperature and Henry's Law coefficient (reflecting air/water phase partitioning) can cause the apparent recharge temperature to be elevated above the annual mean temperature where the water table is shallow. In addition, fine-grained soils can isolate the air phase in the unsaturated zone from the atmosphere. At the USGS' Mirror Lake, New Hampshire fractured-rock research site CFC concentrations near the water table are depleted where dissolved oxygen is low. CFC-11 and CFC-113 are completely absent under anaerobic conditions, while CFC-12 is as low as one-third of modern concentrations. Anaerobic biodegradation apparently consumes CFC's near the water table at this site. One area of active degradation appears to be associated with streamflow loss to ground water. Soil gas concentrations are generally close to atmospheric levels, although some spatial correlation is observed between depleted concentrations of CFC-11 and CFC-113 in soil gas and water-table samples. Results of unsaturated-zone monitoring indicate that recharge occurs throughout the year in the watershed, even during summer evapotranspiration periods, and that seasonal temperature fluctuations occur as much as 5 meters below land surface. Application of ground-water age and CFC-11 transport models to the large-scale ground-water system at Mirror Lake

illustrates the similarities between age and chemical transport. Generally, bedrock porosities required to match observed apparent ages from CFC concentrations are high relative to porosities measured on cores. Although matrix diffusion has no effect on steady-state age, it can significantly reduce CFC concentrations in fractured rock in which the effective porosity is low.

Table of Contents

Abstract iii

Table of Contents v

List of Figures ix

List of Tables xviii

Acknowledgments xix

Chapter 1 Introduction 1

References 4

Chapter 2 Direct Simulation of Ground-Water Age 5

2.1 Introduction 5

2.2 Derivation of Mean-Age Transport Equation 9

2.2.1 Residence-Time Distribution 9

2.2.2 Conservation of Age Mass 11

2.2.3 Boundary and initial conditions 14

2.2.4 Internal source of age mass 16

2.2.5 Effect of matrix diffusion at steady state 17

2.3 Examples 19

2.3.1 Regional Flow in Cross Section 19

2.3.2 Matrix Diffusion from a Single Fracture 32

2.3.3 Age of Pumped Samples from a Heterogeneous Formation 35

2.3.4 Two-Dimensional Age Distribution in Mildly-Heterogeneous Porous Media 42

2.4 Summary 47

2.5 References 49

Chapter 3 Effects of Temperature Fluctuations on CFC-11 Transport from the Atmosphere to the Water Table 52

3.1 Introduction 52

3.2 Governing Equations, Constitutive Relations, and Numerical Solution 54

3.2.1 Governing Equations and Boundary Conditions 54

3.2.2 Constitutive Relations 57

3.2.2 Numerical Solution 61

3.2.3 Benchmark Simulation 62

3.3 Homogeneous Media 65

3.3.1 Static Water 65

3.3.2 Steady Water Flow 67

3.3.3 Seasonal Temperature Cycle 69

3.4 Layered Soil 78

3.4.1 Static Water 78

3.4.2 Steady Water Flow and Seasonal Temperature Cycle 79

3.5 Henry's Law Coefficient for Recharge 83

3.6 Summary 87

3.7 References 89

Chapter 4 Field Study of CFC Concentrations at the Water Table at the Mirror Lake Site, New Hampshire 90

4.1 Introduction 90

4.1.1 CFC's as Environmental Tracers 90

4.1.2 Mirror Lake Field Site 92

4.1.3 Ground-Water Ages from CFC Data at Mirror Lake 94

4.1.4 Scope and Objectives 96

4.2 Methods 97

4.2.1 Moisture Content and Pressure 97
4.2.2 Soil Temperature 98
4.2.3 Water Sample Collection and Analysis 99
4.2.4 Soil Gas Sampling and Analysis 103
4.3 Results 108
4.3.1 Moisture Content and Pressure 108
4.3.2 Soil Temperature 114
4.3.3 General Chemistry 117
4.3.4 Chlorofluorocarbon Concentrations 130
4.4 Discussion 146
4.5 Summary 152
4.6 References 153

Chapter 5 Regional-Scale Simulation of Ground-Water Age and CFC-11 Transport at the Mirror Lake Site, New Hampshire 157

5.1 Introduction 157
5.2 Background 158
5.2.1 Regional-Scale Flow Modeling at Mirror Lake site 158
5.2.2 Environmental Tracers and Ground-Water Age at the Mirror Lake Site 160
5.2.3 Scope of this study 162
5.3 Model Construction 163
5.3.1 Flow model results 166
5.4 Ground-Water Age 169
5.5 CFC-11 Transport 175
5.5.1 Advective Transport 175
5.5.2 Matrix Diffusion 182
5.6 Summary 188

5.7 References……188

Chapter 6 Summary and Conclusions ……190

Future Work……193

List of Figures

Figure 2-1 Flow boundary conditions on top of cross-sectional model of regional aquifer system showing specified-flux values for recharge nodes and specified-head values for discharge nodes. 21

Figure 2-2 Results of direct simulation of groundwater age in a **uniform** regional aquifer system in which the hydraulic conductivity is 10^{-6} m/s. 22

Figure 2-3 Results of direct simulation of groundwater age in a cross-section through a **layered** regional aquifer system in which the bottom layer is 30 m thick with hydraulic conductivity 10^{-5} m/s, and the overlying layer is 70 m thick with hydraulic conductivity 10^{-6} m/s. 23

Figure 2-4 Percent difference in simulated age distribution between advection only and advection-dispersion cases in a **layered** regional aquifer system. 26

Figure 2-5 Contours of simulated groundwater age in a **layered** regional aquifer system for advection and diffusion obtained by using proposed transport equation method, and by using a particle tracking and random walk method. 27

Figure 2-6 Results of direct simulation of groundwater age in a cross-section through a **discontinuous layered** regional aquifer system in which three high-permeability zones occur at the bottom. 28

Figure 2-7 Results of direct simulation of groundwater age in a cross-section through a **stratified heterogeneous** regional aquifer system in which eight discontinuous high-permeability zones occur at three different depths. 30

Figure 2-8 Results of direct simulation of groundwater age in a cross-section through a **stratified heterogeneous** regional aquifer system in which eight discontinuous high-permeability zones occur at three different depths. 31

Figure 2-9 Age at x = 9.5 m from the inflow boundary of a one-dimensional rock column having fracture porosity 0.01, rock matrix porosity 0.09, and specific discharge 1 m/day. 35

Figure 2-10 Hydraulic conductivity distribution for three-dimensional highly-heterogeneous case. 37

Figure 2-11 Results of direct simulation of steady-state groundwater age in a highly-heterogeneous fractured bedrock. The colors correspond to age, ranging from less than 3 years (white) to greater than 700 years (black). 38

Figure 2-12 Results of direct simulation of steady-state groundwater age in a highly-heterogeneous fractured bedrock: (a) Y-Z cross-section along the middle of the model at column 7 (x=53 m), variable contour intervals in years. (b) X-Z cross-section at the outflow end of the model along row 21 (y=160 m). 39

Figure 2-13 Sample age as a function of pumping time in a highly-heterogeneous aquifer. 41

Figure 2-14 Age simulation in a mildly heterogeneous two-dimensional aquifer. 43

Figure 2-15 Age variation along lines oriented longitudinal (a) and lateral (b) to the average flow direction for a mildly heterogeneous two-dimensional aquifer. 45

Figure 3-1 Moisture retention and relative unsaturated hydraulic conductivity for a sandy loam and a silty loam soil using Mualem - van Genuchten constitutive model. 59

Figure 3-2 Henry's Law coefficient (K_w) for CFC-11; the ratio of the volumetric concentration in water having zero salinity to the volumetric concentration in air at sea level. 60

Figure 3-3 CFC-11 in water (c) and air (c_a) with depth, 1993, for unsaturated zone conditions of Cook and Solomon (1995, p. 265): uniform moisture and air content; isothermal; and water table at depth of 30 meters. 64

Figure 3-4 Air content (θ_a), tortuosity (τ), and their product versus depth for sandy loam moisture retention curve and water table depth at 5 meters. 66

Figure 3-5 CFC-11 concentrations in 1993 versus depth for two no-flow cases having a water table at 5 meters depth: (a) uniform air content, and (b) sandy loam hydrostatic moisture retention curve. 67

Figure 3-6 CFC-11 concentration versus depth with constant vertical flux of 0.3 m/yr and water-table depth of 5 m for cases (a) with uniform air content above the water table and (b) sandy loam moisture retention and hydraulic conductivity functions. 68

Figure 3-7 Annual temperature cycle for analytical model with sinusoidal surface temperature (mean and amplitude of 9.2681 °C) and uniform thermal diffusivity (D_h = 27.2 m^2/yr). 70

Figure 3-8 Temperature and Henry's Law coefficient versus depth on 1 January 1993 for nonisothermal conditions simulated by analytic model..... 71

Figure 3-9 CFC-11 concentrations versus time from 1990 to 1993 for water table at depth of 5 m and steady water flux of 0.3 m/yr, under nonisothermal conditions..... 72

Figure 3-10 Air content, moisture content, and effective dispersion coefficient versus depth for sandy loam with water table at depth of 5 m and steady flow of 0.3 m/yr..... 74

Figure 3-11 CFC-11 concentration versus depth on 1 January 1993 for water table at depth of 5 m and steady water flux of 0.3 m/yr. Results for isothermal and nonisothermal conditions are shown..... 75

Figure 3-12 CFC-11 concentration versus depth on 1 January 1993 for water table at depth of 1 m and steady water flux of 0.3 m/yr..... 76

Figure 3-13 CFC-11 concentrations versus time from 1990 to 1993 for water table at depth of 1 m and steady water flux of 0.3 m/yr, under nonisothermal conditions..... 77

Figure 3-14 CFC-11 concentrations versus depth for case having water table at 5 m depth and no flow for cases uniform moisture content, homogeneous sand loam, and layered sand with a silt layer between 1 and 2 m depth. 79

Figure 3-15 CFC-11 concentrations versus depth for case having water table at depth of 5 m, steady flow of 0.3 m/yr, and silt layer between 1 and 2 m depth for cases isothermal, and nonisothermal conditions. 80

Figure 3-16 Air content, moisture content, and effective dispersion coefficient versus depth for layered case with water table at depth of 5 m and steady flow of 0.3 m/yr..... 81

Figure 3-17 Annual cycle in temperature and Henry's Law coefficient at 4 m depth..... 84

Figure 3-18 Annual cycle in temperature and Henry's Law coefficient at land surface.... 85

Figure 3-19 Henry's Law coefficients for CFC-11, CFC-12, and CFC-113, normalized by their respective values at T = 0 °C, as a function of temperature. 86

Figure 4-1. Global atmospheric concentration of CFC-12, CFC-11, and CFC-113. 91

Figure 4-2. Mirror Lake site location and bedrock wells..... 93

Figure 4-3. Ground-water ages in bedrock estimated from CFC-12 concentrations in 1990 & 1991 along projected cross-sections (a) A-A', and (b) B-B'. 95

Figure 4-4. Locations of individual piezometers, well clusters, and seep sampled for this study.....100

Figure 4-5. Locations of soil gas sampling tubes installed for this study. 104

Figure 4-6. Schematic of typical soil gas well.....106

Figure 4-7. Moisture content during 1996 and 1997 near W2 at depth of 18 cm and average over depth range 50-80 cm.....109

Figure 4-8. Suction pressure head at W2 TDR site during (a) the summer of 1996, and (b) the summer of 1997. 110

Figure 4-9. Gypsum block electrical resistance during summer 1997: (a) at W2 TDR site, and (b) in separate borehole at W2 TDR site. 112

Figure 4-10. Water table elevations during summer 1997 in six piezometers near W2 TDR, tensiometer, and gypsum block sites. 114

Figure 4-11. Air, surface and soil temperature near FS3.....115

Figure 4-12. Air, surface and soil temperature near FS4.....116

Figure 4-13 Spatial distribution of dissolved oxygen concentrations in water samples from piezometers at the Mirror Lake site, Grafton County, New Hampshire.....126

Figure 4-14 Piper plot of major ions in samples from piezometers. 127

Figure 4-15 Concentrations of dissolved argon and nitrogen in water samples from piezometers and packer-isolated zones of bedrock wells at the Mirror Lake site, Grafton County, New Hampshire. 129

Figure 4-16 Concentrations of CFC-11 and CFC-12 in water samples from water-table piezometers at the Mirror Lake site, Grafton County, New Hampshire.....131

Figure 4-17 Concentrations of CFC-12 and dissolved oxygen in water samples from piezometers at the Mirror Lake site, Grafton County, New Hampshire.....132

Figure 4-18 Concentrations of CFC-11 and dissolved oxygen in water samples from piezometers at the Mirror Lake site, Grafton County, New Hampshire.....133

Figure 4-19 Concentrations of CFC-113 and dissolved oxygen in water samples from piezometers at the Mirror Lake site, Grafton County, New Hampshire.....134

Figure 4-20 Concentrations of CFC-11 and CFC-12 in water samples from water-table piezometers at the Mirror Lake site, Grafton County, New Hampshire.....136

Figure 4-21 Concentrations of CFC-11, CFC-12, and dissolved oxygen in water samples from water-table piezometers at the Mirror Lake site, Grafton County, New Hampshire.....137

Figure 4-22 Concentrations of CFC-11 and tritium in water samples from piezometers at the Mirror Lake site, Grafton County, New Hampshire.....138

Figure 4-23 Box plot of CFC concentrations in soil gas at the Mirror Lake site, Grafton County, New Hampshire.....140

Figure 4-24 Spatial distribution of CFC-11 concentrations in soil gas samples from sampling tubes at the Mirror Lake site, Grafton County, New Hampshire.....145

Figure 4-25 Iron (II) and sulfate as a function of CFC-11 concentrations.....149

Figure 4-26 Water table elevations in the lower part of the W stream drainage basin.....150

Figure 4-27 Cross-section in the lower part of the W stream drainage basin showing the land surface elevation, water table elevation, and concentrations of dissolved oxygen (DO) and total organic carbon (TOC) in samples from water-table piezometers. 151

Figure 5-1 Location map of Mirror Lake site, New Hampshire, regional-scale finite-difference grid, and flow and transport subgrids. 159

Figure 5-2. Mirror Lake ground-water drainage basin. 160

Figure 5-3 Tritium concentrations versus apparent recharge dates from CFC-12 concentrations in ground-water samples from drift piezometers and bedrock wells at Mirror Lake site. 162

Figure 5-4. Stream cells and shading of uppermost active model layer containing water table in flow subgrid using model structure and calibrated parameters of Tiedeman and others (1997). 164

Figure 5-5 Simulated water-table elevation in flow subgrid using model structure and calibrated parameters of Tiedeman and others (1997). 167

Figure 5-6 Hydraulic head in bottom model layer (5) representing bedrock between 90 and 150 m below bedrock surface. 168

Figure 5-7 Simulated ground-water age in upper bedrock from bedrock surface to 30 meters below bedrock surface for advection only using bedrock effective porosity of 0.05. 170

Figure 5-8 Simulated ground-water age in deep bedrock from 90 meters below bedrock surface to 150 meters below bedrock surface for advection only using bedrock effective porosity 0.05. 171

Figure 5-9 Simulated ground-water age in upper bedrock from bedrock surface to 30 meters below bedrock surface for advection only using bedrock effective porosity of 0.005. 173

Figure 5-10 Simulated ground-water age in deep bedrock from 90 meters below bedrock surface to 150 meters below bedrock surface for advection only using bedrock effective porosity of 0.005. 174

Figure 5-11 Simulated CFC-11 concentrations in upper bedrock from bedrock surface to 30 meters below bedrock surface for advection only using bedrock effective porosity of 0.05. 176

Figure 5-12 Simulated CFC-11 concentrations in deep bedrock from 90 meters below bedrock surface to 150 meters below bedrock surface for advection only using bedrock effective porosity of 0.05. 177

Figure 5-13 Simulated CFC-11 concentrations in upper bedrock from bedrock surface to 30 meters below bedrock surface for advection only using bedrock effective porosity of 0.005……179

Figure 5-14 Simulated CFC-11 concentrations in deep bedrock from 90 meters below bedrock surface to 150 meters below the bedrock surface for advection only using bedrock effective porosity of 0.005. ……180

Figure 5-15 CFC-11 concentrations versus time in recharge areas for transport by advection only using bedrock effective porosity of 0.005……181

Figure 5-16 Simulated CFC-11 concentrations in upper bedrock from bedrock surface to 30 meters below bedrock surface for advection and matrix diffusion using bedrock effective porosity of 0.005, rock matrix porosity of 0.045 and exchange rate coefficient of 10^{-4} day^{-1}……183

Figure 5-17 Simulated CFC-11 concentrations in deep bedrock from 90 meters below bedrock surface to 150 meters below bedrock surface for advection and matrix diffusion using bedrock effective porosity of 0.005, rock matrix porosity of 0.045 and exchange rate coefficient of 10^{-4} day^{-1}……184

Figure 5-18 CFC-11 concentrations versus time in recharge areas for transport by advection and matrix diffusion using bedrock effective porosity of 0.005, rock matrix porosity of 0.045 and exchange rate coefficient of 10^{-4} day^{-1}..……186

Figure 5-19 CFC-11 concentrations versus time for deep bedrock in recharge area for cases of transport by advection using bedrock effective porosities of 0.05 and 0.005, and transport by advection and matrix diffusion using bedrock effective porosity of 0.005, rock matrix porosity of 0.045 and exchange rate coefficients of 10^{-6} and 10^{-4} day^{-1}……187

List of Tables

Table 2-1. Hydraulic Properties of Three-Dimensional Model of Highly-Heterogeneous Formation 36

Table 3-1. Simulated air-phase concentrations in 1992 of CFC's and Krypton-85 immediately above the water table 53

Table 3-2. Moisture retention and unsaturated hydraulic conductivity parameters for van Genuchten - Mualem model of a sandy loam and silty loam. 59

Table 3-3. General flow and transport parameters used for CFC-11 transport simulation 63

Table 4-1. Selected piezometer construction data. 101

Table 4-2. Overview of water sampling procedures. 102

Table 4-3. Selected soil gas tube construction data. 105

Table 4-4. Geochemical data from water samples. 118

Table 4-5. Concentrations of CFC's in soil gas. 141

Acknowledgments

I am most indebted to my life partner, Cynthia Emily Ward Goode, whose constant support and emphatic encouragement made this work possible. More practically, she cared for me and for our daughters, Emily Ethel Goode and Robin Imogene Goode, when I could not, and still allowed me to enjoy the benefits of fatherhood. I hope they will forgive me this selfishness. I also thank my parents, Jamie Joseph Goode and Imogene Medlock Talley Goode, for being my first teachers; a lifelong job, it turns out.

Mike Celia has been an outstanding advisor and continues to be a friend and mentor. His clarity of thought and broad knowledge of hydrology and computational methods have been a boon, and an inspiration, to me.

I thank my second reader, Catherine Peters, and committee members Jim Smith, Peter Jaffé, and Chris Milly.

Thanks to current and former colleagues and professors who have contributed in many ways to my long journey, so far, including Allen Shapiro, Paul Hsieh, Lenny Konikow, John Wilson, Lloyd Townley, George Slaughter, Matt Gordon, Dick Codell, Claire Tiedeman and Ward Sanford.

The help and friendship received from fellow students at Princeton has been wonderful. Thanks to Paul Reeves, Jon Johnson, Rudi Held, Jonathan Miller, Philip Binning, Johathan Stevens, Beverly Shimada, Paula Sturdevant, and Saumyen Guha. I've benefited from working with, and getting to know, Helge Dahle, Ulrich Fischer, Andrea Amantia, and others I'm unfortunately forgetting.

Support for the Mirror Lake field study was provided by numerous colleagues at the U.S. Geological Survey including Rick Perkins, Allen Shapiro, Paul Hsieh, Tom Winter, Ed Busenberg, Niel Plummer, Don Rosenberry, Warren Wood, Tom Kraemer, Don Vroblesky, Fred Robertson, Gary Paulachok, Bill Werkheiser, Dick Yager, Lisa Senior, Drew Reif, Kevin Breen, Bob Michel, Julian Waylan, Mike Doughten, Art Baehr

and Matt Lahvis. I'm especially grateful for the dedicated field assistance, and good company, of Johannes Voitleithner.

The Mirror Lake site is part of the Hubbard Brook Experimental Forest, administered by the U.S. Department of Agriculture Forest Service, Northeast Experiment Station, Radnor, Pennsylvania. A number of individuals at the Forest Service contributed to this work, including Wayne Martin, Amey Bailey, and Scott Bailey. Individuals at the Institute of Ecosystems Studies also helped me in a number ways; they include Don Buso, Torsten Berger, Gene Likens, and Scott Nolan. I thank the Science Advisory Committee of the Hubbard Brook Ecosystem Study for permission to carry out my field activities, and all the participants in the study for sharing their data so freely with me. The scientific leadership and logistical management of the USGS fractured-rock research effort at Mirror Lake by Allen Shapiro and Paul Hsieh is gratefully acknowledged. Tom Winter pioneered the study of ground water at Mirror Lake, and has freely shared his data and wisdom throughout this study.

Funding and other support for this work was provided by several programs within the Water Resources Division of the U.S. Geological Survey: Graduate School Training Program, Toxic Substances Hydrology Program, National Research Program, and Pennsylvania District. I received funding from Princeton University as an Assistant Instructor for one semester, and the Graduate School paid my medical insurance fee for one year. Other, less tangible support from the Princeton University community is gratefully acknowledged.

Chapter 1 Introduction

Estimation of flow and transport properties of large-scale ground-water systems is difficult because small-scale measurements cannot be directly up-scaled, and because large-scale field experiments cannot be easily conducted. The presence of environmental tracers, such as atmospheric gases, can serve as ongoing experiments on the large-scale system (e.g. Plummer et al., 1993). Interpretation of tracer transport via quantitative simulation can yield estimates of large-scale properties. In this approach, the historic source function is used as a boundary condition for the transport model, and simulated concentrations are compared directly to measurements. If tracer concentrations are affected by processes other than advection and dispersion, then those additional processes must be included in the transport model.

A simple method of interpreting environmental tracer data is by age dating; the measured concentration is used to estimate ground-water age. For example, Chlorofluorocarbon (CFC) concentrations in ground water can be converted to a recharge date when the water was isolated from the atmosphere, based on the record of increasing atmospheric levels. The difference between the recharge date and the sampling date is the ground-water age. The ground-water age can be compared to advective travel times, and hydraulic properties and effective porosity can be estimated (e.g. Reilly et al., 1994). This method ignores dispersion.

This thesis explores two main topics in the use of ground-water age-dating tracers, and CFC's in particular, in estimation of large-scale flow and transport properties. The first topic is the relation between solute concentration and ground-water age in systems affected by dispersion, mixing, and matrix diffusion. In Chapter Two, a method is presented that bridges the gap between modeling ground-water age using advection alone, and simulating tracer concentrations using advection, dispersion and

exchange processes. Simulations of ground-water age and CFC concentration are compared and contrasted for a fractured-rock field site in Chapter Five.

The second topic is the effect of additional processes, primarily temperature fluctuations and degradation reactions, on transport of CFC's from the atmosphere to ground water. The effects of fluctuating temperature and nonuniform soil properties on CFC concentrations at the water table are simulated in Chapter Three. A previously observed problem with CFC's as tracers is that under certain low-oxygen conditions degradation can significantly reduce concentrations (Plummer et al., 1993). In Chapter Four, a field study of CFC concentrations at the water table focuses on degradation reactions that may completely remove CFC's from recharge waters. Based on this field study, the input source function of CFC-11 to ground water is modified in Chapter Five for the large-scale transport model to account for degradation in some areas of the watershed.

Chapter Two presents a theory of direct simulation of ground-water age by transport modeling. The theory bridges the two current approaches for interpretation of age-dating environmental tracers: comparison of ground-water age dates to advective (piston flow) travel times, and simulation of environmental tracer concentrations using the advective-dispersive transport equation. The impact of matrix diffusion, an important process in fractured rocks, on ground-water age is theoretically examined. Several examples illustrate the application of the theory to characterize age in different ground-water systems. Chapter Two is an extension of Goode (1996).

The effects of temperature fluctuations and material heterogeneities on dissolved gas transport from the land surface to the water table are examined in Chapter Three. A one-dimensional transport model is developed and applied to unsaturated-zone conditions representative of humid eastern climates. Simulations examine CFC-11 transport under nonisothermal conditions in which partitioning into the air and water phases changes as a

function of temperature. The impact of a fine-grained soil above the water table on air-phase diffusion is also examined.

Chapter Four is a field study of the unsaturated zone at the Mirror Lake site (Hsieh et al, 1993). Use of CFC's to age date saturated-zone ground water is based on an assumption of chemical equilibrium between the water table and the atmosphere. However, CFC concentrations at the water table are significantly degraded in some locations in the Mirror Lake watershed. The relation between CFC's, dissolved oxygen, redox indicators, and stream/aquifer interaction is examined based on field data collected over a three-year period at the site. Preliminary summaries of the findings reported here have been presented at scientific meetings (see abstracts: Goode, 1997; Goode et al., 1997).

Large-scale ground-water age and CFC-11 transport is simulated in Chapter Five. These simulations use the theory of Chapter Two, and modifications to a USGS transport model (Konikow et al., 1996) to approximate the effects of matrix diffusion on transport. The flow model used is derived from that of Tiedeman and others (1997). Results of the transport and age simulation are compared and contrasted. CFC-11 results are qualitatively compared to results from field sampling (Busenberg and Plummer, 1996).

References

Busenberg, E., and Plummer, L.N., 1996, Concentrations of chlorofluorocarbons and other gases in ground water at Mirror Lake, New Hampshire: in Morganwalp, D.W., and Aronson, D.A., eds., U.S. Geological Survey Toxics Program Meeting, Colorado Springs, Colo., September 20-24, 1993: U.S. Geological Survey WRIR 94-4015.

Goode, D.J., 1996, Direct simulation of groundwater age: Water Resources Research, 32(2), 289-296.

Goode, D.J., 1997, CFC transport to and degradation near a shallow water table, Mirror Lake area, Grafton County, New Hampshire: (abs.), p. S176 in 1997 Spring Meeting, supplement to Eos, 29 April 1997, American Geophysical Union, Washington DC.

Goode, D.J., Busenberg, Eurybiades, Plummer, L.N., Shapiro, A.M., and Vroblesky, D.A., 1997, CFC degradation under anaerobic water table conditions in glacial drift at Mirror Lake New Hampshire: (abs.), Geological Society of America 1997 Annual Meeting, 20-23 October 1997, Salt Lake City, Utah, GSA Abstracts with Programs, vol. 29, no. 6, p. 77.

Hsieh, P. A., Shapiro, A. M., Barton, C. C., Haeni, F. P., Johnson, C. D., Martin, C. W., Paillet, F. L., Winter, T. C., and Wright, D. L., 1993, Methods of characterizing fluid movement and chemical transport in fractured rock: in Chaney, J. T., and Hepburn, C., (eds.) Field Trip Guidebook for northeastern United States, Geological Society of America, annual Meeting, October 25-28, 1993, Boston, Mass., v. 2, chap. R, p. R1-R23.

Konikow, L.F., D.J. Goode and G.Z. Hornberger, 1996, A three-dimensional method-of-characteristics solute-transport model (MOC3D): U.S. Geological Survey Water-Resources Investigations Report 96-4267, 87 p.

Plummer, L. N., R.L. Michel, E.M. Thurman, and P.D. Glynn, 1993,. Environmental tracers for age dating young ground water, in *Regional Ground-Water Quality* , edited by W. M. Alley, pp. 255-294, Van Nostrand Reinhold, New York.

Reilly, T. E., L.N. Plummer, P.J. Phillips, and E. Busenberg, The use of simulation and multiple environmental tracers to quantify flow in a shallow aquifer, Water Resour. Res., 30(2), 421-433, 1994.

Tiedeman, C.R., Goode, D.J., and Hsieh, P.A., 1997, Numerical simulation of ground-water flow through glacial deposits and crystalline bedrock in the Mirror Lake area, Grafton County, New Hampshire: U.S. Geological Survey Professional Paper 1572, 50 p.

Chapter 2 Direct Simulation of Ground-Water Age

2.1 Introduction

The age of water in a groundwater system is useful for quantitative analysis. Various environmental tracers can be used to estimate the time since recharge for groundwater samples collected from various locations. These age data can be used in turn to constrain the parameters of models of flow and transport. Isotopic information is typically interpreted by using a travel time approach, simulating groundwater movement as 'piston' flow. Reilly and others (1994) show that an advective model of groundwater age, simulated by numerical particle tracking, is consistent with the distribution of chlorofluorocarbons and tritium observed in a shallow sand and gravel aquifer. In the advective model, the age is determined by the travel time of water, computed from Darcy's law. However, isotope transport in groundwater is often not by advection alone.

Several studies have indicated that estimates of groundwater travel time can be in error if the effects of dispersion and mixing on isotope concentrations are ignored. Plummer and others (1993, p. 287) give an overview of current methods for age-dating groundwater, and point out, as have many others, that "Because environmental tracers are dissolved solutes which are transported along with the ground water, it is usually necessary to consider effects of hydrodynamic dispersion on the modeled age." Walker and Cook (1991, p. 41) "show how neglecting diffusion can lead to serious underestimates of groundwater ages in unconfined aquifers where recharge rates are similarly low" when using the isotope carbon-14. Maloszewski and Zuber (1991) demonstrate the effects of matrix diffusion and exchange reactions on carbon-14 movement in fractured rocks and on groundwater age. Geyh and Backhaus (1978)

examine the effects of diffusion and mixing during pumping on carbon-14 distribution and age. The diffusion of carbon-14 from a confined aquifer into adjacent aquitards, and the resulting effect on interpreted ages, is quantified by Sudicky and Frind (1981). In their review, Mazor and Nativ (1992, p. 211) identify "problem areas" in the interpretation of groundwater age, including "lack of single recharge and discharge areas; . . . entrapment of ground water in 'dead' volumes . . .; (and) mixing of ground water of various ages."

Incorporation of the effects of transport processes other than advection allows additional information to be extracted from tracer distributions. For example, Torgersen and others (1978) estimate vertical diffusivity from observed tritium/helium-3 distributions in lakes. Weeks and others (1982) used fluorocarbon distribution in the unsaturated zone to estimate soil diffusion coefficients. A model of age that incorporates dispersion can be helpful in identifying the dispersive properties of the groundwater system (Robinson and Tester, 1984), in addition to the mean flow properties. Egboka and others (1983) estimate longitudinal dispersivity from the observed tritium distribution by fitting a one-dimensional model of tritium transport. Musgrove and Banner (1993) use isotopic information to help quantify mixing of distinct saline waters in a regional scale flow system.

The effects of diffusion, dispersion, and mixing can be incorporated in a transport simulation of the tracer or tracers of interest, for example tritium (Nir, 1964; Simpkins and Bradbury, 1992; Solomon, et al., 1993). Tritium is an isotope of hydrogen that is incorporated in water molecules. Simulation of tritium transport by use of a model that accounts for dispersion and diffusion reflects the underlying dispersion and diffusion of water molecules, and these water molecules have different ages. Thus, the age of the water *itself* is affected by diffusion, dispersion, and other hydrodynamic processes.

In the same way that particle tracking is used to generate groundwater age for the case of advection alone, simulation of groundwater age as affected by dispersion and

mixing, without resort to separate models for separate tracers, can be useful. Such an analysis complements, but does not replace, simulation of transport of the tracer of interest, which can be affected by processes, such as sorption and chemical exchange (Fritz et al. 1979), that do not affect the water.

The concept of a residence-time distribution has been used for many years to describe the statistics of the lifetimes of components in a flowing reactor (MacMullin and Weber, 1935; Danckwerts, 1953). This approach is chosen because molecules do not behave identically, rather mixing, diffusion, and variability in flow conditions result in different paths and residence times for different molecules. Residence-time distributions have been widely applied to the analysis of chemical reaction systems (Levenspiel, 1972). Eriksson (1958), Bolin and Rodhe (1973), and Nir and Lewis (1975) discuss the application of residence-time-distribution theory to steady and transient geophysical systems. Robinson and Tester (1984) use residence-time distributions determined from tracer tests to analyze dispersion in a fractured geothermal reservoir. Campana and Simpson (1984) apply some of these concepts to isotopic age dating of groundwater with a discrete-state (as opposed to continuous-state) compartment model in which separate areas of the groundwater system are treated as mixed reservoirs.

The underlying connection between the residence-time distribution and transport of an ideal tracer can be exploited to develop residence-time distributions corresponding to solutions of the advection-dispersion transport equation (Danckwerts, 1953; Wen and Fan, 1975; Nauman, 1981; Zuber, 1986). Danckwerts (1953) describes how the residence-time distribution can be determined experimentally from the outflow concentration of a nonreactive tracer. In this context, the mean age at a point, determined from temporal integrals of the concentration (described below), is affected by all of the processes accounted for in the solute-transport equation, including dispersion and mixing. The connection between resident concentration and probabilistic travel-time approaches to simulating groundwater transport is described by Shapiro and Cvetkovic (1988) and by

Dagan and Nguyen (1989), who discuss advantages of the travel-time approach for some analyses. Recently, Harvey and Gorelick (1995) present a general framework for application of temporal moment-generating equations to reactive transport.

It is shown in this chapter that the distribution of groundwater age obeys a special form of the solute-transport equation. The mean age can be simulated directly in an analytical or numerical transport model and the result of the simulation—that is, the predicted 'concentration'—is the mean age. This spatial age distribution is obtained directly, without further manipulation external to the transport simulation. For steady-state flow conditions, the age transport equation is derived from previous results on the residence-time distribution in systems governed by the advection-dispersion equation. This form has been presented previously for analysis of mean or 'local' age of air in a room during ventilation (Sandberg, 1981). A more general derivation here for transient flow conditions is based on the assumption of conservation of imaginary 'age mass.' This derivation also incorporates exchange processes; this framework is used to examine the impact of matrix diffusion on steady-state age. The method is illustrated by several example simulations, including cases representative of mildly-heterogeneous porous media and highly-heterogeneous fractured rock.

2.2 Derivation of Mean-Age Transport Equation

2.2.1 Residence-Time Distribution

Danckwerts (1953) defined a function C(t) to characterize the residence-time distribution for molecules in a chemical reactor. This function corresponds to the concentration at the reactor exit of a solute that is injected as an impulse (unit mass in an infinitely small time period) at the reactor entrance at time zero. For one-dimensional piston flow (advection only) conditions, the function C(t) is zero except at the time equal to the advective travel time of the system, at which time the function is a Dirac delta. In the case of complete mixing, C(t) is an exponentially decaying function; the outflow concentration is equal to the uniform concentration within the reservoir, which decreases because of the addition of tracer-free fluid at the inflow. For transport in porous media, the function C is analogous to the outflow mass flux (mass per unit time) of a column, that is c, the concentration measured in flux (Kreft and Zuber, 1978). In multi-dimensional systems, the mass injected on all inflow boundaries is proportional to the fluid flux across the boundary. Levenspiel (1972) and Wen and Fan (1975) present several models for transport in flowing reactors and their respective C functions.

The mean residence time in a steady-flow domain can be determined from the concentration of a tracer injected as an impulse at time zero as:

$$A = \frac{\int_0^\infty t\, c\, dt}{\int_0^\infty c\, dt} = \frac{E}{M} \tag{2.1}$$

where A is the mean residence time, or the mean age of molecules, in the reactor (Spalding, 1958). The numerator of (2.1) is a concentration-weighted average time,

which I will denote as E. This form is similar to the expectation of a random variable t with probability density function c. The denominator normalizes the numerator such that c divided by the time integral of c has the properties of a probability density function. This integral, which is constant and uniform for steady flow (Spalding, 1958), will be denoted as M. This term is uniform for multi-dimensional systems provided the mass injected on inflow boundaries is proportional to fluid flux across the boundary (see Harvey and Gorelick, 1995).

For transport by advection and dispersion in a constant-density fluid, the concentration satisfies

$$\frac{\partial c\theta}{\partial t} = \nabla \bullet \theta \mathbf{D} \bullet \nabla c - \nabla \bullet \mathbf{q} c \tag{2.2}$$

where θ is the moisture content (porosity for saturated flow); **D** is the dispersion tensor; and **q** is the specific-discharge vector. A standard model of dispersion in groundwater is assumed such that the product of moisture content and the dispersion tensor, **D**, is given by

$$\theta D_{ij} = \left(\theta D_m + \alpha_T q\right)\delta_{ij} + \left(\alpha_L - \alpha_T\right)\frac{q_i q_j}{q} \tag{2.3}$$

where D_m is the diffusion coefficient; the Kronecker delta is $\delta_{ij} = 1$ if i=j and $\delta_{ij} = 0$ if $i \neq j$; α_L and α_T are, respectively, the longitudinal and transverse dispersivities; q_i is a component of the specific discharge vector; and q is the magnitude of specific discharge. Multiplying (2.2) by time and integrating through all time gives (Spalding, 1958):

$$-\theta M = \nabla \bullet \theta \mathbf{D} \bullet \nabla E - \nabla \bullet \mathbf{q} E \quad . \tag{2.4}$$

The left side of (2.4) is obtained through integration by parts of the time derivative term. Dividing by M, which is uniform and can be brought inside the spatial derivatives, and assuming porosity is also uniform, gives

$$\nabla \cdot \mathbf{D} \cdot \nabla A - \frac{1}{\theta} \nabla \cdot \mathbf{q} A + 1 = 0 \tag{2.5}$$

where the defined mean age A = E / M has been substituted (see Sandberg, 1981, for comparison). Thus, the mean age at a point satisfies a steady-state advection-dispersion transport equation with an internal source of unit (1) strength. A more general form of (2.5) is derived in the next section by assuming that age is conserved under mixing. This derivation also leads to natural choices for boundary conditions for (2.5) to complete the mathematical framework.

Computing age by particle tracking corresponds to solution of (2.5) without the dispersion term. In this case, particle paths are defined by the characteristics of the governing equation and the increasing travel time corresponds to the unit source in (2.5). Equation (2.1) can be used to calculate mean age within a small volume from a particle tracking analysis to include, for example, the mixing induced by sampling. The methods presented here for age simulation also may be useful in accounting for the effects of dispersion and mixing on other analyses involving groundwater and travel time such as contamination from landfills (Lee and Kitanidis, 1993) and time-dependent capture zones (Bair et al., 1990).

2.2.2 Conservation of Age Mass

In this section, a more general form of the age transport equation is derived from mass-conservation principles. Assuming that the mean age of mixed waters is a mass-weighted average, then the mean age is analogous to a conservative solute concentration. Although age is not a directly-measurable physical property, and thus this assumption

cannot be verified experimentally, it seems suitable for our conceptual model that when two water masses are mixed, the mean age of the mixture is the mass-weighted average age of the mixed components. It may be possible to experimentally verify this assumption using a tracer that has an input function that varies linearly with time. A given mass of water with a mean age A can be assumed to be characterized by its 'age mass,' the product of the mean age and the water mass, $A \rho V$, where ρ is water density and V is water volume. Assuming that the density of the water is constant, the mean age of a two-component mixture is a volume-weighted average:

$$A = \frac{A_1 V_1 + A_2 V_2}{V_1 + V_2} \tag{2.6}$$

where the subscripts distinguish the components. This is completely analogous to the concentration of a conservative solute under mixing in constant-density water. This analog can be exploited to derive a governing transport equation for mean age.

A governing equation for age-mass transport can be derived from a simple box balance similar to the derivation of the mass-transport equation by Konikow and Grove (1977; see also Bear, 1979). Consider conservation of age mass in a control volume (dimensions Δx by Δy by Δz) of aquifer material. The age mass within the control volume is the product of the age (A) and the mass of water, $\theta \rho \Delta x \Delta y \Delta z$. The age-mass flux (per unit area) across the boundaries of the control volume is designated **J**, with components J_x, J_y, and J_z, and includes advection with the water as well as dispersive flux. Over a time step of length Δt, the age mass of the water initially in the control volume increases by the product of Δt and the mass of water. Additionally, an internal net source of age mass of rate F is included to account for, for example, net exchange of age mass with separate phases. Physical processes included in F are described below. Assuming that the age mass is conserved, a difference form of a conservation equation is

$$A(t+\Delta t)\,\theta\,\rho\,\Delta x\,\Delta y\,\Delta z = A(t)\,\theta\,\rho\,\Delta x\,\Delta y\,\Delta z + \Delta t\,\theta\,\rho\,\Delta x\,\Delta y\,\Delta z +$$

$$\Delta t\Big\{\,\Delta y\,\Delta z\big[J_x(-\Delta x/2) - J_x(+\Delta x/2)\big] + \Delta x\,\Delta z\big[J_y(-\Delta y/2) - J_y(+\Delta y/2)\big] + \tag{2.7}$$

$$\Delta x\,\Delta y\big[J_z(-\Delta z/2) - J_z(+\Delta z/2)\big]\Big\} + F\,\Delta t\,\Delta x\,\Delta y\,\Delta z \quad .$$

Dividing by the volume and the time-step length, and allowing the size of the control volume and the time-step length to go to zero in the limit gives the governing partial differential equation for mean-age transport:

$$\begin{aligned}\frac{\partial A\theta\rho}{\partial t} &= \theta\rho - \frac{\partial J_x}{\partial x} - \frac{\partial J_y}{\partial y} - \frac{\partial J_z}{\partial z} + F \\ &= \theta\rho - \nabla\bullet\mathbf{J} + F \quad .\end{aligned} \tag{2.8}$$

This form of the mean-age transport equation is more general than (2.5) in that the water density is allowed to vary, the model of dispersive flux is not specified, and the equation is transient. The mean age spatial distribution can be determined from (2.8) even for aquifer systems with unsteady flow, provided the flow history is known. The ability to simulate the transient evolution of groundwater age may be useful, for example, in assessing the impact of climate change on large aquifer systems.

To complete the governing equation, a description of dispersive age-mass flux in terms of age, or its gradient, is needed. Here, I adopt the standard model of mass flux such that **J** is composed of advection, diffusion, and dispersion modeled as Fickian diffusion. That is, **J** in (2.8) is replaced by

$$\mathbf{J} \approx A\,\rho\,\mathbf{q} - \theta\rho\mathbf{D}\bullet\nabla A \tag{2.9}$$

where **D** is the dispersion tensor and includes a diffusion term. By substitution, the governing equation becomes

$$\frac{\partial A\theta\rho}{\partial t} = \theta\rho - \nabla\bullet A\rho\mathbf{q} + \nabla\bullet\theta\rho\mathbf{D}\bullet\nabla A + F \quad . \tag{2.10}$$

If the porosity and density are constant in time and uniform in space, (2.10) becomes

$$\frac{\partial A}{\partial t} = 1 - \nabla\bullet A\frac{\mathbf{q}}{\theta} + \nabla\bullet\mathbf{D}\bullet\nabla A + \frac{F}{\theta\rho} \quad . \tag{2.11}$$

Under steady flow conditions the time derivative in (2.11) (or (2.10)) can be set to zero to derive a governing equation for steady-state mean-age spatial distribution. A steady-state age distribution does not exist if both **q** and **D** are zero. The steady-state equation derived from (2.11) is the same as (2.5) derived above from residence-time distribution theory, with an additional source term F, which is discussed below. Initial and boundary conditions for the mean-age transport equation can be specified from the control-volume balance.

2.2.3 Boundary and initial conditions

The age of groundwater is relative to the time at which the water entered the system. That is, recharge to the system is assumed to have age zero. From the definition of age mass, the age-mass flux, the product of age and water-mass flux, is also zero at all inflow boundaries. Furthermore, the age-mass flux across all no flow boundaries is also zero. These conditions can be written as:

$$\mathbf{J}|_{\Gamma_1} \bullet \mathbf{n} = 0 \tag{2.12}$$

where Γ_1 is a noflow or inflow boundary and **n** is its unit outward normal. Note that (2.12) uses the previous notation for total age-mass flux, **J**, which includes dispersion as well as advection. Thus, no dispersion is assumed to occur upstream across the boundary against the direction of the incoming flow.

The boundary condition on outflow boundaries depends on the physical situation. A common assumption, which I will adopt here, is that mass flux across an outflow boundary occurs only by advection. This condition of no dispersion across the boundary can be written

$$\mathbf{D}\,\nabla A\big|_{\Gamma_2} \bullet \mathbf{n} = 0 \tag{2.13}$$

where Γ_2 is the outflow boundary. This condition probably is most appropriate for discharge to surface-water bodies. Alternate boundary conditions for other physical situations, such as advection and dispersion into a separate aquifer outside of the simulation domain, also can be formulated, but they are not pursued here.

The general form of the governing equation for mean age transport is transient. If the flow field is steady, then the steady distribution of mean age is determined by solution of the steady-state form of the governing equation, similar to (2.5). In this case, an initial condition is not required. If the flow field is not steady, then the transient form of the governing equation for age transport must be used and an initial condition is required. That is, the initial mean age at every point within the aquifer system must be specified. For simulation times that are very long, relative to the rate of advection through the aquifer system, the groundwater age is insensitive to the initial age distribution, although the initial age is required mathematically to yield a solution.

2.2.4 Internal source of age mass

The internal net source of age mass, F, can account for several processes. Many aquifer systems are modeled in only the horizontal dimensions because vertical head gradients and flow rates are assumed to be small. A governing equation for this case can be obtained from (2.5) or (2.11) by vertical integration across the saturated thickness. In the resulting two-dimensional model, F could include the age-mass flux due to inflow from an underlying hydrogeologic unit. For example, for the case of leakage through an aquitard, F would be the product of the leakage water mass flux rate and the age of the leakage, and would be positive for the case of inflow to the aquifer of interest. Similarly, evapotranspiration from a two-dimensional horizontal model would be treated as a net sink of age mass and F would be negative.

The internal sink/source term F could represent age-mass exchange between phases, for exmaple during unsaturated flow through partially frozen soil. In this case, some of the flowing water may freeze, acting as a sink for age mass, or stationary ice of a different age may melt, acting as a source of age mass for the flow system. Of course, as with the other examples, for the case of age-mass sources such as melting ice, the age of the source water must be specified or determined from a separate, possibly coupled, mathematical model.

For the general three-dimensional model, F could represent sources and sinks of age mass due to multi-continua exchange. For example, flow in fractured rock can be modeled as a two-domain system, with separate transport equations for high-permeability fractures and for the rock matrix. Exchange of water between the fractures and the rock matrix would include an exchange of age mass. For the fracture domain, F would be the product of the rate of water-mass inflow from the matrix and the age of that water. The F term for the rock-matrix equation would be of equal magnitude but opposite in sign.

Low-flow or stagnant zones are not necessarily included in this internal source term, but can be handled directly in the governing equation. In such zones, the advective

flux is small and the groundwater age is determined primarily by diffusion, which is included in the dispersion tensor **D**. In the absence of diffusion, the age of water at a stagnation point in a steady flow field is by definition infinite. However, this infinite age applies only to a point which has infinitesimally small fluid volume.

2.2.5 Effect of matrix diffusion at steady state

The age-mass concept can be used to evaluate the effect of matrix diffusion on steady-state age distribution. Consider age-mass transport in a fractured rock system which is modeled as advection and dispersion in a continuum of connected fractures, coupled with diffusion to and from the rock matrix. In this case, F represents the rate of age-mass transfer between the rock matrix and the fractures. Hence, F appears as the boundary flux for an equation governing age-mass transport within the rock matrix. In general, the solution of this problem would require solution of two coupled transport equations. However, for the case of steady-state age distribution, F can be computed directly.

Under steady-state conditions, an integrated age-mass conservation equation for the rock matrix has only three components: (1) accumulation of age-mass (zero for steady state), (2) boundary flux, and (3) production of age-mass by aging. Because (1) is zero in steady state, (2) and (3) must balance. Hence, the net boundary flux F of age-mass out of the rock matrix into the fracture is equal to the total age-mass production rate in the matrix, which is the product of the rock porosity and the water density in the rock matrix Hence, at steady state (2.10) can be written

$$0 = \theta\rho - \nabla\bullet A\rho\mathbf{q} + \nabla\bullet\theta\rho\mathbf{D}\bullet\nabla A + \theta_m\rho_m \quad , \tag{2.14}$$

where θ_m is the bulk porosity of the rock matrix and ρ_m is the density of water in the matrix. In this case, the porosity of fracture system (θ) is the bulk fracture porosity: the

total volume of the fractures per unit volume of aquifer. Assuming that the density of water is constant, and that both fracture and rock porosities are uniform, (2.14) can be simplified to:

$$0 = 1 - \nabla \bullet A \frac{\mathbf{q}}{\theta + \theta_m} + \frac{1}{\theta + \theta_m} \nabla \bullet \theta \mathbf{D} \bullet \nabla A \quad . \tag{2.15}$$

Thus, the age distribution is identical to that of a single continuum system in which the porosity is the sum of the fracture and rock matrix porosities. The apparent velocity is 'retarded' compared to the velocity of water in the fractures alone, and the rate of dispersive spreading is likewise reduced by the total porosity. Of course, this analysis assumes that the age distribution is in steady state. Because of the slow rate of diffusion in rock, disequilibrium between the age-mass production in the rock and diffusion out into the fracture may exist for millions of years.

2.3 Examples

2.3.1 Regional Flow in Cross Section

The mathematical theory for simulation of groundwater age developed in the previous section is applied to a regional model of groundwater flow and transport in cross-section. This application demonstrates the practical simulation of groundwater age distribution using the age transport equation, both with and without dispersion. The impact of heterogeneous hydraulic conductivity and porosity, and of matrix diffusion on age distributions are illustrated. Six hypothetical aquifer systems are considered:

- **uniform** aquifer with homogeneous hydraulic conductivity and porosity;
- **layered** aquifer in which a high-permeability layer exists at depth;
- **discontinuous layered** aquifer in which a high permeability layer at the aquifer bottom is discontinuous; in this case, the permeability contrast is 100:1;
- **stratified heterogeneous** aquifer in which several discontinuous horizontal high-permeability (100:1) zones occur at different depths; results are presented for uniform porosity and nonuniform porosity.

The uniform and layered configurations are similar to those analyzed by Freeze and Witherspoon (1967) in a landmark series of papers in which they used numerical flow models to study the characteristics of regional groundwater flow. The flow equation is solved using a block-centered finite-difference flow model, MODFLOW (McDonald and Harbaugh, 1988). A three-dimensional method-of-characteristics solute transport model, MOC3D (Goode and Konikow, 1991; Konikow and others, 1996), is modified to solve the age transport equation, including the zero-order source term for age in equation (2.10). In contrast to finite-difference or finite-element numerical solutions of the transport equation, MOC3D is well suited to the case of advection alone, $\mathbf{D}=\mathbf{0}$.

The domain geometry and boundary conditions are identical for the six hypothetical regional aquifers considered. The domain is 1 km long and 100 m thick.

Except where noted, this spatial domain is discretized by 10 rows in the vertical direction, each 10 m thick, and 50 columns in the horizontal direction, each 20 m long. Noflow boundary conditions are specified on the left, right, and bottom boundaries. The top boundary represents the water table and is modeled here with a combination of specified-flux and specified-head conditions. The change in the position of the domain boundary due to movement of the water table is considered to be a minor effect, and is ignored here.

The uniform and layered regional flow systems modeled here are similar to those considered by Freeze and Witherspoon (1967), but a different water-table boundary condition is used. Freeze and Witherspoon (1967) used numerical flow models to study the effects of nonuniform hydraulic conductivity on regional groundwater flow. As previously noted by Freeze and Cherry (1979, p. 204), the results obtained by Freeze and Witherspoon (1967) were affected by the choice of specified-head boundary conditions along the entire water table, the top boundary of the flow domain. With this approach, variations in subsurface permeability lead to significant changes in recharge magnitude and distribution, without affecting water-table altitudes. For the simulations here, I choose boundary conditions at the opposite extreme, where the recharge is modeled as a specified-flux boundary condition (fig. 2-1). In reality, both water-table altitudes and net groundwater recharge are sensitive to subsurface permeability. Specified-head conditions similar to those of Freeze and Witherspoon (1967) are used at discharge locations. Thus, water-table altitudes are free to change in response to various hydraulic-conductivity configurations, but the recharge distribution is identical in both cases. These simulations yield greater changes in hydraulic heads but smaller changes in flow rates compared to the simulations of Freeze and Witherspoon (1967).

The first two cases are identical except that in the layered case a high-permeability layer occurs at the aquifer bottom. The isotropic hydraulic conductivity of the homogeneous aquifer is $K_1 = 10^{-6}$ m/s and its porosity is 0.2. The hydraulic

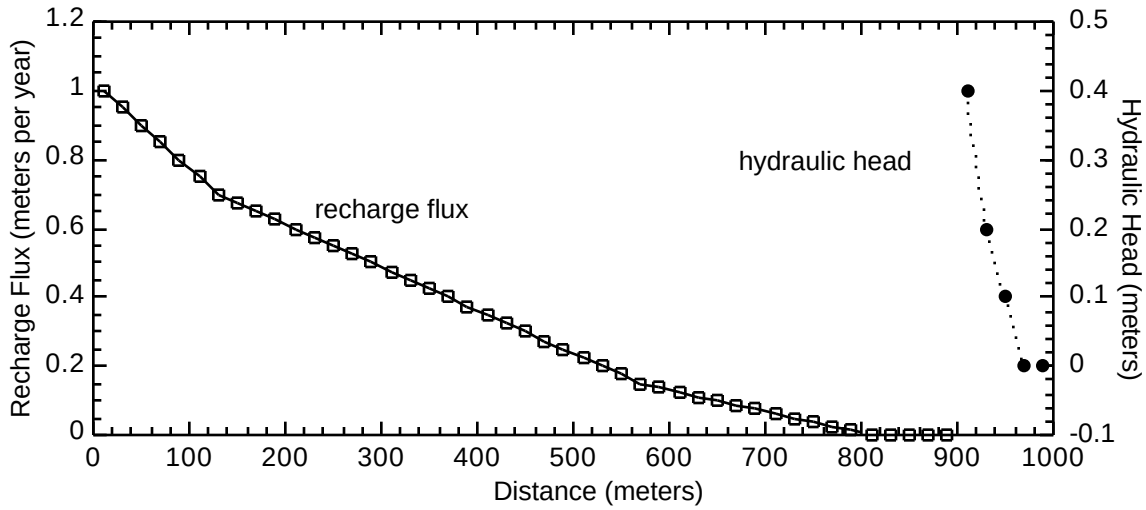

Figure 2-1 Flow boundary conditions on top of cross-sectional model of regional aquifer system showing specified-flux values for recharge nodes and specified-head values for discharge nodes.

conductivity of the layered aquifer system is the same in the upper 70 m of the system, but is ten times greater, $K_2 = 10 \times K_1 = 10^{-5}$ m/s, in the lower 30 m . The porosity is the same for both layers, 0.2.

Figures 2-2a and 2-3a show the head distribution and groundwater-flow velocities for steady-state conditions, and figures 2-2b and 2-3b show corresponding streamlines for the **uniform** and **layered** cases. The imposed boundary conditions and uniform properties lead to a smooth distribution of head and gradual variations in velocity for the uniform aquifer (fig. 2-2a). In the layered case, most flow occurs through the deep layer , where the hydraulic conductivity is greater (fig. 2-3a). Because the transmissivity is greater, water-table altitudes are lower in the layered than in the uniform case. Velocity changes abruptly at the interface in the layered case, yielding refracting streamlines (fig. 2-3b), that contrast with the smooth streamlines throughout the uniform aquifer (fig. 2-2b).

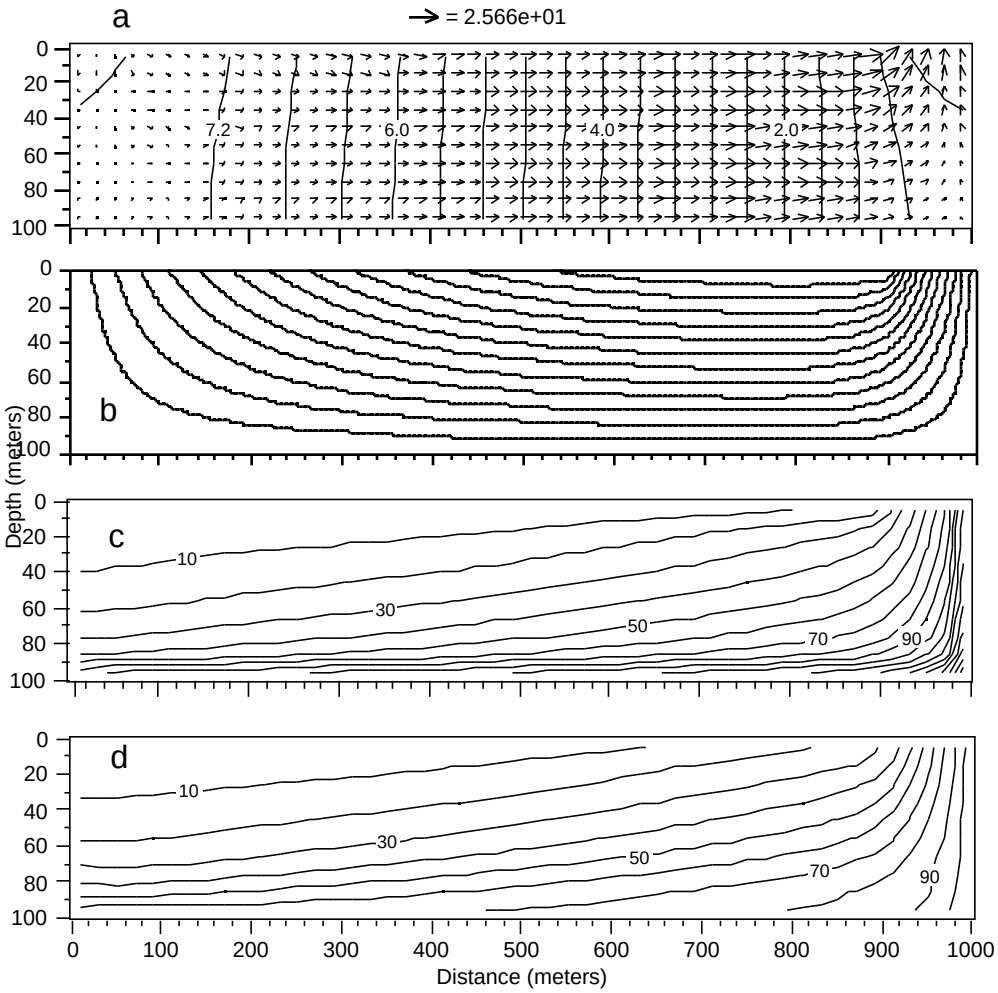

Figure 2-2 Results of direct simulation of groundwater age in a **uniform** regional aquifer system in which the hydraulic conductivity is 10^{-6} m/s: (a) Cross-sectional domain with hydraulic-head contours (0.4 m interval) and velocity vectors. Vertical exaggeration is 2X and the 10 row by 50 column finite-difference grid used for the numerical flow and transport solutions is indicated by the small ticks on each axis. (b) Streamlines from recharge to discharge locations. (c) Contours of simulated groundwater age for advection only ($D_m = \alpha_L = \alpha_T = 0$). Contour interval 10 years. (d) Contours of simulated groundwater age for advection and dispersion using $D_m = 1.16 \times 10^{-8}$ m^2/s, $\alpha_L = 6$ m, and $\alpha_T = 0.6$ m. Contour interval 10 years.

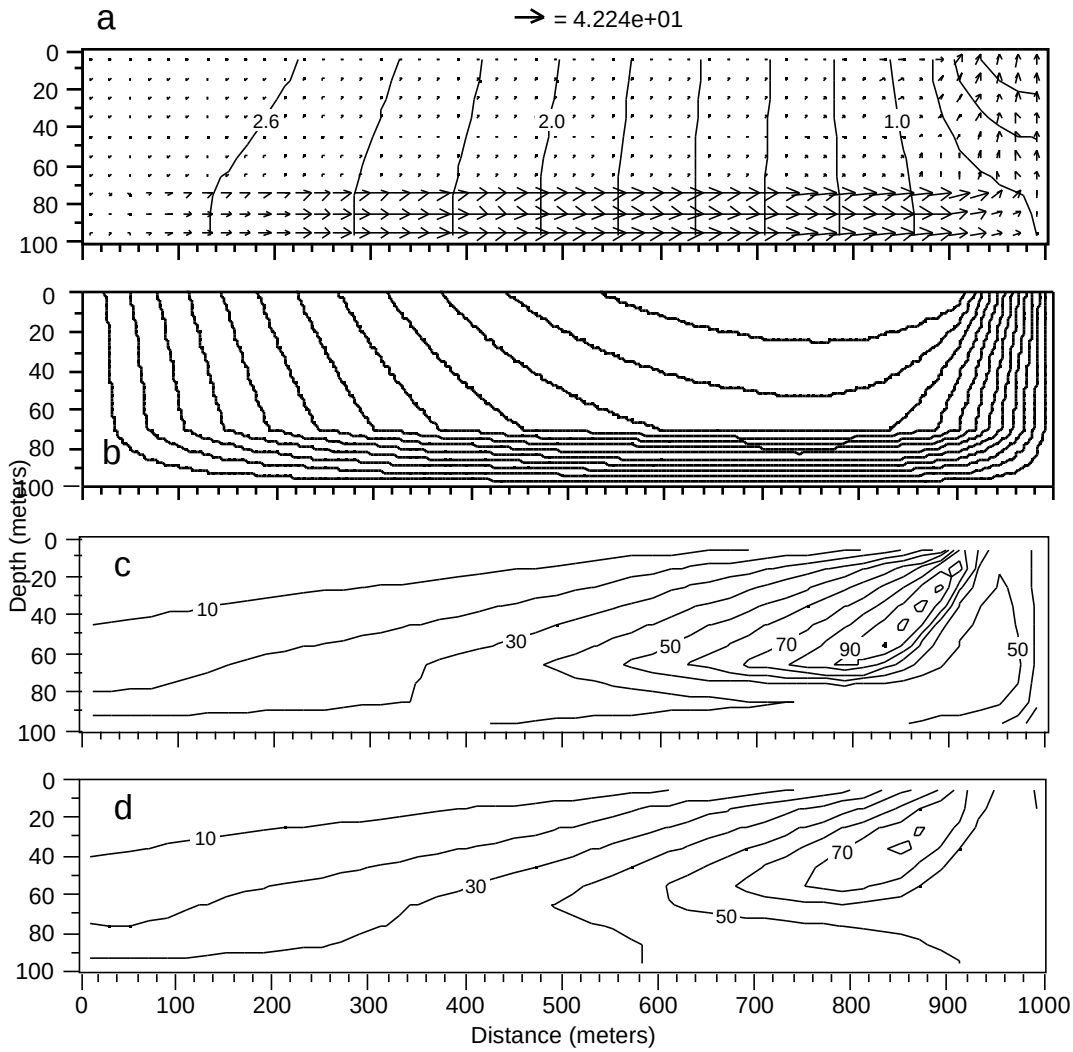

Figure 2-3 Results of direct simulation of groundwater age in a cross-section through a **layered** regional aquifer system in which the bottom layer is 30 m thick with hydraulic conductivity 10^{-5} m/s, and the overlying layer is 70 m thick with hydraulic conductivity 10^{-6} m/s: (a) Cross-sectional domain with hydraulic-head contours (0.2 m interval) and velocity vectors. Vertical exaggeration is 2X and the 10 row by 50 column finite-difference grid used for the numerical flow and transport solutions is indicated by the small ticks on each axis. (b) Streamlines from recharge to discharge locations. (c) Contours of simulated groundwater age for advection only ($D_m = \alpha_L = \alpha_T = 0$). Contour interval 10 years. (d) Contours of simulated groundwater age for advection and dispersion using $D_m = 1.16 \times 10^{-8}$ m^2/s, $\alpha_L = 6$ m, and $\alpha_T = 0.6$ m. Contour interval 10 years.

The groundwater age throughout the aquifer is readily simulated by solving the advection transport equation with the zero-order source term that accounts for aging (figs. 2-2c and 2-3c). For the uniform case, velocities are lowest along the no-flow boundaries on the left, bottom, and right. Along the right boundary, ages are the greatest at the bottom and decrease toward the discharge boundary at the top. Ages might be expected to increase continually toward the top of the right boundary, and this in fact occurs on individual streamlines. But the ages portrayed in Figures 2-2c and 2-3c are volume averages over 10 x 20 m cells. These cell-averaged values do not increase because converging streamlines near the discharge boundary bring younger water into the cells along the right boundary. That is, the maximum age at a point is at the top right corner of the domain, but the average age for the cell containing this point is less because of the convergence of streamlines in the cell.

The age distribution in the layered case is nonuniform and ages are greatest in the central part of the system, away from the boundaries (fig. 2-3c). Because the permeability of the lower layer is higher, the lowest velocities do not occur along the bottom of the system, but along the bottom of the upper layer. As with the homogeneous case, volume-averaged ages decrease toward the discharge boundary because the streamlines converge. The maximum water age in the layered aquifer system is about 90 years, whereas the maximum age in the uniform case is about 180 years. As discussed above, the total discharge through the aquifers is identical as a result of the specified-flux boundary conditions for recharge to the water table.

This result of greater maximum ages in the uniform case is highly dependent on aquifer structure and boundary-condition configuration. Simulation of a layered aquifer system identical to that shown here, but with the hydraulic conductivity of the lower layer decreased to 10^{-7} m/s, yields very different results. In this case, the upper portion of the system is more conductive than the lower and ages in the upper layer are similar to those in the homogeneous case. In the lower layer, however, flux and velocity are significantly

reduced because of the low permeability, and very old water is present, especially towards the right side of the domain. Maximum volume-average ages for this case, with advection alone, are more than 1,000 years.

The effect of dispersion on the groundwater age distribution is easily obtained by re-solving the transport equation and including dispersivities of α_L = 6 m and α_T = 0.6 m for the longitudinal and transverse components, respectively. In addition, a diffusion coefficient of $D_m = 1.16 \times 10^{-8}$ m^2/s is added to the dispersion tensor. This diffusion coefficient is about ten times higher than realistically expected values, and is used to illustrate the maximum likely effect of diffusion in these hypothetical aquifer systems. The effect of this diffusion alone is examined below.

Dispersive and diffusive mixing of water of different ages tends to limit the maximum ages (figs. 2-2d and 2-3d). Solute dispersive flux occurs, according to the generally accepted Fick's law model, in the direction of decreasing concentration. In complete analogy, the dispersive flux of age mass occurs in the direction of decreasing age, away from areas of maximum age. Where advective flux is relatively small—that is, where velocity is small—the effect of this dispersive flux on age distribution is greatest. The effect of longitudinal dispersion is mitigated in the case of age transport because, along a streamline, age increases smoothly in the direction of flow due to aging. Thus the steep longitudinal gradients typically associated with an advancing solute front are not present. However, steep gradients in age are present transverse to the flow direction, particularly in the layered case (figs. 2-3c and 2-3d). In these areas of steep gradients dispersion can have the greatest effect on groundwater age. Figure 2-4 is a contour map of the percent change in groundwater age, ranging from -37 to +64 percent, due to diffusion and dispersion for the layered case.

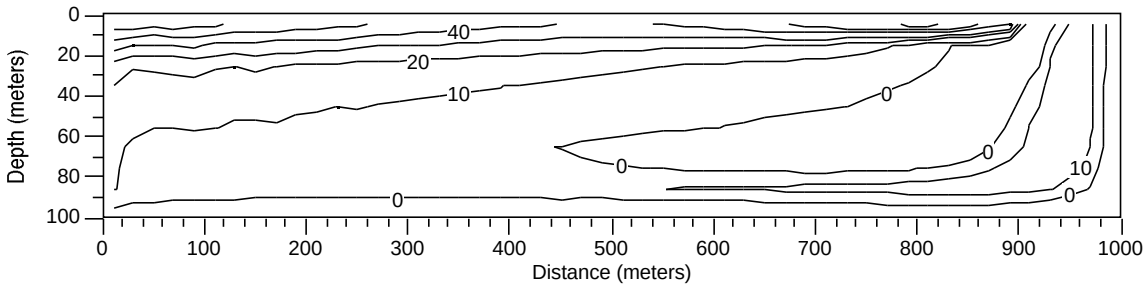

Figure 2-4 Percent difference in simulated age distribution between advection only and advection-dispersion (D_m = 1.16 x 10^{-8} m^2/s, α_L = 6 m, α_T = 0.6 m) cases in a **layered** regional aquifer system. The percent difference in simulated age ranges from -37 to +64 percent.

To examine further the relative contribution of diffusion and dispersion to the previous results, and to compare the theory developed here with residence-time-distribution (particle tracking) methods, a simulation of the layered case is conducted with advection and diffusion, but without dispersion. Figure 2-5 shows the results obtained by the theory proposed here, which are similar to those for advection alone, but exhibit a slight reduction in maximum ages. In the bottom layer, where velocities are high, diffusion has no observable effect on age distribution. Figure 2-5 also shows results of a particle-tracking model applied to the same problem. Particle paths and travel times are computed by linear velocity interpolation (Goode, 1990) and a random walk (Kinzelbach, 1988) to simulate diffusion. The groundwater age distribution is computed by numerical integration of equation (2.1). The close agreement between results obtained by using these alternative methods further supports the theoretical arguments presented in section 2.2.

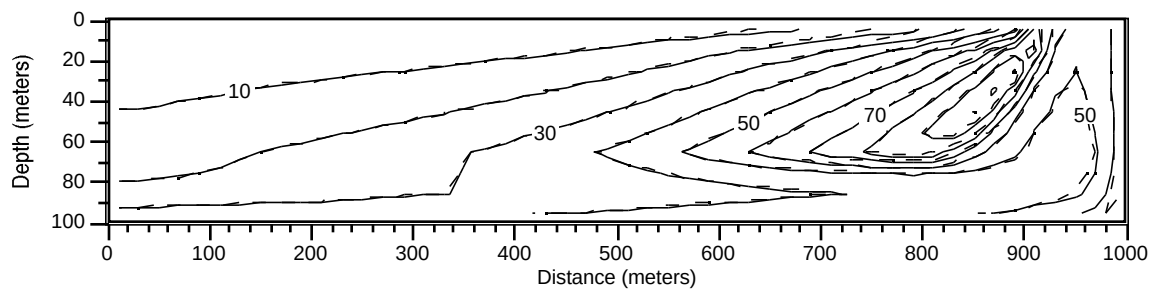

Figure 2-5 Contours of simulated groundwater age in a **layered** regional aquifer system for advection and diffusion obtained by using proposed transport equation method (solid lines), and by using a particle tracking and random walk method (dashed lines). The diffusion coefficient is 1.16 x 10^{-8} m^2/s and the contour interval is 10 years.

The **discontinuous layered** case is derived from the layered case but has a discontinuous bottom layer of even higher permeability. Here the high-permeability layer occurs only across part of the regional flow system in three sections. The bottom 30 m of the aquifer system has hydraulic conductivity $K_3 = 100 \times K_1 = 10^{-4}$ m/s in zones between 0-200 m, 400-600 m, and 800-1000 m distance from the left. The hydraulic conductivity is the same as the uniform case, $K_1 = 10^{-6}$ m/s, in the rest of the aquifer. The same value of porosity is used throughout the aquifer system, 0.2.

Flow is significantly diverted into the discontinuous high-permeability zones because of the 100 fold higher permeability (fig. 2-6a). The flow system is characterized by downward flow in the areas upgradient of and over the high-permeability zones, and upward flow at the downgradient end.

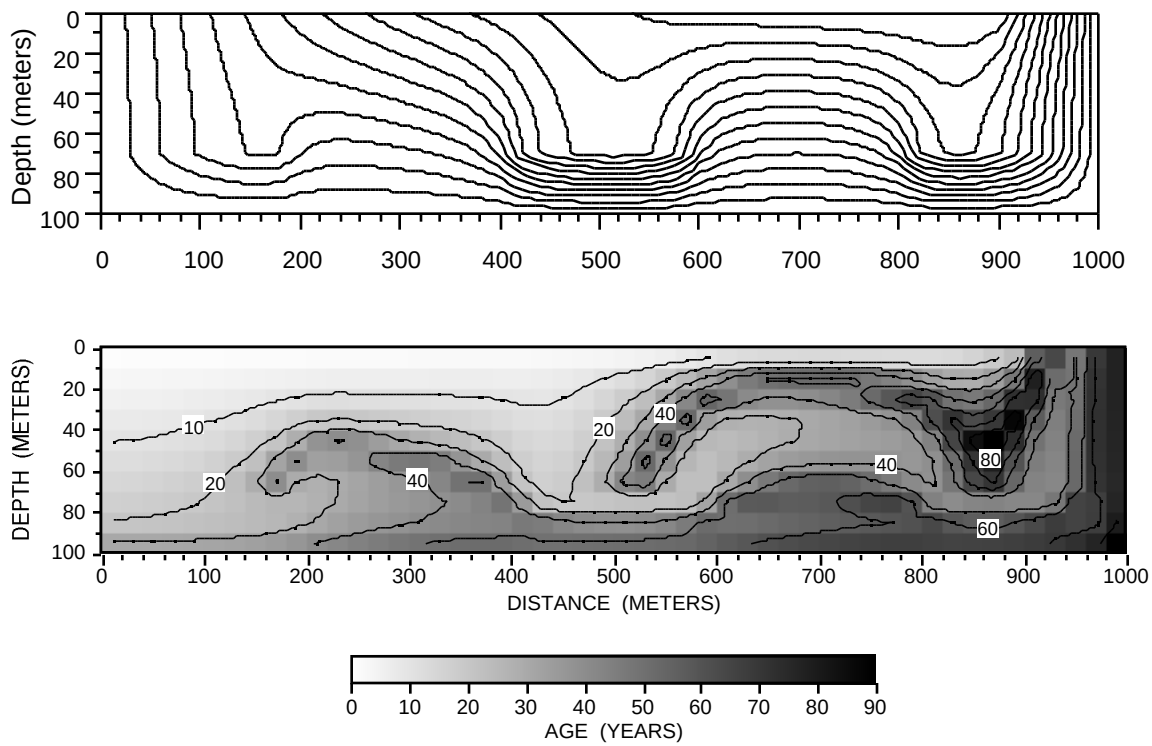

Figure 2-6 Results of direct simulation of groundwater age in a cross-section through a **discontinuous layered** regional aquifer system in which three high-permeability zones occur at the bottom. Each zone is 30 m thick with hydraulic conductivity 10^{-4} m/s and the horizontal extents are between 0 - 200 m, 400 - 600 m, and 800 - 1000 m from the left boundary. The remainder of the aquifer system has hydraulic conductivity 10^{-6} m/s. (a) Streamlines from recharge to discharge locations. Vertical exaggeration is 2X and the 10 row by 50 column finite-difference grid used for the numerical flow and transport solutions is indicated by the small ticks on each axis. (b) Contours of simulated groundwater age for advection only ($D_m = \alpha_L = \alpha_T = 0$). Contour interval 10 years.

The pattern of ages from advection alone is complex, even for this relatively simple case with only three high-permeability zones. As shown in Figure 2-6b, the nonuniform permeability distribution leads to widely varying travel times. As in the layered case, low horizontal velocities occur immediately adjacent to the high-permeability zones because their presence significantly reduces the local hydraulic

gradient. Hence, ground-water ages change significantly between adjacent flow lines depending on their history - whether they pass into high-permeability zones or pass through low-velocity areas adjacent to high-permeability zones.

The **stratified heterogeneous** case has several discontinuous high-permeability zones at different depths. The bulk of the aquifer has $K_1=10^{-6}$ m/s. Several very high permeability features are included; these features have $K_3 = 100\ K_1 = 10^{-4}$ m/s. The porosity is uniform, $\theta=0.2$. The two-order-of magnitude contrast in hydraulic conductivity causes a very complex flow pattern. Much of the horizontal flow occurs within the horizontal high-permeability features (fig. 2-7a). However, these features do not connect with each other, or with the top boundary. Outside of the high-permeability features, flow is primarily vertical, either between separate high-K zones, or between the upper high-K zones and the recharge/discharge boundaries at the top.

Although ages generally increase from left to right, in the direction of the overall flow, the age distribution is so complex that interpretation of the ages alone would be difficult (fig. 2-7b). For example, several closed contours of ages less than 40 years occur for $600 \leq x \leq 1000$ m. As with the layered case above, these closed contours occur because of the averaging of ages in model cells. Within high-K zones, the age is an average of many streamlines, some of which are very old. As these streamlines diverge downstream of the high-K zone, the youngest streamlines occupy cells in which no very-old streamlines occur, yielding younger cell-average ages. Conceptually, the cell-average age may represent the age of a sample taken from that location that mixed waters from the entire cell space, rather than the age at a point. This particular configuration yields youngest average ages outside the high-K zones, which is somewhat counter-intuitive. However, the occurrence of the oldest waters beneath the lower high-K zones re-emphasizes the shadowing effect of high-permeability features which reduce gradients in surrounding low-K areas.

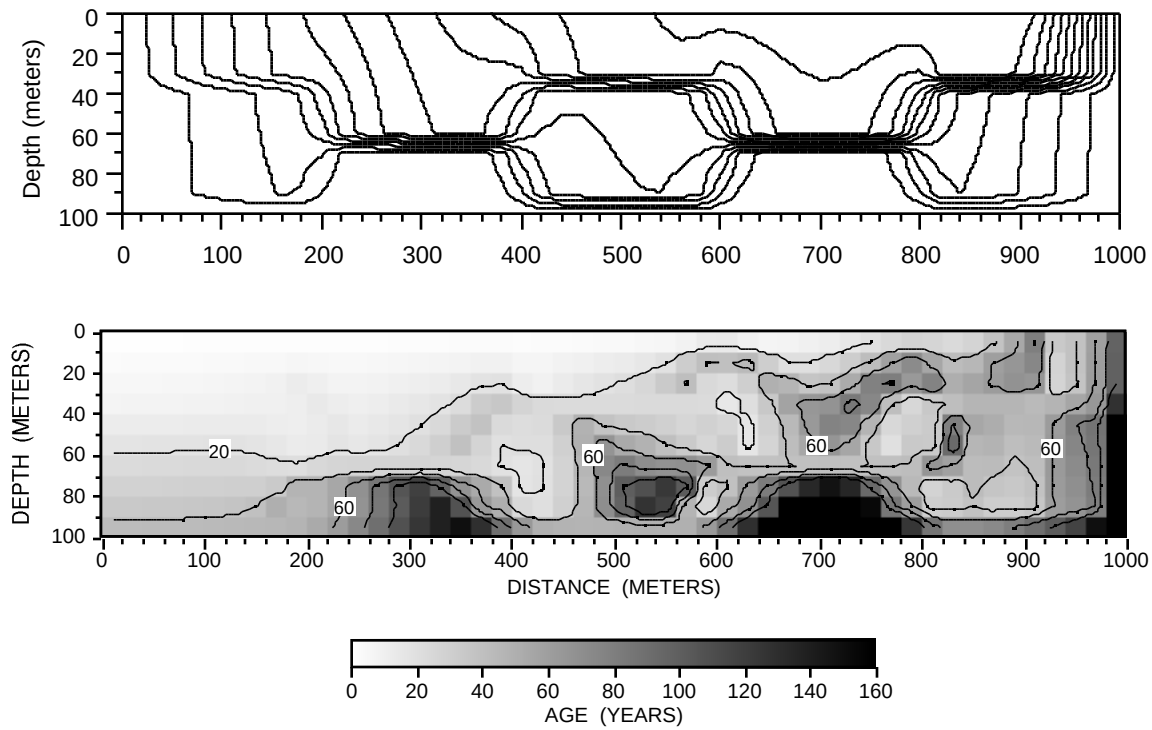

Figure 2-7 Results of direct simulation of groundwater age in a cross-section through a **stratified heterogeneous** regional aquifer system in which eight discontinuous high-permeability zones occur at three different depths. Each zone is 30 m thick with hydraulic conductivity 10^{-4} m/s and with horizontal extent of 200 m. The remainder of the aquifer system has hydraulic conductivity 10^{-6} m/s. Porosity is uniform, θ=0.2. (a) Streamlines from recharge to discharge locations. Vertical exaggeration is 2X and the 10 row by 50 column finite-difference grid used for the numerical flow and transport solutions is indicated by the small ticks on each axis. (b) Contours of simulated groundwater age for advection only ($D_m = \alpha_L = \alpha_T = 0$). Contour interval 10 years.

The second **stratified heterogeneous** case is derived from the previous case by changing the porosity of the lower 90 m of the system to θ_2=0.01. The hydraulic conductivity distribution is the same as the previous case, so the head gradients and fluxes are the same, but the velocity is increased by a factor of 20 in the lower part of the aquifer. This case illustrates the effect of stratified porosity; here the upper zone may represent a weathered rock zone with high porosity, and the lower zone may represent

unweathered rock with both highly-fractured and less-fractured zones. The ages in the fractured rock are lower than the previous case because of the reduced porosity, although the pattern of age variability is similar in many respects. However, the 20X large porosity in the overburden layer causes ages to be highest at the top of the system where significant horizontal flow occurs in the top layer. Maximum ages of about 40 years occur near the left end of the discharge region, and these ages are similar to the ages in the previous simulation at the same location. For this location, the main control on the age is the time spent in the top layer, and that has not changed because the porosity of the top layer, and of course the specific discharge everywhere, is identical to the previous simulation.

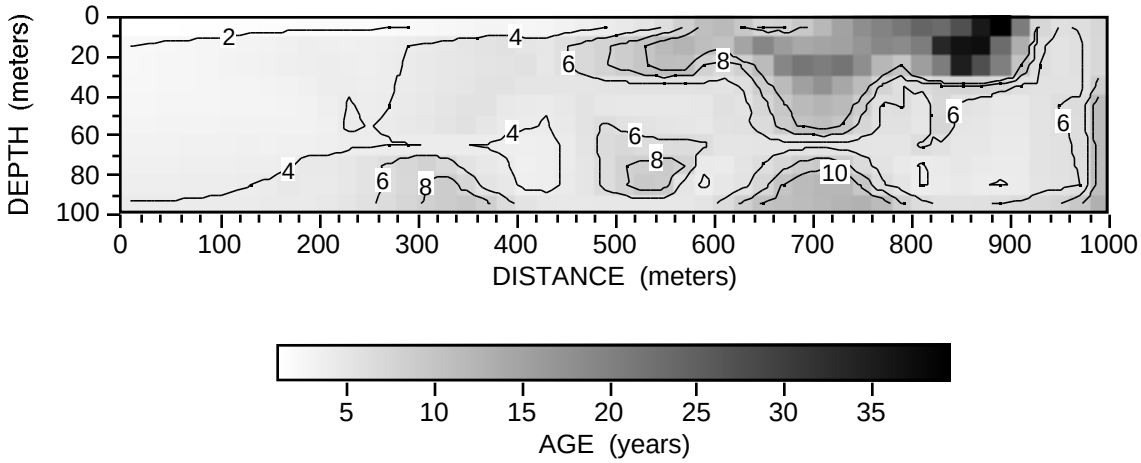

Figure 2-8 Results of direct simulation of groundwater age in a cross-section through a **stratified heterogeneous** regional aquifer system in which eight discontinuous high-permeability zones occur at three different depths. Each zone is 10 m thick with hydraulic conductivity 10^{-4} m/s and with horizontal extent of 200 m. The remainder of the aquifer system has hydraulic conductivity 10^{-6} m/s. Porosity is θ=0.2 in the upper 10 m and is θ_2=0.01 in the remainder of the aquifer. (Streamlines are the same as fig. 2-7a) Contours of simulated groundwater age for advection only ($D_m = \alpha_L = \alpha_T = 0$). Contour interval 10 years.

In summary, these regional cross-section examples illustrate the utility of the method of direct simulation of ground-water age, and the complexity in spatial age patterns that can be created by heterogeneities in hydraulic conductivity and porosity. The methods presented here for direct simulation of ground-water facilitate computation of age throughout an aquifer with simple modifications to existing solute transport models. Although environmental tracers offer additional information, compared to hydraulic head measurements, it may not be easy to unravel the underlying permeability distribution from spatially variable age distributions; highly complex age patterns emerge from relatively simple simulations, albeit ones with at least one order of magnitude variability in permeability.

2.3.2 Matrix Diffusion from a Single Fracture

Matrix diffusion can be an important aspect of transport of solutes in ground water, particularly in fractured-rock settings. Matrix diffusion generally refers to diffusive exchange between high-permeability fractures or fracture zones and low-permeability rock *matrix*, whether much less fractured or unfractured. Water flow occurs primarily in the fractures and flow is often modeled ignoring the permeability of the rock matrix. However, diffusive exchange of solutes between the flowing water in the fractures and the immobile water in the rock matrix can have significant impacts on solute migration (Grisak and Pickens, 1980; Sudicky and Frind, 1982).

The impact of matrix diffusion on age transport is examined here for a one-dimensional flow system using MOC3D (Goode and Konikow, 1991; Konikow and others, 1996) modified to solve the transient age transport equation (2.10). A 1 m long column is discretized with 10 cells ($\Delta x = 0.1$ m). Imposed fixed-head boundary conditions yield a specific discharge of 1 m/day, and the porosity of 0.01 results in a uniform velocity of 100 m/day. This porosity represents the high-permeability fractures in the rock column. Ignoring dispersion and matrix diffusion, the steady-state age at a x = 9.5 m is simply the travel time: A (x=9.5) = x / V = 9.5 m / 100 m/day = 0.095 day.

At steady state, the effect of matrix diffusion is an apparent increase in porosity, from that of the fractures alone, to the sum of both fracture and matrix porosity (θ_m ; eq. 2.15). In this case, the apparent travel time to x = 9.5 m, and the steady-state age, is A = x / [q/($\theta + \theta_m$)] = 9.5 m / [1 m/day / (0.01 + 0.09)] = 0.95 day, or an increase by an order-of-magnitude. This increase corresponds directly to the increase in porosity from 0.01 to 0.10. However, the rate at which this steady state is approached depends on the system properties.

The exchange of age-mass between the fractures and the rock matrix is the term F in the governing equation (2.10). In the rock matrix, the age transport processes are limited to accumulation, production, and diffusion. Diffusion is assumed to be one-dimensional in the rock matrix, orthogonal to fractures. An integral balance equation for age-mass in the rock matrix is

$$\frac{d\,A_m}{dt} = 1 - \frac{\beta\left(A_m - A\right)}{\theta_m} \quad . \tag{2.16}$$

where A_m is the average age in the rock matrix, A is the age in the fracture system at the same location, β [T^{-1}] is a linear exchange coefficient characterizing diffusion between the fracture and the rock matrix, and the density is assumed to be constant. The term F in the fracture governing equation is F = $\rho\beta$ (A_m - A) and corresponds to the age-mass flux into the fractures per unit volume of aquifer.

The linear exchange coefficient is generally proportional to the diffusion coefficient (D_m) divided by a characteristic length (b) squared:

$$\beta \propto \frac{D_m}{b^2} \quad . \tag{2.17}$$

For example, for the case of planar fractures, the linear exchange coefficient corresponding to a 1-node finite-difference approximation is given by:

$$\beta = \frac{1}{2}\frac{D_m}{b^2} \quad . \tag{2.18}$$

where b is the block half-thickness. This simple linear model of matrix diffusion is strictly accurate only for relatively small diffusion distances, i.e. small b. However, this kinetic exchange model can be considered a first-order approximation of the impact of exchange between high-permeability and much lower-permeability portions of a flow system, whether limited strictly to diffusion or not.

The initial age is assumed to be zero throughout the aquifer. At early time, water at all locations ages as simulation time progresses (fig. 2-9). If the linear exchange coefficient is low ($\beta = 10^{-4}$ m^2/day in fig. 2-9), then the age temporarily stabilizes at a level corresponding to the travel time in the fractures alone, 0.095 day. However, eventually the age in the matrix builds up to such high levels that the age-mass flux into the fracture is sufficient to increase the age in the fractures, and eventually reach a new plateau corresponding to the travel time computed from the total porosity, 0.95 day. The magnitude of the linear exchange coefficient (β) controls the time at which matrix diffusion has a significant impact on computed ages. For very high β, the initial plateau is not present because the fracture and matrix ages are essentially in equilibrium at all times (fig. 2-9).

Equation (2.16) can be used to compute the steady-state age in the rock matrix from the steady-state age in the fracture: $A_m = A + \theta_m / \beta$. Hence for this case the steady-state ages in the matrix at x = 9.5 m for $\beta = 1$, 10^{-2}, and 10^{-4} day^{-1} are $A_m = 0.185$, 9.095 and 900.095 days., respectively.

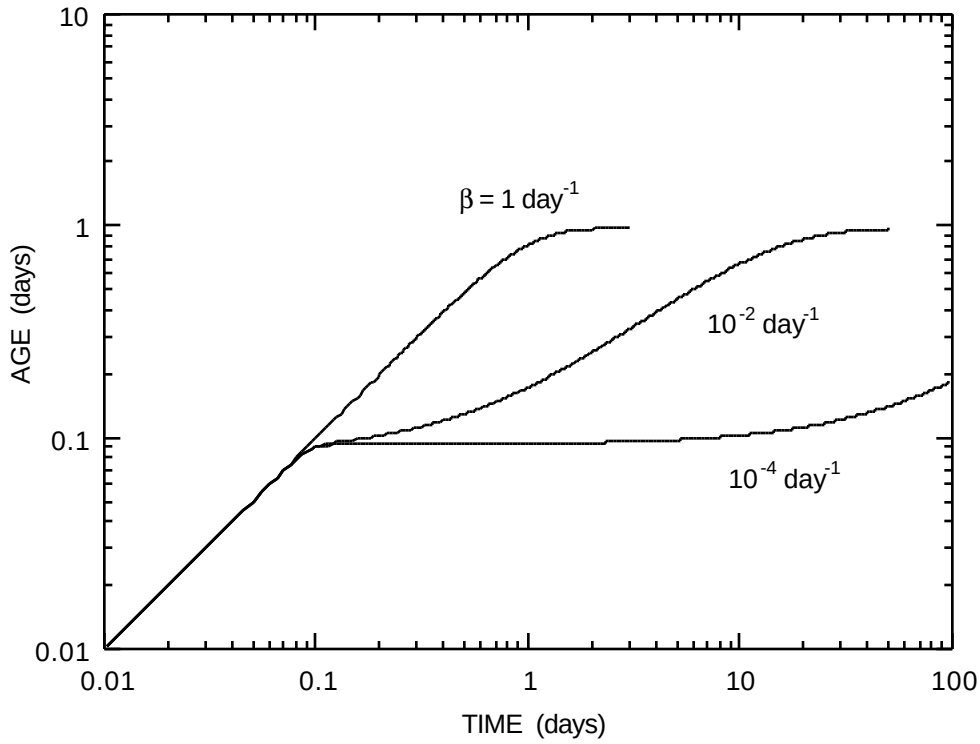

Figure 2-9 Age at x = 9.5 m from the inflow boundary of a one-dimensional rock column having fracture porosity 0.01, rock matrix porosity 0.09, and specific discharge 1 m/day. The initial condition is age = 0 at all locations. Age is shown as a function of simulation time for three values of linear exchange coefficient (β) characterizing the rate of mass transfer by diffusion between the flowing water in the fractures and the immobile water in the rock matrix.

2.3.3 Age of Pumped Samples from a Heterogeneous Formation

The age in a ground-water system can be estimated from concentrations of environmental tracers in samples pumped from wells. For example, the time since water has been isolated from the atmosphere can be estimated from CFC concentrations because the atmospheric concentration has been increasing for about the last 50 years (Plummer et al., 1993). When drawing water from a well, particularly one with a long screened or open interval, the pumped water is a mixture of water from different parts of the aquifer. This mixing can significantly complicate or add uncertainty to estimation of

ground-water age. Furthermore, the age of discharging water after a pump is turned on would change in time as water from a larger and larger capture volume enters the well.

A hypothetical simulation illustrates use of the direct age method to model the time-evolution of age in water discharging from a pumping well in a highly heterogeneous formation. This simulation is based on a well-field scale model developed by Paul Hsieh (USGS, Menlo Park, California, written communication, 1994) of ground-water flow during an aquifer test in fractured rock at Mirror Lake NH. Aquifer hydraulic properties (Table 2-1) were estimated by calibrating steady-state and transient models of three-dimensional flow during the test. These properties are used here in a model of both steady-state age distribution and age transport during pumping tests.

Table 2-1. Hydraulic Properties of Three-Dimensional Model of Highly-Heterogeneous Formation (Paul A. Hsieh, U.S. Geological Survey, written communication, 1994).

		Hydraulic Conductivity (m/s)	
Hydrogeologic Unit	Model Layers	Horizontal	Vertical
Overburden	1-5	1.8×10^{-6}	1.8×10^{-6}
Bedrock Surface	between 5 & 6	--	1.9×10^{-8}
Highly-Fractured	parts of 11, 22 & 38	5.6×10^{-5}	--
Less-Fractured	6-38	3.3×10^{-8}	1.9×10^{-7}

The model grid is 22 rows x 14 columns x 38 layers. The grid spacing is uniform throughout the grid with $\Delta x = \Delta y = 7.62$ m, $\Delta z = 1.5$ m. The highly-fractured zones of the bedrock are simulated as 1.5 m thick porous media units with much higher hydraulic conductivity than the surrounding bedrock (fig. 2-x).

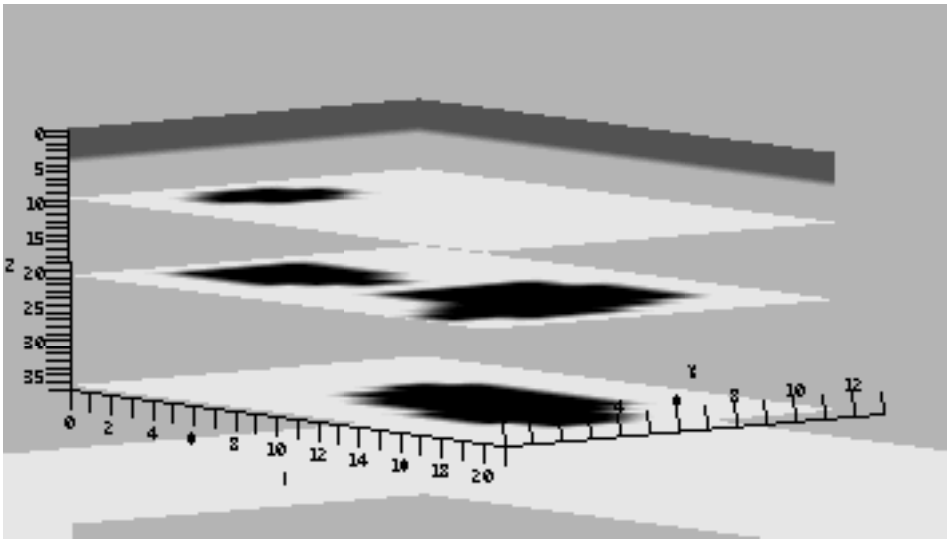

Figure 2-10 Hydraulic conductivity distribution for three-dimensional highly-heterogeneous case. Weathered zone at top (dark gray) has K = 2.7 x 10^{-6} m/s; four horizontal highly-fractured zones (black) occur at three different depths and have K = 8.4 x 10^{-5} m/s; the remainder of the less-fractured bedrock has K = 5 x 10^{-8} m/s.

The initial steady-state distribution of ground-water age is assumed to represent conditions prior to pumping. The average annual recharge of 368 mm/yr is distributed over the top of the model. All other boundaries are no-flow, except the face at y = 168 m where the head in all model layers is fixed at 0.0. Age is simulated only in the bedrock portion of the aquifer and it is assumed that all water inflowing from the overburden has age zero. For advection alone, the age distribution is efficiently computed using particle tracking and equation (2.1). For the age simulation, the bedrock porosity is assumed to be 0.001, which corresponds to a bulk porosity of fracture volume per unit volume of rock.

Maximum ages occur at the bottom of the system where less-fracture bedrock underlies the highly-fractured zones (fig. 2-11; fig. 2-12). Flow is generally downward from the overburden into the horizontal fracture zones, and then laterally out along the downgradient face (front face in fig. 2-11; right end of cross-section in fig 2-12 (a)). The fracture zone at the bottom of the model is shown as the area of blue age in fig. 2-11.

The maximum ages are diluted downgradient from the red area by much younger waters in the fracture flow system. Resulting outflow face ages are high only at the very bottom of the aquifer (fig. 2-12(b)).

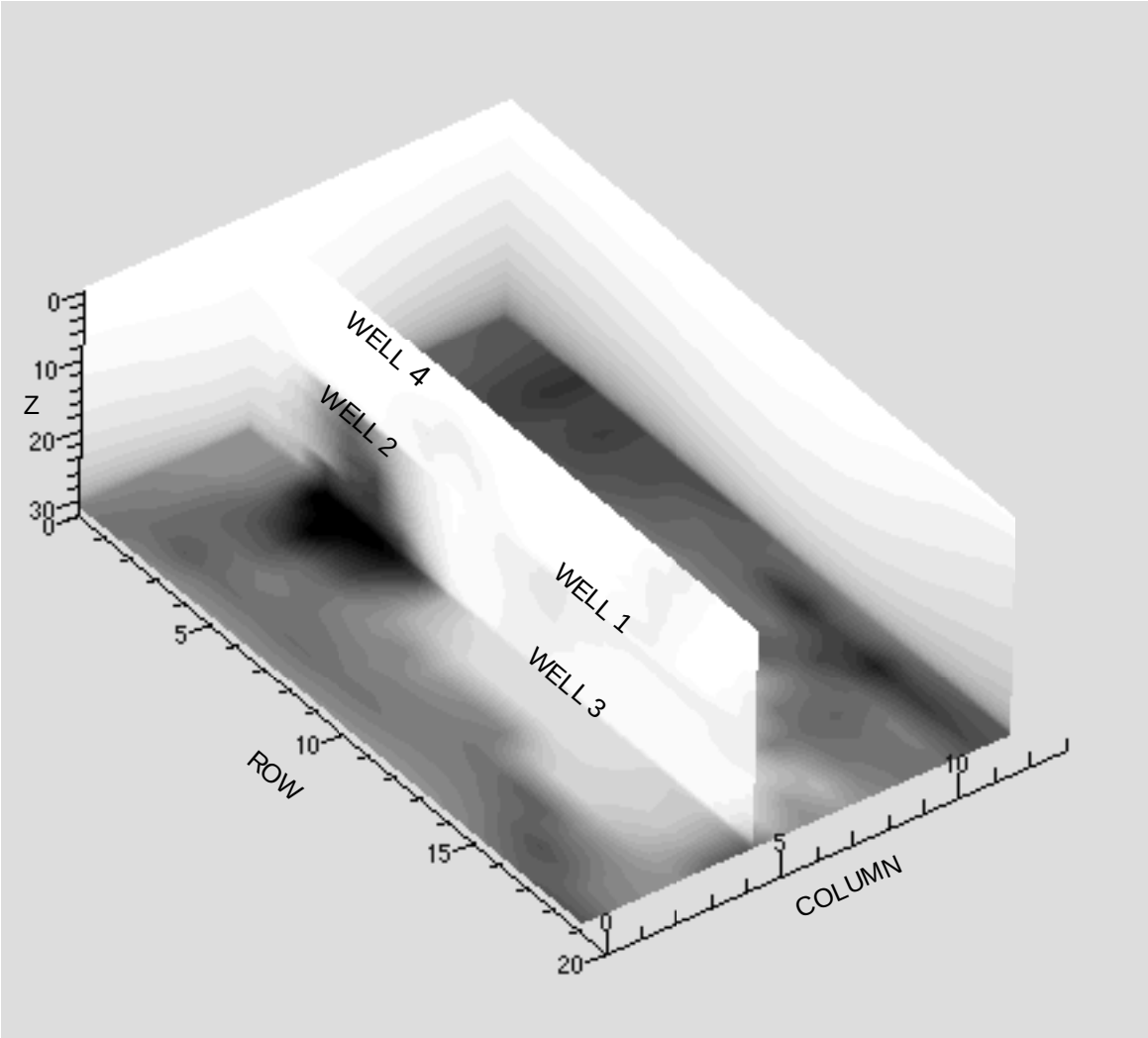

Figure 2-11 Results of direct simulation of steady-state groundwater age in a highly-heterogeneous fractured bedrock. Hydraulic properties are shown in fig. 2-10 and summarized in table 2-1. Also shown are locations of wells which are not pumping in this simulation. The colors correspond to age, ranging from less than 3 years (white) to greater than 700 years (black).

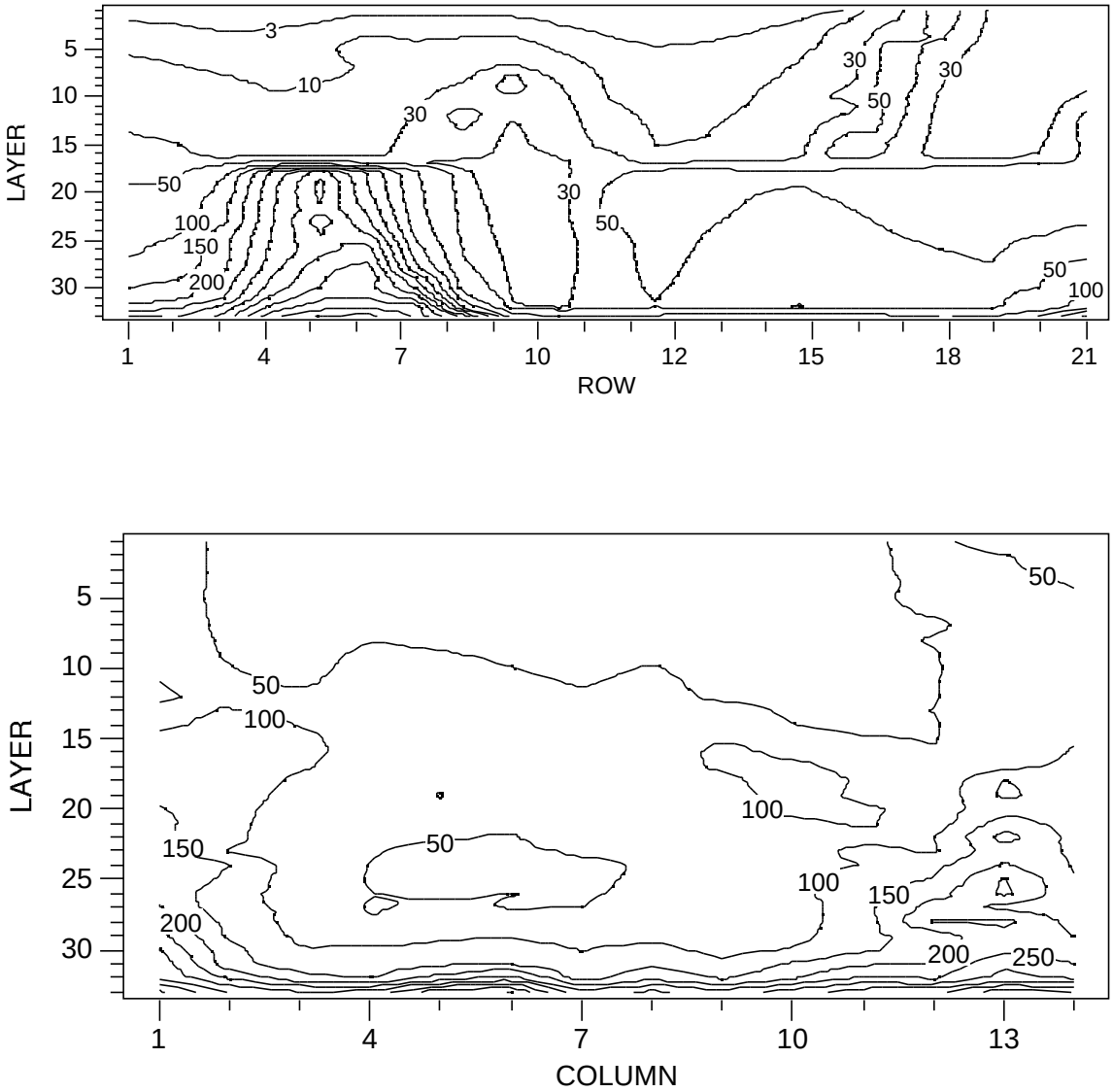

Figure 2-12 Results of direct simulation of steady-state groundwater age in a highly-heterogeneous fractured bedrock. Hydraulic properties are shown in fig. 2-10 and summarized in table 2-1. (a) Y-Z cross-section along the middle of the model at column 7 (x=53 m), variable contour intervals in years. (b) X-Z cross-section at the outflow end of the model along row 21 (y=160 m), contour intervals are 50 years.

Ground-water age in pumped samples is evaluated for four fracture-zone well locations. In each case, the initial age distribution is that from the previous steady-state age simulation. A steady-state flow field is generated for each pumping scenario by imposing no-flow boundaries on the model bottom and all four sides. The top layer of the overburden is modeled as a fixed-head boundary from which all of the flow to the well is ultimately derived. Each well is pumped separately at a rate of 10.6 L/min.

The evolution of ground-water age of pumped samples is different for each well (fig. 2-13). Wells 1 and 2 are in downgradient and upgradient fracture zones near mid-depth in the model. Age in downgradient well 1 increases sharply at early time from about 37 years to over 40 years, levels off near 43 years, and appears to be gradually increasing after 10 hours of pumping. Well 2 is in the upgradient fracture zone at the same depth, and its age is initially higher. Age in well 2 drops, but not as sharply in time, from 54 years to less than 46 years and then increases to about 56 years at the end of the simulation. The small-scale fluctuations in the age are numerical artifacts of the discrete method-of-characteristics model (Konikow and other, 1996).

Ground-water age in samples from wells 3 and 4 decrease logrithmically in time from the initial values (fig. 2-13). Well 3 is located (fig. 2-11) in the bottom fracture zone and has the highest initial age, over 200 years. However, the age decreases sharply to less than 120 years after 2 hours of pumping and is less than 100 years after 10 hours. Well 4 shows a similar pattern, but at much younger ages. This well is located in the top fracture zone, much closer to the recharge source in the overburden. Ages in samples from well 4 decrease from over 12.5 years initially to less than 8.5 years after 10 hours.

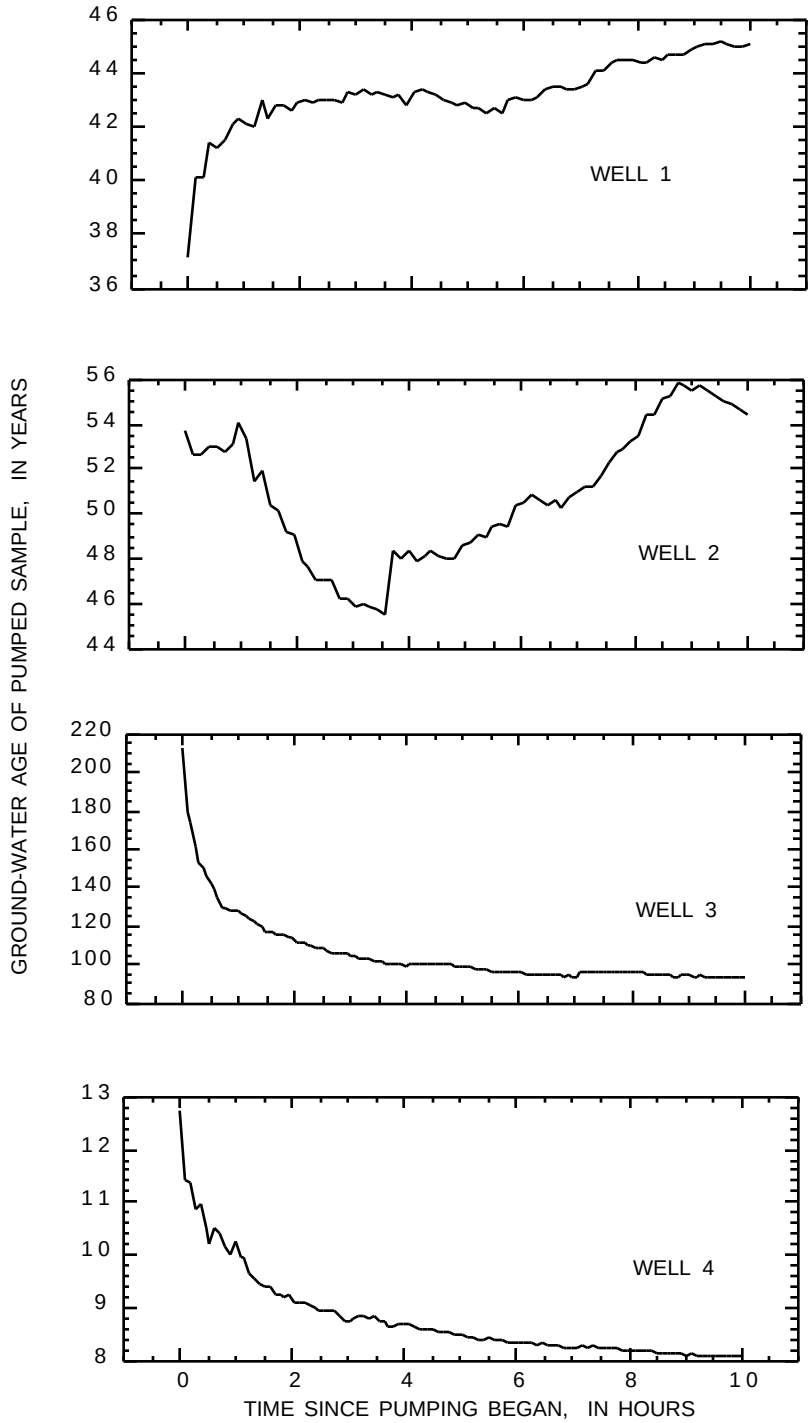

Figure 2-13 Sample age as a function of pumping time in a highly-heterogeneous aquifer. Age transport to the pumping well is simulated with four different steady-state flow models having only the well of interest pumping. The initial age distribution for each case is the steady-state age shown in fig. 2-11. Hydraulic properties are shown in fig. 2-10 and summarized in table 2-1. Locations for each well are shown in fig. 2-11.

2.3.4 Two-Dimensional Age Distribution in Mildly-Heterogeneous Porous Media

Simulation of the age distribution in a hypothetical aquifer illustrates features of ground-water age in relatively homogeneous systems. Intensive field tracer experiments have been conducted at a military reservation on Cape Cod, Massachusetts. LeBlanc and others (1991) describe a natural gradient tracer test conducted over 2 years using nonreactive and reactive tracers in a relatively homogeneous sand and gravel aquifer. Garabedian and others (1991) analyze the spreading of a nonreactive tracer and estimate asymptotic dispersivities from the temporal growth in the spatial moments of the tracer distribution. Hess and others (1992) compare field and laboratory measurements of hydraulic conductivity and estimate macrodispersivities from theoretical relations.

A hypothetical two-dimensional aquifer is generated that has heterogeneous hydraulic conductivity with spatial statistics similar to those from the Cape Cod tracer test. The turning bands methods (Mantoglou and Wilson, 1982; Zimmerman and Wilson, 1989) is used to generate a spatially correlated field of hydraulic conductivity (K). K is assumed to be lognormally distributed with mean 110 m/d (Garabedian et al., 1991) and variance of the natural log of K = 0.24 (Hess et al., 1992). An exponential spatial covariance function is assumed with zero nugget and isotropic correlation length of 2.6 m (Hess et al., 1992). The grid is 100 m by 20 m and is discretized by 500 x 100 square blocks having $\Delta x = \Delta y = 0.2$ m. The single realization of K used (fig. 2-14a) reflects the underlying statistical properties: most of the K values are clustered near and below the mean value, the size of the high and low zones are larger than individual grid blocks and smaller than the grid dimensions; only a few isolated zones exhibit K > 300 m/d.

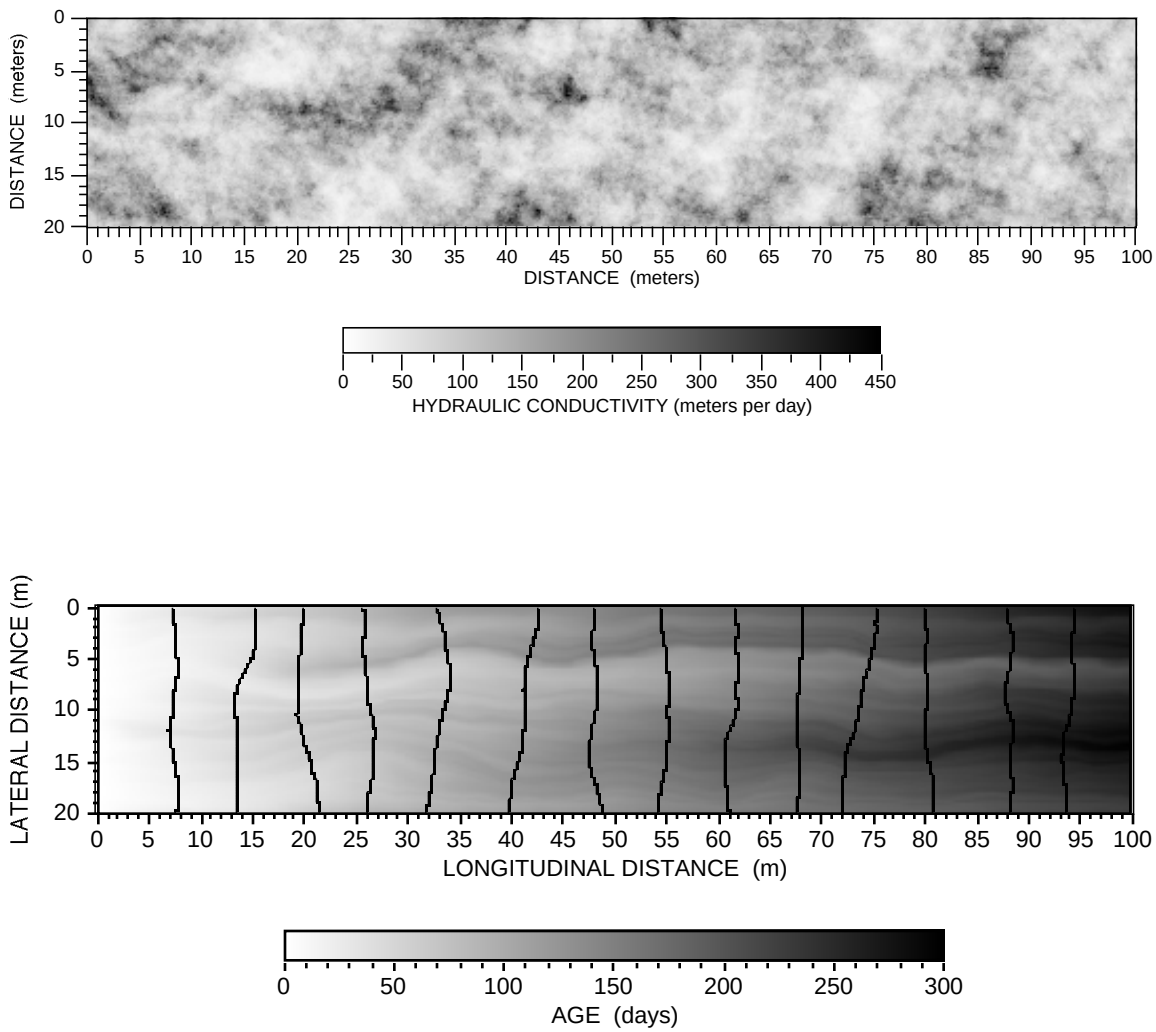

Figure 2-14 Age simulation in a mildly heterogeneous two-dimensional aquifer: (a) Hydraulic conductivity distribution; (b) Hydraulic head contours (0.01 m interval) and age distribution for advection-only.

The boundary conditions for the steady-state flow model are h(x=0) = 0.148 m; h(x=100 m) = 0 m; and no-flow at y = 0 and y = 20 m. These boundary conditions, along with an assumed porosity of 0.39 (LeBlanc et al, 1991) yield an average velocity of about 0.4 m/d.

The steady-state age distribution (fig. 2-14b) is more variable than the head distribution and indicates significant persistence of thin ‘fingers’ of contrasting age.

Youngest ages occur along a somewhat continuous zone of elevated K in the upper half (y<10m) of the aquifer. However, an adjacent zone with older water reflects the impact of a large zone of low K located at about (x,y)=(20m,5m). The resulting large difference in age between closely space streamlines persists downstream to the end of the aquifer. This 'slip' between adjacent streamlines would be modeled as longitudinal dispersion if the small-scale K variability were not explicitly accounted for.

The spatial variability of the steady-state age distribution can also be illustrated by plots of age as a function of distance. In the longitudinal direction, the age generally increases more or less smoothly in the average direction of flow (fig. 2-15a). For much of the domain, the variability in the x-direction is relatively smooth, as illustrated by the lines at y = 7.3 and 13.3 m. The overall rate of increase in age versus x shown for these two lines essentially brackets all longitudinal transects in this simulation. Significantly more variability along x is illustrated near the position of the large low-K zone, as shown by the line at y = 5.3 m. At this position, the age does not monotonically increase in the mean direction of flow. For example, the water at (x,y) = (45m,5.3m) is about 30 days older than water 5 m further down (the mean) gradient at (x,y) = (50m,5.3m). Close examination of other lines indicates that in this simulation all lines have portions where age decreases in the mean flow direction. This decrease in age in the mean flow direction is due to the difference between the actual streamlines and the mean path.

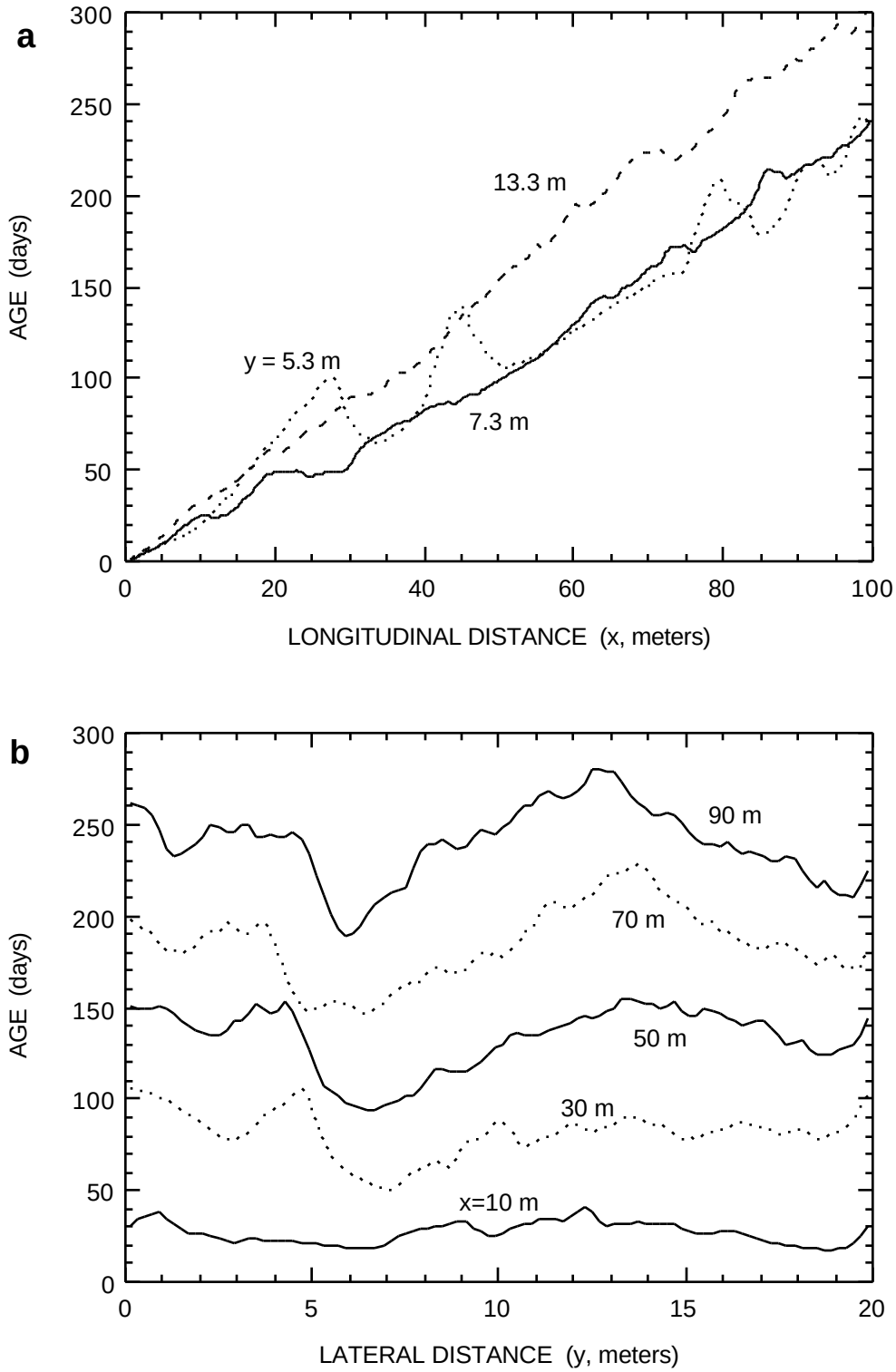

Figure 2-15 Age variation along lines oriented longitudinal (a) and lateral (b) to the average flow direction for a mildly heterogeneous two-dimensional aquifer.

Variability in age is pronounced in the y-direction, lateral or transverse to the mean flow direction (fig. 2-15b). The variability is less at the upstream boundary because by definition the age is uniform at 0 days at x=0. A significant peak of older water develops between x = 10 and 30 m because of the large low-K zone discussed above. Although the y position of this peak shifts due to shifting flowlines, the magnitude of the difference between the age on this peak and on adjacent streamlines persists through the simulated domain.

2.4 Summary

A new method is developed to simulate groundwater age. The spatial distribution of groundwater age is governed by a transport equation that has an internal source of unit (1) strength, corresponding to the rate of aging. This governing equation is derived both from residence-time-distribution concepts, and from mass-conservation principles applied to conceptual age mass. This method of groundwater age simulation falls between existing approaches of, on one hand, simulation of groundwater age as governed by advection alone, by using a particle tracking model and, on the other hand, simulation of isotopes or chemical markers of interest in a solute transport model. Use of the theory presented here allows general simulation of groundwater age, without solute-specific modeling, by incorporating the physical effects of diffusion, dispersion, mixing, and exchange processes on age. These methods can be incorporated easily in existing models of transport in aquifers.

Application of this theory is illustrated for several examples. The impact of layered heterogeneity on regional scale age distribution is examined in cross-section for cases with and without dispersion and diffusion. Average ages are not highest at the discharge boundary in many cases, and the shadowing effect of high-permeability units on gradients in surrounding low-permeability units is illustrated. Matrix diffusion causes a ‘retardation’ of apparent velocity at steady state, but the rate at which steady state is approached may be slow, as controlled by diffusion in the rock matrix. The age transport equation is a convenient method of examining the time variation of age of pumped samples. For the case examined, the time history of age of pumped samples depends on the local conditions near the well and may result in large changes in age during pumping at some locations. Finally, a relatively homogeneous example illustrates that even when the spatial variability of hydraulic conductivity is relatively small, the age distribution is not smooth. The age is much more sensitive to variability in K than the head. Hence,

deviation of age from the mean value can provide significant information about heterogeneity. On the other hand, interpretation of mean age from a limited number of point samples is complicated by this sensitivity.

2.5 References

Bair, E. S., R.A. Sheets, and S.M. Eberts, Particle-tracking analysis of flow paths and travel times from hypothetical spill sites within the capture area of a wellfield, Ground Water, 28(6), 884-892, 1990.

Bear, J., *Hydraulics of Groundwater*, McGraw-Hill, New York, 1979.

Bolin, B., and Henning Rodhe, A note on the concepts of age distribution and transit time in natural reservoirs, Tellus, 25(1), 58-62, 1973.

Campana, M. E., and E.S. Simpson, Groundwater residence times and recharge rates using a discrete-state compartment model and 14C data, J. Hydrol., 72, 171-185, 1984.

Dagan, G., and V. Nguyen, A comparison of travel time and concentration approaches to modeling transport by groundwater, J. Contaminant Hydrology, 4, 79-91, 1989.

Danckwerts, P. V., Continuous flow systems: Distribution of residence times, Chemical Eng. Sci., 2, 1-13, 1953.

Egboka, B. C. E., J.A. Cherry, R.N. Farvolden, and E.O. Frind, Migration of contaminants in groundwater at a landfill: A case study, 3, Tritium as an indicator of dispersion and recharge, J. Hydrol., 63, 51-80, 1983.

Eriksson, E., The possible use of tritium for estimating groundwater storage, Tellus, 10(4), 472-478, 1958.

Freeze, R.A., and J.A. Cherry, *Groundwater*, Prentice-Hall, Englewood Cliffs, New Jersey, 1979.

Freeze, R. A., and P.A. Witherspoon, Theoretical analysis of regional groundwater flow. 2. Effect of water-table configuration and subsurface permeability variation, Water Resour. Res., 3(2), 623-634, 1967.

Fritz, P., J.E. Gale, and E.J. Reardon, Comments on carbon-14 dating of groundwaters in crystalline environments, Geoscience Canada, 6(1), 10-15, 1979.

Garabedian, S.P., D.R. LeBlanc, L.W. Gelhar, and M.A. Celia, 1991, Large-scale natural gradient tracer test in sand and gravel, Cape Cod, Massachusetts 2. Analysis of spatial moments for a nonreactive tracer: Water Resources Research, v. 27, no. 5, p. 911-924.

Geyh, M. A., and G. Backhaus, Hydrodynamic aspects of carbon-14 groundwater dating, in *Isotope Hydrology 1978*, v. 2, pp. 631-643, International Atomic Energy Agency, Vienna, 1978.

Goode, D. J., Particle velocity interpolation in block-centered finite difference groundwater flow models, Water Resour. Res., 26(5), 925-940, 1990.

Goode, D.J., Direct simulation of groundwater age: Water Resources Research, 32(2), 289-296, 1996.

Goode, D. J., and L. F. Konikow, Testing a method-of-characteristics model of three-dimensional solute transport in ground water, in Proc. *Symposium on Ground Water*, Nashville, Tenn., July 29–August 2, 1991, edited by G.P. Lennon, pp. 21-27, Am. Soc. Civ. Eng., New York, 1991.

Grisak, G.E., and J.F. Pickens, 1980, Solute transport through fractured media, 1, The effect of matrix diffusion: Water Resources Research, 16, 719-730.

Harvey, C.F., and S.M. Gorelick, Moment generating equations: Modeling transport and mass transfer in heterogeneous aquifers, Water Resour. Res., 31(8), 1895-1911, 1995.

Hess, K.M., S.H. Wolf, and M.A. Celia, Large-scale natural gradient tracer test in sand and gravel, Cape Cod, Massachusetts 3. Hydraulic conductivity variability and calculated macrodispersivities: Water Resources Research, 28(8), 2011-2027, 1992.

Kinzelbach, W., The random walk method in pollutant transport simulation, in *Groundwater Flow and Modeling*, edited by E. Custodio et al., pp. 227-245, D. Reidel, Hingham, Mass., 1988.

Konikow, L.F., and D.B. Grove, Derivation of equations describing solute transport in ground water, U.S. Geological Survey Water-Resources Investigations Report 77-19, 1977.

Konikow, L.F., D.J. Goode and G.Z. Hornberger, A three-dimensional method-of-characteristics solute-transport model (MOC3D): U.S. Geological Survey Water-Resources Investigations Report 96-4267, 87 p., 1996.

Kreft, A., and A. Zuber, On the physical meaning of the dispersion equation and its solutions for different initial and boundary conditions, Chemical Eng. Sci., 1471-1780, 1978.

LeBlanc, D.R., S.P. Garabedian, K.M. Hess, L.W. Gelhar, R.D. Quadri, K.G. Stollenwerk, and W.W. Wood, Large-scale natural gradient tracer test in sand and gravel, Cape Cod, Massachusetts 1. Experimental design and observed tracer movement: Water Resources Research, 2( )5, 895-910, 1991.

Lee, S.-I., and P.K. Kitanidis, Analysis of groundwater flow and travel times for a landfill site in an arid region with a thick vadose zone, Hydrological Processes, 7, 373-387, 1993.

Levenspiel, O., *Chemical Reaction Engineering*, Wiley, New York, 1972.

MacMullin, R. B., and M. Weber, Jr., The theory of short-circuiting in continuous-flow mixing vessels in series and kinetics of chemical reactions in such systems, Transactions of American Institute of Chemical Engineers, 31(2), 409-458, 1935.

Mantoglou, A., and J.L. Wilson, The turning bands method for simulation of random fields using line generation by a spectral method: Water Resources Research, 18(5), 1379-1394, 1982.

Maloszewski, P., and Andrzej Zuber, Influence of matrix diffusion and exchange reactions on radiocarbon ages in fissured carbonate aquifers, Water Resour. Res., 27(8), 1937-1945, 1991.

Mazor, E., and Ronit Nativ, Hydraulic calculation of groundwater flow velocity and age: Examination of the basic premises, J. Hydrol., 138, 211-222, 1992.

McDonald, M.G., and A.W. Harbaugh, A modular three-dimensional finite-difference ground-water flow model, U.S. Geological Survey Techniques of Water-Resources Investigations, book 6, chapter A1, 1988.

Musgrove, M., and J.L. Banner, Regional ground-water mixing and the origin of saline fluids: Midcontinent, United States, Science, 259, 1877-1882, 1993.

Nauman, E. B., Residence time distributions in systems governed by the dispersion equation, Chemical Eng. Sci., 36, 957-966, 1981.

Nir, A., On the interpretation of tritium 'age' measurements of groundwater, J. Geophys. Res., 69(12), 2589-2595, 1964.

Nir, A., and S. Lewis, On tracer theory in geophysical systems in the steady and non-steady state, Part I, Tellus, 27(4), 372-383, 1975.

Plummer, L. N., R.L. Michel, E.M. Thurman, and P.D. Glynn,. Environmental tracers for age dating young ground water, in *Regional Ground-Water Quality* , edited by W. M. Alley, pp. 255-294, Van Nostrand Reinhold, New York, 1993.

Reilly, T. E., L.N. Plummer, P.J. Phillips, and E. Busenberg, The use of simulation and multiple environmental tracers to quantify flow in a shallow aquifer, Water Resour. Res., 30(2), 421-433, 1994.

Robinson, B. A., and J.W. Tester, Dispersed fluid flow in fractured reservoirs: An analysis of tracer-determined residence time distributions, J. Geophys. Res., 89(B12), 10374-10384, 1984.

Sandberg, M., What is ventilation efficiency?, Building and Environment, 16(2), 123-135, 1981.

Shapiro, A. M., and V.D. Cvetkovic, Stochastic analysis of solute arrival time in heterogeneous porous media, Water Resour. Res., 24(10), 1711-1718, 1988.

Simpkins, W. W., and K. R. Bradbury, Groundwater flow, velocity, and age in a thick, fine-grained till unit in southeastern Wisconsin, J. Hydrol., 132, 283-319, 1992.

Solomon, D. K., S.L. Schiff, R.J. Poreda, and W.B. Clarke, A validation of the 3H/3He method for determining groundwater recharge, Water Resour. Res., 29(9), 2951-2962, 1993.

Spalding, D. B., A note on mean residence-times in steady flows of arbitrary complexity, Chemical Eng. Sci., 9, 74-77, 1958.

Sudicky, E. A., and E.O. Frind, Carbon 14 dating of groundwater in confined aquifers: Implications of aquitard diffusion, Water Resour. Res., 17(4), 1060-1064, 1981.

Sudicky, E.A., and E.O. Frind, Contaminant transport in fractured porous media: Analytical solutions for a system of parallel fractures: Water Resources Research, 18, 1634-1642, 1982.

Torgersen, T., W.B. Clarke, and W.J. Jenkins, The tritium/helium-3 method in hydrology, in *Isotope Hydrology 1978*, pp. 917-930 , International Atomic Energy Agency, 1978.

Walker, G. R., and P.G. Cook, The importance of considering diffusion when using carbon-14 to estimate groundwater recharge to an unconfined aquifer, J. Hydrol., 128, 41-48, 1991.

Weeks, E. P., D.E. Earp, and G.M. Thompson, Use of atmospheric fluorocarbons F-11 and F-12 to determine the diffusion parameters of the unsaturated zone in the southern high plains of Texas, Water Resour. Res., 18(5), 1365-1378, 1982.

Wen, C. Y., and L.T. Fan, *Models for Flow Systems and Chemical Reactors*, Marcell Decker, New York, 1975.

Zimmerman, D.A., and Wilson, J.L., Description and user's manual for TUBA: A computer code for generating two-dimensional random fields via the turning bands method: unpublished report, Geosci. Dep., N.M. Inst. of Min. and Technol., Socorro, 1989.

Zuber, A., Mathematical models for the interpretation of environmental radioisotopes in groundwater systems, in *Handbook of Environmental Isotope Geochemistry*, edited by P. Fritz and J. Ch. Fontes, pp. 1-59, Elsevier, Amsterdam, 1986.

Chapter 3 Effects of Temperature Fluctuations on CFC-11 Transport from the Atmosphere to the Water Table

3.1 Introduction

Transport of atmospheric gases from the land surface to ground water beneath the water table is impacted by unsaturated-zone flow and transport processes. The effect of these processes on concentrations of dissolved gases in ground water may impact the use of these gases as environmental tracers for ground-water age dating and estimation of saturated-zone transport properties. Much attention has been focused on the behavior of chlorofluorocarbons (CFC's) and other gases in arid regions, where the unsaturated zone is relatively thick. However, less attention has been paid to processes affecting dissolved gas concentrations in humid regions, or in regions where the water table is close to the land surface.

Cook and Solomon (1995) used a simple one-dimensional transport model to characterize transport of CFC-11, -12, and -113, and Krypton-85 (^{85}Kr) from the land surface to the water table. When the water table is deep, concentrations of these gases in water at the water table lag behind atmospheric concentrations because of the time required for diffusion in the unsaturated zone (Table 3-1). Cook and Solomon (1995) also examined the impact of temperature, unsaturated-zone moisture content, sorption, and recharge rate on concentrations at the water table. Some of the simplifying assumptions used by Cook and Solomon (1995) include isothermal conditions (constant and uniform temperature) and uniform moisture content throughout the unsaturated zone, with a step change in moisture content at the water table.

In this Chapter, the work of Cook and Solomon (1995) is extended by including the effects of more realistic moisture-content distributions in the unsaturated zone, and by

simulating a seasonal temperature profile. Moisture content varies in the unsaturated zone as a function of both elevation above the water table and recharge rate. Furthermore, layers of fine-grained soil have different moisture retention properties than coarser-grained soil, so material heterogeneities can influence unsaturated-zone transport. Similarly, the seasonal temperature profile caused by the seasonal pattern in land surface temperatures, and the heat-transport properties of the porous media effect dissolved-gas transport. The simulations here include these additional factors, and focus on cases with shallow water-table depths, compared to those of Cook and Solomon (1995); these shallow water-table depths may be more characteristic of humid locations in the northeastern U.S., such as the Mirror Lake NH site. After describing the mathematical and numerical model used to simulate one-dimensional water flow and dissolved gas transport, the effect of depth-varying moisture content and nonisothermal conditions are examined for homogeneous and layered unsaturated zones.

Table 3-1. Simulated air-phase concentrations in 1992 of CFC's and Krypton-85 immediately above the water table (Cook and Solomon, 1995) [apparent lag time, in years, given in parentheses]

Water Table Depth (m)	CFC-11 (pptv)	CFC-12 (pptv)	CFC-113 (pptv)	^{85}Kr (dpm cm^{-3})
0	292	523	86	59
5	289 (0.4)	519 (0.3)	85 (0.3)	59 (0.1)
10	278 (1.5)	504 (1.0)	79 (1.4)	56 (0.6)
20	237 (5.6)	445 (3.9)	57 (4.4)	48 (2.2)
30	174 (12.4)	356 (8.6)	35 (8.2)	37 (4.6)
40	117 (17.2)	263 (14.1)	20 (12.7)	28 (7.3)

3.2 Governing Equations, Constitutive Relations, and Numerical Solution

3.2.1 Governing Equations and Boundary Conditions

In this section, the governing partial differential equations for flow and transport in the unsaturated zone are presented. The flow equation is a mixed form of the Richards' equation for one-dimensional vertical unsaturated water flow. Under steady water flow conditions, air flow is assumed to be zero. Although transport occurs in both the air and water phases, a single transport equation written in terms of only one concentration can be developed because of the equilibrium assumption for local equilibrium air/water partitioning.

Water Flow

Assuming that water is incompressible, a one-dimensional mass conservation equation for the water can be written:

$$\frac{\partial \theta}{\partial t} = -\frac{\partial q}{\partial z} \tag{3.1}$$

where θ [-] is the moisture content and q [LT^{-1}] is the water flux. It is assumed that the water density is unaffected by pressure, temperature, or solute concentration.

Substitution of Darcy's Law for water flow in porous media into the mass conservation equation (3.1), a mixed-form of Richards' equation can be written (Hillel, 1982):

$$\frac{\partial \theta}{\partial t} = \frac{\partial}{\partial z}\left[K(\theta)\left(\frac{\partial h}{\partial z} - 1\right)\right] \tag{3.2}$$

where $K(\theta)$ [LT^{-1}] is the unsaturated hydraulic conductivity; and h [L] is the pressure head. The coordinate system is oriented downward so that the gravitational gradient acts in the positive z direction. The constitutive relations between the moisture content and

the pressure head, and between moisture content and unsaturated hydraulic conductivity, are presented in Section 3.2.2. Cases presented here are limited to steady flow, in which case (3.2) becomes a nonlinear ordinary differential equation in the pressure head.

The flow equation boundary conditions are either specified flux or specified pressure head at the top and bottom of the domain. Specified pressure boundary conditions at the domain top and bottom are:

$$h = H_0 \text{ at } z = 0 \qquad h = H_L \text{ at } z = L \tag{3.3}$$

Alternatively, the fluxes can be specified:

$$K(\theta)\left(1 - \frac{\partial h}{\partial z}\right) = q_0 \text{ at } z = 0 \qquad K(\theta)\left(1 - \frac{\partial h}{\partial z}\right) = q_L \text{ at } z = L \tag{3.4}$$

Mixed boundary conditions can be used such that one boundary is specified pressure and the other is specified flux.

Transport

A one-dimensional transport equation considering advection and dispersion/diffusion in both air and water phases can be written (c.f. Cook and Solomon, 1995):

$$\frac{\partial(\theta c + \theta_a c_a)}{\partial t} = \frac{\partial}{\partial z} D \frac{\partial c}{\partial z} - \frac{\partial(qc)}{\partial z} + \frac{\partial}{\partial z} D_a \frac{\partial c_a}{\partial z} - \frac{\partial(q_a c_a)}{\partial z} \tag{3.5}$$

where c [ML^{-3}] is the volumetric concentration in the water phase; c_a [ML^{-3}] is the volumetric concentration in the air phase; θ_a [-] is the air content; q_a [LT^{-1}] is the volumetric air flux; D [L^2T^{-1}] is the water-phase dispersion coefficient; and D_a [L^2T^{-1}] is the air-phase dispersion coefficient. Assuming that partitioning between the air and water phases occurs quickly, relative to vertical transport processes, the air and water phase concentrations can be assumed to be in thermodynamic equilibrium, as expressed by Henry's Law:

$$c_a = \frac{c}{K_w} \tag{3.6}$$

where the Henry's Law coefficient, K_w [-], is generally a function of temperature, pressure and salinity (Warner and Weiss, 1985). The effects of pressure and salinity on K_w are ignored here, and the temperature dependence is described in Section 3.2.2. Substitution of (3.6) into (3.5) and rearrangement gives

$$\frac{\partial(\theta + \theta_a / K_w)c}{\partial t} = \frac{\partial}{\partial z}\left[D\frac{\partial c}{\partial z} + D_a \frac{\partial(c/K_w)}{\partial z}\right] - \frac{\partial qc}{\partial z} - \frac{\partial q_a\, c/K_w}{\partial z} \tag{3.7}$$

The governing transport equation is a linear partial differential equation in the water-phase concentration. However, coefficients in the equation may change in time and space due to water and air flow, and changing temperature. The transport equation could also be formulated in term of the air phase concentration (Cook and Solomon, 1995).

Terms appearing in the transport equation related to the divergence of air and water fluxes can be simplified, for example:

$$\begin{aligned} \frac{\partial \theta c}{\partial t} + \frac{\partial qc}{\partial z} &= c\left(\frac{\partial \theta}{\partial t} + \frac{\partial q}{\partial z}\right) + \theta\frac{\partial c}{\partial t} + q\frac{\partial c}{\partial z} \\ &= \theta\frac{\partial c}{\partial t} + q\frac{\partial c}{\partial z} \end{aligned} \tag{3.8}$$

because the parenthetical term is zero, from eq. (3.1). Using the same simplification for air-phase continuity, (3.3) can be written:

$$\theta\frac{\partial c}{\partial t} + \theta_a \frac{\partial(c/K_w)}{\partial t} = \frac{\partial}{\partial z}\left[D\frac{\partial c}{\partial z} + D_a \frac{\partial(c/K_w)}{\partial z}\right] - q\frac{\partial c}{\partial z} - q_a \frac{\partial(c/K_w)}{\partial z} \tag{3.9}$$

If the spatial and temporal gradients in the Henry's Law coefficient are zero, for example under isothermal conditions, or if the gradients are assumed to be essentially zero, then (3.10) can be written (c.f. Cook and Solomon, 1995):

$$(\theta + \theta_a / K_w)\frac{\partial c}{\partial t} = \frac{\partial}{\partial z}\left[(D + D_a / K_w)\frac{\partial c}{\partial z}\right] - (q + q_a / K_w)\frac{\partial c}{\partial z} \tag{3.10}$$

In the numerical model used here, the more general form (3.7) is used because cases are considered with nonisothermal conditions, hence spatially and temporally variable K_w. Also, the iterative solution of this mixed form numerically conserves mass (Celia et al., 1990).

The land-surface boundary condition used here is a specified concentration in the air phase, which corresponds to a specified water-phase concentration by the equilibrium assumption

$$c(t) = K_w C_a(t) \qquad z = 0 \tag{3.11}$$

where C_a is the atmospheric concentration. The bottom boundary condition is no-flow for the case of q=0, or natural outflow by advection alone if flow is occurring:

$$\frac{\partial c}{\partial z} = 0 \qquad z = L \tag{3.12}$$

Cook and Solomon (1995) solved this transport equation for several cases with different moisture content distributions, water fluxes, and uniform temperatures. In all cases, the moisture content was assumed to be uniform in the unsaturated zone down to the water table, and then to change abruptly at the water table to the porosity. A more realistic representation of the moisture content distribution is possible by solving the one-dimensional flow equation and using computed moisture contents and fluxes in the transport equation solution.

3.2.2 Constitutive Relations

Water Flow

The moisture retention curve describes the relation between pressure head and moisture content. The simple model of van Genuchten (1980) is chosen here to represent the moisture retention curve:

$$\theta = \theta_r + \frac{\theta_s - \theta_r}{\left[1 + \left(-\alpha_\theta h\right)^n\right]^{1-1/n}} \tag{3.13}$$

where θ_s [-] is the saturated moisture content; θ_r [-] is the residual moisture content; α_θ [L^{-1}] and n [-] are empirical coefficients. By volume conservation, the air content is the total porosity, ϕ [-], minus the moisture content: $\theta_a = \phi - \theta$.

Unsaturated hydraulic conductivity is generally a nonlinear function of moisture content. The Mualem (1976) - van Genuchten (1980) constitutive relation is chosen for unsaturated hydraulic conductivity:

$$k_{rw} \equiv \frac{K}{K_s} = \theta_e^{1/2}\left[1 - \left(1 - \theta_e^{1/m}\right)^m\right]^2 \tag{3.14}$$

where K_s [LT^{-1}] is the saturated hydraulic conductivity; k_{rw} [-] is the relative hydraulic conductivity, $m \equiv 1 - 1/n$; and θ_e [-] is the normalized moisture content:

$$\theta_e \equiv \frac{\theta - \theta_r}{\theta_s - \theta_r} \tag{3.15}$$

Two soils are considered here, a sandy loam and a silty loam. The parameters for the van Genuchten and Mualem constitutive models are listed in Table 3-2, and the corresponding moisture retention and relative hydraulic conductivity functions are shown in Figure 3-1.

Transport

The dispersion coefficients include the effects of molecular diffusion and macroscopic dispersion, caused by spatial variability in velocity, modeled as Fickian diffusion:

$$\begin{aligned} D &= \theta D_m + \alpha q \\ D_a &= \theta_a \tau D_g + \alpha_a q_a \end{aligned} \tag{3.16}$$

in which D_m [L^2T^{-1}] is the effective diffusion coefficient in the porous medium; α [L] is the porous media dispersivity for the water phase; τ [-] is the air-phase tortuosity; D_g

Table 3-2. Moisture retention and unsaturated hydraulic conductivity parameters for van Genuchten - Mualem model of a sandy loam and silty loam

Parameter	Sandy Loam	Silty Loam
θ_s, saturated moisture content	0.35	0.35
θ_r, residual moisture content	0.149	0.149
α_θ, van Genuchten coefficient	0.5 m^{-1}	0.5 m^{-1}
n, van Genuchten coefficient	7	2
K_s, saturated hydraulic conductivity	100 m/yr	1 m/yr

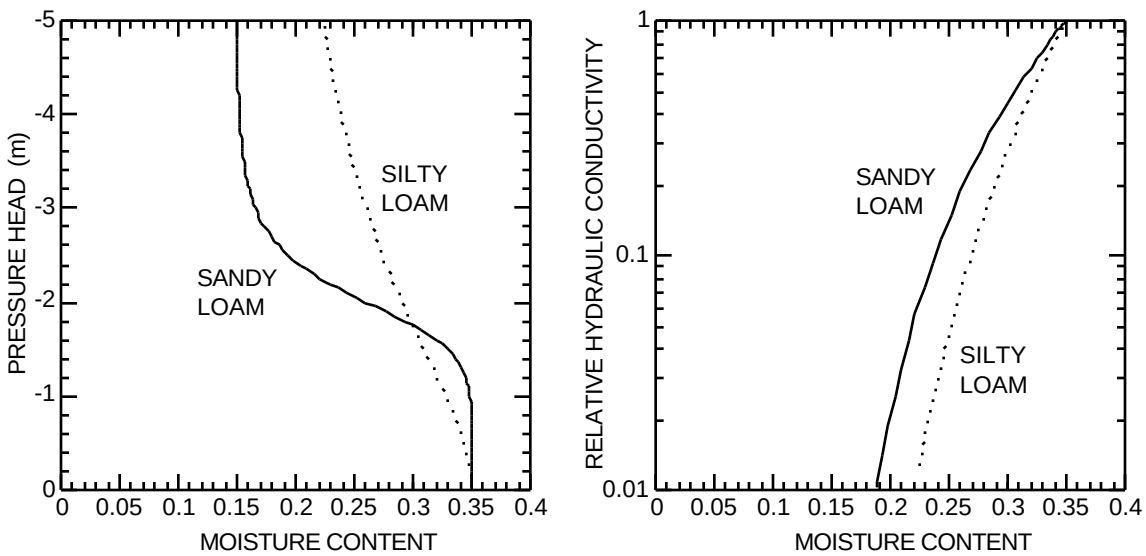

Figure 3-1 Moisture retention and relative unsaturated hydraulic conductivity for a sandy loam and a silty loam soil using Mualem - van Genuchten constitutive model.

$[L^2T^{-1}]$ is the free gas diffusion coefficient; and α_a [L] is the porous media dispersivity for the air phase. The effective water-phase diffusion coefficient includes the effects of tortuosity in the water phase. The air phase tortuosity is assumed to be a power law function of air content and total porosity (Millington, 1959):

$$\tau = \left(\frac{\theta_a}{\theta_a + \theta} \right)^2 \theta_a^{1/3} \tag{3.17}$$

Like many thermodynamic properties, the Henry's Law coefficient, that is the ratio of the concentration in water to the concentration in air, is a function of temperature (fig. 3-2). Cold water in equilibrium with air contains more CFC-11 than warm water. Warner and Weiss (1985) report the experimentally determined Henry's Law coefficient for CFC-11 as a function of temperature in degrees Kelvin (°K):

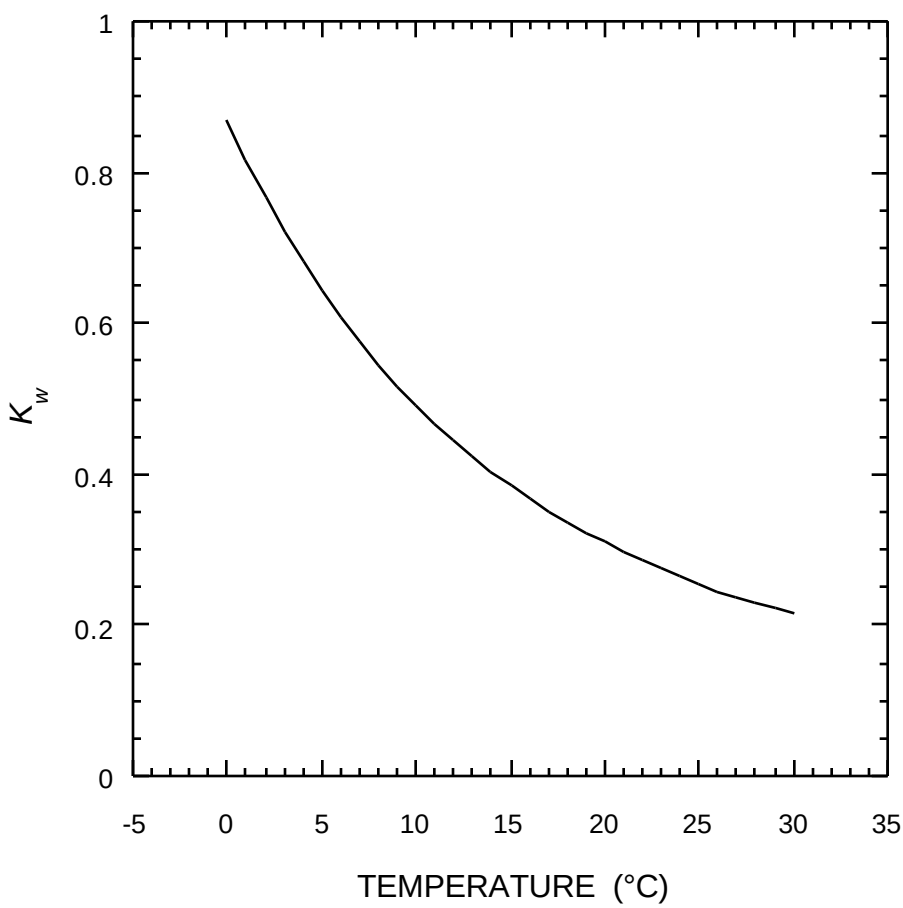

Figure 3-2 Henry's Law coefficient (K_w) for CFC-11; the ratio of the volumetric concentration in water having zero salinity to the volumetric concentration in air at sea level.

$$K_w = 0.0821\,°K \exp\left[a_1 + \frac{100\ a_2}{°K} + a_3 \ln\left(\frac{°K}{100} \right) \right] \tag{3.18}$$

where a_1, a_2, and a_3 are gas-specific coefficients (volumetric form of Warner and Weiss, 1985). The units of the Henry's Law coefficient here are dimensionless: the mass in water per unit volume of water divided by the mass in air per unit volume of air.

The Henry's Law coefficient for CFC-11 as a function of temperature (fig. 3-2) is given by (3.18) with a_1= -134.1536; a_2= 203.2156, and a_3= 56.2320 (Warner and Weiss, 1985). With these coefficients, the K_w value used by Cook and Solomon (1995) corresponds to an equilibration temperature of about 9.3 °C. Water in equilibrium with the atmosphere contains about 4 times more CFC-11 near freezing than it does at 30 °C. Warner and Weiss (1985) also present Henry's Law coefficients for CFC-12, and Bu and Warner (1995) present the CFC-113 coefficients.

3.2.2 Numerical Solution

The governing flow and transport equations are solved using standard finite-difference methods. The numerical model used here is a modified version of a flow and transport model developed by Michael A. Celia (personal communication, 1994; Celia and Binning, 1992). These modifications are primarily associated with incorporation of the air-phase transport terms into the transport equation solution. The numerical solution of the flow equation is based on the mixed form to guarantee numerical mass conservation (Celia et al., 1990). The flow equation solution is essentially that of Celia and others (1990) and is not described further here.

Approximation of the derivatives in the governing transport equation by centered differences in time and space on a uniformly-spaced finite-difference grid yields the numerical form for each node of the finite-difference grid:

$$
\begin{aligned}
&\frac{\left(\theta+\theta_a/K_w\right)_i^{n+1} c_i^{n+1}-\left(\theta+\theta_a/K_w\right)_i^{n} c_i^{n}}{\Delta t}= \\
&\frac{1}{2\Delta z}\left[D_{i+1/2}^{n+1}\frac{c_{i+1}^{n+1}-c_i^{n+1}}{\Delta z}+\left(D_a\right)_{i+1/2}^{n+1}\frac{c_{i+1}^{n+1}/\left(K_w\right)_{i+1}^{n+1}-c_i^{n+1}/\left(K_w\right)_i^{n+1}}{\Delta z}\right. \\
&\left.-D_{i-1/2}^{n+1}\frac{c_i^{n+1}-c_{i-1}^{n+1}}{\Delta z}-\left(D_a\right)_{i-1/2}^{n+1}\frac{c_i^{n+1}/\left(K_w\right)_i^{n+1}-c_{i-1}^{n+1}/\left(K_w\right)_{i-1}^{n+1}}{\Delta z}\right] \\
&+\frac{1}{2\Delta z}\left[D_{i+1/2}^{t}\frac{c_{i+1}^{n}-c_i^{n}}{\Delta z}+\left(D_a\right)_{i+1/2}^{n}\frac{c_{i+1}^{n}/\left(K_w\right)_{i+1}^{n}-c_i^{n}/\left(K_w\right)_i^{n}}{\Delta z}\right. \\
&\left.-D_{i-1/2}^{n+1}\frac{c_i^{n}-c_{i-1}^{n}}{\Delta z}-\left(D_a\right)_{i-1/2}^{n}\frac{c_i^{n}/\left(K_w\right)_i^{n}-c_{i-1}^{n}/\left(K_w\right)_{i-1}^{n}}{\Delta z}\right] \\
&-\frac{q_{i+1/2}^{n+1}\left(c_{i+1}^{n+1}+c_i^{n+1}\right)-q_{i-1/2}^{n+1}\left(c_{i-1}^{n+1}+c_i^{n+1}\right)}{4\Delta z}-\frac{q_{i+1/2}^{n}\left(c_{i+1}^{n}+c_i^{n}\right)-q_{i-1/2}^{n}\left(c_{i-1}^{n}+c_i^{n}\right)}{4\Delta z} \\
&-\frac{\left(q_a\right)_{i+1/2}^{n+1}\left[c_{i+1}^{n+1}/\left(K_w\right)_{i+1}^{n+1}+c_i^{n+1}/\left(K_w\right)_i^{n+1}\right]-\left(q_a\right)_{i-1/2}^{n+1}\left[c_{i-1}^{n+1}/\left(K_w\right)_{i-1}^{n+1}+c_i^{n+1}/\left(K_w\right)_i^{n+1}\right]}{4\Delta z} \\
&-\frac{\left(q_a\right)_{i+1/2}^{n}\left[c_{i+1}^{n}/\left(K_w\right)_{i+1}^{n}+c_i^{n}/\left(K_w\right)_i^{n}\right]-\left(q_a\right)_{i-1/2}^{n}\left[c_{i-1}^{n}/\left(K_w\right)_{i-1}^{n}+c_i^{n}/\left(K_w\right)_i^{n}\right]}{4\Delta z}
\end{aligned}
\tag{3.19}
$$

where i is the grid index, Δz is the uniform grid spacing, and $\Delta t = t^{n+1} - t^n$ is the time step. Identical equations for all nodes are assembled in a tri-diagonal matrix form, with appropriate modifications for flux or specified concentration boundary conditions at the top and bottom of the domain. The resulting matrix equation is solved directly at each time step using the Thomas algorithm for a tri-diagonal matrix equation. At each time step, the only unknowns are the water-phase concentrations at the new time level, $n+1$; all other terms are known from the previous time level or from the flow and temperature models.

3.2.3 Benchmark Simulation

A benchmark transport simulation is made to qualitatively compare the results of the modified transport model to those of Cook and Solomon (1995) for one of the cases they examined. General flow and transport parameters are in Table 3-3. Cook and

Solomon (1995) estimated the gas-phase diffusion coefficient for CFC-11 using the empirical equation of Slattery and Bird (1958). Using this same method for CFC-12 yielded an estimated value within 10 percent of the measured diffusion coefficient (Monfort and Pellegatta, 1991). The water table depth is 30 m and the moisture content of the unsaturated zone is uniformly 0.15. The bottom boundary condition, at z = 40 m, is no-flow for transport, and the top boundary condition is the specified CFC-11 concentration in the atmosphere. Cook and Solomon (1995) present profiles of CFC-11 concentration in the air phase above the 30 m deep water table for an isothermal case with K_w = 0.51.

Table 3-3. General flow and transport parameters used for CFC-11 transport simulations (after Cook and Solomon, 1995)

Parameter	Value
L, domain length	40 m
α, dispersivity in water phase	0.02 m
ϕ, total porosity	0.35
D_m, effective diffusion coefficient in water	0.03 m^2/yr
D_g, free gas diffusion coefficient	260 m^2/yr

Using parameter values identical or very similar to those of Cook and Solomon (1995), the profile of CFC-11 air-phase concentrations computed here (fig. 3-3) is essentially the same as their results (their fig. 2, p. 265). The CFC-11 concentration in the water has an identical shape but concentrations are reduced by the factor K_w = 0.51. Below the water table, only the water phase is present, and diffusion into the stagnant

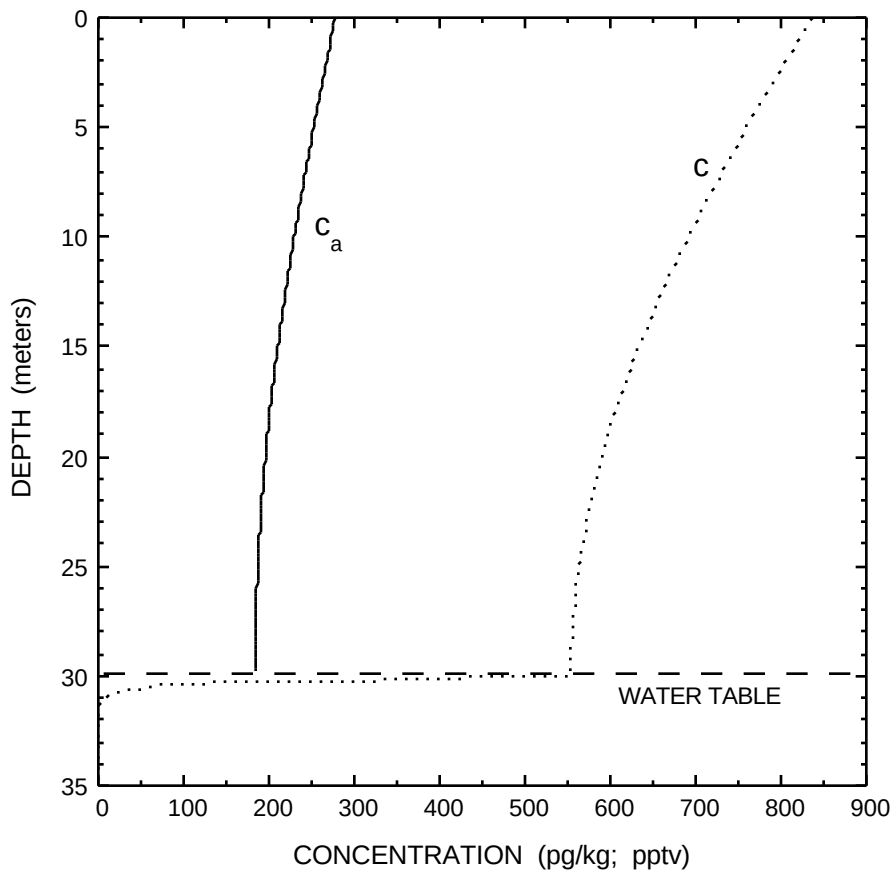

Figure 3-3 CFC-11 in water (c) and air (c_a) with depth, 1993, for unsaturated zone conditions of Cook and Solomon (1995, p. 265): uniform moisture and air content; isothermal; and water table at depth of 30 meters.

water is so slow that CFC-11 has diffused less than a meter below the water table. This result also reflects the very low atmospheric concentrations at the beginning of the simulation period in the 1940's.

3.3 Homogeneous Media

The simulations in this section are for the case of a homogeneous porous medium, as was considered by Cook and Solomon (1995) for their one-dimensional simulations.

3.3.1 Static Water

The impact of moisture retention above a water table on CFC-11 transport is examined for the case of a sandy loam (Table 3-2) and a water-table depth of 5 m. The porosity is assumed to be the same as the cases considered by Cook and Solomon (1995) to facilitate comparison with their results. The soil is near saturated for about 1 m above the water table because of the holding capacity of the fine-grained fraction of the soil. The associated reduction of air content significantly reduces the effective diffusion coefficient in the air phase (fig. 3-4), because the effective diffusion coefficient is the free coefficient times the product $\theta_a \tau$. These moisture-retention parameters are chosen to yield a relatively thick capillary fringe and a sharp reduction in moisture content above the capillary fringe.

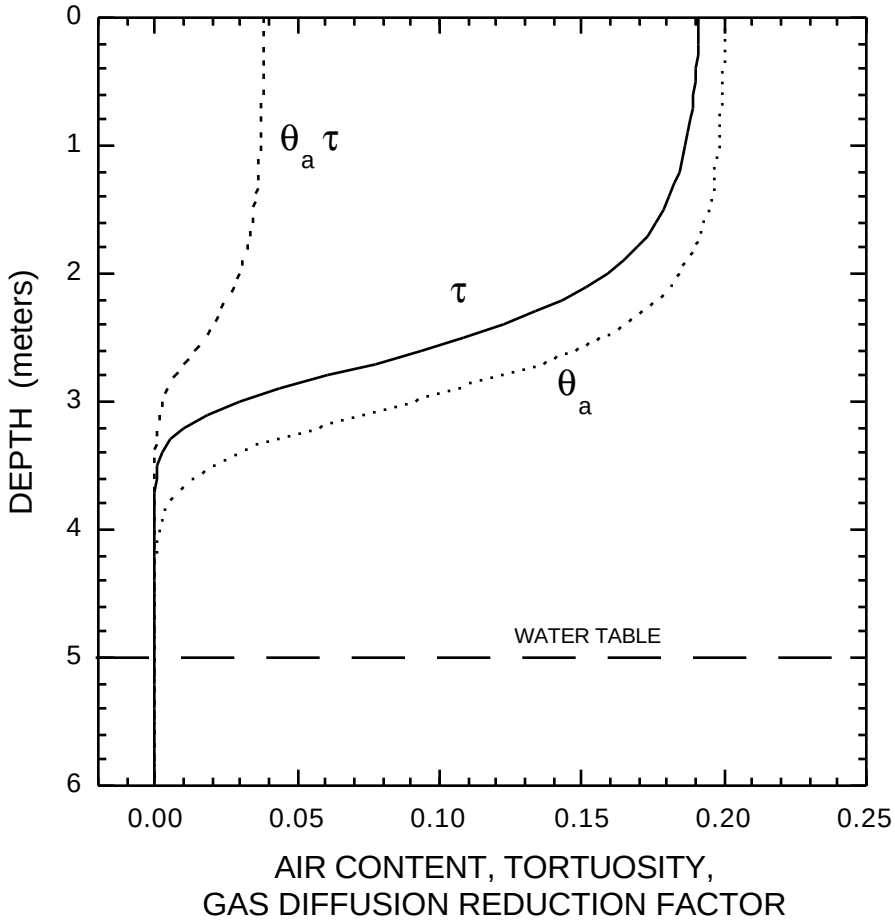

Figure 3-4 Air content (θ_a), tortuosity (τ), and their product versus depth for sandy loam moisture retention curve and water table depth at 5 meters.

The nonuniform moisture profile in the unsaturated zone reduces vertical transport (fig. 3-5). The primary effect is that downward gaseous diffusion stops at the capillary fringe, not at the water table. Without flow of water below the saturated zone, the concentrations at the water table are close to zero. The continuous variation of moisture content at the top of the capillary fringe results in more gradual changes in the CFC-11 profile, compared to the abrupt change in gradient for the case of Cook and Solomon (1995).

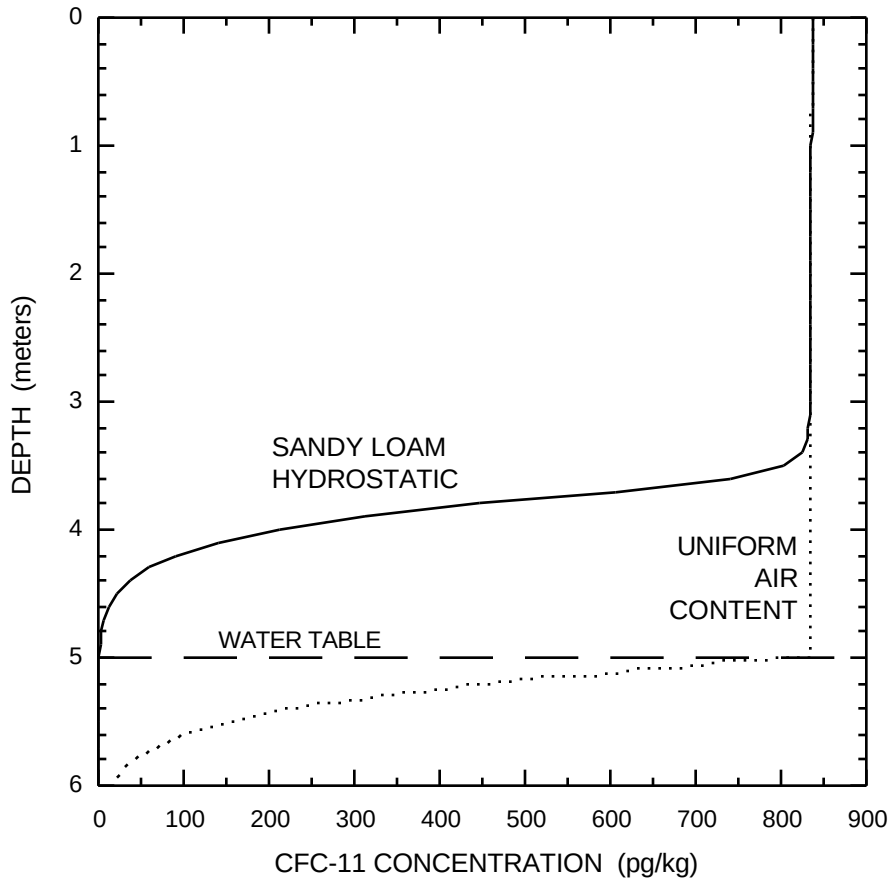

Figure 3-5 CFC-11 concentrations in 1993 versus depth for two no-flow cases having a water table at 5 meters depth: (a) uniform air content, and (b) sandy loam hydrostatic moisture retention curve.

3.3.2 Steady Water Flow

Cook and Solomon (1995) examine the impact of water flux rates on the unsaturated zone CFC-11 concentrations, but with a model having uniform moisture content in the unsaturated zone. A more realistic model of flow in the unsaturated zone leads to an even greater reduction in downward gaseous diffusion because the moisture contents are somewhat higher during downward flow.

Steady-state flow conditions are assumed with a downward water flux of $q = 0.3$ m/yr. Diffusion and dispersion in the saturated zone have little impact, because the

concentration gradients are small, hence advection is the dominant transport process for CFC-11 below the water table. The CFC-11 profile below the water table is essentially an image of the time history of CFC-11 concentrations in the atmosphere (fig. 3-6).

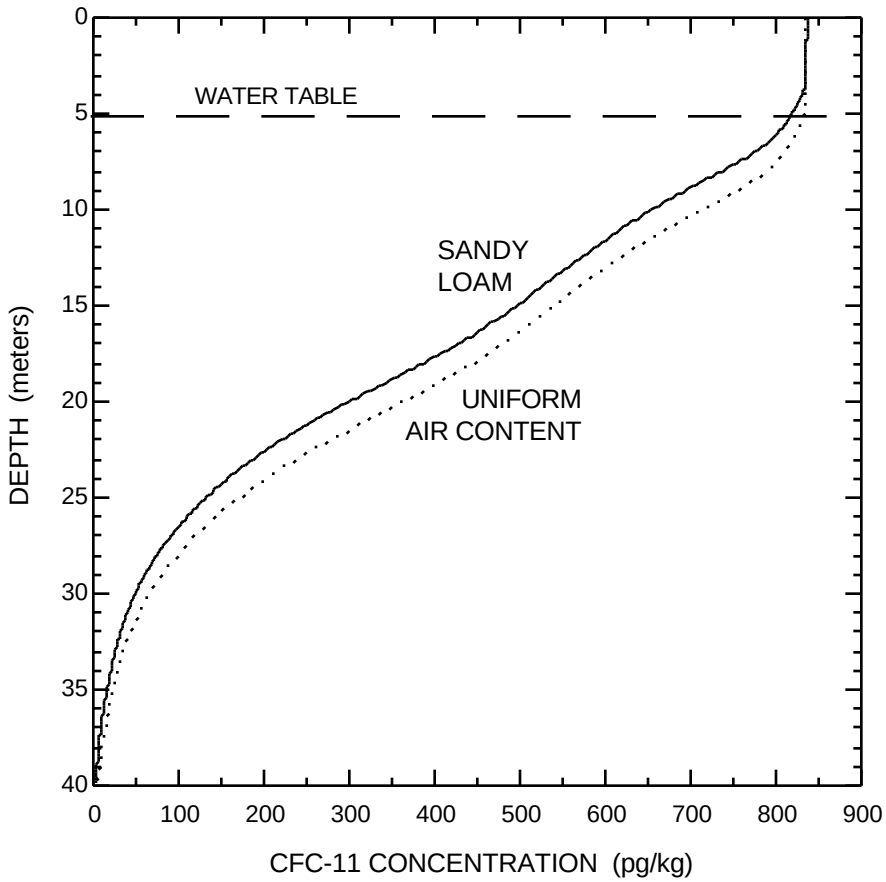

Figure 3-6 CFC-11 concentration versus depth with constant vertical flux of 0.3 m/yr and water-table depth of 5 m for cases (a) with uniform air content above the water table and (b) sandy loam moisture retention and hydraulic conductivity functions.

The increased moisture content above the water table for the sandy loam leads to a lag in the transport of CFC-11 into the saturated zone (fig. 3-6). This lag at the top of the saturated zone is propagated downward by the flowing water. The differences in CFC-11 concentrations at any location correspond to about 10 percent difference in apparent ages for the uniform moisture content and the sandy loam cases.

3.3.3 Seasonal Temperature Cycle

Because the Henry's Law coefficient for CFC-11 is a function of temperature, the transport of CFC-11 from the atmosphere to the water depends on temperature in the unsaturated zone. Cook and Solomon (1995) evaluated the effect of temperature on CFC-11 transport for isothermal cases with uniform temperature distribution. However, temperature is not uniform with depth in real soils, and near the land surface strong seasonal cycles occur due to the seasonal cycle in air temperature and solar radiation. In this section CFC-11 transport is examined under conditions of a seasonal temperature cycle.

Temperatures in the subsurface fluctuate seasonally near the land surface due to the annual cycle in air temperatures and solar radiation. A classic and simple model of the subsurface temperature profile is based on a sinusoidal annual temperature at the land surface and uniform heat conduction in the subsurface. Assuming that at infinite depth the subsurface remains at the mean annual temperature, and that the minimum surface temperature occurs on January 1 (t=0 yr), then the temperature as a function of depth and time of year can be written (Hillel, 1982)

$$T(z,t) = \bar{T} + A \sin\left[2\pi\left(t - 0.25\text{yr} - z/d\right)\right] \exp\left(-z/d\right) \tag{3.20}$$

where t is the time of year in years, $\bar{T}$ is the mean annual temperature, A is the amplitude of the land surface temperature cycle, and d [L] is the damping depth defined as

$$d \equiv \left(\frac{2D_h}{2\pi\ \text{yr}^{-1}}\right)^{1/2} \tag{3.21}$$

where D_h [L^2T^{-1}] is the uniform thermal diffusivity. The denominator in (3.21) is the frequency of the temperature cycle in radians per time, in this case for an annual cycle. For the simulations here, the thermal diffusivity is D_h = 27.2 m^2/yr, corresponding to a wet sand (Hillel, 1982), and the damping depth is d = 2.94 m. The mean annual temperature is taken as 9.2681 °C, and the temperature amplitude is equal to the mean annual temperature. Thus, the annual cycle in temperature at the land surface exhibits a

minimum of 0 °C on 1 January and a maximum of 18.54 °C on 1 July. Transport and storage of heat in the subsurface causes the temperature amplitude to drop off with depth, and causes the temperatures at depth to lag behind the surface forcing (fig. 3-7).

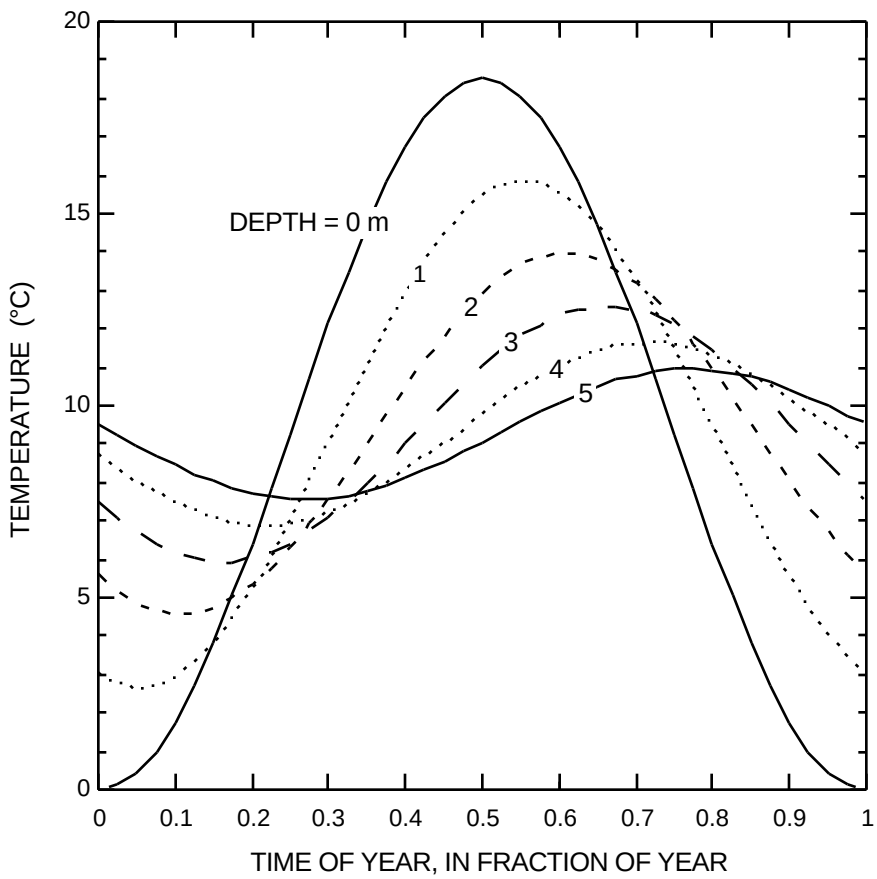

Figure 3-7 Annual temperature cycle for analytical model with sinusoidal surface temperature (mean and amplitude of 9.2681 °C) and uniform thermal diffusivity (D_h = 27.2 m^2/yr).

The amount of CFC-11 partitioned between the air and water phases changes as the temperature changes, hence the seasonal cycle in temperature within the unsaturated zone causes a seasonal cycle in the Henry's Law coefficient. Furthermore, the lag in temperature with depth yields a spatially variable K_w. For example, on 1 January the land surface temperature is at its minimum and K_w is at its maximum at this location (fig. 3-8).

At this time, temperatures beneath the land surface are decreasing from the higher temperatures of the summer period. As K_w changes in time, the partitioning between air and water is assumed to adjust instantly. As temperatures are dropping, CFC-11 moves from the air phase to the water phase, and vice versa. This re-partitioning can only occur where both phases are present.

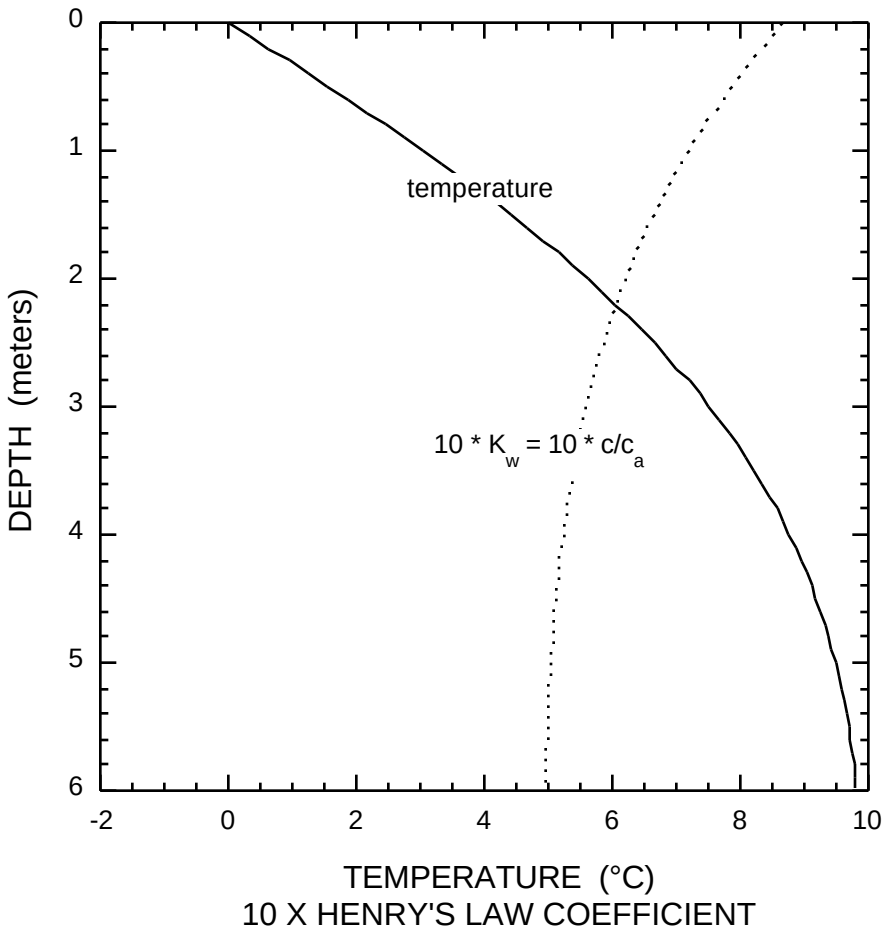

Figure 3-8 Temperature and Henry's Law coefficient versus depth on 1 January 1993 for nonisothermal conditions simulated by analytic model.

Above the capillary fringe, CFC-11 concentrations in water exhibit a strong seasonal cycle that corresponds to, but lags, the temperature cycle (fig. 3-9). At depths of 3 and 3.5 m, the water concentration mirrors the temperature cycle, with maximum

concentrations slightly lagged from minimum temperatures. This lag is due to the diffusion in the air phase within the unsaturated zone. For example, at 3.5 m, as the soil cools, CFC-11 is removed from the air phase and added to the water phase. This reduction in air-phase concentrations will lead to increased diffusion downward from the land surface, except that temperatures above this depth are even cooler. These cooler temperatures at shallower depths mean that CFC-11 air-phase concentrations are depleted, hence air-phase concentrations gradients cause upward diffusion. After the temperature minimum at 3.5 m, shallower depths are warmer hence have excess CFC-11 in the air phase which leads to increased air- and water-phase concentrations by air-phase

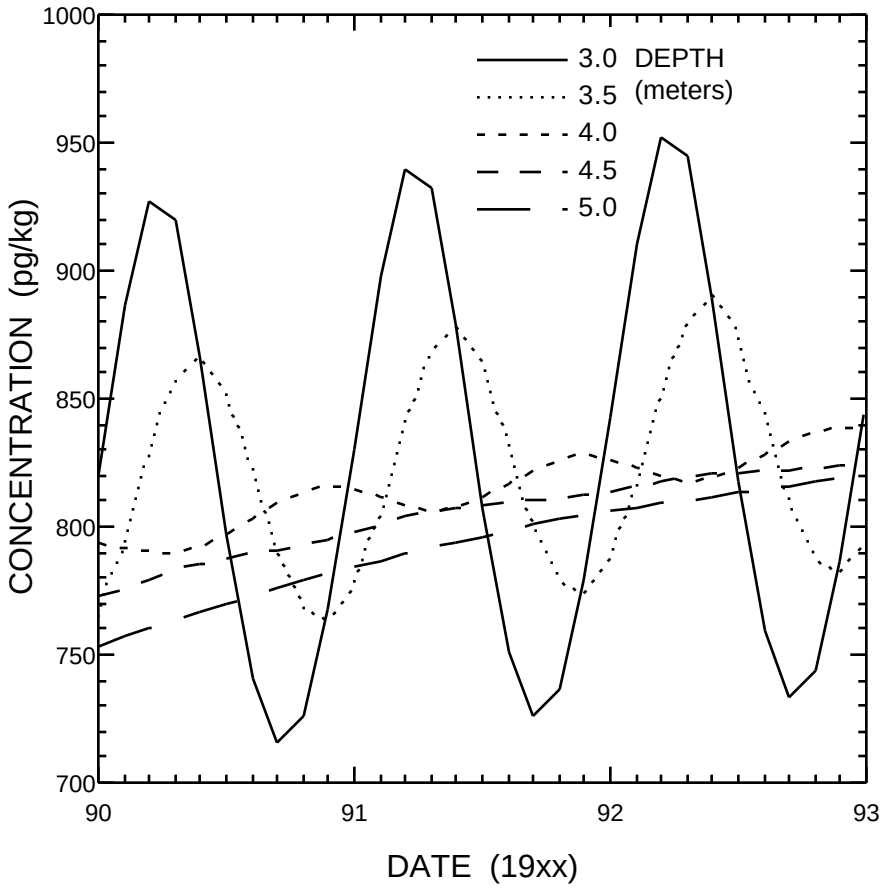

Figure 3-9 CFC-11 concentrations versus time from 1990 to 1993 for water table at depth of 5 m and steady water flux of 0.3 m/yr, under nonisothermal conditions.

diffusion downward. The direction of air-phase diffusion is changing throughout the year because the temperature cycles lead to large fluctuations in air-phase concentrations, relative to the gradual long-term atmospheric trend.

Within and below the capillary fringe, the volume of the air phase is small, hence water concentrations are not significantly affected by re-partitioning. Concentration cycles in this zone correspond to advective transport of water which carries the concentration cycle at the top of the capillary fringe down into the saturated zone. The approximately 0.5 yr lag in concentrations between 3.5 and 4 m depth is not the same as the temperature lag, but is close to the advective travel time between these depths, which is approximately 0.5 m / (q / θ) = 0.5 m / (0.3 m/yr / 0.35) = 0.58 yr.

The temporal cycle in CFC-11 concentrations in water is lagged compared to the temperature cycle above the capillary fringe, while below the capillary fringe the concentration cycle is approximately the cycle at the top of the capillary fringe advected downward by the flowing water. The break between these two different regimes is more specifically controlled by the magnitude of the effective diffusion coefficient, which is the sum of the air and water phase diffusion coefficients, weighted by the air and moisture contents (fig. 3-10). Where this term is large, the concentration cycle is controlled by temperature fluctuations, re-partitioning, and air phase diffusion. Where the effective diffusion coefficient is small, the concentration cycle is controlled by advection in the water and further dampening by water phase diffusion and dispersion.

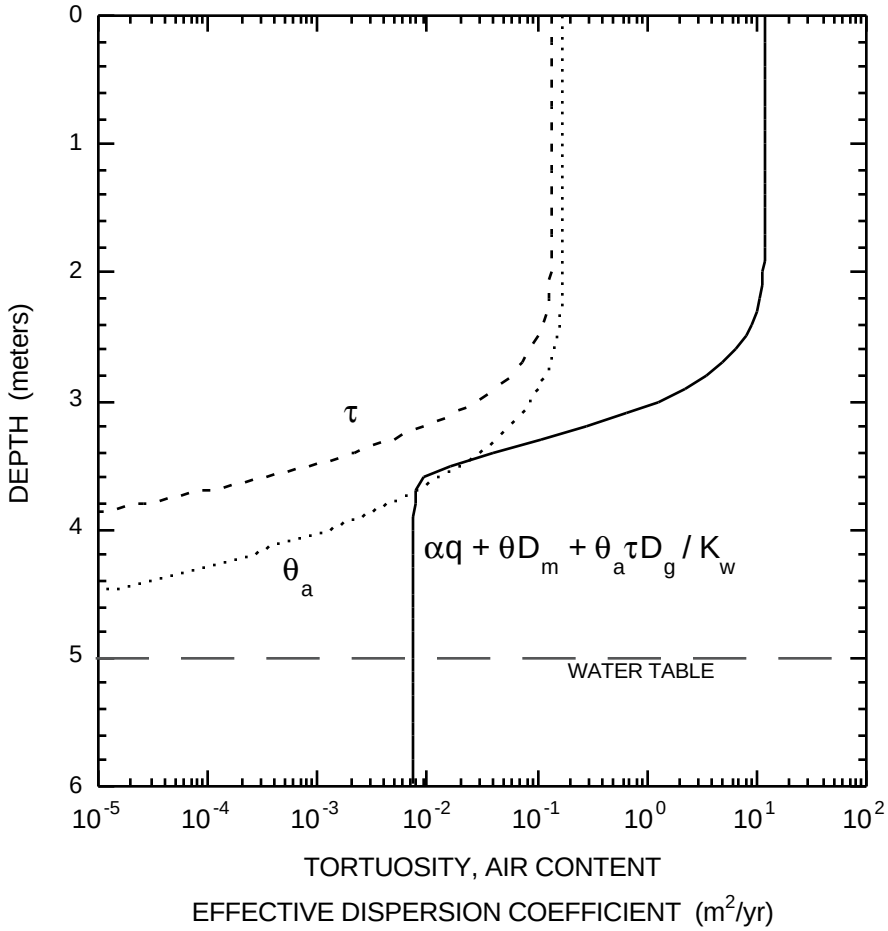

Figure 3-10 Air content, moisture content, and effective dispersion coefficient versus depth for sandy loam with water table at depth of 5 m and steady flow of 0.3 m/yr.

Although the water- and air-phase concentrations of CFC-11 fluctuate under nonisothermal conditions, the resulting saturated-zone concentrations are essentially unaffected by these fluctuations (fig. 3-11). Air-phase diffusion is the dominant transport mechanism from the land surface to the top of the capillary fringe, and temperature fluctuations are not large at that depth.

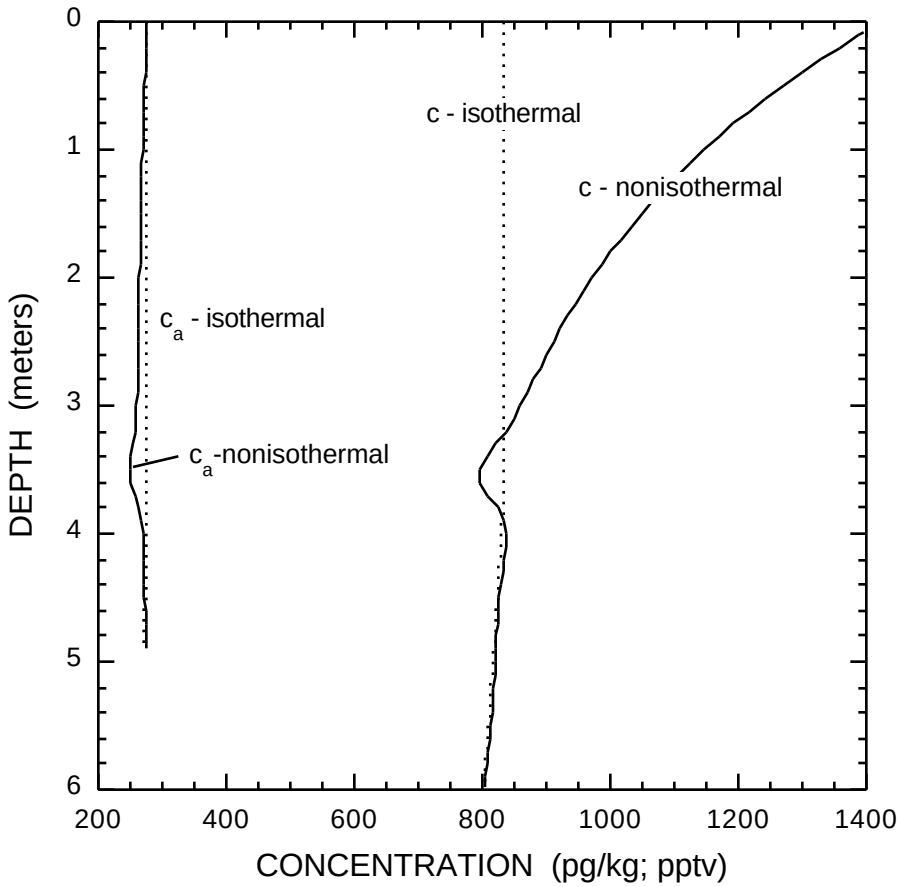

Figure 3-11 CFC-11 concentration versus depth on 1 January 1993 for water table at depth of 5 m and steady water flux of 0.3 m/yr. Results for isothermal and nonisothermal conditions are shown.

If the water table is at a depth of 1 m, instead of 5 m, then the saturated-zone concentrations are impacted significantly by nonisothermal conditions. For the same water flux rate, 0.3 m/yr, but with a water table depth of 1 m, the saturated-zone concentrations are about 10 percent higher under nonisothermal conditions (fig. 3-12).

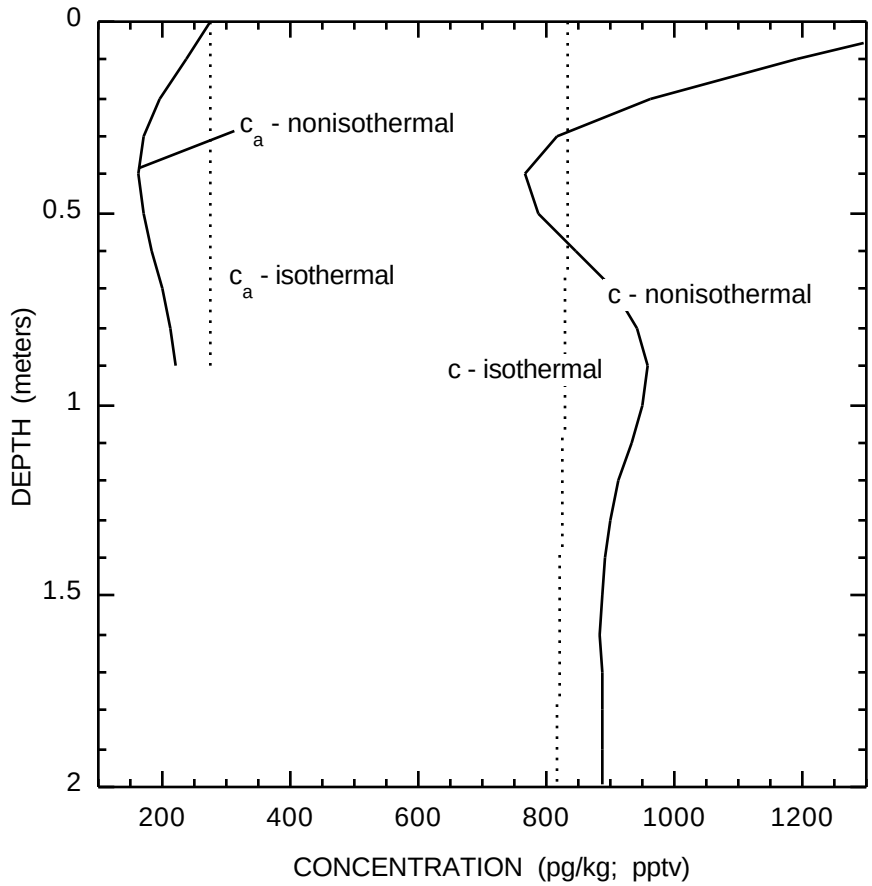

Figure 3-12 CFC-11 concentration versus depth on 1 January 1993 for water table at depth of 1 m and steady water flux of 0.3 m/yr. Results for isothermal and nonisothermal conditions are shown.

The fluctuations of water-phase concentrations within the unsaturated zone in the case of a water-table depth of 1 m do not correspond to the temperature fluctuations (fig. 3-13). Rather, the water-phase concentration at the land surface fluctuates according to the land-surface temperature, and that fluctuation is advected down by the flow of water, with subsequent dampening by dispersion. The capillary fringe extends to the land surface in this case, and air-phase transport is negligible.

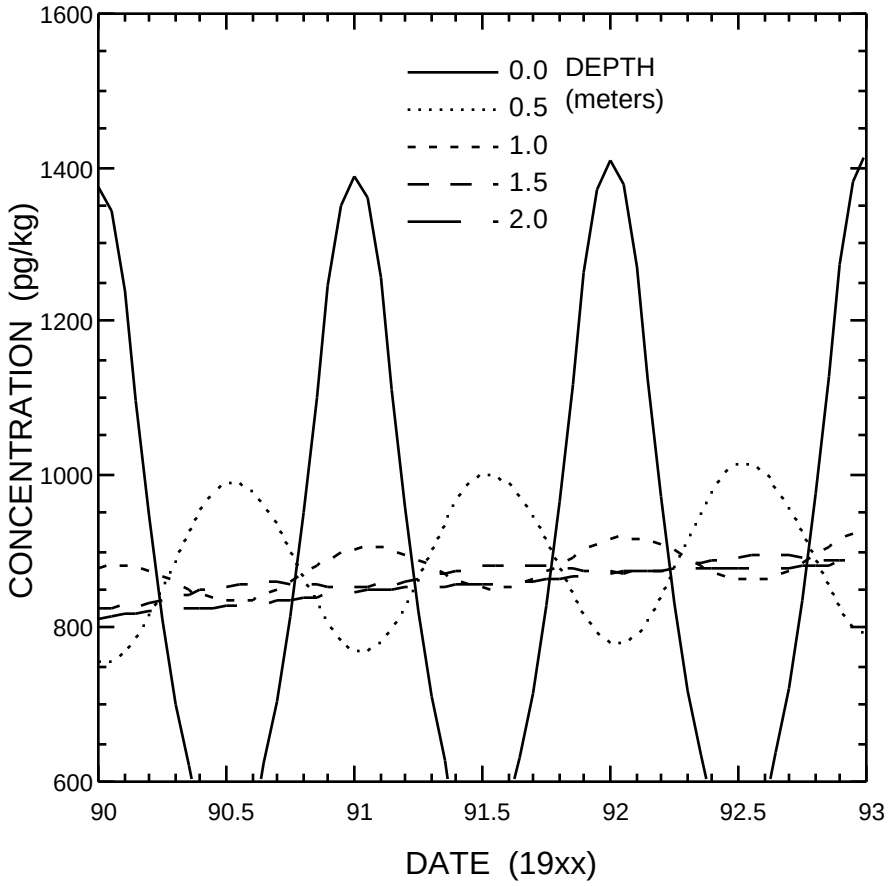

Figure 3-13 CFC-11 concentrations versus time from 1990 to 1993 for water table at depth of 1 m and steady water flux of 0.3 m/yr, under nonisothermal conditions.

3.4 Layered Soil

Natural porous media are not homogeneous, and inhomogeneities can have significant effects on flow and transport. Simulations for conditions analogous to those examined in previous sections are re-run with a simple layered porous medium to examine some of these effects. The majority of the porous-media system is the sandy loam of the previous section. A silty-loam layer occurs in the soil column between 1 and 2 m below the land surface. As described in the previous section on constitutive relations, this silt loam has a lower saturated hydraulic conductivity than the sandy loam, and retains more moisture at higher negative pressures.

3.4.1 Static Water

Under static-water conditions, the pressure and moisture-content distribution is independent of hydraulic conductivity. Inclusion of the silty layer in the column has no effect on pressure in this case, but leads to higher moisture contents within the layer compared to the homogeneous sandy loam case. This is because of the moisture-retention characteristics of the silty loam; it holds more water at an equivalent pressure. However, the moisture content is not close enough to saturation to significantly impact air-phase diffusion. Hence, the water-phase concentrations of CFC-11 are essentially the same as the homogeneous case (fig. 3-14).

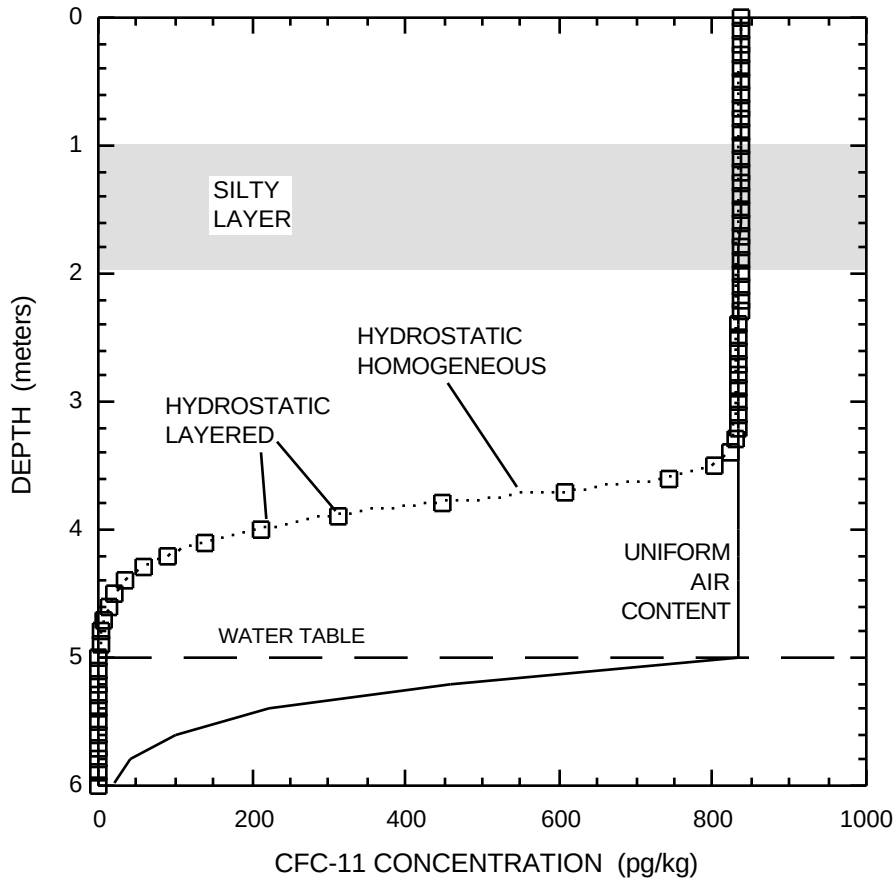

Figure 3-14 CFC-11 concentrations versus depth for case having water table at 5 m depth and no flow for cases (dashed) uniform moisture content, (solid) homogeneous sand loam, and(symbols) layered sand with a silt layer between 1 and 2 m depth.

3.4.2 Steady Water Flow and Seasonal Temperature Cycle

The silt layer has more effect on transport during steady flow because the hydraulic conductivity of the silt layer impedes flow and increases moisture contents in the unsaturated zone above the water table (fig. 3-15). CFC-11 concentrations at the water table (5 m) are lower for both isothermal and nonisothermal conditions, when compared to the results for the same conditions with a homogeneous porous medium (fig 3-11). For the previous simulation of a water table at 5 m depth in a homogeneous column, the impact of nonisothermal conditions on the concentrations at the water-table

are insignificant. However, nonisothermal conditions cause a noticeable increase in concentrations at the water-table in the layered case.

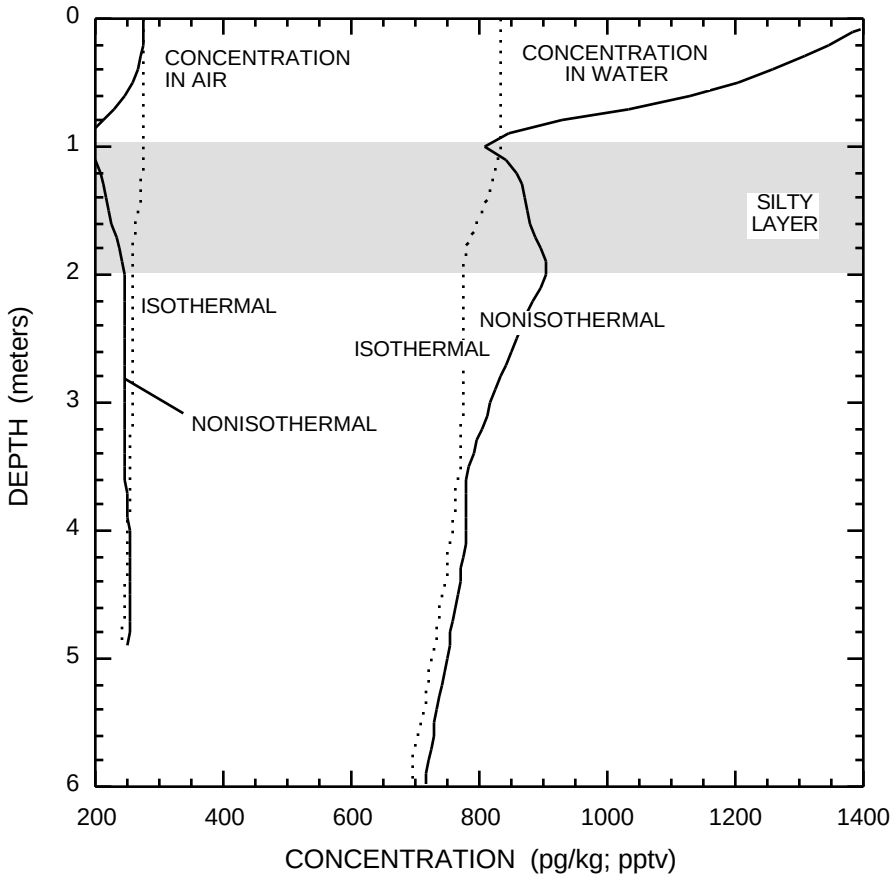

Figure 3-15 CFC-11 concentrations versus depth for case having water table at depth of 5 m, steady flow of 0.3 m/yr, and silt layer between 1 and 2 m depth for cases (dashed) isothermal, and (solid) nonisothermal conditions.

The specified flow rate of 0.3 m/yr is close to the saturated hydraulic conductivity of the silt material (1.0 m/yr). Hence saturations must be high in this layer and pressures must be close to zero at the top of the silt layer. Pressures will be close to zero in the sand layer as well because pressure is continuous. At the particular pressures simulated, the sand is more saturated than the silt at the top of the silt layer (see fig. 3-1), and hence the air phase content is lower, the tortuosity is lower, and the overall effective dispersion

coefficient is lower (fig 3-16). This high moisture content limits air-phase diffusion and results in lower water-table concentrations.

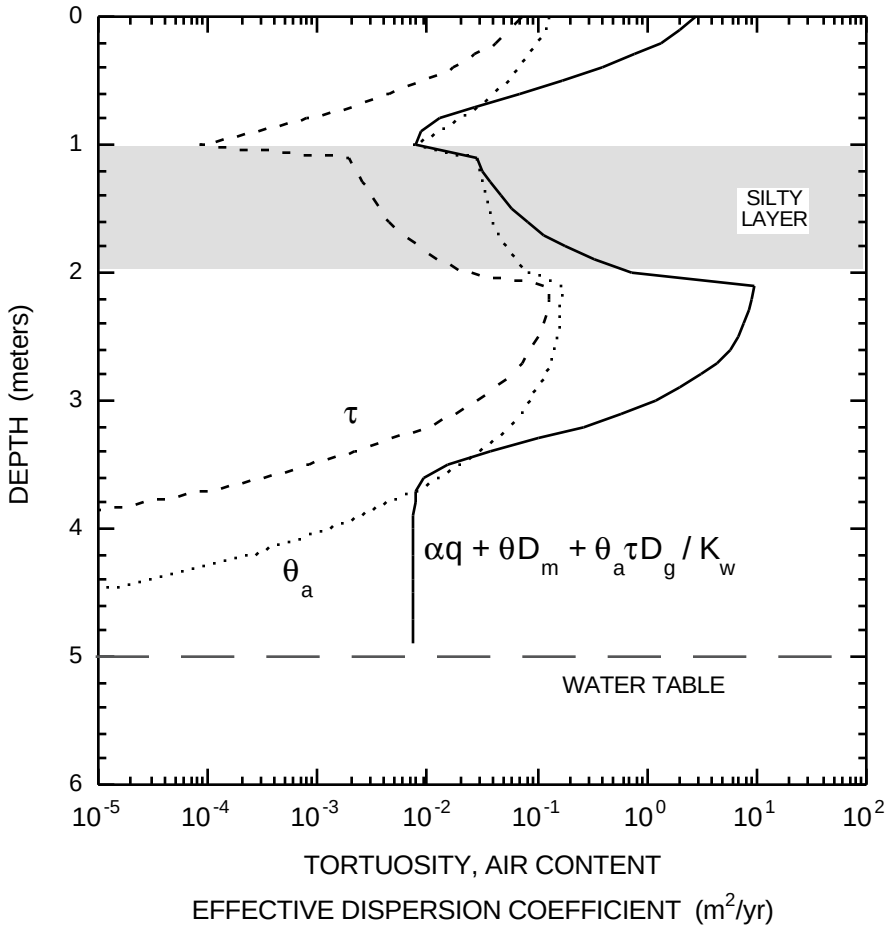

Figure 3-16 Air content, moisture content, and effective dispersion coefficient versus depth for layered case with water table at depth of 5 m and steady flow of 0.3 m/yr.

Nonisothermal conditions lead to noticeably higher water-table concentrations for this layered case compared to the isothermal conditions. This result is in contrast to the corresponding homogeneous case, in which temperature fluctuations had little impact on water-table concentrations for the 5 m deep water table (fig. 3-11). In the layered case, the high moisture content at the top of the silt layer isolates the air at greater depths from the near-surface air. Transport from this point downward is essentially controlled by the

water-phase concentration, and not the air-phase concentration, because diffusion in the air phase is so small. Of course, the water-phase concentration at this depth varies seasonally with temperature because the temperature is fluctuating at this depth.

3.5 Henry's Law Coefficient for Recharge

To determine a date of isolation from the atmosphere from CFC concentrations in a ground-water sample, the equilibration temperature between the sampled water and the atmosphere must be known. Equilibration temperatures are typically estimated from actual air temperature, taking the annual average, or from concentrations of other dissolved gases in the sample, such as nitrogen and argon (see Chapter 4).

The extent to which water-table concentrations are affected by fluctuating temperature is determined not by the extent of temperature fluctuations at the water table, but the extent of temperature fluctuations at the shallowest depth where air-phase diffusion is negligible; that is where the moisture content is near saturation. The air phase below this point is essentially isolated from the atmosphere, and deeper migration is controlled by the water-phase concentration there, because the air phase is essentially absent. If the temperature is fluctuating at this depth, then the water-phase concentration fluctuates as well because of equilibrium exchange with the overlying air column.

In the homogeneous column case, fluctuating temperature had no impact on water-table concentrations for a 5 m-deep water table. Air-phase diffusion is high down to the top of the capillary fringe (at about 4 m), and temperature fluctuations there are small, ranging from about 7 to 11.5 °C (fig 3-17). The average Henry's Law coefficient, 0.513, is very close to the Henry's Law coefficient at the average temperature, 0.510; a difference of about 0.6 percent.

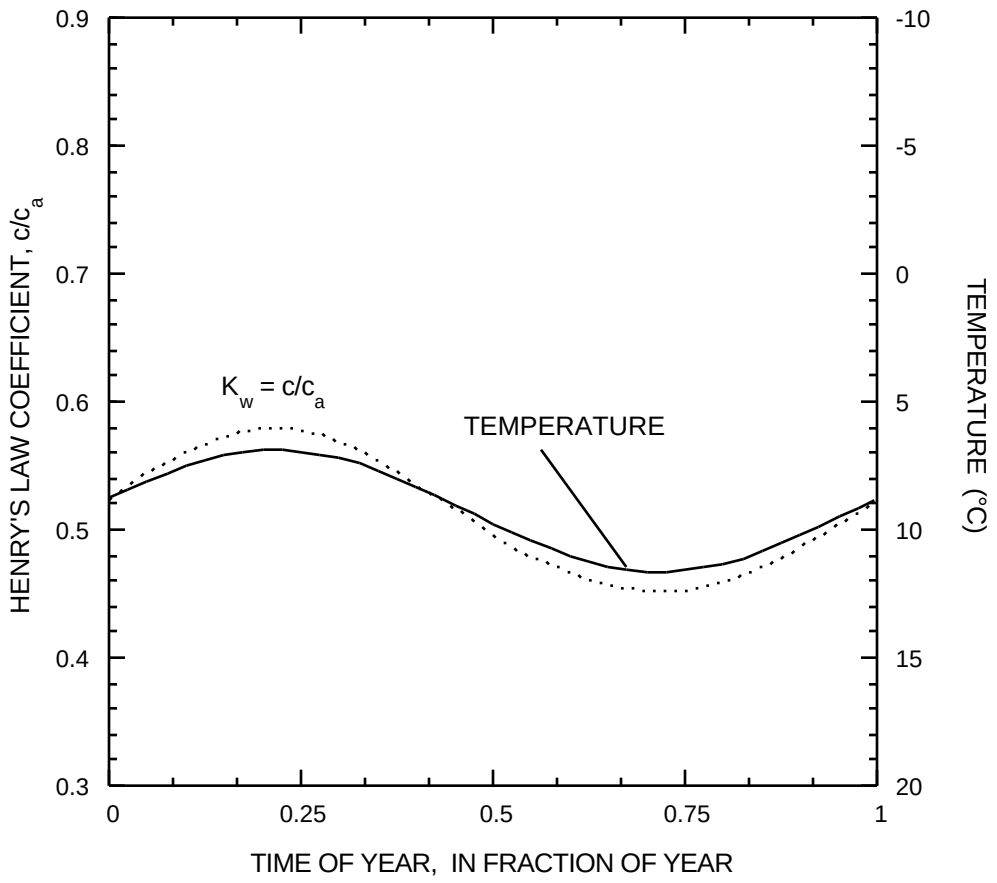

Figure 3-17 Annual cycle in temperature and Henry's Law coefficient at 4 m depth.

If the water table is close to the land surface, then temperature fluctuations at the top of the capillary fringe will be large. In this case, the average Henry's Law coefficient at that point will be higher than the Henry's Law coefficient at the average temperature. This is illustrated here by the case of the homogeneous column with the water table at a depth of only 1 m. In this case, for the sand-loam soil, the column is essentially saturated all the way to the land surface. The average Henry's Law coefficient, 0.554, is over 8 percent higher than the Henry's Law coefficient at the average temperature, 0.510 (fig. 3-18).

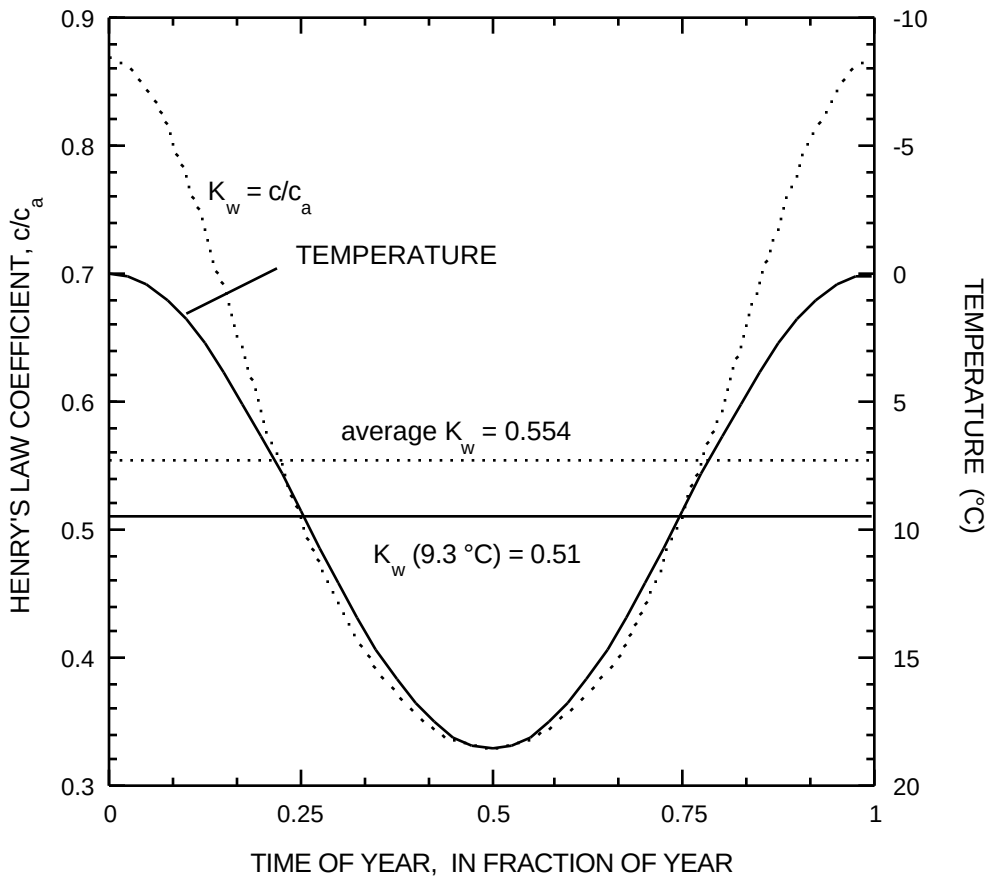

Figure 3-18 Annual cycle in temperature and Henry's Law coefficient at land surface.

The average Henry's Law coefficient at the highest nearly-saturated depth will be higher than the Henry's Law coefficient at the average temperature, because of the shape of the K_w(°C) function. The magnitude of this difference depends on the temperature range experienced at that location. The best method to estimate this quantity would be to measure the temperature monthly or more frequently, compute the corresponding Henry's Law coefficients, and take the annual average K_w.

The same nonlinear effect shown here for CFC-11 will also impact CFC-12 and CFC-113 concentrations to about the same extent. The temperature dependence of the Henry's Law coefficients from CFC-113 and CFC-12 have essentially the same relative shape as the CFC-11 function (fig. 3-19), hence will be affected in much the same way.

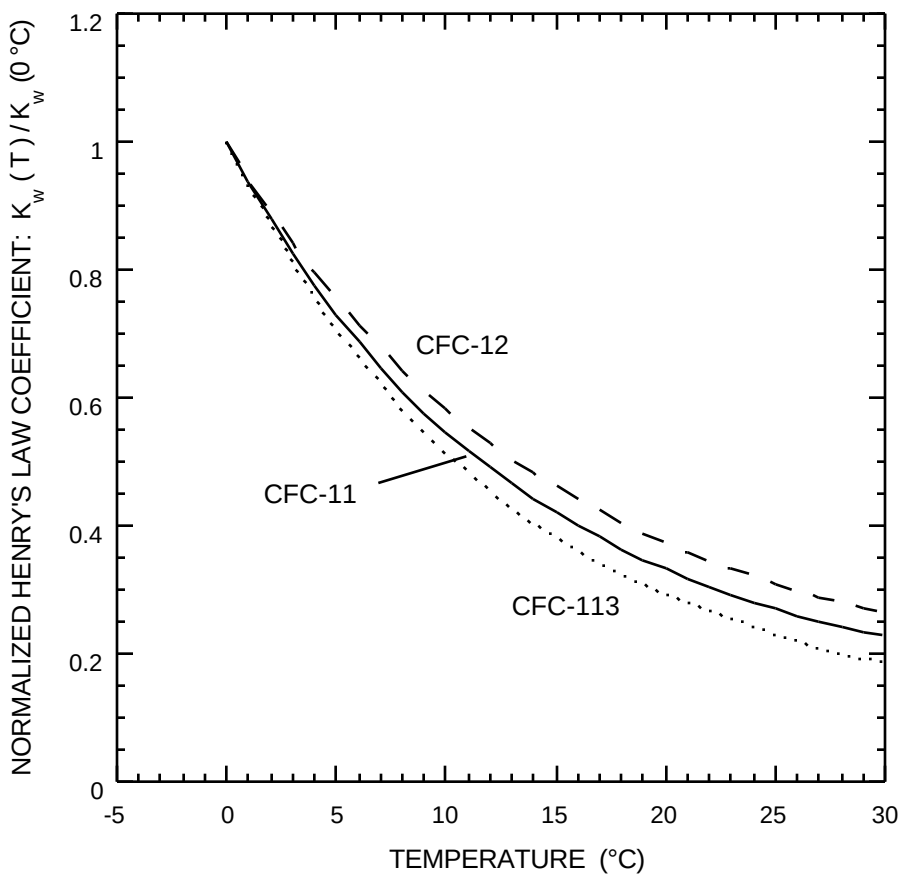

Figure 3-19 Henry's Law coefficients for CFC-11, CFC-12, and CFC-113, normalized by their respective values at T = 0 °C, as a function of temperature.

The saturations of most gases in water are nonlinear functions of temperature. Hence, this effect should also be observed to some extent in noble gas concentrations. The standard methods for estimating recharge temperature from these gas concentrations assume isothermal conditions, which may be expected to yield erroneous results for cases where isolation from the atmosphere occurs at shallow depth. If the Henry's Law coefficient is only weakly dependent on temperature, or the temperature range is small, then these effects can be safely ignored.

3.6 Summary

Transport of CFC-11 (and other gases) from the land surface to the saturated zone is characterized by rapid air-phase diffusion in the unsaturated zone down to a depth where the moisture content is nearly saturated. Below this point, transport is dominated by advection in flowing water, with minor diffusion and dispersion. Horizontal flow, which is not considered here, dominates solute advection in the saturated zone in many cases. CFC-11 concentrations at the water table will generally reflect a lag from atmospheric levels due to air-phase diffusion and advection through the capillary fringe. The former is small in cases with shallow water tables and increases with water-table depth, while the latter depends primarily on the moisture retention function and the recharge rate, and is independent of water-table depth.

At some distance above the water table, moisture contents are sufficiently high that air-phase diffusion no longer dominates vertical transport. Usually this would be at the top of the capillary fringe. However, in layered or inhomogeneous media, zones may exist well above both the water table and the capillary fringe where moisture contents are near saturation.

Temperature fluctuations will have an impact on CFC-11 transport to the water table only if temperature fluctuations are large (> 5 °C) at the shallowest point where air diffusion is negligible. In these cases, CFC-11 concentrations at the water table will be higher than those corresponding to isothermal conditions. This increase is due to the nonlinear relation between the Henry's Law coefficient and temperature. For the cases considered here, CFC-11 concentrations at the water table increased at most by about 10 percent for nonisothermal cases, compared to isothermal cases at the same average temperature.

CFC-11 concentrations within the unsaturated zone fluctuate throughout the year at depths where the temperature fluctuates. Hence, diffusion gradients can change

direction during the course of a year. Fluctuations in concentration at the top of the (nearly) saturated zone are propagated downward by the flowing water, and water-phase dispersion will dampen the fluctuations as advection progresses. These fluctuations in the unsaturated zone can cause air-phase concentrations to fluctuate around atmospheric levels by several 10's of percent.

Ideally, average Henry's Law coefficients can be computed from measured temperatures if fluctuating temperatures are significant at the top of the capillary fringe. The difference between the average Henry's Law coefficient and the Henry's Law coefficient at the average temperature is small if the temperature range is small. The relative temperature dependence of Henry's Law coefficients for CFC-12 and CFC-113 are similar to that of CFC-11, hence similar results would be expected for those gases. Fluctuating temperatures will have similar impacts on water-phase concentrations of other gases that have a nonlinear functional dependence on temperature, and the impact will depend on the sensitivity of the Henry's Law coefficient to the temperature.

The impact of fluctuating temperatures on CFC-11 concentrations in ground water is likely to be small in most cases. However, differences in computed atmospheric concentrations translate directly into age-estimation errors. In extreme cases, age-dating errors of 10 percent, or about 5 years, would be expected for cases having 20 °C temperature fluctuations at the top of the capillary fringe.

3.7 References

Bu, W., and M.J. Warner, 1995, Solubility of chlorofluorocarbon 113 in water and seawater, Deep Sea Research, v. 42, no. 7, p. 11512-1161.

Celia, M.A., and Binning, Philip, 1992, A mass conservative numerical solution for two-phase flow in porous media with application to unsaturated flow: Water Resources Research, v. 28, no. 10, p. 2819-2828.

Celia, M.A., Bouloutas, E.T., and Zarba, R.L., 1990, A general mass-conservative numerical solution for the unsaturated flow equation: Water Resources Research, v. 26, no. 7, p. 1483-1496.

Cook, P.G., and D.K. Solomon, 1995, Transport of atmospheric trace gases to the water table: Implications for groundwater dating with chlorofluorocarbons and krypton 85, Water Resources Research, v. 31, no. 2, p. 263-270.

Hillel, Daniel, 1982, *Introduction to Soil Physics*: Academic Press, Orlando, Fla., 364 p.

Millington, R.J., 1959, Gas diffusion in porous media, Science, v. 130, p. 100-102.

Montfort, J.-P., and Pellegatta, J.-L., 1991, Diffusion coefficients of the halocarbons CCl2F2 and C2Cl2F4 with simple gases: Journal Chemical Engineering Data, v. 36, p. 135-137.

Mualem, Y., 1976, A new model for predicting the hydraulic conductivity of unsaturated porous media: Water Resources Research, v. 12, no. 3, p. 513-522.

Slattery, J.C., and Bird, R.B., 1958, Calculation of the diffusion coefficient of dilute gases and of the self-diffusion coefficient of dense gases: American Institute Chemical Engineers Journal, v. 42, p. 137-142.

van Genuchten, M.Th., 1980, A closed-form equation for predicting the hydraulic conductivity of unsaturated soils: Soil Science Society of America Journal, v. 44, p. 892-898.

Warner, M.J., and R.F. Weiss, 1985, Solubilities of chlorofluorocarbons 11 and 12 in water and seawater, Deep-Sea Research, v. 32, p. 1485-1497.

Chapter 4 Field Study of CFC Concentrations at the Water Table at the Mirror Lake Site, New Hampshire

4.1 Introduction

4.1.1 CFC's as Environmental Tracers

Chlorofluorocarbons (CFC's; also called Freon, chlorofluoromethane) have emerged as useful age-dating tracers for young ground water (Thompson et al., 1974; Thompson and Hayes, 1979; Plummer et al., 1993). For atmospheric tracers, the age of ground water is defined as the time since the water was in contact with the atmosphere. Conceptually, recharge to the saturated zone is in chemical equilibrium with the atmosphere at the water table, and below in the saturated zone that concentration is maintained. Hence, if the atmospheric concentration changes in time, then different concentrations in ground water presumably correspond to different recharge times, and different ages. Knowledge of the atmospheric source term allows calibration of flow and transport models, yielding estimates of hydraulic and transport properties (e.g. Reilly et al., 1994; Szabo et al., 1996). These methods are most useful where the flow system under investigation is too large or responds too slowly to test through traditional field tracer experiments.

CFC's are useful ground-water tracers because the atmospheric source term is relatively well known and is almost linear in time, and because the CFC concentration of fresh water in equilibrium with the atmosphere is well described as a function of temperature alone (Warner and Weiss, 1985; Bu and Warner, 1995). CFC-12, CFC-11, and CFC-113 are man-made volatile organic compounds widely used as refrigerants and

occurring in many manufactured goods. The atmospheric concentration of CFC's has been increasing since their creation in the 1940's (fig. 4-1). Atmospheric concentrations have been measured for approximately 30 years and concentrations before 1960 are estimated from manufacturing records. Recently, concentrations of CFC's have leveled off and in the case of CFC-11 and CFC-113 have begun to decrease somewhat due to reduced production, atmospheric loss (by reaction) and transfer of CFC's from the atmosphere to the oceans (Khalil and Rasmussen, 1993).

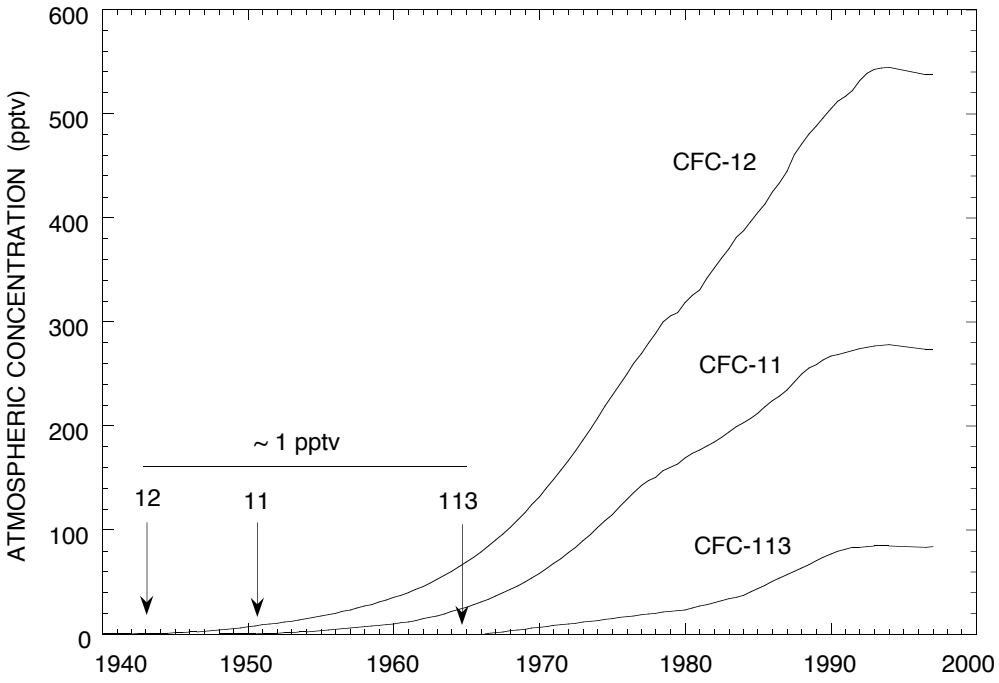

Figure 4-1. Global atmospheric concentration of CFC-12, CFC-11, and CFC-113 (after Plummer et al., 1993)

Assuming that recharging ground water is in CFC equilibrium with the atmosphere, a measured CFC concentration in water can be converted to a corresponding atmospheric concentration, which in turn can be used to compute a corresponding date of recharge from Figure 4-1. The difference between the date of recharge and the date of sampling is the age of the ground water.

The dating of ground water from CFC's depends, in part, on the assumption that CFC's are inert; once isolated from the atmosphere, the CFC concentration in a moving volume of water is constant in time. Processes which may change CFC concentrations include mixing and dispersion, exchange with solids, gases, or immobile waters, and degradation by biotic or abiotic reactions (Busenberg and Plummer, 1992). Degradation of CFC's in water has been identified for anaerobic conditions (Khalil and Rasmussen, 1989; Lovely and Woodward, 1992; Semprini et al., 1990; Terauds et al., 1993; Bullister and Lee, 1995; Oster et al., 1996; Plummer et al., in press). However, in oxygenated waters CFC's appear to be essentially inert. Furthermore, the relatively linear increase in the atmospheric concentrations over time means that CFC concentrations are less affected by mixing and dispersion than tracers with highly variable source terms, such as tritium (Plummer et al., 1993). Exchange processes may be important for CFC's, especially in highly heterogeneous formations, such as fractured rock (Shapiro, 1996; Wood et al., 1996). Sorption of CFC's to most natural aquifer materials is believed to be insignificant (Russell and Thompson, 1983; Lovely and Woodward, 1992). Despite these beneficial factors, CFC concentrations in ground water are not always easy to interpret. The U.S. Geological Survey Mirror Lake, New Hampshire site is one location where CFC's have not been as useful as hoped in characterizing large-scale transport properties (Busenberg and Plummer, 1996; Shapiro et al., 1996).

4.1.2 Mirror Lake Field Site

The U.S. Geological Survey (USGS) is investigating multi-scale flow and transport in a glaciated fractured rock setting at the Mirror Lake site, Grafton County, New Hampshire (fig. 4-2) (Winter, 1984; Shapiro and Hsieh, 1991; Hsieh et al., 1993). These investigations are multi-disciplinary and use tools ranging from detailed geologic and fracture mapping, to surface seismic and borehole radar, to crosshole hydraulic and tracer tests (Hsieh and Shapiro, 1996) and large-scale flow model calibration (Tiedeman et al., 1997). Ground water from both the fractured bedrock and from the overlying

glacially deposited formations has been analyzed for numerous environmental tracers (Busenberg and Plummer, 1996; Drenkard et al., 1996). The Mirror Lake site is within the Hubbard Brook drainage basin that also contains the Hubbard Brook Experimental Forest, a long-term ecological research site of the U.S. Forest Service, the Institute of Ecosystem Studies (IES), and several universities (Bormann and Likens, 1979; Likens, 1985; Federer et al., 1990; USDA Forest Service, 1991; Likens and Bormann, 1995).

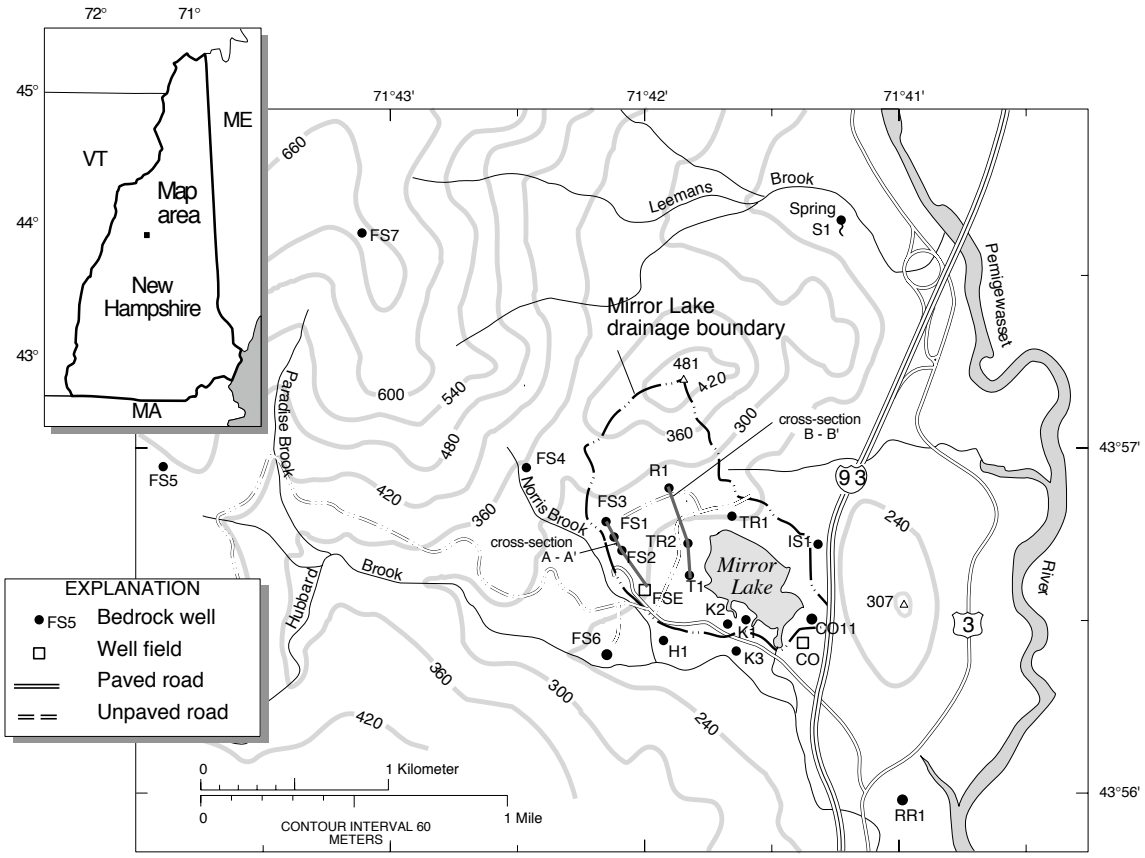

Figure 4-2. Mirror Lake site location and bedrock wells.

The hydrogeologic setting of the Mirror Lake site is glacial drift overlying crystalline bedrock (Winter, 1984; Winter 1985). The glacial drift has a highly variable composition ranging from uniform sandy terraces to fine-grained till filled with large

boulders (Winter, 1984; Harte, 1992; Harte and Winter, 1996). The permeability of the glacial drift is generally low (Wilson, 1991; Harte, 1997). Regional-scale flow modeling indicates that the transmissivities of the glacial drift and the underlying fractured bedrock are low and of the same order of magnitude (Tiedeman et al., 1997). Baseflow to streams in the Mirror Lake drainage basin is significantly higher than in other parts of the Hubbard Brook drainage basin because of the increased thickness of glacial drift (Winter et al., 1989; Mau and Winter, 1997). Sandy terrace deposits located throughout the watershed may have strong local control on ground-water flow and ground-water/surface water interaction (Shattuck, 1991; Harte and Winter, 1996). The climate is humid and long-term average recharge to ground water is on the order of 30 cm/yr (Mau and Winter, 1997).

4.1.3 Ground-Water Ages from CFC Data at Mirror Lake

In contrast to results from some relatively homogeneous coastal plain sediments (e.g. Reilly et al., 1994; Szabo et al., 1996), ground-water ages derived from CFC concentrations in samples from site bedrock wells do not follow a readily apparent spatial distribution. Figure 4-3 shows cross-sections of ground-water ages determined from samples collected from packer-isolated portions of open bedrock boreholes at the Mirror Lake site (Busenberg and Plummer, 1996; Shapiro et al., 1996). In homogeneous formations, ground-water age is expected to increase gradually from recharge to discharge locations, as shown in Chapter 2. However, in the highly heterogeneous fractured rock at Mirror Lake, in which the small-scale hydraulic conductivity varies over at least 7 orders of magnitude (Hsieh and Shapiro, 1996), complex patterns such as those shown in Figure 4-3 may be expected. This is consistent with ground-water age simulation results shown in, for example, Figure 2-8.

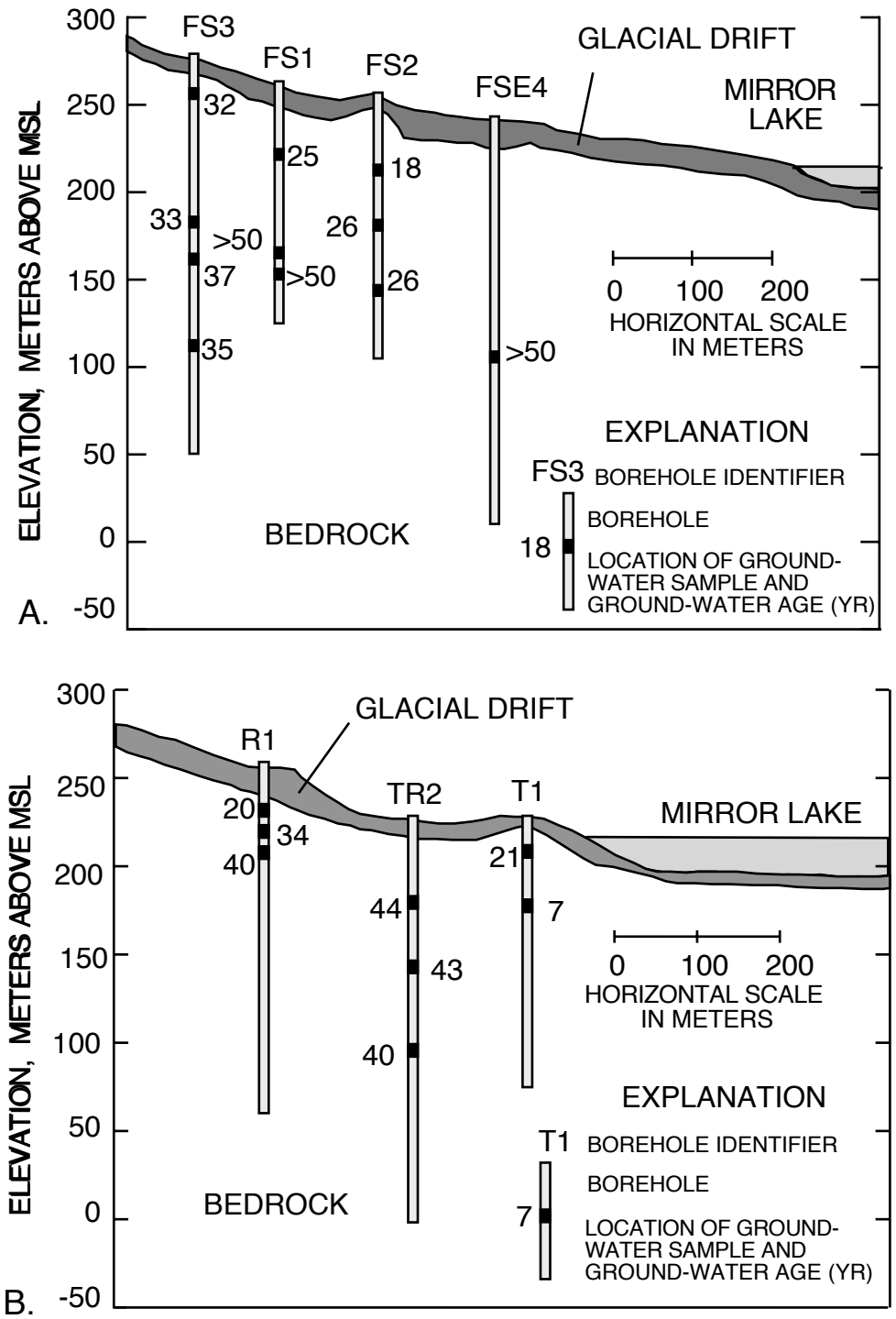

Figure 4-3. Ground-water ages in bedrock estimated from CFC-12 concentrations in 1990 & 1991 along projected cross-sections (a) A-A' (data from Busenberg and Plummer, 1996), and (b) B-B' (Shapiro et al., 1996).

Other possible causes of the complex age spatial pattern at Mirror Lake, and the corresponding CFC concentration pattern, involve in situ processes that modify CFC concentrations. Possible processes include, but may not be limited to, sorption, exchange, and degradation. Furthermore, seasonal temperature cycles may cause corresponding cycles in CFC concentrations in recharging waters (Chapter 3). These cycles may lead to variability in CFC concentrations along a flow path that may be misinterpreted as highly variable ages. Previous and concurrent work indicates that CFC's, particularly CFC-11 and CFC-113, are degraded under anaerobic conditions in ground water (Semprini et al., 1990; Terauds et al., 1993; Plummer et al., in press).

4.1.4 Scope and Objectives

The goals of this field study are to characterize the concentrations of CFC's in water recharging the saturated zone at Mirror Lake, to identify the processes that control those concentrations, and to describe the source function for CFC's in infiltrating waters that recharge the saturated zone. The field program investigates the following properties and processes: CFC concentrations at or near the water table, and in the unsaturated zone; temperature cycles where CFC air/water equilibrium is occurring; biogeochemical factors that may be related to CFC concentrations; and hydraulic properties of the unsaturated zone. Section 4.2 describes methods used in this field study, and results are presented in section 4.3. These results are discussed and processes controlling CFC in recharge water at the Mirror Lake site are identified in section 4.4. Preliminary summaries of the findings here have been presented at scientific meetings (see abstacts: Goode, 1997; Goode et al., 1997).

4.2 Methods

Some of the data used in this study were obtained from previous and ongoing research at Mirror Lake and at Hubbard Brook Experiment Forest conducted by U.S. Forest Service, Institute of Ecosystems Studies (IES), U.S. Geological Survey, and numerous universities. Geochemical data, including CFC results from bedrock wells and isolated piezometers were provided by USGS. Water level measurements are also provided by USGS and IES. Barometric pressure data were provided by IES. Precipitation and air temperature data were provided by USFS, Radnor Pa. Hydrogen concentrations in water reported here were provided by USGS (Don A. Vroblesky, written communication, 1997).

4.2.1 Moisture Content and Pressure

Unsaturated zone hydraulic conditions were monitored during 1996 and 1997, with most data collected during the summers. A Time-Domain-Reflectometry (TDR) system from CSI and Tektronix was used to measure soil moisture near W2 (fig. 4-4). The system consists of a CR10 datalogger with special TDR PROM chips, a Tektronix 1502B cable tester, a CSI multiplexer, coax cable, and CSI model 605 3-rod TDR probes. TDR measures the reflection time of an electrical pulse, which is a function of the moisture content around the 3-rod 30-cm probe. The measurement is the average moisture content within an elliptical cylinder 30 cm long, about 10 cm maximum cross-section and about 5 cm minimum cross-section. One of the first long-term field applications of automated TDR was performed at Hubbard Brook Experimental Forest by Herkelrath and others (1991).

Soil suction pressure head was measured at four depths near the TDR system, near W2. Soil Moisture Inc. tensiometers were used with depths of approximately 30, 60, and 90 cm. These tensiometers consist of a porous ceramic cup at the end of a clear plastic rigid tube of the appropriate length. A calibrated pressure gage in installed near

the top of the tensiometer, and a water reservoir with 'quick-fill' system is mounted on the top. The gage reading was recorded periodically by field personnel.

A secondary automatic measure of soil suction pressure head was obtained during the last part of this study using gypsum blocks. These gypsum blocks were also installed near the TDR system, near W2. Gypsum blocks were installed at depths ranging from 10 to 90 cm. The CSI datalogger of the TDR system was additionally programmed to measure the electrical resistance of the gypsum blocks which is a function of the moisture content in the block. The block's moisture content depends in turn on the prevailing soil pressure head in the surrounding material. These gypsum blocks were not calibrated in the laboratory and give only qualitative measures of pressure, but were used because the measurements are continuous, and supplement the direct tensiometer measurements.

Well water levels were measured throughout this study using manual electrical tape, and using continuous pressure transducer measurements. The water level indicator used was a Slope Indicator Inc. model 51453 which is marked in 0.01 ft (about 0.3 cm) intervals. Druck submersible pressure transducers were used with CSI dataloggers, and these were continuously calibrated in the field from manual water level measurements.

4.2.2 Soil Temperature

Average hourly soil temperature was monitored from June 1996 through September 1997 at several depths at two locations in the study area: near the FS3 and FS3C well clusters, and near FS4 and FS4-WT. Campbell Scientific Inc. (CSI) model 107B soil temperature probes were installed in natural backfill in hand augered boreholes. The average hourly temperature was recorded from measurements made every 5 minutes. Data collection was automated with CSI CR10 dataloggers. At the FS3C site, one temperature probe was installed in the bottom of piezometer FS3C-14, which was dry throughout the monitoring period. At each location, a CSI model 107U air temperature probe was installed on the ground in a small plastic box. At the FS3C site,

the depths of measurement of soil temperature were 0, 0.8 m, 1.9 m, and 3.5 m. At the FS4 site, the measurements depths were 0, 42 cm and 75 cm.

4.2.3 Water Sample Collection and Analysis

Water samples were collected from 31 shallow piezometers during the summers of 1995, 1996, and 1997. Figure 4-4 shows the locations of these wells within the Mirror Lake watershed, Grafton County, New Hampshire. These wells were constructed by the U.S. Geological Survey over approximately 20 years as part of ground-water/lake interaction studies (Winter, 1984) and of fractured rock research (Shapiro and Hsieh, 1996). Wells are constructed of either steel or PVC (Table 4-1) and are almost all screened over 0.6 to 0.9 m long intervals. This sampling effort focused primarily on wells screened near the water table, but also included some wells screened in the glacial drift beneath the water table. New wells constructed for the present study are W16A, W33, W34, W35, W36, and FS4-WT. These wells were installed by the USGS New Hampshire District drill rig crew under supervision by the author. These boreholes were power augered without adding any water during drilling, and the wells were constructed of threaded PVC to minimize CFC contamination. Except where the borehole caved during auger withdrawal, coarse sand was placed in the annulus around the screen, followed by natural backfill, followed by a layer of ground silica flour, and natural backfill to the surface. The purpose of the fine-grained ground silica is to minimize vertical flow within the borehole annulus.

The general procedures for sampling (Table 4-2) consisted of pumping at least 1 borehole volume and then collecting water samples using standard procedures and equipment developed by USGS. CFC samples were collected using procedures and equipment developed at the USGS CFC Lab, Reston Virginia (Busenberg and Plummer, 1992).

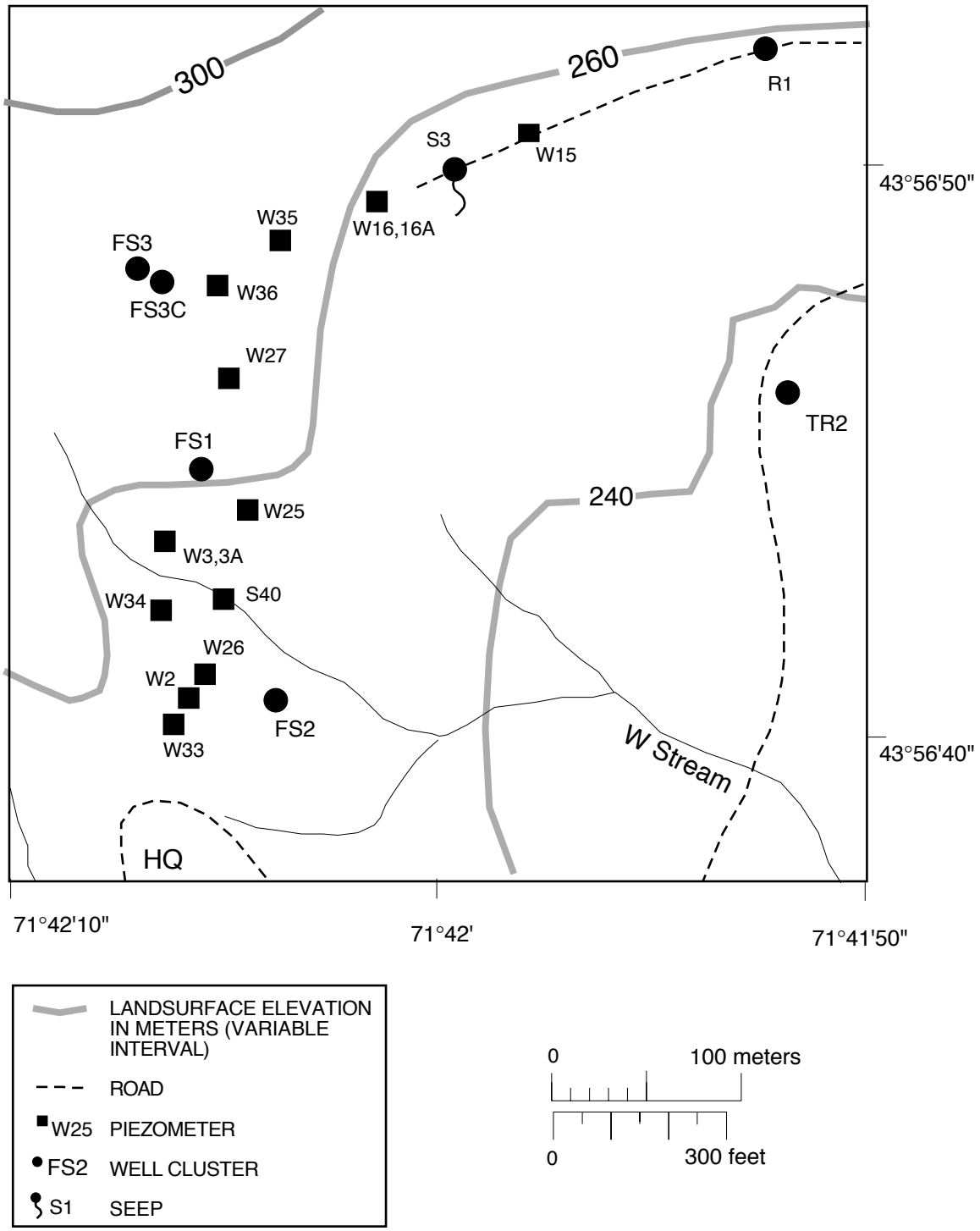

Figure 4-4. Locations of individual piezometers, well clusters, and seep sampled for this study.

Table 4-1. Selected piezometer construction data. [Primary references: W84, Winter, 1984; W94, T.C. Winter, personal commun., 1995; H91, P.T. Harte, written commun., 1991; H97, Harte, 1997; S91, Shattuck, 1991]

Well ID	Date installed	Casing material	Casing Diam. (cm)	Screen type	Screen Length (cm)	Screen top depth (m)	Top of casing elevation (m)	Land surface elevation (m)	Primary reference
W2	Nov-78	PVC	5.1	PVC wound	91	4.6	256.78		W84
W3	Nov-78	PVC	3.2	PVC slotted	76	5.9	258.56		W84
W3A	Nov-78	PVC	5.1	PVC slotted	76	1.7	259.11		W84
W6	Jul-82	Steel	5.1	Steel wound	91	9.4	239.27		W84
W11	Jul-82	ABS	5.1	PVC wound	61	7.3	240.97	240.1	W84
W15	Jul-82	Steel	3.2	Steel wound	91	0.9	263.26		W84
W16	Jul-82	Steel	3.2	Steel wound	91	5.5	264.82		W84
W16A	Jul-96	PVC	5.1	PVC wound	61	2.1		263.8	this study
W25	Oct-88	PVC	5.1	PVC wound	61	6.7	262.34	261.0	W94
W26	Oct-88	PVC	5.1	PVC wound	61	4.9	258.05	256.8	W94
W27	Aug-90	PVC	5.1	PVC slotted	152	4.9	266.93	265.9	H91
W33	Jul-96	PVC	5.1	PVC wound	61	5.2		256.0	this study
W34	Jul-96	PVC	5.1	PVC wound	61	4.5		258.0	this study
W35	Jul-96	PVC	5.1	PVC wound	61	2.4		271.0	this study
W36	Jul-96	PVC	5.1	PVC wound	61	5.2		272.0	this study
FS1-17	Jul-82	Steel	5.1	Steel wound	91	4.9	262.64	261.3	W84
FS1-25	Aug-79	PVC	5.1	PVC wound	61	6.9	262.35	261.2	W94
FS1-35	Aug-79	PVC	5.1	PVC wound	61	9.5	262.22	260.7	W94
FS3-11		PVC	5.1		61	2.7	275.04	274.0	
FS3-22		PVC	5.1		61	6.1	275.05	274.0	
FS3-29		PVC	5.1		61	8.2	275.02	274.0	
FS3C-14	Aug-91	PVC	5.1	PVC slotted	15	3.9	273.81	273.6	H97
FS3C-19	Aug-91	PVC	5.1	PVC slotted	15	5.5	274.27	273.7	H97
FS3C-24	Aug-91	PVC	5.1	PVC slotted	15	7.2	274.32	273.7	H97
FS3C-29	Aug-91	PVC	5.1	PVC slotted	15	8.8	274.13	273.7	H97
FS4-WT	Jul-96	PVC	5.1	PVC wound	61	1.1		349.7	this study
R1-36	Aug-90	PVC	5.1	PVC slotted	152	9.6	257.30	256.5	H91
R1-55		PVC	5.1		61	15.5	257.32	256.2	
S40	Aug-88	PVC	5.1	PVC slotted	24	0.5	255.30	254.3	S91
T1-8	Jul-82	Steel	5.1	Steel wound	91	1.5	229.62	228.9	W84
TR1-63	Sep-83	PVC	5.1	PVC wound	183	17.4	249.30	248.4	W94

Table 4-2. Overview of water sampling procedures.

Step	Procedures and Parameters	Equipment	Notes
1	measure water level and total well length	electric tape	compute volume of water in well
2	install submersible piston pump, or intake tubing for peristaltic pump	stainless steel piston pump or peristaltic pump	either copper or nylon tubing
3.	purge well of at least 1 well volume		monitor pH, specific conductivity, temperature, and dissolved oxygen; collect discharge for volume measurements; intermittent water level measurements
4	Tritium	1 L poly bottle	overflow at least 1 volume
5	Carbon Isotopes	1 L brown or clear glass bottle with polyseal cap	overflow at least 1 volume; small air bubble at top
6	Alkalinity	50 ml in graduated cylinder	analyze in field by titration
7	Total Organic Carbon	4 oz brown glass bottle with Teflon cap	store on ice and express mail to USGS Lab
8	Deuterium and Oxygen-18	2 oz glass bottle with polyseal cap	no air bubble
9	Dissolved Gases	200 ml clear glass bottles with rubber septum	duplicate samples; no air bubble; store on ice and express mail to USGS Lab
10	Sulfur Hexafluoride	1 L clear glass bottle with polyseal cap	no air bubble, store on ice and express mail to USGS Lab
11	CFC's	75 ml clear glass ampules	collect and seal in ultra-pure apparatus provided by USGS Lab; 3-6 samples
12	shutdown		record final field parameters

Field water quality parameters included temperature, pH, specific conductivity, dissolved oxygen, and alkalinity. Specific conductivity and pH were measured with separate Orion probes, both of which also measured temperature. In some cases the probes were lowered into the piezometer prior to sampling to record in situ values. Dissolved oxygen was measured in the field using the Winkler titration method (Hach kit) or a YSI self-stirring BOD probe (model 5905). Alkalinity was measured using 0.16 N sulfuric acid titration of 50 ml samples. Collected samples were analyzed at the following USGS laboratories: CFC Lab and Isotope Lab in Reston; National Water Quality Lab in Denver; and Tritium Lab in Menlo Park.

4.2.4 Soil Gas Sampling and Analysis

Soil gas samples were collected during the summers of 1996 and 1997, and in January 1997 from steel dry wells installed by hand or power auger, or manual drive point in one case (fig. 4-5; Table 4-3). Figure 4-6 shows a schematic of the a steel gas well consisting of 0.6 cm diameter stainless steel tubing, stainless steel or brass swagelok compression fittings, a stainless steel screen, and glass wool. The borehole annulus around the sampling port is filled with coarse sand, followed by natural backfill, followed by ground silica flour, and natural backfill to the surface.

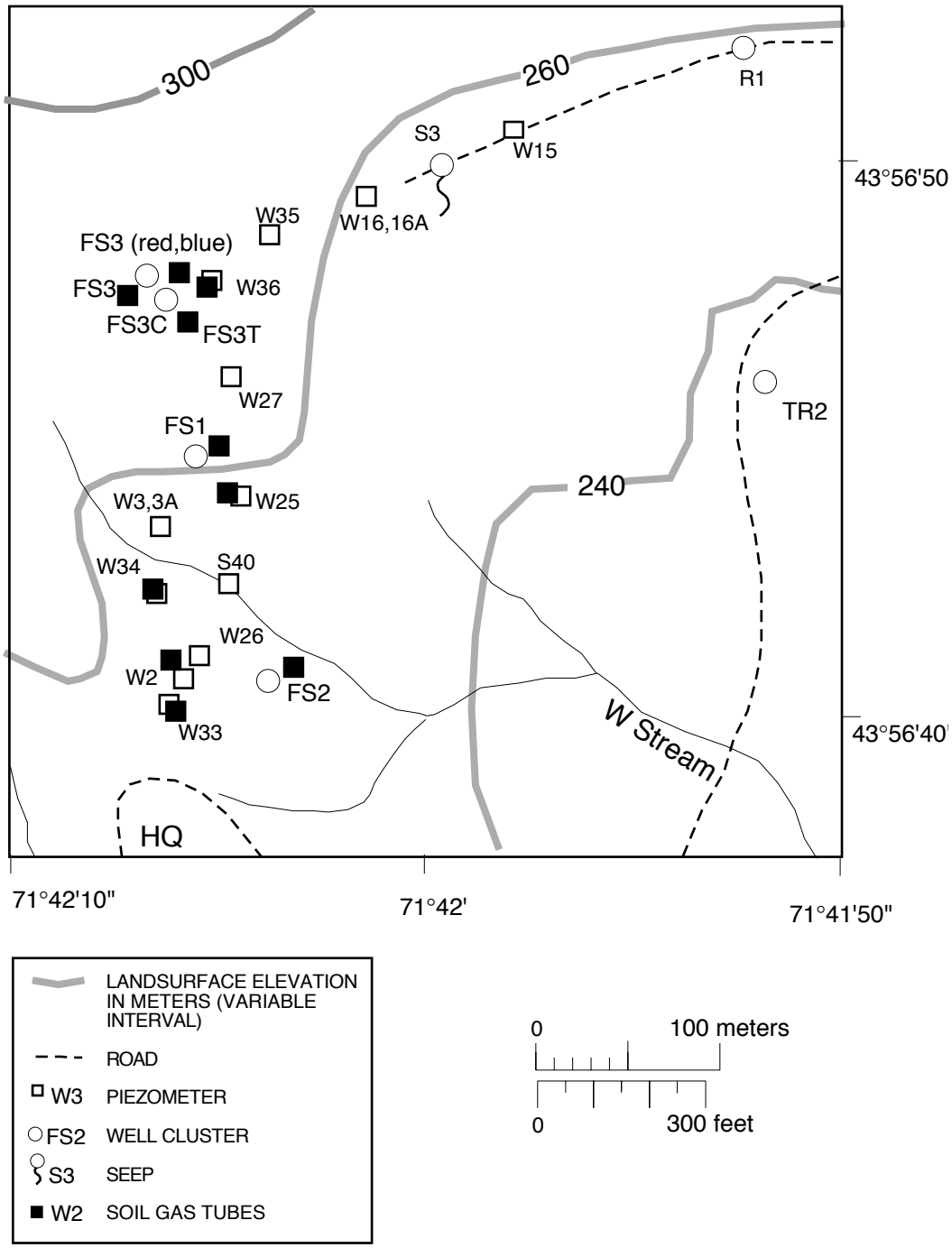

Figure 4-5. Locations of soil gas sampling tubes installed for this study.

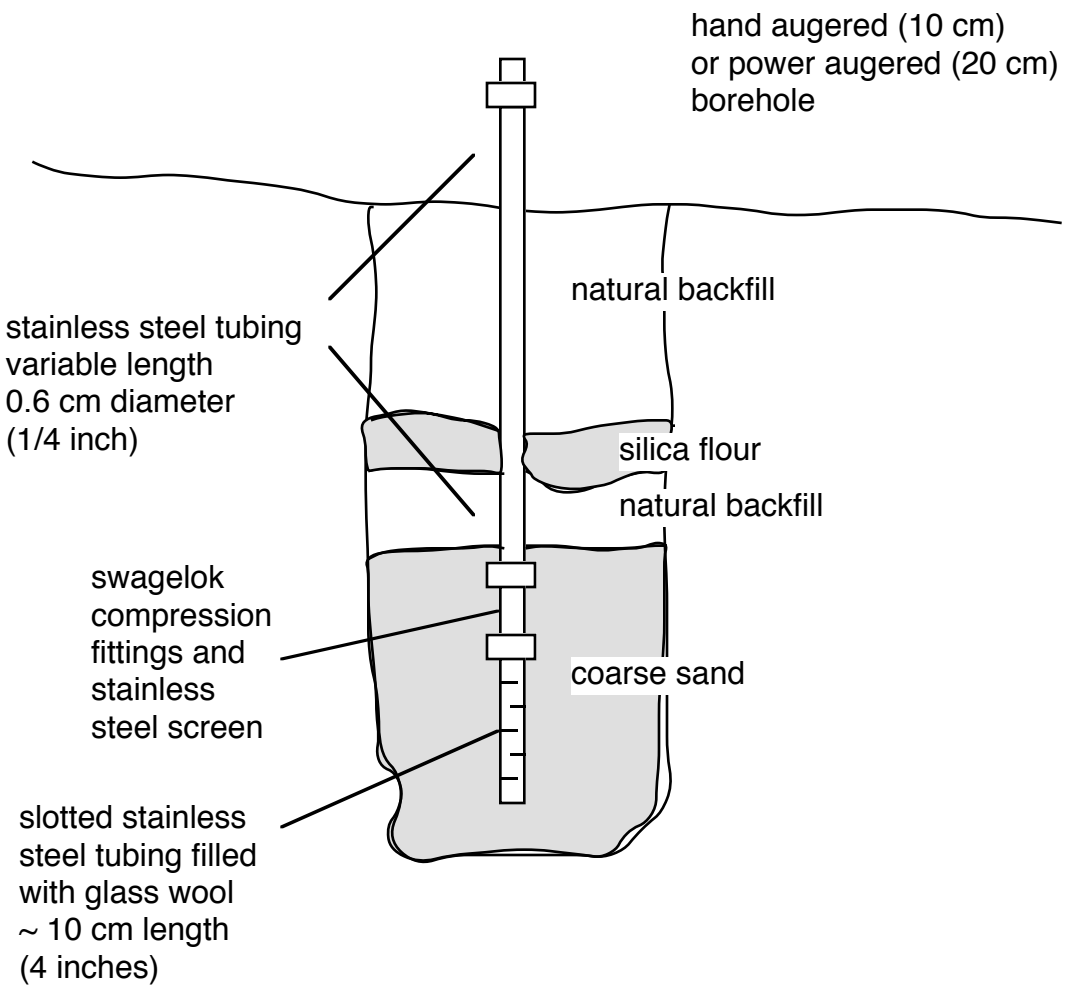

Figure 4-6. Schematic of typical soil gas well.

Soil gas samples were pumped from the dry well into glass ampules which were sealed by welding. A Rasmussen stainless steel gas pump with Teflon diaphragm (40 psig model) was attached to the dry well and pumped for 2-3 minutes to purge the well. All metal (aluminum and stainless steel) tubing was used. Samples were collected after purging in 150 ml glass ampules which were sealed by welding the ampule neck closed with a MAP gas torch. Three samples were normally collected from each dry well. All CFC gas samples were analyzed at the USGS CFC Lab in Reston.

Air samples were also collected to ascertain the local CFC gas concentrations. Samples were collected using the Rasmussen pump with aluminum tubing and a stainless steel cylinder provided by the USGS CFC Lab in Reston. Additional samples were collected using the same apparatus and sample ampules as the soil gas, but with the pump intake in air, 1-2 m above ground. These samples provide further information on local CFC air concentrations, and possible sample apparatus contamination.

4.3 Results

4.3.1 Moisture Content and Pressure

Soil moisture was relatively high from late fall through early summer, and was relatively low in the summer, except immediately after rainfall (fig. 4-7). Overall, the moisture content was significantly higher at the shallower depth. Moisture content at 18 cm is 0.2 - 0.25 in late spring and falls to as low as 0.09 during late summer. Average moisture content over the 50-80 cm depth range is 0.12 - 0.17 in spring and fell to 0.07 in mid-September 1997. When the 18-cm moisture content is above about 0.2, then the 50-80 cm moisture content responds relatively quickly to rainfall, although the response is smaller in magnitude than at the shallower depth. However, when the shallow moisture content falls below about 0.2, the deeper moisture content responds only very gradually to rainfall.

Precipitation during 1996 was very high, but 1997 precipitation was below average through September (U.S. Forest Service files, 1997). However, this difference in precipitation is not reflected by soil moisture differences. Overall, the ranges of soil moisture contents during the wet summer of 1996 and the dryer summer of 1997 are similar. Some differences are apparent. For example, moisture contents in July 1996 are significantly higher than in July 1997. However, even in the dryer July 1997, recharge of soil moisture is occurring at the 50-80 cm depth following sufficient precipitation.

Moisture content was relatively constant in time under snow cover during February 1997 (fig. 4-7), increasing during a partial melt at the end of February and again during final melt at the end of March and beginning of April 1997. The relatively small changes in moisture content during winter are consistent with previous observations in other parts of the Hubbard Brook drainage basin (Herkelrath et al., 1991).

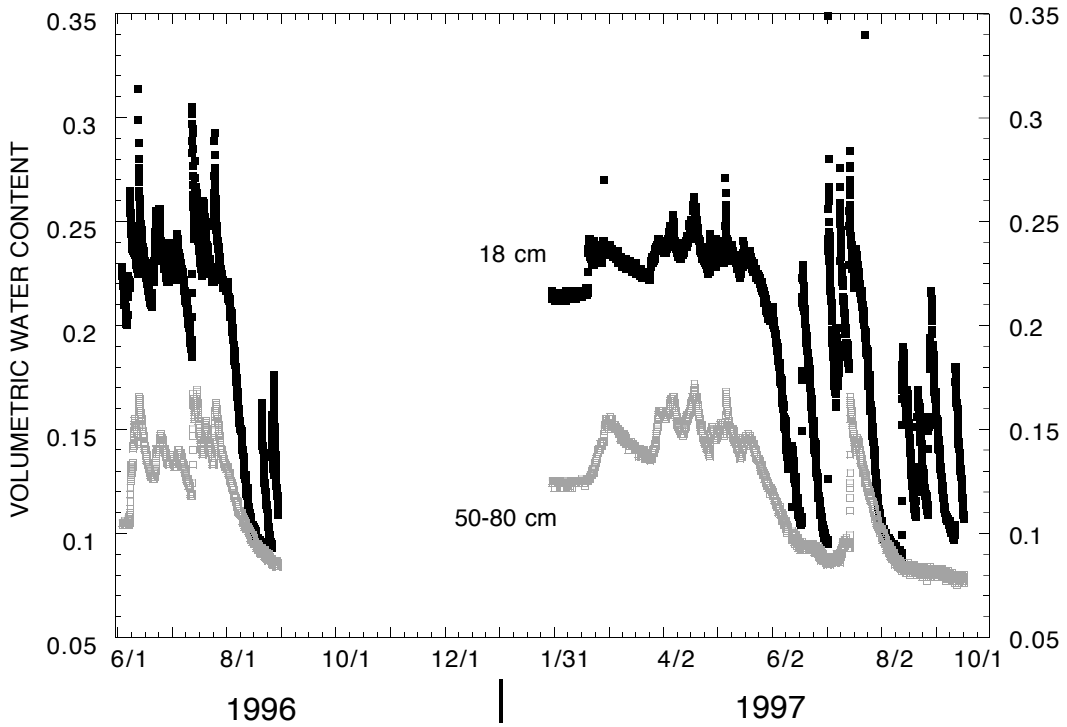

Figure 4-7. Moisture content during 1996 and 1997 near W2 at depth of 18 cm and average over depth range 50-80 cm.

Tensiometer measurements of pressure head in the unsaturated zone are similar to the soil moisture results, although tensiometer results are available only for the summers of 1996 and 1997 (fig 4-8). Suction head (negative pressure head) is low in the early summer at all depths but increases significantly at the 30 cm depth as the upper soil zone dries out. Fluctuations in suction head at 30 cm generally mirror soil moisture fluctuations, with high moisture content and low suction head after rainfall, and then falling moisture content and increasing suction head as drying proceeds. The deeper 60- and 90-cm suction pressure heads changed much less during the monitored period. The 90-cm results were essentially constant in the range 10-14 centibars, while the 60-cm suction head increased somewhat only after extended drying, and then increased only to about 30 centibars.

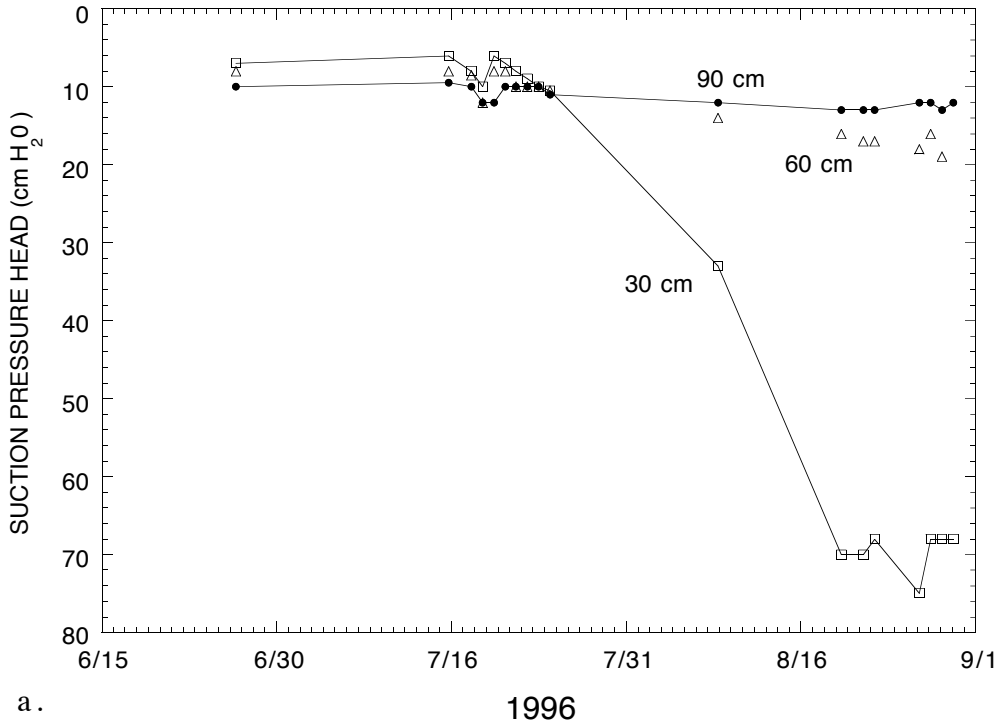

a.

1996

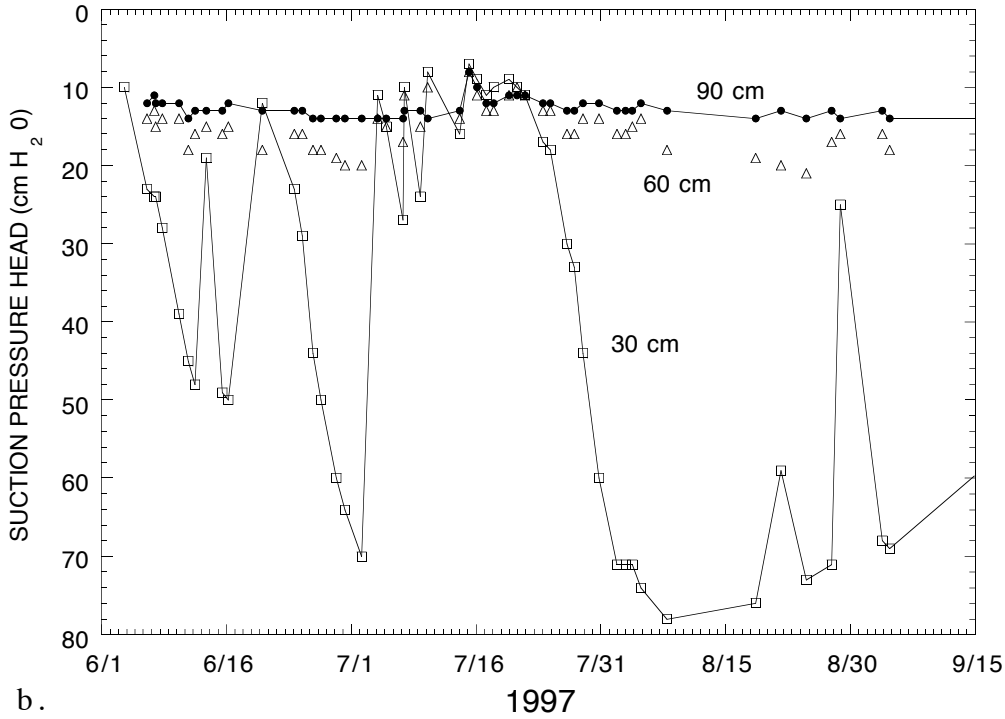

b.

1997

Figure 4-8. Suction pressure head at W2 TDR site during (a) the summer of 1996, and (b) the summer of 1997.

Although uncalibrated, the gypsum block results provide a continuous record of relative fluctuations of suction pressure head during the summer of 1997. The 3 blocks installed with the tensiometers show similar, but not identical, responses (fig. 4-9a). The deepest probe (90 cm) shows a very slow decrease in resistance, corresponding to increasing wetness. The resistance change at 60 cm is similar in pattern to the observed suction pressure head (fig. 4-8b). The significant decreases in suction pressure head at 30 cm depth during the early part of the summer of 1997 correspond to only minor changes in electrical resistance at 30 cm. However, the subsequent drying in the latter part of the summer is represented similarly by both suction pressure head and electrical resistance changes. Notably, the electrical resistance changes following recharge are more gradual than the tensiometer data, suggesting a time-lag in the gypsum block, probably due to moisture diffusion.

The temporal fluctuations are more rapid for the 5 gypsum blocks installed in a separate shallow hole (fig. 4-9b). The overall pattern of the electrical resistance in the gypsum block at 20 cm depth is very similar to the pressure head fluctuations measured at 30 cm (fig. 4-8b). However, the block at 10 cm apparently has much lower resistance, relative to the other gypsum blocks, but has a similar temporal pattern. The rapid decrease in resistance in the first week of August 1997 is observed only for the 10 cm block, suggesting that wetness increased very near the surface, but infiltration did not occur to 20 cm. The resistance changes also appear to be most rapid at the 10 cm depth. The 30 and 40 cm block respond very similarly to each other, and their response slightly lags that at 20 cm. The 58 cm block responds most slowly, but indicates significant drying at that depth during August 1997.

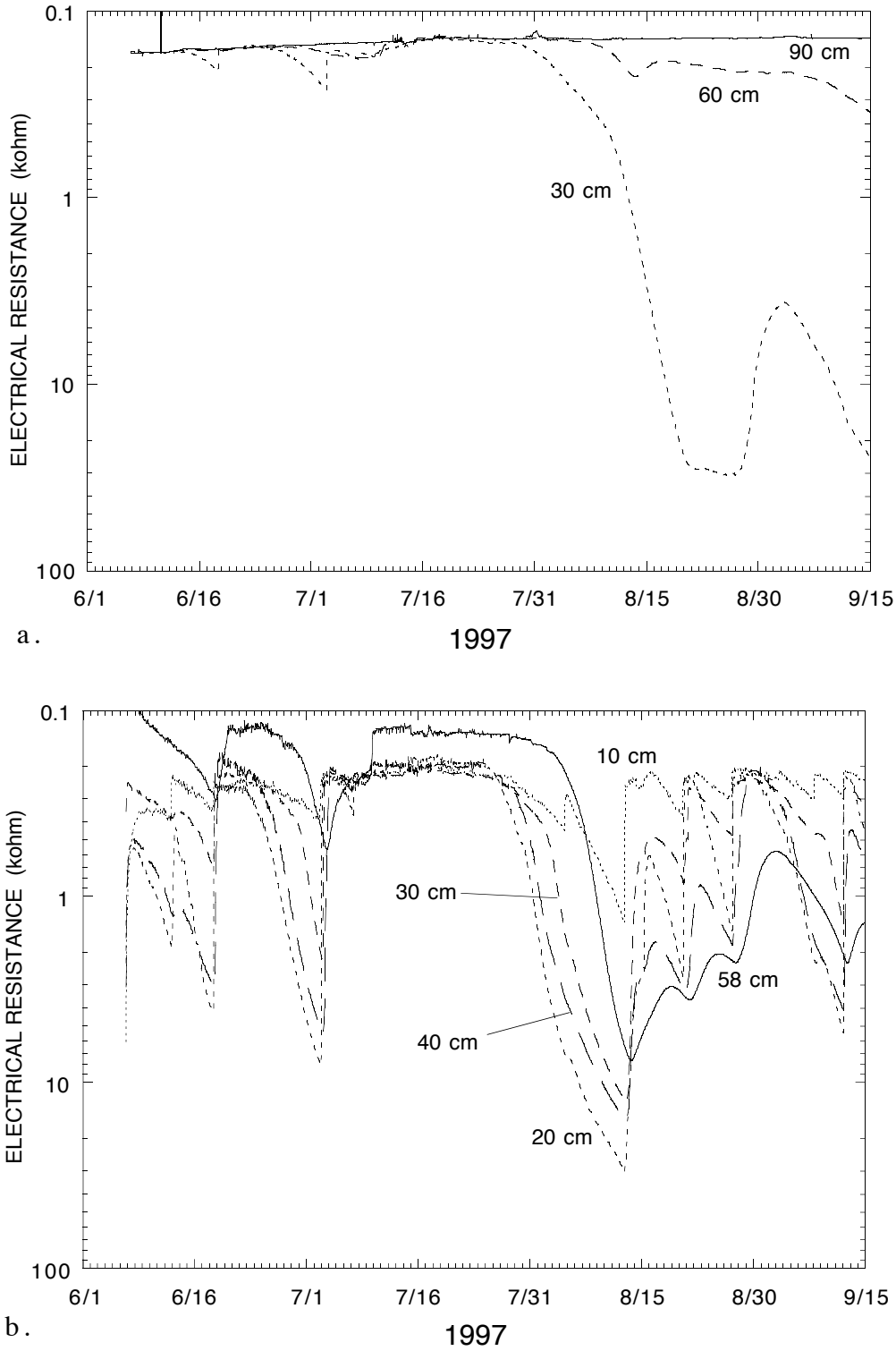

Figure 4-9. Gypsum block electrical resistance during summer 1997: (a) at W2 TDR site, and (b) in separate borehole at W2 TDR site.

Overall, these soil moisture, tensiometer, and gypsum block data indicate that a dynamic unsaturated zone exists at Mirror Lake. Although moisture contents are generally constant during the winter, significant infiltration can occur during temporary warm periods. The summer is not characterized by very low moisture contents and high soil moisture suction. Rather several drying/wetting cycles occur during the summer to depths of at least 60 cm. The unsaturated zone is not in static equilibrium with zero recharge during the summer. Soil moisture and suction pressure data show that infiltration to depths of at least 60 cm routinely occurs following sufficient precipitation, even during the peak evapotranspiration period. These data are consistent with observations of static and occasionally increasing hydraulic head in saturated-zone wells during the summer (fig. 4-10). Without this recharge during the 3-to-4-month growing season, water levels in these wells would be expected to drop throughout the summer due to discharge to streams.

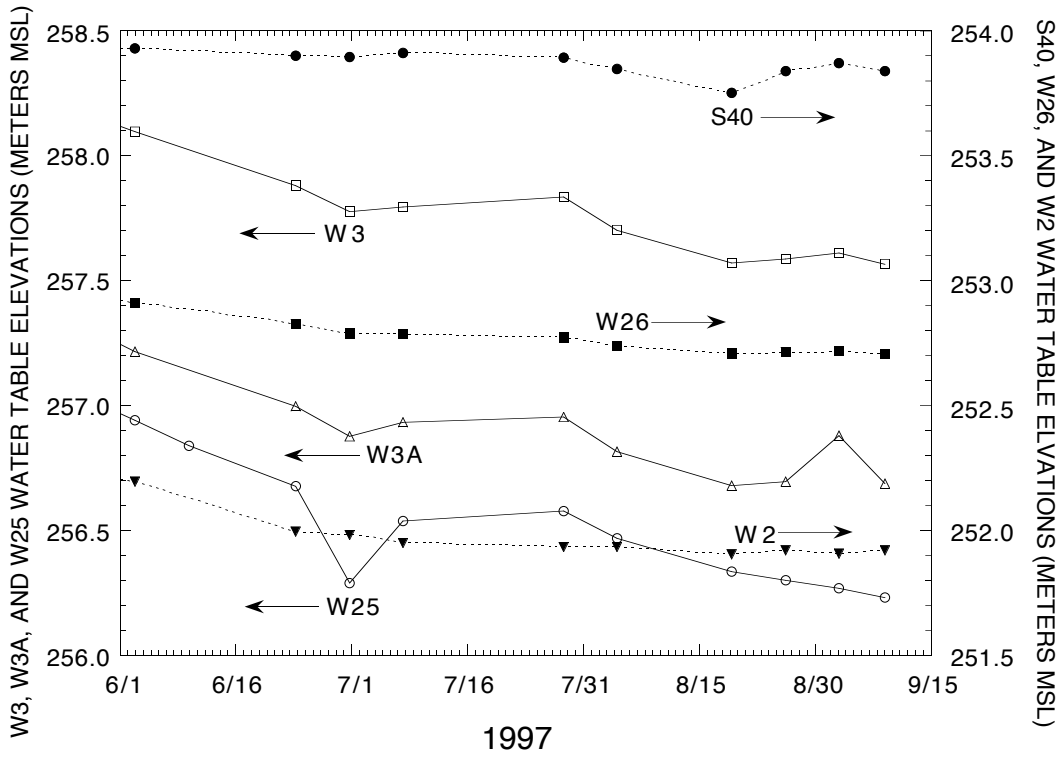

Figure 4-10. Water table elevations during summer 1997 in six piezometers near W2 TDR, tensiometer, and gypsum block sites. Arrows point to the corresponding elevation axis.

4.3.2 Soil Temperature

Soil temperature at FS3 was monitored continuously from early June 1996 until mid-September 1997. All of the soil temperatures change gradually from hour to hour (fig. 4-11). The most rapid changes are associated with infiltration events during heavy storms or snowmelt. The surface temperature changes rapidly except when the surface is covered by snow in the winter.

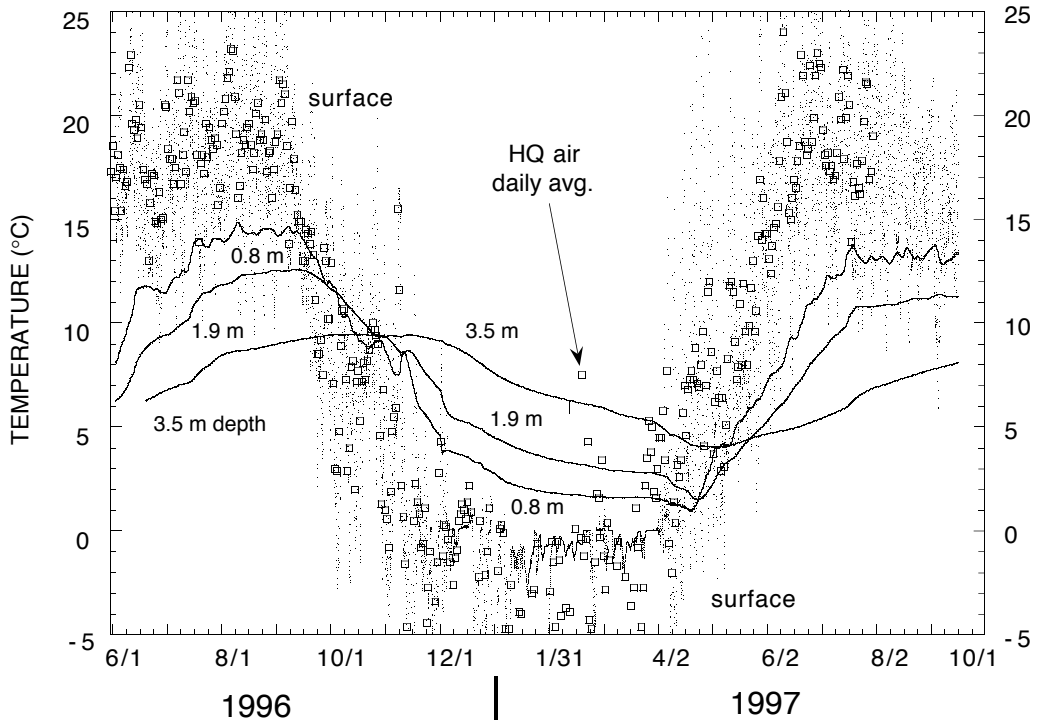

Figure 4-11. Air, surface and soil temperature near FS3. Hourly soil temperatures at 0.9 and 1.8 m depth and at 3.5 m depth at bottom of dry well FS3C-14 are solid lines. Hourly surface temperatures are dots. Daily average air temperature at Forest Service Headquarters (HQ) is squares.

The general temporal and spatial trends in temperature follow the classic diffusion controlled profile, as reported by Federer (1973) for other parts of the Hubbard Brook drainage basin. The lag and dampening of temperature fluctuations increases with depth. Surface temperatures range from about -5 °C to over 25 °C with minimum temperatures in November-April and maximum in June-August. At 3.5 m depth, the temperature range is only 4 to 9.5 °C with the minimum in April and the maximum in November. The mean temperature at the 3.5 m depth is about 7 °C. At intermediate soil depths the cycle in temperature is not symmetric. Cooling in the fall and winter is more gradual than the rapid heating that occurs for about 3.5 months after snow melt.

Soil temperatures at the FS4 site (fig. 4-12) are similar to those as FS3. FS4 is higher in the watershed and this elevation change is reflected in the slightly lower summer temperatures at FS4. The maximum temperature at 75 cm at FS4 is 13°C, whereas the maximum temperature at 80 cm at FS3 is 14 °C. Conversely, the minimum temperature at 75 cm at FS4, 3.5°C, is higher than that at 80 cm at FS3, 1°C.

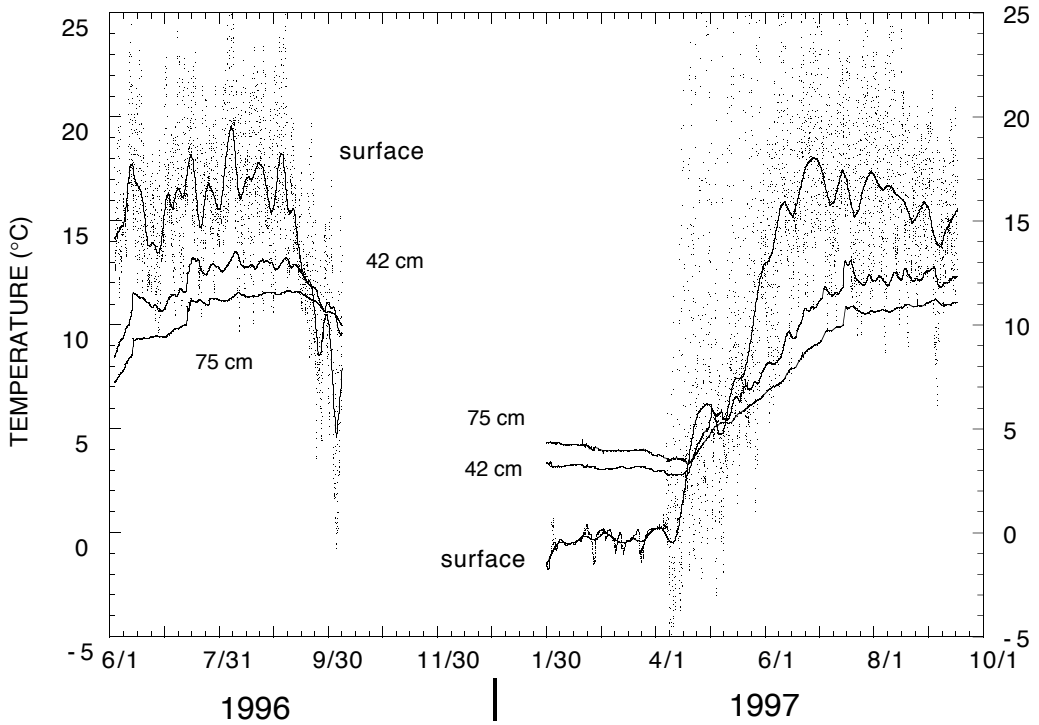

Figure 4-12. Air, surface and soil temperature near FS4: Hourly soil temperatures at 42 and 75 cm depth (solid lines); Hourly surface temperature (dots) with smoothed curve (solid line).

Rapid air and surface temperature fluctuations are often associated with precipitation or melting events which serve to advect relatively hot or cold water down with infiltrating water. For example, very rapid soil temperature increases in 1996 are associated with a moving cold front that caused rapid drops in air and surface temperature (hail was observed at the site). Even though the precipitation was cold, the result of the heavy precipitation (mostly rain) was to carry relatively warm water down into the soil

column. Inflections in soil temperature at 3.5 m in July 1996, April 1997, and July 1997 are caused by heat advection in moving water during significant infiltration events.

Snow cover in winter insulates the surface from air temperature fluctuations. During November-December 1996 snow cover was minimal and surface temperatures closely followed air temperature. January-March 1997 was a period with more snow cover and stable surface temperature near zero. A melt in February 1997 lead to subsequent decreased surface temperatures because of the loss of the insulating snow cover. Gradual cooling occurs at the intermediate depths while snow cover is present. Snow melt in April 1997 caused rapid decreases in soil temperature as large amounts of nearly frozen water infiltrated. These dynamics cause the upper soil column to experience minimum temperatures during the spring snow melt event. The minimum temperatures in April 1997 were 1°C at 0.8 m and 1.5°C at 1.9 m depth.

4.3.3 General Chemistry

Field water-quality parameters exhibit significant variability in water-table piezometers at the Mirror Lake site (Table 4-4). In general, specific conductance values are relatively low compared to bedrock wells at the site (Shapiro et al., 1998). The pH ranges from 5 to 11 with most values between 5 and 7. High pH has been associated with cement grout installed at older piezometers (P.T. Harte, written commun., 1991).

Dissolved oxygen (DO) concentrations are significantly below saturation levels in many samples from water-table piezometers at the Mirror Lake site (Table 4-3). In several areas the water table is apparently anaerobic, or nearly so (fig. 4-13). This corresponds with the wide-spread observation of low-DO in bedrock wells (Busenberg and Plummer, 1996).

Table 4-4. Geochemical data from water samples.

Well ID	Date	Pumping Rate (L/min)	Temp. (°C)	pH	Sp. Cond. (µS/cm)	Field DO (mg/L)	Ca2+ (mg/L)	Mg2+ (mg/L)	Sr2+ (mg/L)	SiO2 (mg/L)
FS1-17	18-Jul-95	0.05	15	6.6	77	0.01	5.5	1.24	0.034	9.24
FS1-17	19-Jul-96	0.1		6.8	74	0.1-0.7	5.3	1.20	0.034	10.7
FS1-25	20-Jul-96	0.1		11	370	3	32.3	0.51	0.069	14.2
FS1-35	20-Jul-96	0.7		5.3	24	4	1.6	0.24	0.011	6.50
FS3C-19	14-Jul-95	0.05	24	5.6	25	9.5	1.56	0.26	0.015	5.65
FS3C-19	18-Jul-96	0.34		5.4	24	8	1.6	0.32	0.014	6.90
FS3C-24	15-Jul-95	0.1	18	5.8	30	8.8	2.19	0.55	0.015	8.17
FS3C-24	18-Jul-96	0.13		5.8	28	6.8	2.1	0.50	0.015	8.80
FS3C-24	12-Jun-97	0.11	8-9	5.5	26	7	1.77	0.44	0.013	7.47
FS3C-29	17-Jul-96	0.1-0.2		6.5	29	6.2	1.5	0.37	0.013	7.20
FS3C-29	11-Jun-97	0.04	7-12	5	22	5.8	1.38	0.37	0.012	5.93
FS4-WT	8-Jul-97	0.06	10.6	4-5	54-76	4.7	4.02	0.36	0.025	9.26
R1-36	10-Jul-95	0.3	8	6.4	23	10.6	1.88	0.31	0.016	4.09
R1-55	11-Jul-95	0.05	18	10.2	190	0				
RR1-PZ	21-Aug-95	0.74	13.5	6.6	575	0.8	30	5.16	0.42	13.0
S1 spring	6-Aug-97		7.7	4.8	10.5	6	2.78	0.48	0.020	8.58
S3 seep	7-Aug-97	0.07	14	5	23-40	0.8-1.6	0.68	0.16	0.007	4.32
S40	1-Jan-96									
S40	25-Jul-97	0.05					0.92	0.21	0.007	8.43
T1-8	12-Jul-95		20	6.4	35	5.3	1.42	0.28	0.015	6.25
T1-8	26-Jun-97	0.07	13-15	6	28	2	1.27	0.27	0.017	5.73
TR1-63	8-Jul-95	0.1	19	7.8	47	9	4.64	0.75	0.026	17.4
TR1-63	25-Jun-97	0.15	9-16	6.1	46	9.2	4.08	0.79	0.023	18.0
W11	25-Jul-97	0.2	10-13	5.5	38	6.9	3.73	0.44	0.019	9.05
W15	28-Jul-97	0.03	17-20	6.2	50-70	1.9	1.56	0.41	0.014	5.33
W16	28-Aug-96	0.1	13	7	120-180	0.1	14.7	6.50	0.131	24.4
W16	13-Jul-97	0.08	10-20	6.6-8	140-170	0.5	14.3	6.21	0.134	25.5
W16A	27-Aug-96	0.1	15	7	80	3	4.30	1.80	0.039	16.5
W16A	8-Jul-97	0.07	12	6	62-86					
W16A	12-Jul-97	0.09	13	6.3	50-72		3.69	1.41	0.031	12.8
W2	20-Jun-95	0.06	17	6.4	74	0	5.16	1.18	0.031	18.7
W2	26-Aug-96	0.2	21	6.3	68	0.2-2.0				
W2	7-Jun-97	0.07	9-12	7	75	0.5-1.0	5.22	1.34	0.027	19.7
W25	21-Jun-95	0.13	11	6.8	85	0.5	7.17	1.84	0.036	16.7
W25	13-Jul-97	0.09	14-17	6.7	93	0.1	7.53	2.02	0.034	18.5
W26	21-Jun-95	0.1	15	6.9	83	0	5.80	1.44	0.032	19
W26	16-Aug-95						6.10	1.48	0.032	19.1
W26	26-Aug-96	0.2		6.4	80	0.05				
W26	8-Jun-97	0.08	10-12	6.7	85	0.5-0.7	5.99	1.62	0.030	20.3
W26	26-Jul-97									
W27	16-Jul-95	0.05	20	6.3	54	5.1	5.55	1.19	0.033	12
W27	19-Jun-97	0.11	10	5.8	50	4	5.16	1.16	0.027	12.6
W3	23-Jun-95	0.1	16	6.3	47	3	3.85	0.89	0.025	16.5
W3	14-Jul-97	0.26	11-20	6	52	2.5	4.30	1.10	0.027	18.6
W3A	23-Jun-95	0.2	19	5.4	23	6.8	1.33	0.25	0.014	7.57
W3A	14-Jul-97	0.09	12-22	5	20-29	5.6	1.45	0.28	0.013	7.30
W33	22-Aug-96	0.4	24	6.8	74	0.04	5	1.3	0.025	21
W33	7-Jul-97	0.15	10	6.4	78	0				
W34	22-Aug-96	0.05		7	55	2.7	3.5	0.79	0.021	15.7
W34	10-Jun-97	0.06	9-14	6.3	37	6-7	3.04	0.61	0.016	13.9
W34	14-Jul-97									
W34	14-Jul-97									
W35	27-Aug-96	0.1	15		60	0.2	1.9	0.72	0.028	15.4
W35	11-Jul-97	0.03	9.3	5-5.8	35	4.6				
W36	26-Aug-96	0.05-0.1	15	6	39	3	2.2	0.71	0.027	10.8
W36	27-Aug-96	0.1	15		40	3				
W36	17-Jun-97	0.1	8	5.4	23	7.8	1.55	0.33	0.017	8.54
W6	26-Jul-97	0.07	10-16	6-6.4	140	0.3-0.8	1.85	0.4	0.017	18.9

Table 4-4. Geochemical data from water samples (continued).

Well ID	Date	Na+ (mg/L)	K+ (mg/L)	Fe2+ (mg/L)	Mn2+ (mg/L)	Al3+ (mg/L)	Alkalinity as HCO3- (mg/L)		Cl- (mg/L)	S042- (mg/L)
							lab	field		
FS1-17	18-Jul-95	2.58	1.54	3.84	0.118	<0.005	31.9	40.8	0.69	2.52
FS1-17	19-Jul-96	2.8	1.8	4.51	0.117	0.008	29		0.71	2.87
FS1-25	20-Jul-96	3.4	2.2	0.023	<0.004	0.241	47.4		0.52	6.33
FS1-35	20-Jul-96	0.8	<0.3	0.039	0.019	0.225	2.5		0.56	3.97
FS3C-19	14-Jul-95	1.17	0.28	0.085	0.023	0.02	5.25	4.39	0.9	4.85
FS3C-19	18-Jul-96	1.3	<0.3	0.012	0.014	0.14	3.1		0.68	5.02
FS3C-24	15-Jul-95	1.46	0.45	0.027	0.019	0.007	7.53	9.29	0.99	5.75
FS3C-24	18-Jul-96	1.4	0.3	<0.010	0.016	0.015	7		0.7	4.61
FS3C-24	12-Jun-97	1.33	0.5	0.010	0.012	0.016	4.5		1.16	5.06
FS3C-29	17-Jul-96	1.2	0.3	0.046	0.037	0.093	4.5		1.04	5.1
FS3C-29	11-Jun-97	1.09	0.4	0.01	0.028	0.061	2.0		1.16	5.06
FS4-WT	8-Jul-97	1.12	1.0	0.79	0.114	0.564	<2		1.21	18.3
R1-36	10-Jul-95	0.81	0.15	0.01	<0.005	0.02	1.8	2.93	0.98	6.19
R1-55	11-Jul-95									
RR1-PZ	21-Aug-95	57.4	11.9	1.46	1.47	0.071	71.1	53.7	115.3	23.6
S1 spring	6-Aug-97	1.42	0.4	<0.007	0.004	0.050	5.0		1.15	5.80
S3 seep	7-Aug-97	0.98	0.2	2.02	0.054	0.192	5.6		1.29	2.95
S40	1-Jan-96									
S40	25-Jul-97	0.93	0.3	0.352	0.062	0.262	3.6		1.12	3.89
T1-8	12-Jul-95	1.1	0.43	1.39	0.074	<0.005	16	22.7	1.14	1.72
T1-8	26-Jun-97	1.01	0.50	2.41	0.072	0.01	10.1		1.29	1.65
TR1-63	8-Jul-95	2.89	1.1	0.017	0.012	0.01	19.5	19	0.98	5.82
TR1-63	25-Jun-97	2.88	1.2	0.009	0.005	0.008	16.9		1.23	5.22
W11	25-Jul-97	2.18	0.6	0.008	0.009	0.022	9.4		2.65	4.05
W15	28-Jul-97	1.11	0.6	10.4	0.215	0.003	28.9		1.18	4.67
W16	28-Aug-96	4.7	3.9	5.65	1.03	0.003	96.9		0.61	1.62
W16	13-Jul-97	4.39	3.5	5.05	1.07	0.003	94		1.11	2.81
W16A	27-Aug-96	2.3	2.1	<0.010	0.463	0.01	27		0.64	5.80
W16A	8-Jul-97									
W16A	12-Jul-97	1.99	1.1	<0.006	0.119	0.007	18.9		1.18	5.60
W2	20-Jun-95	3.28	1.06	4.77	0.085	<0.005	20.1	25.9	0.67	11.1
W2	26-Aug-96									
W2	7-Jun-97	3.33	1.2	3.42	0.092	0.007	19.8		1.25	13.9
W25	21-Jun-95	3.79	1.82	2.45	0.108	<0.005	33.4	33.7	0.71	11.2
W25	13-Jul-97	3.87	2.0	2.2	0.086	0.003	31.3		1.16	14.2
W26	21-Jun-95	3.43	1.33	4.83	0.114	<0005	22.5	29.3	0.71	12.4
W26	16-Aug-95	3.48	1.34	5.07	0.097	0.006	23.4		1.26	12.1
W26	26-Aug-96									
W26	8-Jun-97	3.63	1.5	3.09	0.089	0.002	22.7		1.14	15.3
W26	26-Jul-97									
W27	16-Jul-95	1.75	1.23	0.2	0.164	0.007	22	22	0.77	6.87
W27	19-Jun-97	1.73	1.3	0.154	0.096	0.007	18.8		1.19	6.11
W3	23-Jun-95	2.69	1.09	0.014	<0.005	<0.005	16	14.2	0.67	8.52
W3	14-Jul-97	2.80	1.3	0.021	<0.003	0.004	16.5		1.12	8.35
W3A	23-Jun-95	1.36	0.14	0.024	0.012	0.092	4.5	6.83	0.63	4.36
W3A	14-Jul-97	1.14	0.2	0.009	0.009	0.131	2.5		1.18	4.31
W33	22-Aug-96	3.4	1.4	3	0.217	0.009	16.1		0.67	13.7
W33	7-Jul-97									
W34	22-Aug-96	3.4	2.1	<0.010	0.209	0.015	15.4		0.66	7.87
W34	10-Jun-97									
W34	14-Jul-97	2.09	1.4	0.023	0.021	0.028	11.4		1.22	5.66
W34	14-Jul-97									
W35	27-Aug-96	3.60	3.6	0.054	1.55	0.006	22.2		0.73	4.31
W35	11-Jul-97									
W36	26-Aug-96	1.80	1.6	<0.010	1.06	0.013	11.3		0.78	6.05
W36	27-Aug-96									
W36	17-Jun-97	1.32	0.6	<0.007	0.042	0.046	3.3		1.19	4.74
W6	26-Jul-97	3.60	2.5	21.5	0.355	0.002	37.9		12.3	6.14

Table 4-4. Geochemical data from water samples (continued).

Well ID	Date	NO3- (mg/L)	F- (mg/L)	Br- (mg/L)	Total Cations meq	Total Anions (meq) lab alk.	Total Anions (meq) field alk.	Charge Bal % lab alk.	Charge Bal % field alk.	Si (mg/L)
FS1-17	18-Jul-95	0.14		0	0.671	0.597	0.743	11.63	-10.21	
FS1-17	19-Jul-96	0.06	0.04	<0.01	0.71	0.56		23.7		5.01
FS1-25	20-Jul-96	0.13	0.06	0.02	1.89	0.93		68.11		6.64
FS1-35	20-Jul-96	0.01	0.06	<0.01	0.16	0.14		14.08		3.02
FS3C-19	14-Jul-95	0.15		0	0.164	0.215	0.201	-26.99	-20.3	
FS3C-19	18-Jul-96	0.02	0.06	<0.01	0.19	0.18		7.14		3.24
FS3C-24	15-Jul-95	0.08		0	0.232	0.272	0.301	-15.85	-25.81	
FS3C-24	18-Jul-96	0.03	0.04	<0.01	0.23	0.23		-0.41		4.12
FS3C-24	12-Jun-97	0.13	<0.05	<0.02	0.2	0.214		-6.68		3.49
FS3C-29	17-Jul-96	0.1	0.08	<0.01	0.21	0.22		-2.61		3.38
FS3C-29	11-Jun-97	0.16	0.01	<0.02	0.166	0.174		-4.27		2.77
FS4-WT	8-Jul-97	<0.10	0.06	<0.02	0.401	0.418		-4.11		4.33
R1-36	10-Jul-95	0.13		0	0.161	0.188	0.207	-15.33	-24.62	
R1-55	11-Jul-95									
RR1-PZ	21-Aug-95	10.5		0	4.846	5.078	4.793	-4.68	1.1	
S1 spring	6-Aug-97	0.62	0.05	<0.02	0.258	0.248		4.09		4.01
S3 seep	7-Aug-97	<0.10	0.05	<0.02	0.192	0.192		0.00		2.02
S40	1-Jan-96									
S40	25-Jul-97	<0.10	0.06	<0.02	0.156	0.174		-10.8		3.94
T1-8	12-Jul-95	0.18		0	0.206	0.333	0.443	-47.3	-73.2	
T1-8	26-Jun-97	<0.10	<0.05	<0.02	0.239	0.236		1.1		2.68
TR1-63	8-Jul-95	0.37		0	0.45	0.474	0.466	-5.31	-3.57	
TR1-63	25-Jun-97	0.30	0.06	<0.02	0.433	0.428		1.16		8.43
W11	25-Jul-97	0.89	0.04	<0.02	0.338	0.33		2.45		4.23
W15	28-Jul-97	<0.10	<0.05	<0.02	0.607	0.604		0.43		2.49
W16	28-Aug-96	<0.01	0.49	<0.01	1.82	1.66		8.99		11.4
W16	13-Jul-97	0.73	0.49	<0.02	1.734	1.668		3.87		11.9
W16A	27-Aug-96	0.09	0.1	<0.01	0.54	0.59		-9.04		7.7
W16A	8-Jul-97									
W16A	12-Jul-97	0.25	0.12	<0.02	0.421	0.470		-11.1		6.0
W2	20-Jun-95	0.08		0	0.699	0.581	0.676	18.5	3.38	
W2	26-Aug-96									
W2	7-Jun-97	<0.10	0.11	<0.02	0.675	0.655		3.03		9.2
W25	21-Jun-95	0.08		0	0.813	0.802	0.807	1.39	0.77	
W25	13-Jul-97	<0.10	0.22	<0.02	0.845	0.853		-1.01		8.66
W26	21-Jun-95	0.08		0	0.769	0.648	0.76	17.04	1.22	
W26	16-Aug-95	0.02		0	0.798	0.671		17.29		
W26	26-Aug-96									
W26	8-Jun-97	<0.10	0.15	<0.02	0.745	0.730		2.00		9.5
W26	26-Jul-97									
W27	16-Jul-95	0.17		0	0.497	0.528	0.528	-6.04	-6.04	
W27	19-Jun-97	<0.10	0.05	<0.02	0.471	0.472		-0.10		5.9
W3	23-Jun-95	0.09		0	0.411	0.46	0.43	-11.17	-4.55	
W3	14-Jul-97	<0.10	0.09	<0.02	0.466	0.481		-2.99		8.7
W3A	23-Jun-95	0.05		0	0.162	0.183	0.221	-12.53	-31.23	
W3A	14-Jul-97	<0.10	0.08	<0.02	0.166	0.168		-1.19		3.41
W33	22-Aug-96	<0.01	0.13	<0.01	0.66	0.57		13.61		9.8
W33	7-Jul-97									
W34	22-Aug-96	0.02	0.08	0.01	0.45	0.44		2.94		7.34
W34	10-Jun-97	0.25	0.05	<0.02	0.335	0.346		-3.06		6.52
W34	14-Jul-97									
W34	14-Jul-97									
W35	27-Aug-96	<0.01	0.07	<0.01	0.46	0.48		-3.07		7.2
W35	11-Jul-97									
W36	26-Aug-96	0.02	0.05	<0.01	0.33	0.34		-2.23		5.03
W36	27-Aug-96									
W36	17-Jun-97	<0.10	0.05	<0.02	0.183	0.192		-4.37		3.99
W6	26-Jul-97	1.79	0.05	0.02	1.141	1.128		1.2		8.85

Table 4-4. Geochemical data from water samples (continued).

Well ID	Date	B3+ (mg/L)	Ba2+ (mg/L)	Li+ (mg/L)	Cu (mg/L)	Zn (mg/L)	trace NO2	trace PO4	trace oxalate	Deuterium (per mil VSMOW)
FS1-17	18-Jul-95									-66.14
FS1-17	19-Jul-96	<0.005	0.005	0.014	0.016	0.275		y	y	-68.4
FS1-25	20-Jul-96	<0.005	0.009	0.016	0.011	0.005	y		y	-66.3
FS1-35	20-Jul-96	<0.005	0.011	0.002	0.121	0.018				-61.1
FS3C-19	14-Jul-95									-66.6
FS3C-19	18-Jul-96	<0.005	0.006	0.002	0.277	0.095				-62.4
FS3C-24	15-Jul-95									-67.02
FS3C-24	18-Jul-96	<0.005	0.003	0.002	0.303	0.178				-63.9
FS3C-24	12-Jun-97	<0.005	0.002	0.002	0.039	0.067				-69.83
FS3C-29	17-Jul-96	<0.005	0.004	0.004	0.841	0.14			y	-66.5
FS3C-29	11-Jun-97	<0.005	0.003	0.003	0.017	0.044				-70.58
FS4-WT	8-Jul-97	<0.005	0.016	0.004	0.018	0.040				-71.03
R1-36	10-Jul-95									-67.21
R1-55	11-Jul-95									-67.37
RR1-PZ	21-Aug-95									-59.88
S1 spring	6-Aug-97	<0.005	0.004	0.002	0.004	0.023				-64.67
S3 seep	7-Aug-97	<0.005	0.007	0.001	0.004	0.058				-68.16
S40	1-Jan-96									
S40	25-Jul-97	<0.005	0.006	0.002	0.010	0.021				-61.48
T1-8	12-Jul-95									-81.32
T1-8	26-Jun-97	<0.005	0.002	<0.001	0.007	0.176				-61.82
TR1-63	8-Jul-95									-67.26
TR1-63	25-Jun-97	<0.005	0.002	0.008	0.173	0.021				-65.41
W11	25-Jul-97	<0.005	0.004	<0.001	0.024	0.057				-65.67
W15	28-Jul-97	<0.005	0.006	0.002	0.003	1.70				-64.25
W16	28-Aug-96	<0.005	0.006	0.029	0.002	0.159				-64
W16	13-Jul-97	<0.005	0.007	0.027	0.002	0.189				-65.64
W16A	27-Aug-96	<0.005	0.003	0.013	0.006	0.028				-65.6
W16A	8-Jul-97									
W16A	12-Jul-97	<0.005	0.002	0.009	0.003	0.010				-63.55
W2	20-Jun-95									-49.51
W2	26-Aug-96									
W2	7-Jun-97	<0.005	0.004	0.008	0.004	0.046				-63.68
W25	21-Jun-95									-69.07
W25	13-Jul-97	<0.005	0.004	0.024	0.019	0.010				-66.89
W26	21-Jun-95									-65.01
W26	16-Aug-95									
W26	26-Aug-96									
W26	8-Jun-97	<0.005	0.004	0.012	0.004	0.041				-64.56
W26	26-Jul-97									
W27	16-Jul-95									-68.97
W27	19-Jun-97	<0.005	0.004	0.004	0.002	0.008				-66.75
W3	23-Jun-95									-63.31
W3	14-Jul-97	<0.005	0.001	0.008	0.124	0.009				-66.13
W3A	23-Jun-95									-65.83
W3A	14-Jul-97	<0.005	0.003	0.001	0.007	0.028				-69.15
W33	22-Aug-96	<0.005	0.003	0.01	0.007	0.023				-63.2
W33	7-Jul-97									
W34	22-Aug-96	<0.005	0.002	0.009	0.016	0.032	y			-66.4
W34	10-Jun-97	<0.005	0.001	0.006	0.004	0.046				-66.41
W34	14-Jul-97									
W34	14-Jul-97									
W35	27-Aug-96	<0.005	0.004	0.003	0.005	0.027				-64.4
W35	11-Jul-97									
W36	26-Aug-96	<0.005	0.004	0.002	0.005	0.016				
W36	27-Aug-96									
W36	17-Jun-97	<0.005	0.003	0.002	0.004	0.011				-66.00
W6	26-Jul-97	<0.005	0.004	0.024	0.003	0.366				-69.20

Table 4-4. Geochemical data from water samples (continued).

Well ID	Date	Oxygen-18 (per mil VSMOW)	Tritium TU	Tritium 1 sig TU	C-13 (per mil VPDB)	CFC-11a	CFC-11b	CFC-11c	CFC-12a	CFC-12b
FS1-17	18-Jul-95	-10.14	13.1	0.4	-22.81	9025.8	5455.4	4206.8	392.8	366.9
FS1-17	19-Jul-96	-10.37	12	0.4	-21.9	6214	8481.4	6223.2	85.8	389.2
FS1-25	20-Jul-96	-10.11	13.2	0.4	-15.7	9403.3	88830.6	9083.3	427.1	393.6
FS1-35	20-Jul-96	-9.42	10.3	0.4	-24.5	ERR	ERR	ERR	1089.6	1355.5
FS3C-19	14-Jul-95	-10.08	12.5	0.4	-16.4	1110.7	1096.3	1060.5	408.7	417.3
FS3C-19	18-Jul-96	-9.71	9.9	0.3	-24.7	812.9	786.6	860.4	389.3	382.7
FS3C-24	15-Jul-95	-10.12	12.3	0.4	-24.05	1116.5	1135.2	1092.7	439.2	461.1
FS3C-24	18-Jul-96	-9.97	11.8	0.4	-20.1	939.8	953.1	976.1	396.5	402.7
FS3C-24	12-Jun-97	-10.58	8.80	0.4	-21.50					
FS3C-29	17-Jul-96	-9.84	10.3	0.4	-20.5	952.3	680	931.7	382.2	281.7
FS3C-29	11-Jun-97	-10.87	9.70	0.4	-17.57					
FS4-WT	8-Jul-97	-10.66	11.80	0.5	-17.16					
R1-36	10-Jul-95	-10.14	12.8	0.4	-22.57	922.1	922.9	892.5	422.1	421
R1-55	11-Jul-95	-9.95	11.1	0.4	-13.52	ERR	342.1	ERR	609.5	441.6
RR1-PZ	21-Aug-95	-9.01	13.7	0.4	-20.76	4133.8	4255.1	4421.6	411.5	376.4
S1 spring	6-Aug-97	-9.99	8.50	0.4	-19.19					
S3 seep	7-Aug-97	-10.37	10.10	0.4	-28.14					
S40	1-Jan-96		12.1	0.4						
S40	25-Jul-97	-9.36	12.60	0.5	-27.10					
T1-8	12-Jul-95	-12.02	9.4	0.3	-16.35	781.8	727.8	736.1	407.2	374.3
T1-8	26-Jun-97	-9.31	8.70	0.4						
TR1-63	8-Jul-95	-10.06	12.2	0.4	-23.42	5770.7	5561	5181.4	347.9	361.4
TR1-63	25-Jun-97	-9.92	11.20	0.5						
W11	25-Jul-97	-9.73	10.30	0.5	-22.31					
W15	28-Jul-97	-9.76	11.00	0.5	-21.51					
W16	28-Aug-96	-9.91	3.4	0.18	-10.6	59.8	89.4	94.3	31.7	42.8
W16	13-Jul-97	-9.88	3.40	0.3	-10.21					
W16A	27-Aug-96	-9.91	11.8	0.4	-18.1	569.3	600	664	303.8	430.4
W16A	8-Jul-97									
W16A	12-Jul-97	-9.85	9.90	0.5	-16.94					
W2	20-Jun-95	-5.62	16.6	0.5	-21.48	8.9	11.2		240	250
W2	26-Aug-96									
W2	7-Jun-97	-9.71	14.80	0.6	-20.96					
W25	21-Jun-95	-10.4			-20.54	137.2	165.7	161.3	166.8	178
W25	13-Jul-97	-10.25	24.40	0.8	-20.25					
W26	21-Jun-95	-9.97	22.4	0.7		6.4	3.9	4.6	172.7	193.3
W26	16-Aug-95									
W26	26-Aug-96									
W26	8-Jun-97	-9.87	17.80	0.6	-20.66					
W26	26-Jul-97									
W27	16-Jul-95	-10.66	12.1	0.4	-23.65	784.5		783.8	390.6	
W27	19-Jun-97	-9.96	9.20	0.4						
W3	23-Jun-95	-9.79	14.4	0.4		503.6	507.5	507.9	333.6	342.4
W3	14-Jul-97	-9.85	12.00	0.5	-22.54					
W3A	23-Jun-95	-10.07	12.5	0.4	-12.67	932.4	947.8	921	423.4	430.7
W3A	14-Jul-97	-10.60	9.60	0.4	-19.24					
W33	22-Aug-96	-9.74	12.8	0.4	-20.6	389	58.9	514.1	254.8	247.9
W33	7-Jul-97	-9.76	14.20	0.6	-20.83					
W34	22-Aug-96	-9.98	12	0.4						
W34	10-Jun-97	-10.22	10.90	0.5	-24.78					
W34	14-Jul-97									
W34	14-Jul-97									
W35	27-Aug-96	-9.79	10.6	0.4	-20.7					
W35	11-Jul-97	-10.15	10.10	0.5						
W36	26-Aug-96		10.1	0.3	-23.3	753.8	737.8	734.4	385.6	387.9
W36	27-Aug-96									
W36	17-Jun-97	-9.98	9.50	0.4	-18.92					
W6	26-Jul-97	-10.45	10.70	0.5	-21.20					

Table 4-4. Geochemical data from water samples (continued).

Well ID	Date	CFC-12c	CFC-113a	CFC-113b	CFC-113c	CFC-11 avg	CFC-12 avg	CFC-113 avg	oldage CFC-11	oldage CFC-12
FS1-17	18-Jul-95	359.3	ERR	63.6	75.7				contam.	6
FS1-17	19-Jul-96	386	48.8	149.4	106.2				contam.	28
FS1-25	20-Jul-96	372.3	224.1	162	119.9				contam.	7.5
FS1-35	20-Jul-96	1128.7	ERR	ERR	ERR				ERR	contam.
FS3C-19	14-Jul-95	419.9	118	131.3	129.5	1089.17	415.3	126.267	contam.	0
FS3C-19	18-Jul-96	377.8	163.6	148.4	153.2				11	7
FS3C-24	15-Jul-95	432.9	242.9	214.5	205	1114.8	444.4		contam.	0
FS3C-24	18-Jul-96	386.2	154.2	161.1	145.8				7	6.5
FS3C-24	12-Jun-97									
FS3C-29	17-Jul-96	381.8	182.8	130.1	169.1				14	13.5
FS3C-29	11-Jun-97									
FS4-WT	8-Jul-97									
R1-36	10-Jul-95	421.1	175.5	173.4	181.7	912.5	421.4		6	0
R1-55	11-Jul-95	234.6	ERR	ERR	ERR				22	15
RR1-PZ	21-Aug-95	415.6	163.4	191	159				contam.	4
S1 spring	6-Aug-97									
S3 seep	7-Aug-97									
S40	1-Jan-96									
S40	25-Jul-97									
T1-8	12-Jul-95	377.5	102.3	105.6	110.3				10.5	4.5
T1-8	26-Jun-97									
TR1-63	8-Jul-95	351.6	80.9	87.5	82.3				contam.	7
TR1-63	25-Jun-97									
W11	25-Jul-97									
W15	28-Jul-97									
W16	28-Aug-96	40.9	57.5	26.7	29.6				34	35.5
W16	13-Jul-97									
W16A	27-Aug-96	313.1	102.9	107.3	98				18	12
W16A	8-Jul-97									
W16A	12-Jul-97									
W2	20-Jun-95		0	0		10.05	245	0	41.5	14.5
W2	26-Aug-96									
W2	7-Jun-97									
W25	21-Jun-95	171	11.3	15.3	15.1	154.733	172	13.9	28	20.5
W25	13-Jul-97									
W26	21-Jun-95	180.1	0	0	0	4.96667	182	0	44	20.5
W26	16-Aug-95									
W26	26-Aug-96									
W26	8-Jun-97									
W26	26-Jul-97									
W27	16-Jul-95	398.8	102.5		97.7	784.15	395	100.1	9	2.5
W27	19-Jun-97									
W3	23-Jun-95	340.2	59	62.3	62.7	506.333	338.667	61.3333	18	8
W3	14-Jul-97									
W3A	23-Jun-95	424.1	104.4	105.4	92.6	933.733	426	100.533	1.5	0
W3A	14-Jul-97									
W33	22-Aug-96	234.9	15.7	5.4	13.9				34	17
W33	7-Jul-97									
W34	22-Aug-96									
W34	10-Jun-97									
W34	14-Jul-97									
W34	14-Jul-97									
W35	27-Aug-96									
W35	11-Jul-97									
W36	26-Aug-96	430.6	115.3	190.7	230.1				12	6.5
W36	27-Aug-96									
W36	17-Jun-97									
W6	26-Jul-97									

Table 4-4. Geochemical data from water samples (continued).

Well ID	Date	oldage CFC-113	CH4 (mg/L)	CH4 b	CO2 (mg/L)	CO2 b	N2 (mg/L)	N2 b	O2 (mg/L)	O2 b
FS1-17	18-Jul-95	10.5								
FS1-17	19-Jul-96	14								
FS1-25	20-Jul-96	6								
FS1-35	20-Jul-96	ERR								
FS3C-19	14-Jul-95	3.5								
FS3C-19	18-Jul-96	contam.								
FS3C-24	15-Jul-95	contam.								
FS3C-24	18-Jul-96	contam.								
FS3C-24	12-Jun-97		0.0000		18.735		17.270		8.655	
FS3C-29	17-Jul-96	4.5								
FS3C-29	11-Jun-97									
FS4-WT	8-Jul-97		0.0003	0.0003	60.638	75.126	17.776	20.749	5.447	5.352
R1-36	10-Jul-95	contam.	0		6.8		28.04		11.7	
R1-55	11-Jul-95	ERR	0.486		0.1		21.86		0.2	
RR1-PZ	21-Aug-95	contam.								
S1 spring	6-Aug-97									
S3 seep	7-Aug-97									
S40	1-Jan-96									
S40	25-Jul-97		0.0174	0.0350	37.805	37.957	16.420	18.105	0.662	0.740
T1-8	12-Jul-95	6	0.013		14.6		19.71		4.7	
T1-8	26-Jun-97		0.0574	0.0488	16.640	17.325	18.701	18.709	4.100	4.229
TR1-63	8-Jul-95	8.5	0		11.6		20.55		8.6	
TR1-63	25-Jun-97		0.0000		10.322		21.804		10.576	
W11	25-Jul-97		0.0000	0.0000	36.689	36.163	21.534	19.509	8.186	7.426
W15	28-Jul-97		0.0139	0.0130	25.765	25.443	18.507	18.434	0.678	0.700
W16	28-Aug-96	18.5	0.5624	0.5663	3.648	2.775	21.55	20.963	0.248	0.115
W16	13-Jul-97		0.1891	0.2847	12.883	12.274	21.248	21.214	0.020	0.080
W16A	27-Aug-96	8.5								
W16A	8-Jul-97		0.0005	0.0005	16.731	16.974	19.708	19.416	5.511	5.432
W16A	12-Jul-97		0.0000	0.0009	15.093	15.050	18.768	18.670	6.833	6.839
W2	20-Jun-95	>30.5								
W2	26-Aug-96		0.0011		19.911		19.507		0.405	
W2	7-Jun-97		0.0000		9.298		16.818		0.048	
W25	21-Jun-95	25.5								
W25	13-Jul-97		0.0000	0.0000	7.425	7.450	21.482	21.485	0.061	0.033
W26	21-Jun-95	>30.5								
W26	16-Aug-95									
W26	26-Aug-96		0		7.083		20.759		0.018	
W26	8-Jun-97		0.0000		13.576		18.865		0.402	
W26	26-Jul-97									
W27	16-Jul-95	6.5								
W27	19-Jun-97		0.0024		19.698		18.503		3.831	
W3	23-Jun-95	11								
W3	14-Jul-97		0.0006	0.0007	17.304	17.317	21.014	20.751	2.682	2.762
W3A	23-Jun-95	6								
W3A	14-Jul-97		0.0000	0.0000	36.813	37.075	20.366	21.253	3.660	3.961
W33	22-Aug-96	30.5	0		6.81		20.32		0.376	
W33	7-Jul-97		0.0004	0.0005	7.968	7.735	20.100	20.291	0.027	0.065
W34	22-Aug-96		0.0014		7.14		20.15		3.618	
W34	10-Jun-97		0.0000		6.285		17.481		8.253	
W34	14-Jul-97		0.0000	0.0001	8.498	8.795	19.384	19.368	7.757	7.239
W34	14-Jul-97		0.0000		8.773		19.526		7.499	
W35	27-Aug-96		0.0051		14.571		34.163		5.947	
W35	11-Jul-97		0.0052	0.0060	21.778	21.049	21.397	21.502	5.693	6.086
W36	26-Aug-96	6.5	0.0025		19.308		19.106		4.005	
W36	27-Aug-96		0.0029		18.707		20.775		4.298	
W36	17-Jun-97		0.0000		19.284		17.639		9.285	
W6	26-Jul-97		0.7135	0.9744	12.952	10.973	19.729	19.838	0.000	0.015

Table 4-4. Geochemical data from water samples (continued).

Well ID	Date	Ar (mg/L)	Ar b	Lab notes
FS1-17	18-Jul-95			
FS1-17	19-Jul-96			FE dropping out in FU
FS1-25	20-Jul-96			
FS1-35	20-Jul-96			
FS3C-19	14-Jul-95			
FS3C-19	18-Jul-96			
FS3C-24	15-Jul-95			
FS3C-24	18-Jul-96			
FS3C-24	12-Jun-97	0.7073		
FS3C-29	17-Jul-96			
FS3C-29	11-Jun-97			
FS4-WT	8-Jul-97	0.6725	0.7257	downhole °C
R1-36	10-Jul-95	0.8659		
R1-55	11-Jul-95	0.7812		
RR1-PZ	21-Aug-95			
S1 spring	6-Aug-97			spring °C
S3 seep	7-Aug-97			downhole °C
S40	1-Jan-96			
S40	25-Jul-97	0.6096	0.6330	
T1-8	12-Jul-95	0.7279		
T1-8	26-Jun-97	0.7030	0.7036	
TR1-63	8-Jul-95	0.7328		
TR1-63	25-Jun-97	0.7849		
W11	25-Jul-97	0.7629	0.7427	
W15	28-Jul-97	0.6767	0.6618	
W16	28-Aug-96	0.7721	0.7543	Fe dropping out in FU
W16	13-Jul-97	0.7715	0.7708	
W16A	27-Aug-96			
W16A	8-Jul-97	0.7393	0.7356	
W16A	12-Jul-97	0.7077	0.7089	
W2	20-Jun-95			
W2	26-Aug-96	0.7361		
W2	7-Jun-97	0.6620		
W25	21-Jun-95			
W25	13-Jul-97	0.7800	0.7760	
W26	21-Jun-95			
W26	16-Aug-95			
W26	26-Aug-96	0.7496		
W26	8-Jun-97	0.7125		
W26	26-Jul-97			
W27	16-Jul-95			
W27	19-Jun-97	0.7054		
W3	23-Jun-95			
W3	14-Jul-97	0.7661	0.7632	
W3A	23-Jun-95			
W3A	14-Jul-97	0.7507	0.7738	
W33	22-Aug-96	0.7262		Fe dropping out in FU
W33	7-Jul-97	0.7570	0.7618	
W34	22-Aug-96	0.7368		
W34	10-Jun-97	0.6774		
W34	14-Jul-97	0.7219	0.7236	
W34	14-Jul-97	0.7175		
W35	27-Aug-96	0.9135		diss.gas leaked?
W35	11-Jul-97	0.7708	0.7636	downhole °C
W36	26-Aug-96	0.7124		4 CFC analyses
W36	27-Aug-96	0.7475		
W36	17-Jun-97	0.7012		
W6	26-Jul-97	0.6980	0.7064	

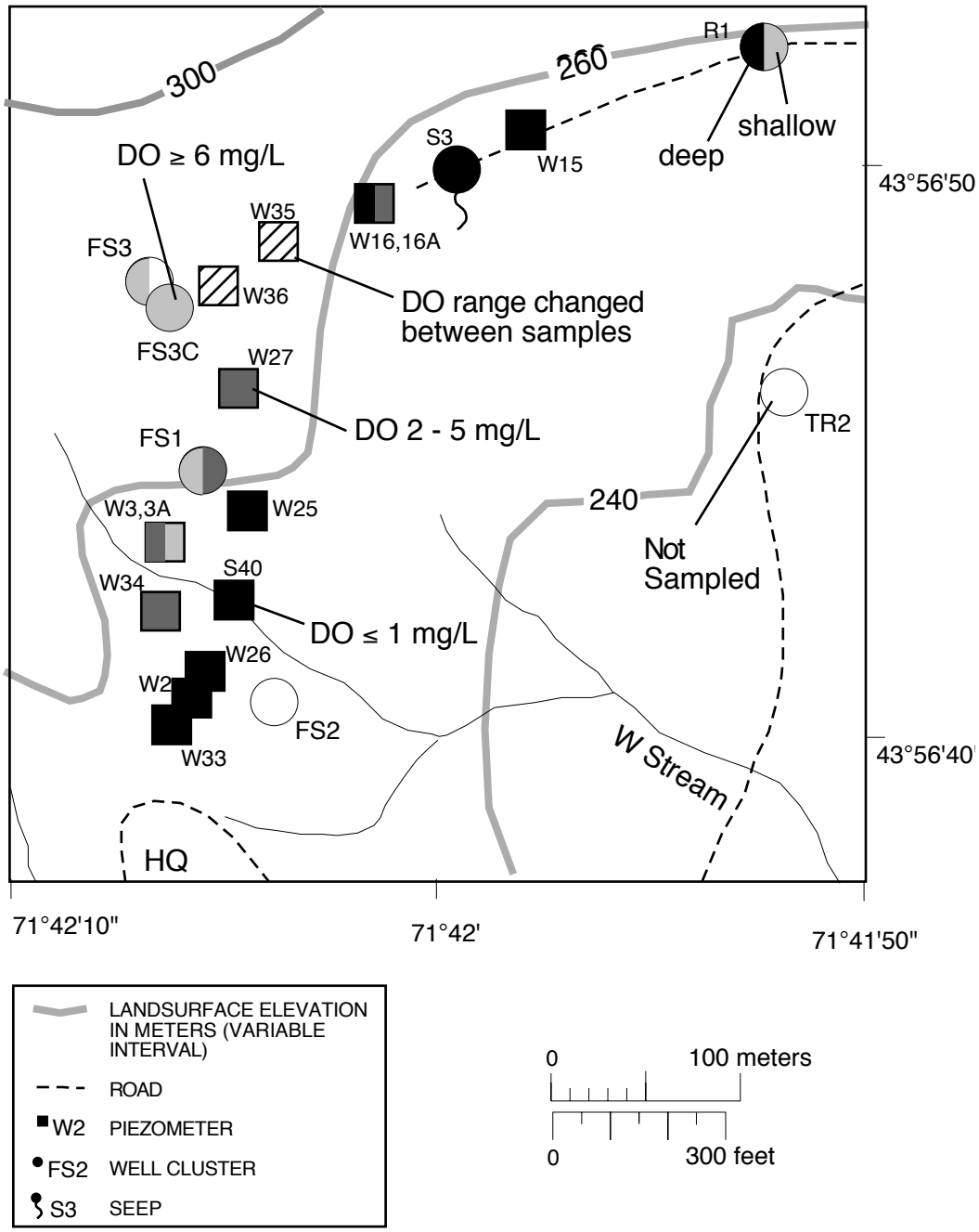

Figure 4-13 Spatial distribution of dissolved oxygen concentrations in water samples from piezometers at the Mirror Lake site, Grafton County, New Hampshire.

Major ion concentrations characterize the overall water quality of the shallow ground-water in the Mirror Lake watershed (Table 4-4). The general water type is calcium-bicarbonate-sulfate in piezometers (fig. 4-14). Outliers include: RR1-PZ located below the Mirror Lake watershed between Route 3 and the Pemigewasset River in an agricultural area; W6 located adjacent to Mirror Lake Road, also contains nitrate; W11 behind an experimental sand plot that has been fertilized, also contains nitrate; FS1-25

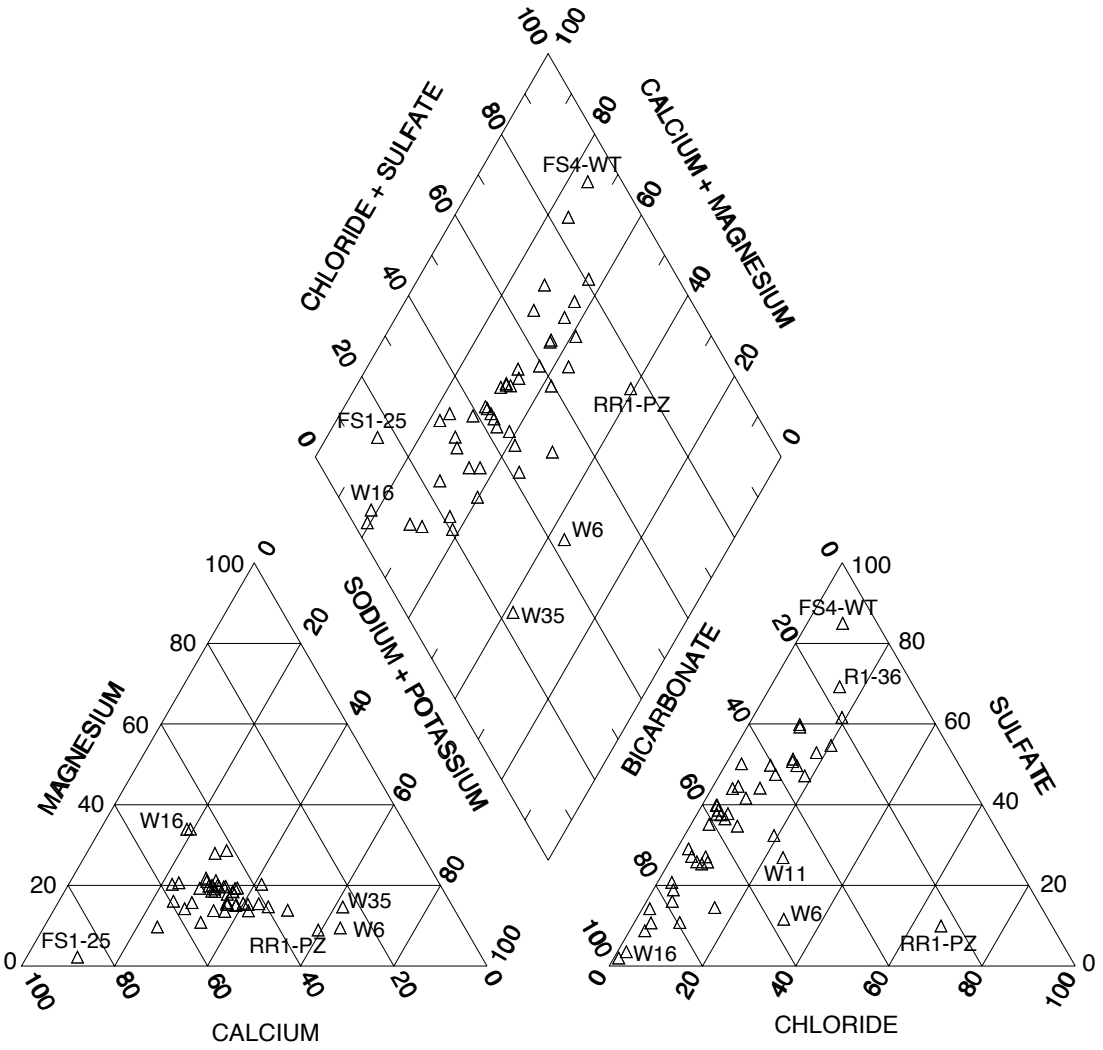

Figure 4-14 Piper plot of major ions in samples from piezometers.

apparently contaminated from well construction materials; W16, a steel well screened several meters below the water table; and R1-36, a high-yielding well with low alkalinity and high sulfate. New piezometers for this study include FS4-WT, installed high in the watershed near the basin divide, that has low alkalinity and high sulfate, and that also contains high CO_2; and W35 that contains high potassium.

Nitrogen and argon dissolved gas concentrations (Table 4-4) indicate that little excess air is present near the water table, and that the recharge temperature is between 5 and 10°C (fig. 4-15). Concentrations of dissolved nitrogen gas and argon in ground water are used to infer the recharge temperature and excess air amounts (Heaton and Vogel, 1981). These quantities are used in turn to determine equilibrium air concentrations from measured water concentrations to date ground water by the CFC method (Busenberg and Plummer, 1992). In contrast to samples from bedrock wells at Mirror Lake (Busenberg and Plummer, 1996), nitrogen and argon concentrations fall approximately along the line corresponding to equilibration with the atmosphere. This suggests that the elevated argon and nitrogen in bedrock waters is not due to entrapped or excess air, but is caused by some other in situ production.

Methane is observed in several samples from water-table piezometers. Measurable methane and lack of DO are consistent with methanogenic biodegradation conditions near the water table.

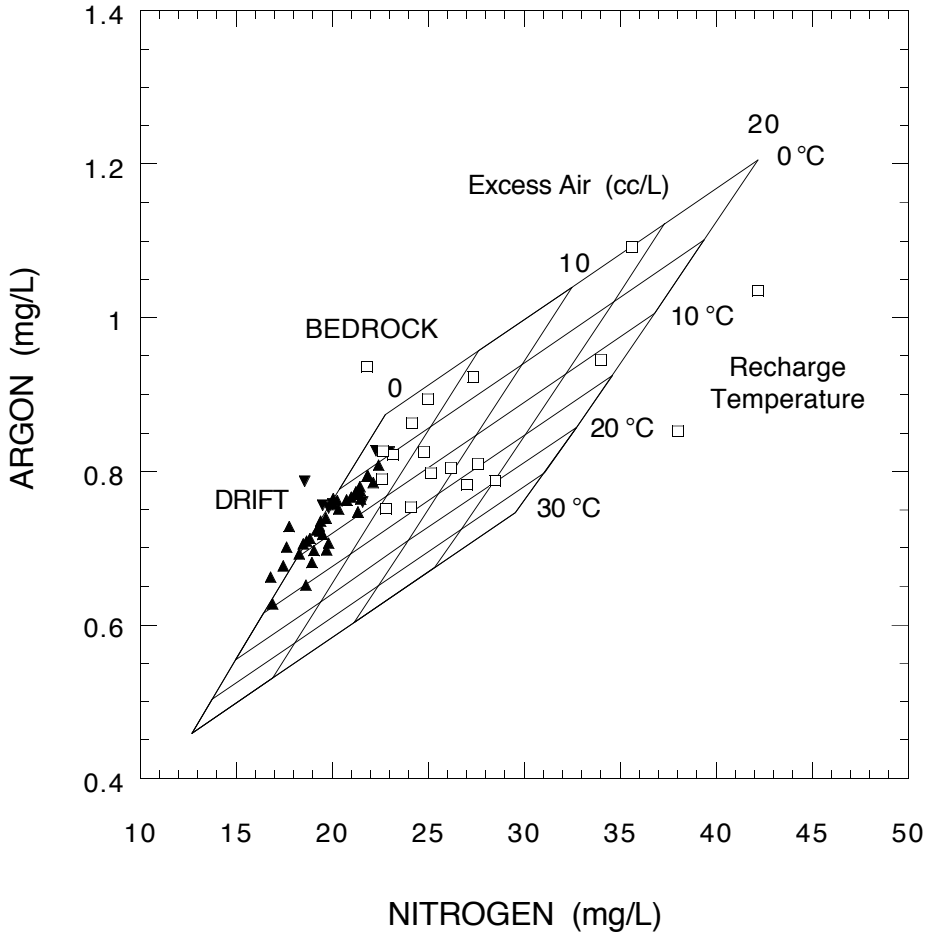

Figure 4-15 Concentrations of dissolved argon and nitrogen in water samples from piezometers (solid symbols) and packer-isolated zones of bedrock wells (open symbols) at the Mirror Lake site, Grafton County, New Hampshire. The superposed grid indicates the concentrations of argon and nitrogen in water that is in equilibrium with the atmosphere as a function of temperature, and that contains varying volumes of entrapped dissolved air.

4.3.4 Chlorofluorocarbon Concentrations

CFC concentrations in water samples from shallow piezometers range from zero to levels greater than those in equilibrium with the modern (1995-1997) atmosphere (Table 4-4). Many samples do contain CFC concentrations near modern atmospheric-equilibrium levels, which are about 950, 450, and 150 pg/kg for CFC-11, -12, and -113, respectively (at 7 °C). This observation supports use of CFC concentrations to date saturated-zone ground water.

Many samples contain CFC concentrations higher than those in equilibrium with the atmosphere (fig. 4-16). Following Busenberg and Plummer (1992), these samples are designated "contaminated." In some cases, contamination of samples was so high that the analytical procedures used to concentrate the normal low levels resulted in analytical responses beyond the instrumentation limits ("ERR" results in Table 4-4).

However, many samples contain CFC concentrations significantly less than those in equilibrium with the modern atmosphere. A preliminary review of the data indicated that CFC concentrations were highly correlated with dissolved oxygen (DO) concentrations. For this reason, the CFC data are plotted here against DO (fig. 4-17).

CFC-12 concentrations range from about 170 pg/kg to about 2,300 pg/kg (Table 4-4). For uncontaminated samples, CFC-12 concentrations are correlated with DO (fig. 4-17). Samples containing zero or very small amounts of oxygen, have CFC-12 concentrations about 1/3 of the concentration of water in equilibrium with modern air. High oxygen concentrations correspond to CFC-12 concentrations near modern levels.

Concentrations of CFC-11 range from zero to 88,000 pg/kg (Table 4-4). Some samples were so highly contaminated with CFC-11 that quantification of the concentrations was not analytically possible (Table 4-4). For uncontaminated samples, CFC-11 concentrations are strongly correlated with DO (fig. 4-18). Samples containing

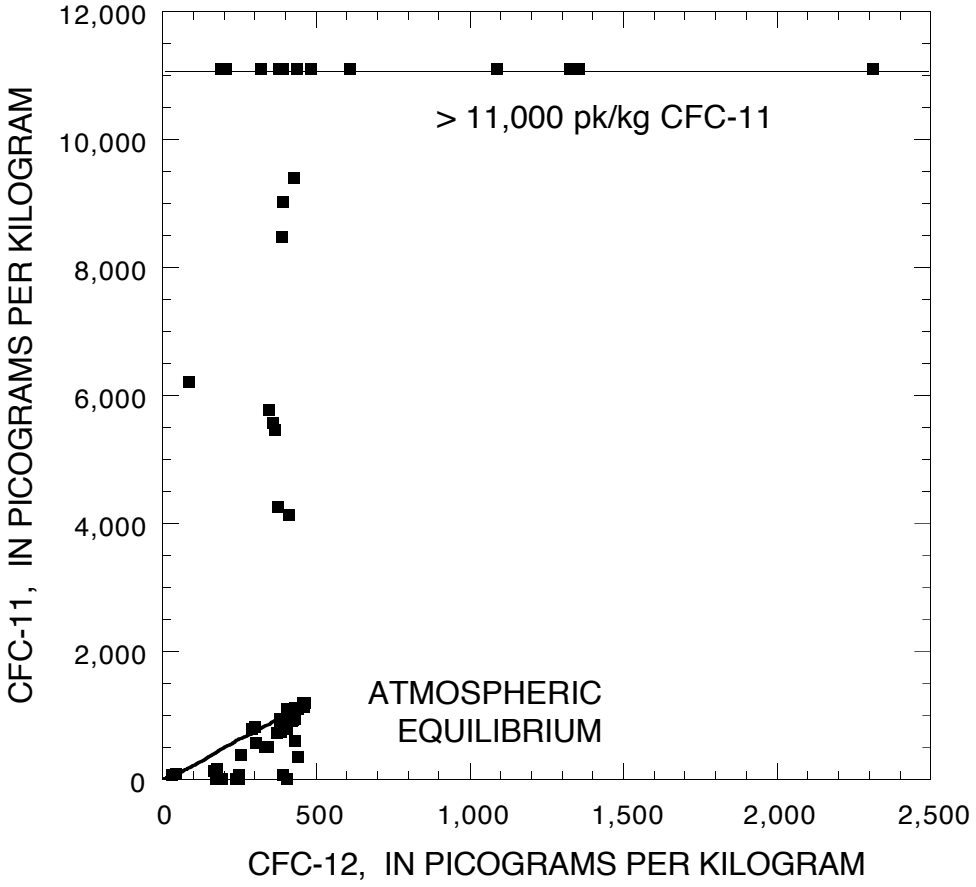

Figure 4-16 Concentrations of CFC-11 and CFC-12 in water samples from water-table piezometers at the Mirror Lake site, Grafton County, New Hampshire. The dashed line is the concentrations in water in equilibrium with the atmosphere during the last 50 years (at 7 °C). The horizontal line indicates CFC-11 concentrations greater than 11,000 pg/kg.

zero or very small amounts of oxygen, also contain zero or very small amounts for CFC-11. High oxygen concentrations corresponds to CFC-11 concentrations near modern levels. Taken at face value, these CFC-11 concentrations corresponds to ages of 0 years, for the high concentrations, to ages of more than 45 years, for the zero-CFC-11 waters.

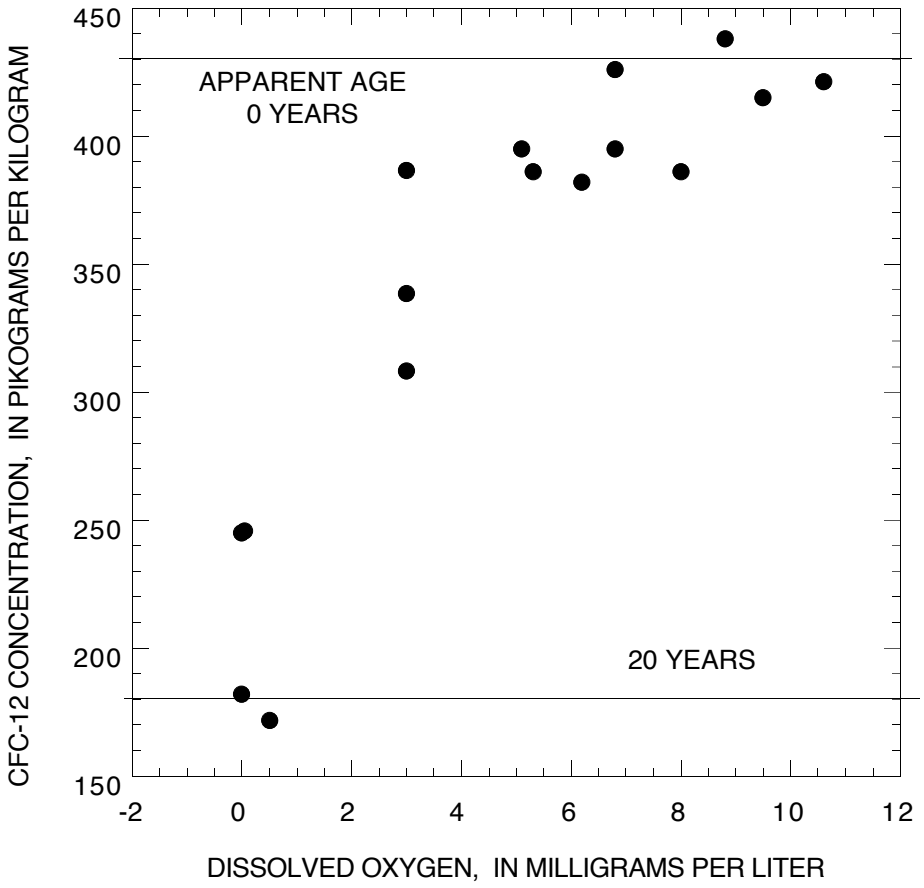

Figure 4-17 Concentrations of CFC-12 and dissolved oxygen in water samples from piezometers at the Mirror Lake site, Grafton County, New Hampshire. The horizontal lines correspond to CFC-12 concentrations in water equilibrated with the atmosphere at the time of sampling (0 years) and 20 years before sampling.

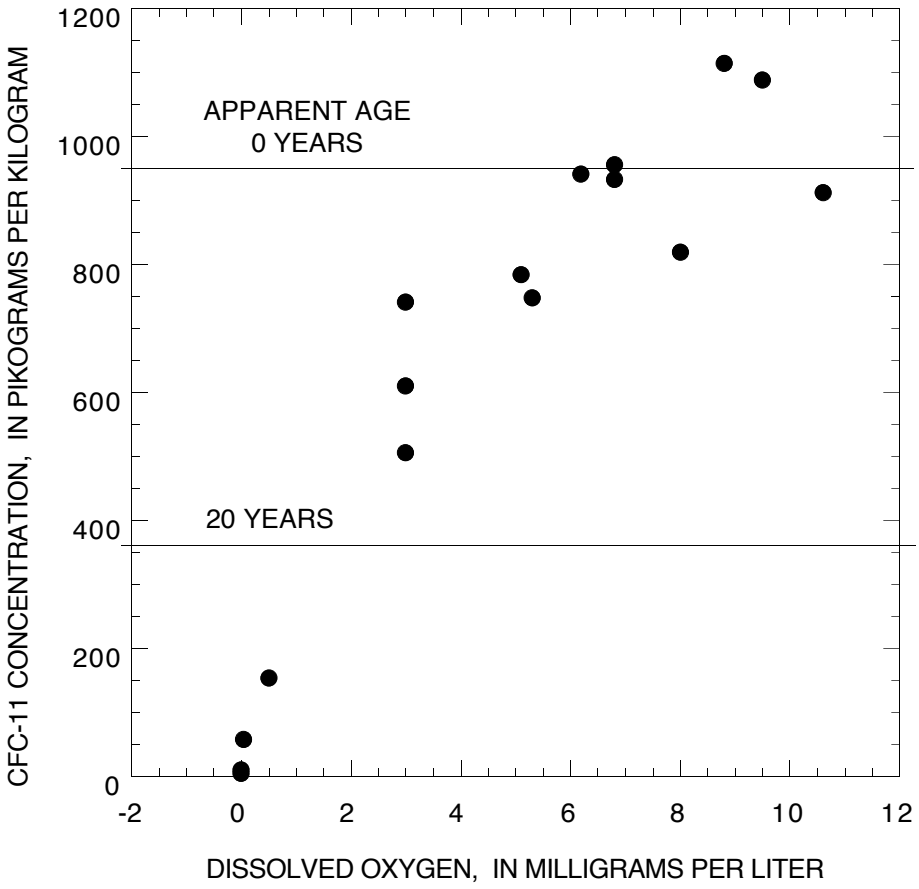

Figure 4-18 Concentrations of CFC-11 and dissolved oxygen in water samples from piezometers at the Mirror Lake site, Grafton County, New Hampshire. The horizontal lines correspond to CFC-11 concentrations in water equilibrated with the atmosphere at the time of sampling (0 years) and 20 years before sampling.

Concentrations of CFC-113 range from zero to 240 pg/kg (Table 4-4). Some samples were so highly contaminated with CFC-113 that quantification of the concentrations was not analytically possible (Table 4-4). For uncontaminated samples, CFC-113 concentrations are strongly correlated with DO (fig. 4-19). Samples containing

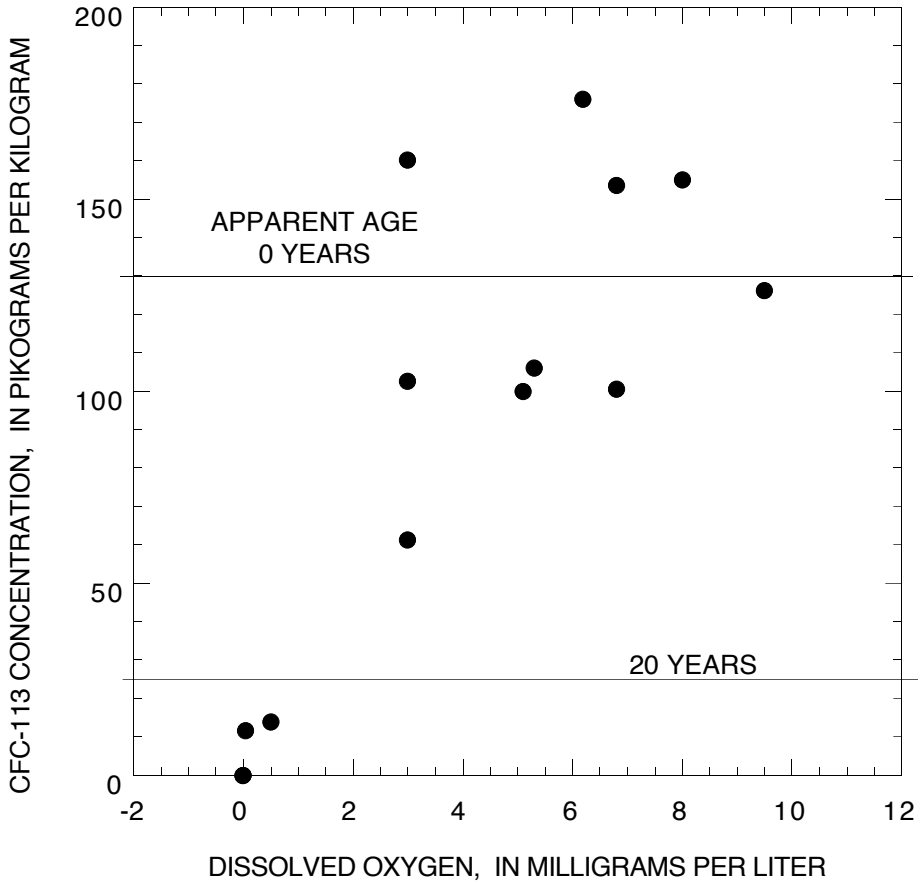

Figure 4-19 Concentrations of CFC-113 and dissolved oxygen in water samples from piezometers at the Mirror Lake site, Grafton County, New Hampshire. The horizontal lines correspond to CFC-113 concentrations in water equilibrated with the atmosphere at the time of sampling (0 years) and 20 years before sampling.

zero or very small amounts of oxygen, also contain zero or very small amounts for CFC-113. High oxygen concentrations corresponds to CFC-113 concentrations near modern levels. The scatter in CFC-113 concentrations in high-DO samples is larger than the scatter for either CFC-12 or CFC-11.

The observed CFC-12 and CFC-11 concentrations indicate that some process is, or several processes are, modifying the concentrations from atmospheric equilibrium (fig. 4-20). Water isolated from the atmosphere during the last 50 years should have CFC-12 and CFC-11 concentrations that lie on the atmospheric equilibrium line shown in Figure 4-21 if the only process affecting concentrations is advection with moving saturated-zone ground water. The fact that most samples fall below this line indicate that more CFC-11 has been removed relative to CFC-12.

The similarity between the correlations of CFC-11 and CFC-12 to DO is shown in Figure 4-21. The only major difference is that the lowest CFC-12 concentrations correspond to about 1/3 of modern levels, whereas the lowest CFC-11 concentrations are zero. The correlation between CFC-113 and DO is essentially the same as the CFC-11 pattern, but with more scatter at the upper concentration levels.

The hypothetical mixing line of Figures 4-20 and 4-21 corresponds to concentrations of CFC-11 and -12, and dissolved oxygen, in a volumetric mixture of two end-members waters: (a) anaerobic water containing no CFC-11 and 150 pg/kg CFC-12, and (b) water containing 7 mg/L DO, 950 pg/kg CFC-11, and 430 pg/kg CFC-12. Without this mixing, the apparent degradation of CFC's in the presence of 1 to 4 mg/L of dissolved oxygen is difficult to explain because it is assumed that degradation is limited to anaerobic conditions.

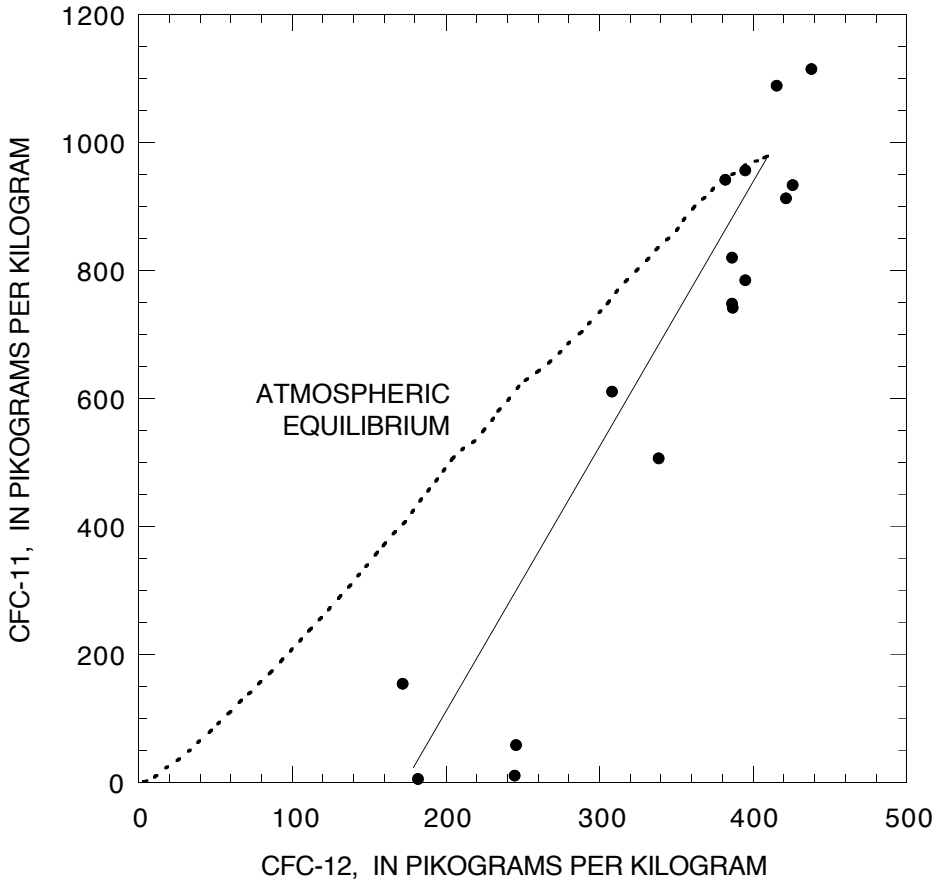

Figure 4-20 Concentrations of CFC-11 and CFC-12 in water samples from water-table piezometers at the Mirror Lake site, Grafton County, New Hampshire. The dashed line is the concentrations in water in equilibrium with the atmosphere during the last 50 years (at 7 °C). The solid line is a suggested mixing line.

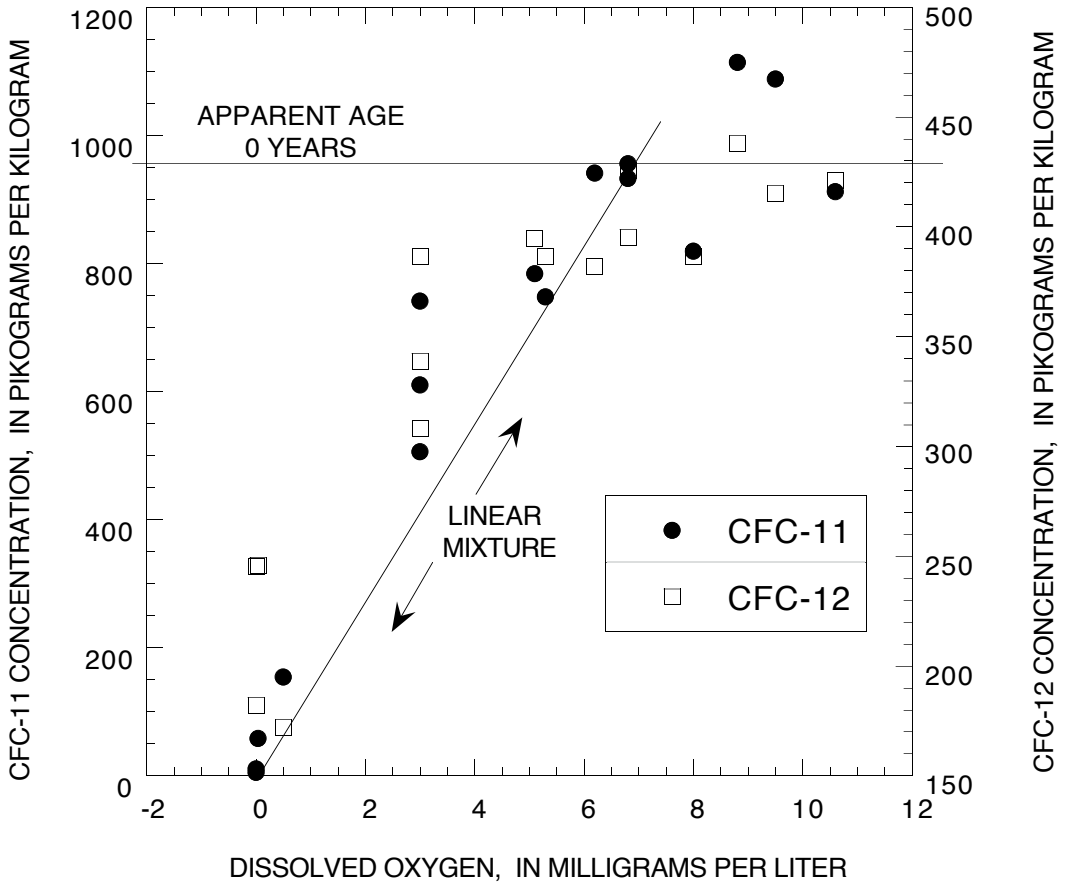

Figure 4-21 Concentrations of CFC-11, CFC-12, and dissolved oxygen in water samples from water-table piezometers at the Mirror Lake site, Grafton County, New Hampshire. The horizontal line corresponds to CFC-11 and CFC-12 concentrations in water equilibrated with the atmosphere at the time of sampling. The solid line is a suggested mixing line.

The relation between CFC-11 and tritium in samples from water-table piezometer is shown in Figure 4-22. Assuming an equilibration temperature of 7 °C, the CFC-11 concentration in water recharged in 1963 would be about 62 pg/kg. The concentration of tritium in waters recharged in 1963, accounting for subsequent radioactive decay until

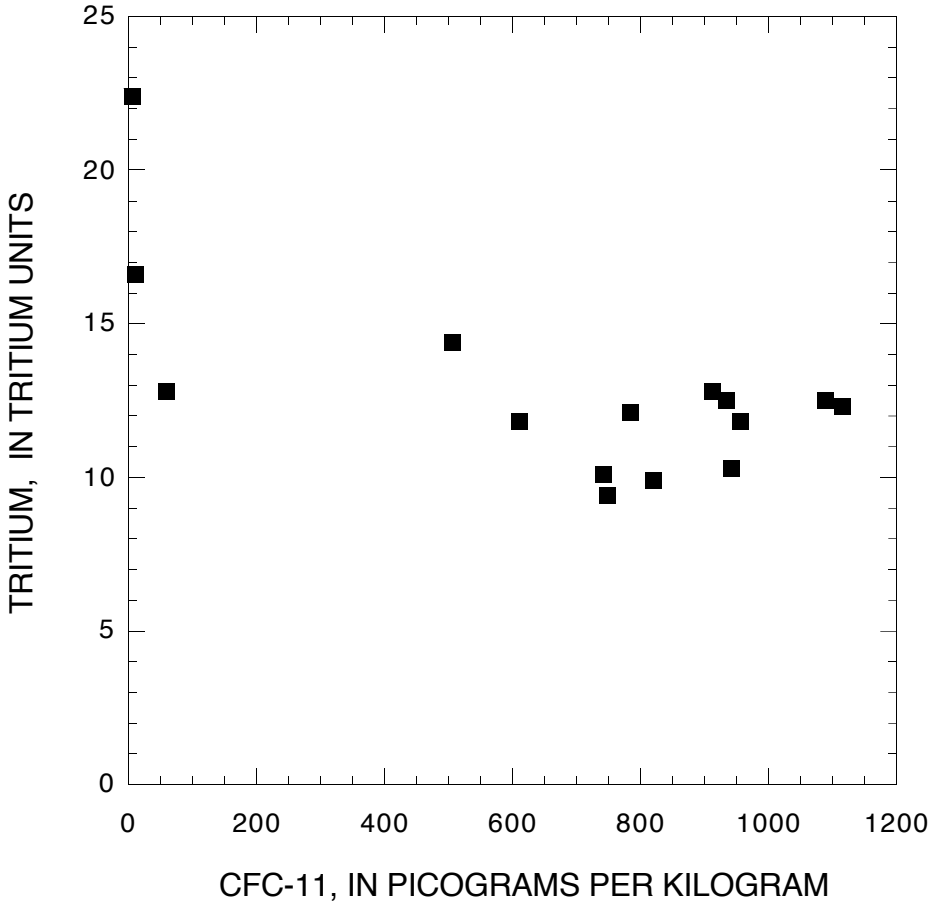

Figure 4-22 Concentrations of CFC-11 and tritium in water samples from piezometers at the Mirror Lake site, Grafton County, New Hampshire.

1995, would be more than 150 tritium units (TU). Thus, under ideal conditions, water samples containing about 63 pg/kg CFC-11 should also contain more than 150 TU tritium. Almost all measured tritium concentrations are about 10-15 TU. The highest observed tritium is 23 TU in a water sample containing no CFC-11. Based on the age-dating assumptions, a sample containing zero CFC-11 was recharged prior to 1945. Tritium in recharge in 1945, decayed to 1995, would amount to less than 5 TU, and older

waters would contain even less tritium. All of these tritium concentrations are significantly below bomb-peak levels dating from the late 50's and early 60's. Busenberg and Plummer (1996) estimate that peak tritium levels in precipitation in New Hampshire from the early 1960's decayed to 1992 would amount to about 300 TU, over an order of magnitude higher than the values observed here. The observed tritium and CFC concentrations suggest that these water samples represent modern recharge, but that CFC concentrations have been reduced by degradation.

Concentrations of CFC's in soil gas exhibit much less variability than liquid concentrations (Table 4-5). All CFC-12 soil gas concentrations are close to 100 percent of modern atmospheric levels (fig. 4-23). The average CFC-12 soil gas concentration at each sampling location ranges from 0.97 to 1.06 times modern air concentrations. CFC-12 concentrations in local air are close to the global average, with individual measurements ranging from 0.97 to 1.01 times the global average.

CFC-11 concentrations vary somewhat more than CFC-12 concentrations and are reduced compared to modern air. The average CFC-11 soil gas concentration at each sampling location range from 0.82 to 1.01 times modern air concentrations. CFC-11 soil gas concentrations are low near well W33 (fig. 4-24), where zero CFC-11 is measured in shallow water-table piezometers, and where the water table is anaerobic (fig. 4-13).

CFC-113 concentrations vary somewhat more than either CFC-12 or CFC-11 concentrations, and several locations exhibit reduced concentrations compared to modern air. The average CFC-113 soil gas concentration at each sampling location ranged from 0.83 to 1.08 times modern air concentrations. CFC-113 soil gas concentrations are low near well W33, where zero CFC-113 is measured in shallow water-table piezometers, and where the water table is anaerobic (fig. 4-13).

CFC concentrations in soil gas show essentially no correlation with depth. However, in a few cases, a systematic pattern in time occurs. In these cases, the winter soil gas CFC-11 and CFC-113 concentrations are a lower fraction of modern air than the

summer concentrations. This may be caused by increasing partitioning into the liquid phase as unsaturated zone temperatures decrease. This temporal pattern is not significant for CFC-12 concentrations.

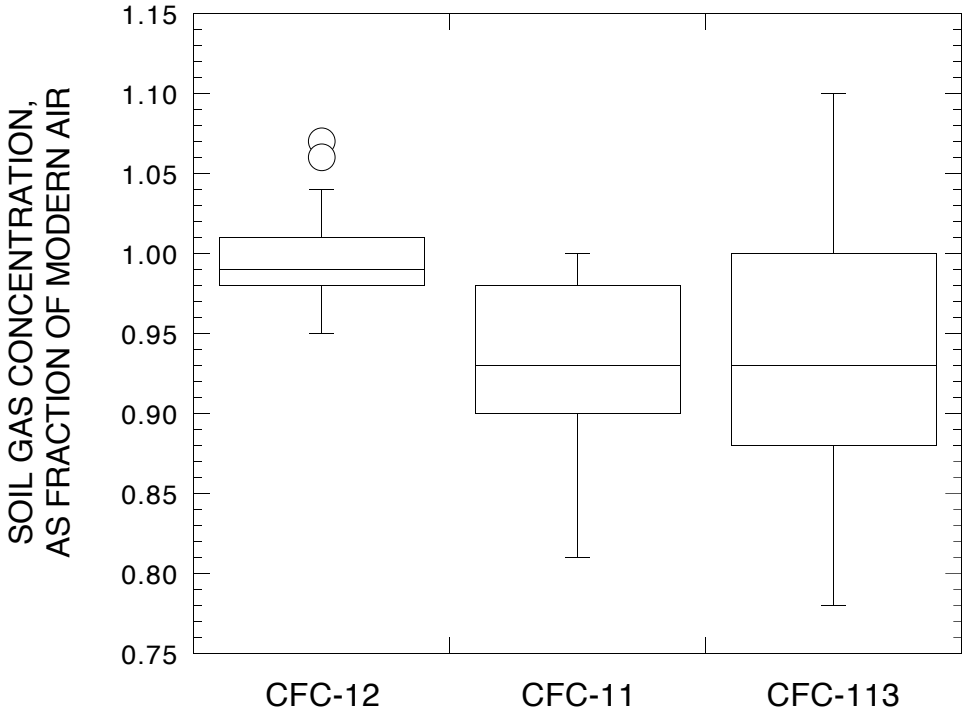

Figure 4-23 Box plot of CFC concentrations in soil gas at the Mirror Lake site, Grafton County, New Hampshire.

Table 4-5. Concentrations of CFC's in soil gas.

ID	Screen depth (cm)	Sample date	Sample time	Sequence Lab	Sequence Field	Concentration in gas (pptv) CFC-12	CFC-11	CFC-113	Fraction of Air Concentration CFC-12	CFC-11	CFC-113	Notes
W33-red	140	30-Jan-97	1536	1		525.4	226.5	70.0	0.98	0.83	0.83	
		30-Jan-97	1546	2		523.3	224.9	69.2	0.97	0.82	0.82	lab time 1548
		avg							0.97	0.82	0.83	
W33-white	200	30-Jan-97	1512	1		525.2	232.3	71.6	0.98	0.85	0.85	
		30-Jan-97	1518	2		535.0	223.1	69.5	0.99	0.81	0.83	
		30-Jan-97	1525	3		521.9	233.5	71.0	0.97	0.85	0.84	
		avg							0.98	0.84	0.84	
W33-blue	240	30-Jan-97	1440	1		529.2	237.1	73.0	0.98	0.87	0.87	
		30-Jan-97	1455	3		526.0	233.9	71.8	0.98	0.85	0.85	
		avg							0.98	0.86	0.86	
W2-blue	100											
FS2-R25	0	29-Jan-97	1600	R-25		530.1	276.6	91.1	0.99	1.01	1.08	
		29-Jan-97	1600	R-25		534.4	275.1	91.1	0.99	1.00	1.08	
		avg							0.99	1.01	1.08	
FS2-air	0	17-Jul-96	910	3		530.9	255.4	79.8	0.99	0.93	0.95	lab date 7/7/96
		17-Jul-96	913	3		526.1	252.8	78.2	0.98	0.92	0.93	
		avg							0.98	0.93	0.94	
FS2-red	65	17-Jul-96	849	1		535.9	258.2	82.3	1.00	0.94	0.98	low flow rate
		17-Jul-96	853	2		530.4	267.5	83.8	0.99	0.98	1.00	
		17-Jul-96	856	3		537.8	273.1	87.5	1.00	1.00	1.05	
		29-Jan-97	1205		1	545.0	253.9	80.1	1.01	0.93	0.95	
		avg							1.00	0.96	1.00	
FS2-blue	180	17-Jul-96	749	1	1	536.5	261.8	82.0	1.00	0.96	0.98	purged 1 min, 50 sec ea. sample
		17-Jul-96	753	2	2	528.9	269.9	91.8	0.98	0.99	1.10	
		17-Jul-96	756	3	3	510.5	257.8	83.1	0.95	0.94	0.99	lab time was 1651?
		29-Jan-97	1237	1	1	537.4	252.7	80.3	1.00	0.92	0.95	
		29-Jan-97	1242	2	2	542.7	246.5	75.5	1.01	0.90	0.90	
		29-Jan-97	1247	3	3	535.7	250.8	77.5	1.00	0.92	0.92	
		avg							0.99	0.94	0.97	

Table 4-5. Concentrations of CFC's in soil gas (continued).

ID	Screen depth (cm)	Sample date	Sample time	Sequence Lab	Sequence Field	Concentration in gas (pptv) CFC-12	CFC-11	CFC-113	Fraction of Air Concentration CFC-12	CFC-11	CFC-113	Notes
W34	180											
W25-red	95											
W25-white	190											
W25-blue	300											
FS1-red	90	29-Aug-96	1715			522.5	271.7	86.6	0.97	0.99	1.04	
		29-Aug-96	1722			529.6	270.9	88.5	0.99	0.99	1.06	
		avg							0.98	0.99	1.05	
FS1-blue	180											
FS3-air	0	31-Jan-97	1034			528.5	260.9	86.0	0.98	0.95	1.02	
FS3	200	31-Jan-97	1012	1	1	538.1	249.4	74.6	1.00	0.91	0.89	
		31-Jan-97	1019	2	2	536.3	242.0	65.9	1.00	0.88	0.78	
		31-Jan-97	1024	3	3	527.8	247.0	73.8	0.98	0.90	0.88	
		avg							0.99	0.90	0.85	
FS3-red	130											
FS3-blue	215	30-Jan-97	1603	1	1	577.8	268.5	75.4	1.07	0.98	0.90	lab fs3c
		30-Jan-97	1608	2	2	568.1	267.2	77.0	1.06	0.98	0.91	
		30-Jan-97	1613	3	3	561.6	273.9	78.6	1.04	1.00	0.93	
		avg							1.06	0.99	0.91	
FS3T-red	60	16-Jul-96	1630	2	1	541.6	266.6	83.0	1.01	0.97	0.99	lab fs3
		16-Jul-96	1635	1	3	532.9	265.0	79.8	0.99	0.97	0.95	
		30-Jan-97	1637	1	1	531.6	252.8	77.2	0.99	0.92	0.92	labeled fs3c-a
		30-Jan-97	1645	2	2	534.7	243.9	73.4	0.99	0.89	0.87	
		30-Jan-97	1651	3	3	532.2	253.2	77.9	0.99	0.92	0.92	
		avg							0.99	0.94	0.93	
FS3T-white	120	16-Jul-96	1559	1	1	535.1	271.8	86.8	1.00	0.99	1.04	
		16-Jul-96	1610		3	536.5	269.7	84.2	1.00	0.98	1.01	
		31-Jan-97	917	1	1	523.3	246.4	77.0	0.97	0.90	0.91	
		31-Jan-97	922	2	2	544.1	241.6	73.1	1.01	0.88	0.87	
		31-Jan-97	927	3	3	524.9	247.4	79.7	0.98	0.90	0.95	
		avg							0.99	0.93	0.95	

Table 4-5. Concentrations of CFC's in soil gas (continued).

ID	Screen depth (cm)	Sample date	Sample time	Sequence Lab	Sequence Field	Concentration in gas (pptv) CFC-12	CFC-11	CFC-113	Fraction of Air Concentration CFC-12	CFC-11	CFC-113	Notes
FS3T-blue	180	16-Jul-96	1548		3	534.5	266.4	89.2	0.99	0.97	1.07	
		16-Jul-96	1534	1	1	530.7	270.2	88.7	0.99	0.99	1.06	lab time 1630?
		31-Jan-97	936	1	1	539.4	262.0	77.2	1.00	0.96	0.92	
		31-Jan-97	941	2	2	547.6	253.7	74.8	1.02	0.93	0.89	
		31-Jan-97	946	3	3	554.0	257.0	76.0	1.03	0.94	0.90	lab fs3c
		avg							1.01	0.96	0.97	
W36-R6	0	31-Jan-97	1400	R-6		529.8	265.6	82.3	0.99	0.97	0.98	
		31-Jan-97	1400	R-6		530.6	264.4	82.3	0.99	0.97	0.98	
		avg							0.99	0.97	0.98	
W36-air	0	29-Aug-96	1453			519.6	254.4	79.8	0.97	0.93	0.95	
W36-red	60	29-Aug-96	1504	1	1	516.3	251.5	77.8	0.96	0.92	0.93	
		29-Aug-96	1511	3	3	520.9	250.6	79.0	0.97	0.91	0.94	lab time 1610?
		31-Jan-97	1538	1	1	525.8	242.6	73.7	0.98	0.89	0.88	
		avg							0.97	0.91	0.92	
W36-white	150	29-Aug-96	1539	1	1	520.8	260.6	83.2	0.97	0.95	0.99	
		29-Aug-96	1546	3	3	534.2	259.7	80.5	0.99	0.95	0.96	
		31-Jan-97	1559	1	1	546.4	253.7	74.4	1.02	0.93	0.88	
		31-Jan-97	1605	2	2	549.7	249.7	71.7	1.02	0.91	0.85	
		31-Jan-97	1610	3	3	542.5	251.6	71.9	1.01	0.92	0.85	
		avg							1.00	0.93	0.91	
W36-blue	260	29-Aug-96	1600	3	2	551.8	270.1	83.8	1.03	0.99	1.00	
		29-Aug-96	1604	1	3	531.6	271.7	88.5	0.99	0.99	1.06	
		31-Jan-97	1623	1	1	546.7	268.5	86.4	1.02	0.98	1.03	
		31-Jan-97	1634	3	3	547.4	270.4	85.8	1.02	0.99	1.02	
		avg							1.01	0.99	1.03	
FS4-R12	0	30-Jan-97	945	R-12		541.9	278.7	95.1	1.01	1.02	1.13	
		30-Jan-97	945	R-12		530.4	280.8	96.8	0.99	1.03	1.15	
		avg							1.00	1.02	1.14	

Table 4-5. Concentrations of CFC's in soil gas (continued).

ID	Screen depth (cm)	Sample date	Sample time	Sequence Lab	Sequence Field	Concentration in gas (pptv) CFC-12	CFC-11	CFC-113	Fraction of Air Concentration CFC-12	CFC-11	CFC-113	Notes
FS4-red	45											
FS4-blue	75	30-Jan-97	1012	1	1	541.3	259.6	82.3	1.01	0.95	0.98	
		30-Jan-97	1017	2	2	537.8	249.6	75.9	1.00	0.91	0.90	
		30-Jan-97	1028	3	3	526.3	254.8	84.8	0.98	0.93	1.01	
		avg							1.00	0.93	0.96	
FS4B-red	30											
FS4B-blue	80											
FS5-red	50											
FS5-blue	115											
Global		30-Jun-96				537.8	273.9	84.2	1.00	1.00	1.00	
average air		1-Jan-97				537.6	273.9	83.7	1.00	1.00	1.00	

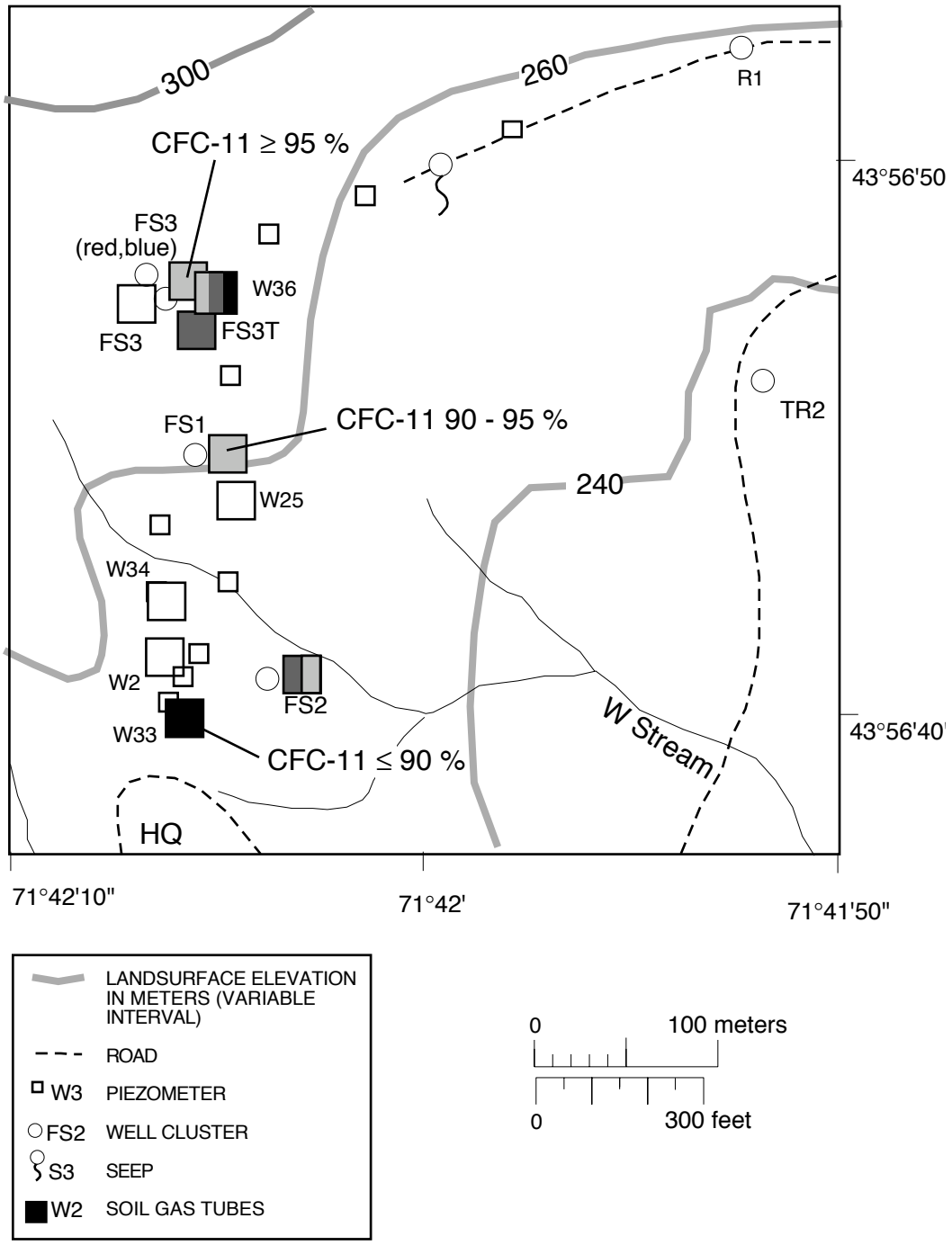

Figure 4-24 Spatial distribution of CFC-11 concentrations in soil gas samples from sampling tubes at the Mirror Lake site, Grafton County, New Hampshire.

4.4 Discussion

The goals of this field study involve characterization of the concentrations of CFC's in water recharging the saturated zone. Where dissolved oxygen concentrations are relatively high (greater than 5 mg/L), CFC concentrations at the water table appear to be approximately in equilibrium with the modern atmosphere. However, even in these well-oxygenated samples, there is significant variability in CFC concentrations. The observed range of concentrations in aerobic water-table samples corresponds to uncertainty in ground-water ages determined from CFC-12, CFC-11, and CFC-113 concentrations on the order of ± 4, 7, and 8 years, respectively. This variability in concentrations at the water table presumably impacts the uncertainty in ages associated with water samples from deeper in the saturated zone at the Mirror Lake site. This uncertainty is significantly larger than the analytical uncertainty in the laboratory (± 1 yr).

The hydraulic data collected during this study suggests that recharge is highest in the early spring and fall, but recharge occurs throughout the year depending on the intensity of precipitation. Significant recharge also occurs slowly throughout the winter, and more rapidly in the winter during mid-winter snowmelt, when it occurs.

Soil temperatures are consistent with measured noble gas concentrations and suggest that recharge temperatures at the water table range between 5 and 10 °C. The average recharge temperature of 7 °C is probably a reasonable approximation for estimating past atmospheric gas concentrations from water samples.

Samples from wells screened near the water table that contain low dissolved oxygen also contain low CFC's, relative to atmospheric equilibrium. In the case of CFC-11 and CFC-113, these compounds are completely absent from some anaerobic samples. CFC-12 is not reduced as much, with concentrations in anaerobic samples as low as 1/3 of modern levels. Ground water in the saturated zone that was anaerobic shortly after recharge near the water table is likely to have low CFC concentrations. These low CFC

concentrations would yield apparent ages for deeper saturated-zone samples much larger than the actual time since recharge.

CFC concentrations are also significantly reduced in samples that have dissolved oxygen concentrations ranging from 1-4 mg/L. This pattern is not consistent with degradation of CFC's only under anaerobic conditions because these DO levels are not low enough to be considered anaerobic. However, this pattern of intermediate CFC concentrations in samples having intermediate DO is consistent with a linear mixing model.

The general pattern of the correlation between CFC's and DO suggests a linear mixing model, although there is scatter in the measurements. This mixing model assumes that samples are linear mixtures of two end-members: (a) aerobic water having about 6 mg/L DO and CFC concentrations in equilibrium with the modern atmosphere; and (b) anaerobic water having no oxygen, no CFC-11 or CFC-113, and CFC-12 concentrations about 1/3 of modern atmospheric-equilibrium levels. That a water sample pumped from a well with a 0.6 to 0.9 m long screen represents a mixture is not surprising. Numerous investigators have reported small-scale water-quality variation in ground water (e.g. Cozarelli et al., 1996). Such small-scale variability is supported by limited diffusion in saturated ground water, and by large variations in permeability. Other evidence of mixing of samples is the presence of iron (II) and methane in oxygenated samples. With this mixing model, the lower concentrations in low-DO waters are explained not as degradation under low-DO conditions, but as degradation under anaerobic conditions, occurring in only a fraction of the total sample volume.

Anaerobic degradation of CFC-11 and CFC-113 has been observed in the laboratory (Lovely and Woodward, 1992) and the field (Cook et al., 1995; Plummer et al., in press), although CFC-12 degradation has only recently been reported for ground waters (Oster et al., 1996). These field results are consistent with the observations reported herein in that CFC-12 is less degraded, but concentrations of CFC-12 are

apparently reduced to about 1/3 of modern levels; not complete degradation, but a significant loss that would cause significant differences between apparent and actual ground-water ages.

Independent evidence of anaerobic biodegradation is presented by hydrogen gas, methane, and carbon dioxide concentrations measured in several piezometers (Table 4-3). Hydrogen gas concentrations can identify the controlling redox processes in anaerobic systems (Lovely and Goodwin, 1988). CFC-11 degradation has been observed in the laboratory for sulfate-reduction and methanogenesis redox conditions (Lovely and Woodward, 1992), both of which are indicated in sampled piezometers. Sulfate and iron (II) are present in shallow ground water at Mirror Lake (fig. 4-25) to support sulfate-reduction and iron-reduction reactions. There is limited laboratory evidence that iron (II) may play a role in abiotic degradation of CFC-11 under anaerobic conditions (Lovely and Woodward, 1992).

Overall, CFC-12 concentrations appear to be least affected by anaerobic degradation or contamination. The use of CFC-12 for age-dating ground water is likely to be more robust in the field, particularly for systems where anaerobic degradation conditions may exist.

Given the variability in geochemical conditions observed in different water-table piezometers, it is not possible to characterize the distribution of CFC's in recharge in the Mirror Lake drainage basin on the basis of these 31 wells. These results suggest that in areas where the shallow water table is anaerobic, CFC's in recharge will be significantly reduced from modern equilibrium levels. Furthermore, concentrations may also be reduced due to anaerobic degradation in micro-environments, even though the apparent redox conditions in pumped samples are not anaerobic. However, it is likely that these micro-environments will have relatively low permeability, and thus may play a less important role in controlling recharge chemistry, which will be weighted toward the conditions occurring in higher permeability zones.

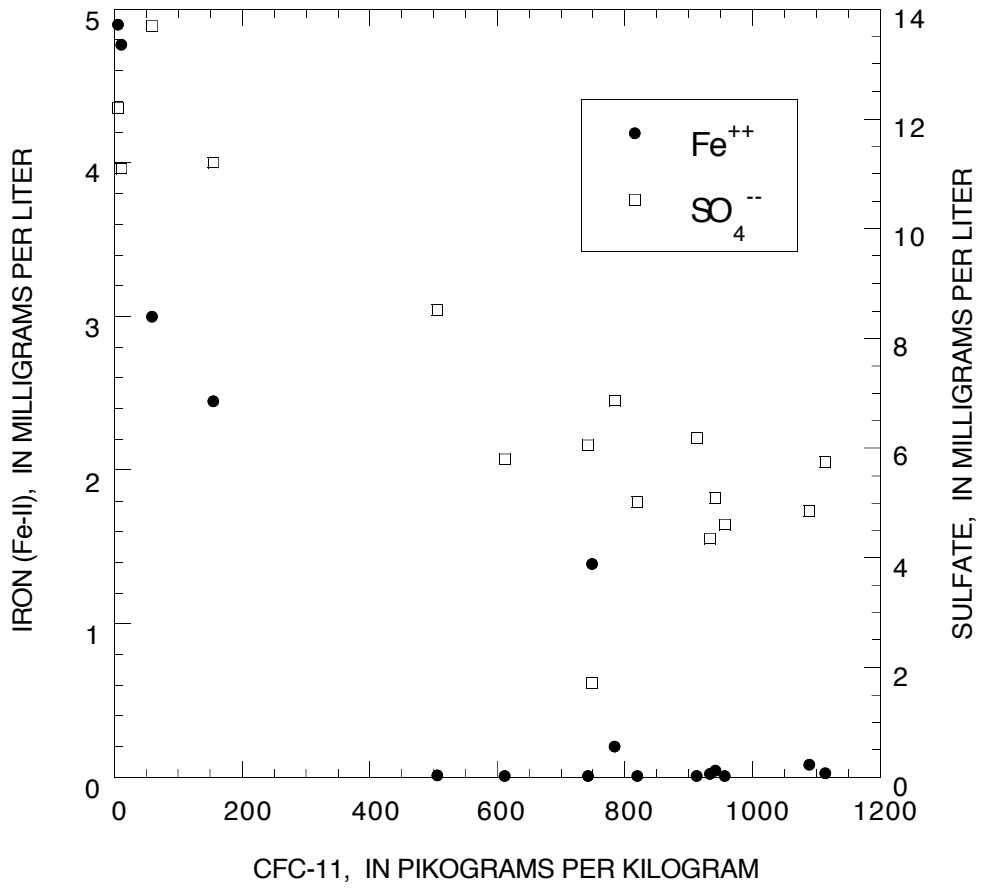

Figure 4-25 Iron (II) and sulfate as a function of CFC-11 concentrations.

A local flow system associated with streamloss and flow across a sandy terrace exhibits strong anaerobic conditions. Shattuck (1991) identified an area in the Mirror Lake drainage basin where the water table gradient is across the W stream (fig. 4-26). It appears that in this area stream water may enter the subsurface and flow across the sandy terrace to another branch of the W stream. Dissolved oxygen (DO) and total organic carbon (TOC) concentrations in water-table piezometers along the apparent flow direction (approximately) suggest that the provision of organic carbon to the aquifer by

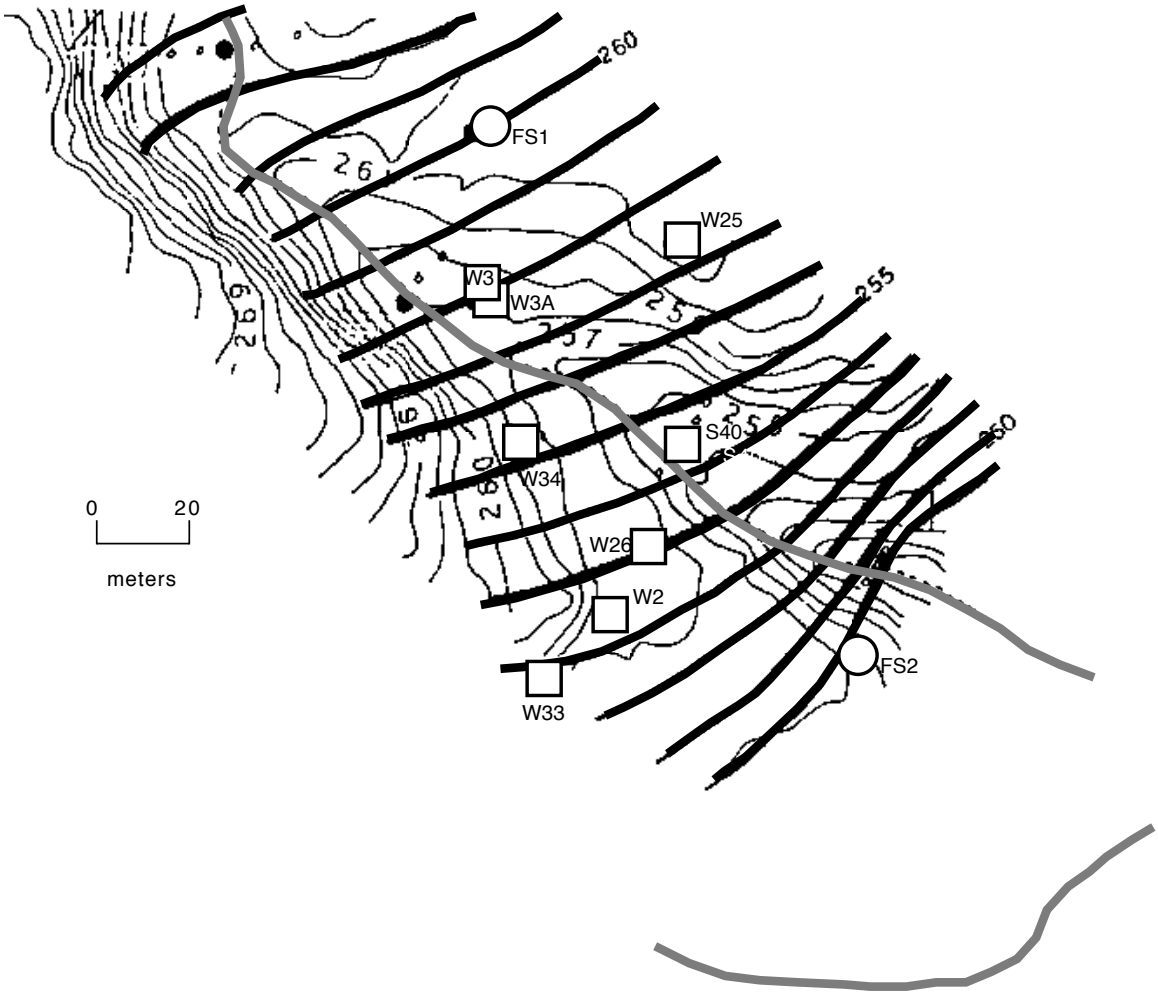

Figure 4-26 Water table elevations in the lower part of the W stream drainage basin (Shattuck, 1991).

the stream may contribute to the anaerobic redox conditions (fig. 4-27). Organic carbon may be carried into the aquifer from the bottom of the stream. Dissolved oxygen is consumed by the biologic activity and is only slowly replenished by diffusion downward through the unsaturated zone. This streamloss is not the only factor contributing to anaerobic conditions because such low-DO environments are also present upgradient of streams (for example, W25 in fig. 4-27).

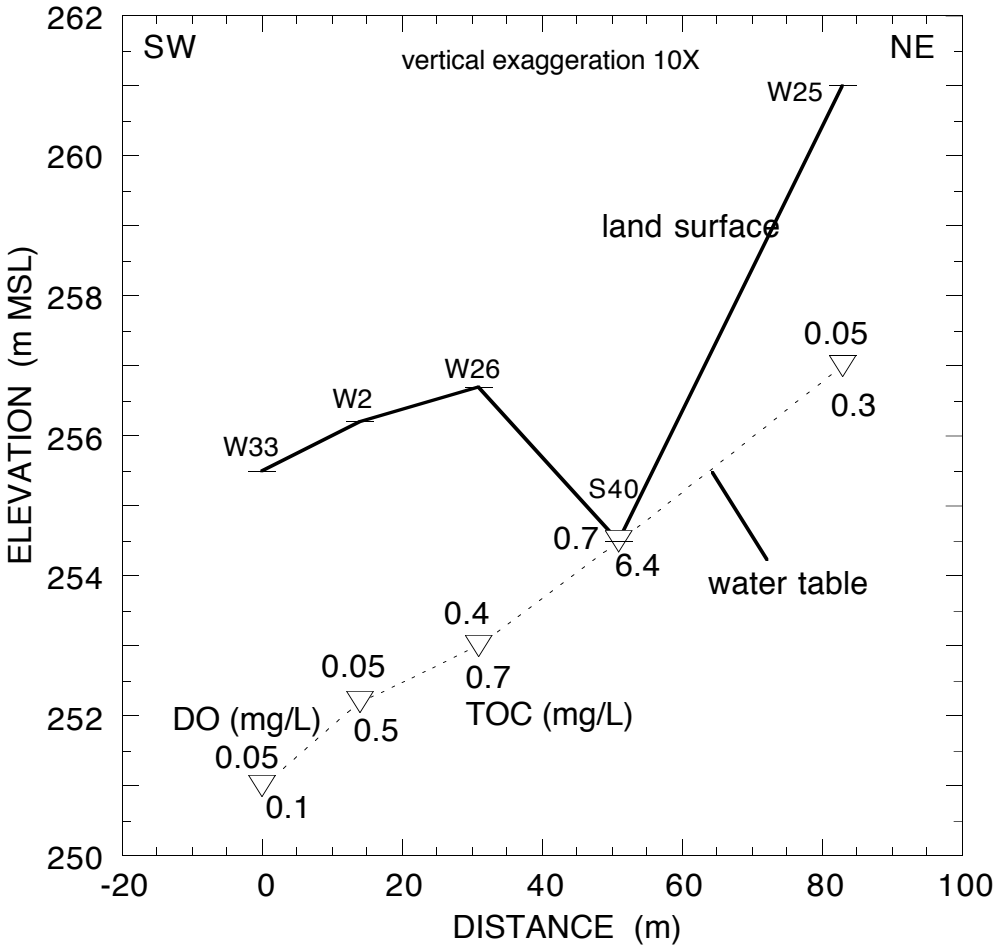

Figure 4-27 Cross-section in the lower part of the W stream drainage basin showing the land surface elevation, water table elevation, and concentrations of dissolved oxygen (DO) and total organic carbon (TOC) in samples from water-table piezometers.

4.5 Summary

The use of chlorofluorocarbons (CFC's) as age-dating tracers for ground water at the Mirror Lake fractured-rock research site may be limited because concentrations of CFC's in at least some areas are significantly reduced by anaerobic degradation. CFC concentrations in water samples from high-conductivity fractures in schist and granite bedrock indicate ages ranging from greater than 45 years to about 7 years, but the spatial pattern of ages is complex and the youngest measured ages occur near the lake at the bottom of the forested watershed. Equilibrium between CFC in the atmosphere and at the water table is needed to date saturated-zone waters. However, samples from piezometers screened just below the water table in the glacial drift indicate that CFC-11, CFC-12, and CFC-113 are substantially degraded where dissolved oxygen (DO) concentrations are low. Anaerobic (DO < 0.1 mg/L) conditions existing in a sandy terrace deposit may be caused by biodegradation of organic carbon in infiltrating stream water. Samples from this and other shallow anaerobic zones lack CFC-11 and CFC-113 and have CFC-12 concentrations that are as low as 1/3 of modern equilibrium concentrations. Furthermore, several hypoxic (0.1 < DO < 3 mg/L) samples have significantly reduced CFC's. As expected, samples with high DO collected at the water table generally contain CFC's near atmospheric-equilibrium concentrations. Many samples plot on a mixing line for CFC's and DO, suggesting that the water sampled can be a mixture of two end members: (1) waters saturated with oxygen and containing CFC's in equilibrium with the modern atmosphere, and (2) zero-DO waters containing no CFC-11 or CFC-113 and containing about 1/3 of modern CFC-12. Several samples contain CFC-11 and CFC-113 concentrations higher than those from equilibration with peak atmospheric levels, suggesting a non-atmospheric source. Possible sources of this contamination include sampling equipment (Busenberg and Plummer, 1996) and well-construction materials, including sand installed at well screens, grout used to seal the borehole annulus and PVC

adhesives. Evidence of active anaerobic biodegradation, which can degrade CFC's, includes high methane and ample iron (Fe-II) and sulfate and generally low DO. Hydrogen gas concentrations in anaerobic samples from water-table piezometers are consistent with methanogenesis or sulfate-reduction as the terminal electron-accepting process.

4.6 References

Bormann, F.H., and Likens, G.E., 1979, *Patterns and Processes in a Forested Ecosystem*: Springer-Verlag, New York, 253 p.

Bu, X., and Warner, M.J., 1995, Solubility of chlorofluorocarbon 113 in water and seawater: Deep Sea Research, v. 42, no. 7, p. 11512-1161.

Bullister, J.L., and Lee, B.-S., 1995, Chlorofluorocarbon-11 removal in anoxic marine water: Geophysical Research Letters, v. 22, no. 14, p. 1893-1896.

Busenberg, E., and Plummer, L.N., 1992, Use of chlorofluorocarbons (CCl_3F and CCl_2F_2) as hydrologic tracers and age-dating tools: Example - The alluvium and terrace system of central Oklahoma: Water Resources Research, v. 28, p. 2257-2283.

Busenberg, E., and Plummer, L.N., 1993, Use of trichlorofluorocarbon-113 (CFC-113) as a hydrologic tracer and age-dating tool of young ground water: GSA Abstracts with Programs, v. 25, no. 6, p. A-365.

Busenberg, E., and Plummer, L.N., 1996, Concentrations of chlorofluorocarbons and other gases in ground water at Mirror Lake, New Hampshire: in Morganwalp, D.W., and Aronson, D.A., eds., U.S. Geological Survey Toxics Program Meeting, Colorado Springs, Colo., September 20-24, 1993: U.S. Geological Survey WRIR 94-4015.

Cook, P.G., Solomon, D.K., Plummer, L.N., Busenberg, E., and Schiff, S.L., 1995, Chlorofluorocarbons as tracers of groundwater transport processes in a shallow, silty sand aquifer: Water Resources Research, v. 31, no. 3, p. 425-434.

Cozzarelli, I.M., Baedecker, M.J., Aiken, G., and Phinney, C.S., 1996, Small-scale chemical heterogeneity's in a crude-oil-contaminated aquifer, Bemidji, Minnesota, in Morganwalp, D. W., and Aronson, D.A., eds., U.S. Geological Survey Toxic Substances Hydrology Program - Proceedings of the Technical Meeting, Colorado Springs, Colorado, September 20-24, 1993: U.S. Geological Survey Water-Resources Investigations Report 94-4015, p. 647-652.

Drenkard, S., Torgersen, T., Weppernig, R., Stute, M., Farley, K., and Schlosser, P., 1993, Helium isotopes and tritium-helium age dating: Mirror Lake, New Hampshire (abs.): GSA Abstracts with Programs, v. 25, no. 6, p. A-364.

Dunkle, S.A., Plummer, L.N., Busenberg, E., Phillips, P.J., Denver, J.M., Hamilton, P.A., Michel, R.L., and Coplen, T.B., 1993, Chlorofluorocarbons (CCl_3F and CCl_2F_2) as dating tools and hydrologic tracers in shallow ground water of the Delmarva Peninsula, Atlantic Coastal Plain, United States: Water Resources Research, v. 29, no. 12, p. 3837-3860.

Federer, C.A., 1973, Annual cycles of soil and water temperatures at Hubbard Brook: U.S. Forest Service Research Note NE-167, 7 p.

Federer, C. A., Flynn, L. D., Martin, C. W., Hornbeck, J. W., and Pierce, R. S., 1990, Thirty years of hydrometeorologic data at the Hubbard Brook Experimental Forest, New Hampshire: U.S. Department of Agriculture, Forest Service, Northeastern Forest Experiment Station, General Technical Report NE-141, 44 p.

Freeze, R.A., and J.A. Cherry, 1979, *Groundwater*, Prentice-Hall, Englewood Cliffs, New Jersey.

Goode, D.J., 1997, CFC transport to and degradation near a shallow water table, Mirror Lake area, Grafton County, New Hampshire: (abs.), p. S176 in 1997 Spring Meeting, supplement to Eos, 29 April 1997, American Geophysical Union, Washington DC.

Goode, D.J., Busenberg, Eurybiades, Plummer, L.N., Shapiro, A.M., and Vroblesky, D.A., 1997, CFC degradation under anaerobic water table conditions in glacial drift at Mirror Lake New Hampshire: (abs.), Geological Society of America 1997 Annual Meeting, 20-23 October 1997, Salt Lake City, Utah, GSA Abstracts with Programs, vol. 29, no. 6, p. 77.

Harte, P.T., 1992, Regional ground-water flow in crystalline bedrock and interaction with glacial drift in the New England uplands: M. S. Thesis, University of New Hampshire, Durham, 147 p.

Harte, P.T., 1997, Prelminary assessment of the lithologic and hydraulic properties of the glacial drift and shallow bedrock in the Mirror Lake area, Grafton County, New Hampshire: U.S. Geological Survey Open-File Report 96-654A, 56 p.

Harte, P.T. and Winter, T.C., 1995, Simulations of flow in fractured crystalline rock in a hypothetical New England setting: Ground Water, v. 33, no. 3, p. 953-964.

Harte, P.T. and Winter, T.C., 1996, Factors affecting recharge to crystalline rock in the Mirror Lake area, Grafton County, New Hampshire: in Morganwalp, D.W., and Aronson, D.A., eds., U.S. Geological Survey Toxics Program Meeting, Colorado Springs, Colo., September 20-24, 1993: U.S. Geological Survey WRIR 94-4015.

Heaton, T.H.E., 1981, Dissolved gases: Some applications to groundwater research: Trans. Geol. Soc. South Africa, v. 84, p. 91-97.

Heaton, T.H.E., and Vogel, J.C., 1981, "Excess air" in groundwater: Journal of Hydrology, v. 41, p. 217-231.

Herkelrath, W.N., Hamburg, S.P., and Murphy, Fred, 1991, Real-time monitoring of soil moisture in a remote field area with time-domain reflectometry: Water Resources Research, v. 27, no. 5, p. 857-864.

Hsieh, P. A., Shapiro, A. M., Barton, C. C., Haeni, F. P., Johnson, C. D., Martin, C. W., Paillet, F. L., Winter, T. C., and Wright, D. L., 1993, Methods of characterizing fluid movement and chemical transport in fractured rock: in Chaney, J. T., and Hepburn, C., (eds.) Field Trip Guidebook for northeastern United States, Geological Society of America, annaul Meeting, October 25-28, 1993, Boston, Mass., v. 2, chap. R, p. R1-R23.

Hsieh, P.A., and Shapiro, A.M., 1996, Hydraulic characteristics of fractured bedrock underlying the FSE well field at the Mirror Lake site, Grafton County, New Hampshire: in Morganwalp, D.W., and Aronson, D.A., eds., U.S. Geological Survey Toxics Program Meeting, Colorado Springs, Colo., September 20-24, 1993: U.S. Geological Survey WRIR 94-4015.

Khalil, M.A.K., and Rasmussen, R.A., 1989, The potential of soils as a sink of chlorofluorocarbons and other man-made chlorocarbons: Geophysical Research Letters, v. 16, no. 7, p. 679-682.

Khalil, M.A.K., and Rasmussen, R.A., 1993, The environmental history and probably future of Fluorocarbon 11: Journal of Geophysical Research, v. 98, no. D12, p. 23,091-23,106.

Likens, G. E., Bormann, F. H, 1995, *Biogeochemistry of a Forested Ecosystem*: Springer-Verlag, New York, 2nd ed., 159 p.

Likens, G. E. (ed.), 1985, *An Ecosystem Approach to Aquatic Ecology, Mirror Lake and its Environment*: Springer-Verlag, New York, 516 p.

Lovely, D.R., and Goodwin, S., 1988, Hydrogen concentrations as an indicator of the predominant terminal electron-accepting reactions in aquatic sediments: Geochmica et Cosmochimica Acta, v. 52, p. 2993-3003.

Lovely, D.R., and Woodward, J.C., 1992, Consumption of Freon CFC-11 and CFC-12 by anaerobic sediments and soils: EST, v. 26, p. 925-929.

Mau, D.P., and Winter, T.C., 1997, Estimating ground-water recharge from streamflow hydrographs for a small mountain watershed in a temperate humid climate, New Hampshire, USA: Ground Water, v. 35, no. 2, p. 291-304.

McConnell, J.B., Busenberg, E., and Plummer, L.N., 1994, Water-resources data for the Valdosta area, south-central Georgia, 1961-93: U.S. Geological Survey Open-file Report 94-350, 58 p.

Oster, H., C. Sonntag, and K.O. Munnich, 1996, Groundwater age dating with chlorofluorocarbons: Water Resources Research, v. 32, no. 10, p. 2989-3001.

Plummer, L. N., R.L. Michel, E.M. Thurman, and P.D. Glynn, 1993,. Environmental tracers for age dating young ground water, in *Regional Ground-Water Quality* , edited by W. M. Alley, pp. 255-294, Van Nostrand Reinhold, New York.

Plummer, L.N., Busenberg, E., Drenkard, S., Schlosser, P., McConnell, J.B., Michel, R.L., Ekwurzel, B., and Weppernig, R., (in press), Flow of river water into a karstic limestone aquifer--2. Dating the young fraction in groundwater mixtures in the upper Floridan Aquifer near Valdosta, Georgia, using tritium/helium-3 and chlorofluorocarbons. (see data report: McConnell et al., 1994).

Reilly, T.E., L.N. Plummer, P.J. Phillips, and E. Busenberg, 1994, The use of simulation and multiple environmental tracers to quantify flow in a shallow aquifer: Water Resources Research, v. 30, no. 2, p. 421-433.

Russell, A.D., and Thompson, G.M., 1983, Mechanisms leading to enrichment of the atmospheric fluorocarbons CCl3F and CCl2F2 in groundwater: Water Resources Research, v. 19, no. 1, p. 57-60.

Semprini, L., Hopkins, G.D., Roberts, P.V., and McCarty, P.L., 1990, In-situ biotransformation of carbon tetrachloride, 1,1,1-trichloroethane, Freon-11, and Freon-113 under anoxic conditions (abs.), *in* Eos, Trans. AGU, San Francisco, American Geophysical Union, p. 1324.

Shapiro, A.M., 1996, Using environmental tracers to estimate matrix diffusion in fractured rock over distances of kilometers: Results from the Mirror Lake site, New Hampshire: Eos, Trans. AGU, v. 77, no. 17, p. S107.

Shapiro, A. M., and P. A. Hsieh, 1991, Research in fractured-rock hydrogeology: Characterizing fluid movement and chemical transport in fractured rock at the Mirror Lake drainage basin, New Hampshire: p. 155-161 in Mallard, G.E., and D. A. Aronson (eds.), U.S. Geol. Survey Toxic Substances Hydrology Program--Proc. Technical Meeting, Monterey, California, March 11-15, 1991: U.S. Geol. Survey Water-Resources Invest. Rep. 91-4034.

Shapiro, A.M., Wood, W.W., Busenberg, E., Drenkard, S., Plummer, L.N., Torgersen, T., and Schlosser, P., 1996, Conceptual model for estimating regional fluid velocity in the bedrock of the Mirror Lake area, Grafton County, New Hampshire, *in* Toxics Program Meeting, Colorado Springs, U.S. Geological Survey WRIR 94-4015.

Shattuck, P. C., 1991, Shallow water-table response to precipitation and evapotranspiration in an ephemeral stream valley, Woodstock, New Hampshire: unpublished M.S. Thesis, Hydrology Program, University of New Hampshire, Durham, 113 p.

Szabo, Z., D.E. Rice, L.N. Plummer, E. Busenberg, S. Drenkard, and P. Schlosser, 1996, Age dating of shallow groundwater with chlorofluorocarbons, tritium/helium 3, and flow path analysis, southern New Jersey coastal plain: Water Resources Research, v. 32, no. 4, p. 1023-1038.

Terauds, V.I., Contaldo, G., McCarthy, C.M., and Smith, G.B., 1993, Field and laboratory evidence for in situ biotransformation of isopropanol and Freon-11 (abs.): Ground Water, v. 31, no. 5, p. 850-851.

Thompson, G.M., and Hayes, J.M., 1979, Trichloromethane in groundwater - A possible tracer and indicator of groundwater age: Water Resources Research, v. 15, p. 546-554.

Thompson, G.M., Hayes, J.M., and Davis, S.N., 1974, Fluorocarbon tracers in hydrology: Geophysical Research Letters, v. 1, p. 177-180.

Tiedeman, C.R., Goode, D.J., and Hsieh, P.A., 1997, Numerical simulation of ground-water flow through glacial deposits and crystalline bedrock in the Mirror Lake area, Grafton County, New Hampshire: U.S. Geological Survey Professional Paper 1572, 50 p.

U.S. Department of Agriculture Forest Service, 1991, The Hubbard Brook Ecosystem Study: Site description and research activities: Northeastern Forest Experiment Station NE-INF0-96-91, 61 p.

Warner, M.J., and R.F. Weiss, 1985, Solubilities of chlorofluorocarbons 11 and 12 in water and seawater, Deep-Sea Research, v. 32, p. 1485-1497.

Weiss, R.F., 1970, The solubility of nitrogen, oxygen, and argon in water and seawater: Deep Sea Research, v. 17, p. 721-735.

Wilson, Alicia, 1991, Distribution of hydraulic conductivity in the glacial drift at Hubbard Brook Experimental Forest, West Thornton, New Hampshire: unpublished Senior Honors Thesis, Dartmouth College, Hanover, New Hampshrie, 56 p.

Winter, T. C., 1984, Geohydrologic setting of Mirror Lake, West Thornton, New Hampshire: U.S. Geological Survey Water-Resources Investigations Report 84-4266, 61 p.

Winter, T. C., 1985, Physiographic setting and geologic origin of Mirror Lake: in Likens, G. E., ed., *An ecosystem approach to aquatic ecology: Mirror Lake and it Environment*: Springer-Verlag, New York, p. 40-53.

Winter, T. C., Eaton, J. S., and Likens, G. E., 1989, Evaluation of inflow to Mirror Lake, New Hampshire: Water Resources Bulletin, vol. 25, no. 5, p. 991-1008.

Wood, W.W., Shapiro, A.M., and Councell, Terry, 1996, Observational experimental and inferred evidence for solute diffusion in fractured granite aquifers: Examples from Mirror Lake Watershed, Grafton County, New Hampshire: in Morganwalp, D.W., and Aronson, D.A., eds., U.S. Geological Survey Toxics Program Meeting, Colorado Springs, Colo., September 20-24, 1993: U.S. Geological Survey WRIR 94-4015.

Chapter 5 Regional-Scale Simulation of Ground-Water Age and CFC-11 Transport at the Mirror Lake Site, New Hampshire

5.1 Introduction

Investigators of the USGS, and others, are trying to characterize large-scale flow and transport properties of the ground-water flow system beneath the Mirror Lake drainage basin, located in north-central New Hampshire (fig. 5-1). Background hydrogeologic information and summaries of previous investigations are provided by Winter (1984; 1985), Winter and others (1989), Shapiro and Hsieh (1991), and Hsieh and others (1993). A wide range of investigative methods are being applied, including the use of large-scale model calibration. A large-scale flow model was calibrated by Tiedeman and others (1997) using measured hydraulic head and streamflow to estimate hydraulic conductivity of the glacial drift and fractured rock. Continuing efforts include calibration of transport models of advective travel time (C.R. Tiedeman, personal commun., 1996) and tritium and CFC-12 transport with matrix diffusion (Shapiro, 1996; Shapiro and others, 1996). Harte (1992) and Harte and Winter (1995) modeled cross-sectional flow between the glacial drift and bedrock, and examined the role of heterogeneity in the glacial drift in controlling local vertical flow. Chapter Four of this thesis addresses degradation of CFC's at the top of the saturated zone that complicates interpretation of saturated-zone concentrations through transport modeling. One method of interpreting environmental tracer information is to convert measured concentrations to ground-water ages. The observed distribution of ages can be compared to a transport model of ground-water age, as developed in Chapter Two.

In this chapter, a numerical transport model is used to simulate ground-water age and CFC-11 concentrations in the Mirror Lake basin. These alternative approaches to

simulating tracer information are compared and contrasted. The effective porosity of bedrock is varied from 0.05 to 0.005. The impact of matrix diffusion and stream-aquifer interaction on CFC-11 concentrations is illustrated.

5.2 Background

5.2.1 Regional-Scale Flow Modeling at Mirror Lake site

Tiedeman and others (1997) calibrated a regional-scale three-dimensional ground-water flow model to measured water levels and streamflow in the Mirror Lake watershed. Calibration of the flow model used a non-linear optimization procedure coupled with the ground-water flow model (Hill, 1992). In addition to providing an estimate of regional-scale hydraulic properties, hydraulic conductivity and recharge, this model was used to characterize the ground-water flow beneath the Mirror Lake watershed. Figure 5-1 shows their finite-difference grid and important hydrologic features of the modeled area. A subset of this model domain, indicated in the figure, is re-gridded for the transport simulations here.

Ground-water pathline analysis was used to identify the ground-water drainage basin of Mirror Lake and streams that flow into Mirror Lake (Tiedeman et al., 1997). Figure 5-2 is a schematic of the three-dimensional ground-water drainage basin for Mirror Lake. The area of the land surface from which infiltration eventually reaches Mirror Lake is considerably larger than the surface-water drainage basin delineated from topography. Furthermore, the subsurface extent of the volume of aquifer containing water that is flowing towards Mirror Lake and its tributaries extends outside the land surface boundaries of the ground-water basin. Some of the infiltration at high elevations flows downward and beneath the adjacent ground-water basin of Norris Brook, before eventually turning towards Mirror Lake and lower elevations of the stream network.

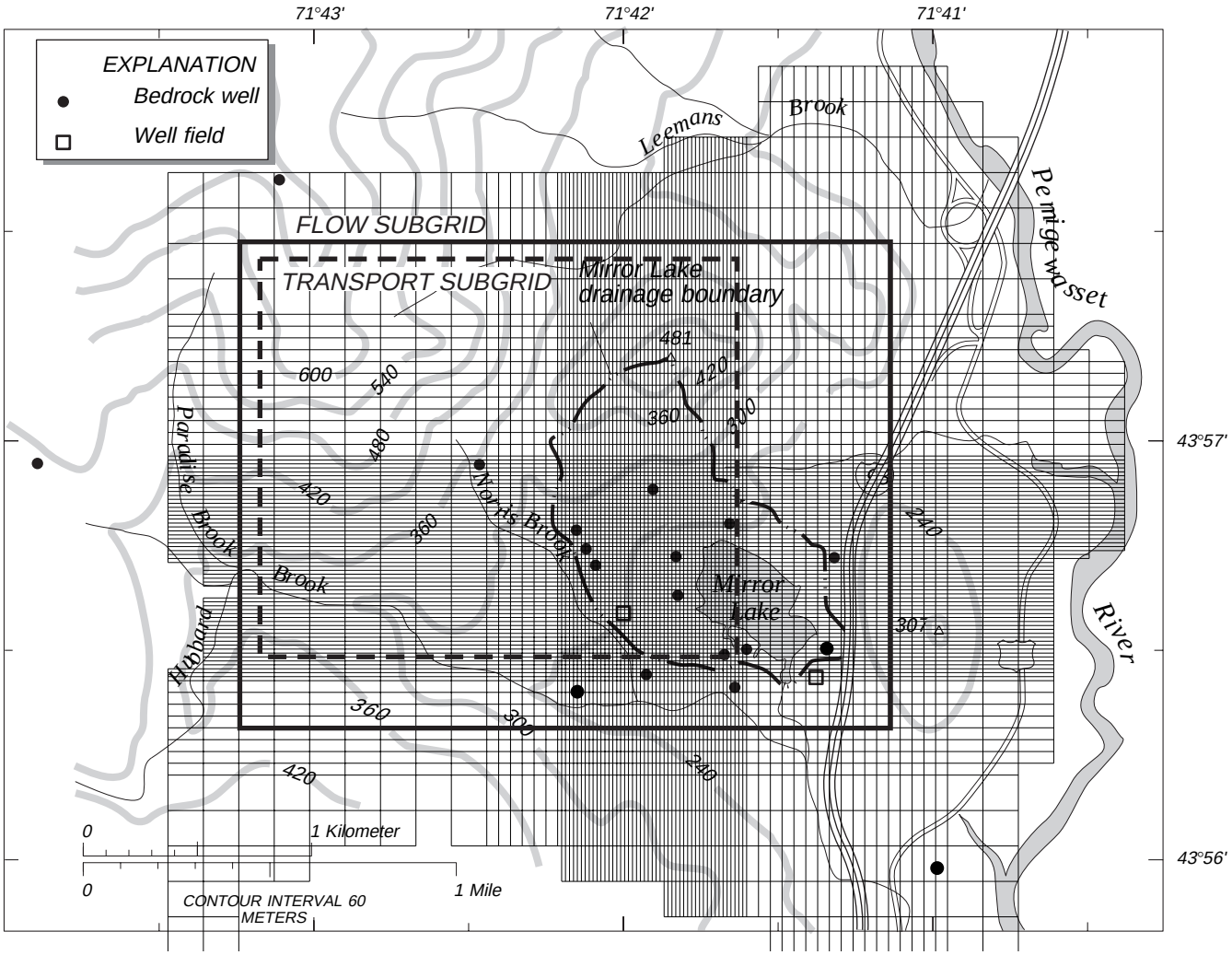

Figure 5-1 Location map of Mirror Lake site, New Hampshire, regional-scale finite-difference grid (Tiedeman et al., 1997), and flow and transport subgrids.

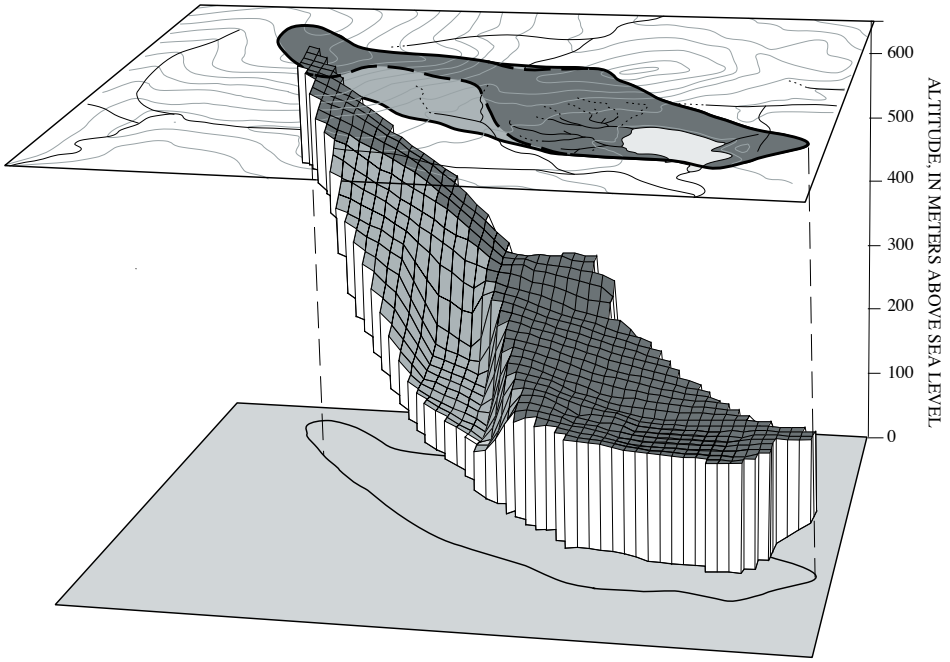

Figure 5-2. Mirror Lake ground-water drainage basin (Tiedeman et al., 1997).

5.2.2 Environmental Tracers and Ground-Water Age at the Mirror Lake Site

Age dating of ground water at the Mirror Lake site has met with limited success. The tritium-helium age-dating method cannot be used in bedrock ground waters because of a local source of helium (Drenkard et al., 1993). Busenberg and Plummer (1996) present results of CFC and tritium sampling. Spatial patterns of CFC-derived ground-water ages cannot be easily related to recharge/discharge in the ground-water basin (see fig. 4-3). The general temporal pattern of CFC-12 dates and tritium concentrations is similar to the tritium input function from the atmosphere (fig. 5-3). Recent recharge has tritium concentrations in the range of 10-20 TU, while water older than about 50 years has very little tritium due to decay. However, the peak tritium concentrations occurred in the atmosphere in 1963 in New Hampshire, while the peak from tritium and CFC-12 data appears to occur several years later. More significantly, the peak tritium concentrations

are well below the 250-300 TU range that would be expected for early-1960's recharge, accounting for decay to 1992 (Busenberg and Plummer, 1996).

Shapiro (1996) suggests that the temporal pattern of tritium and CFC-derived recharge dates may be caused by large-scale matrix diffusion. Matrix diffusion affects tritium and CFC concentrations differently because of differences in diffusion coefficients, but more importantly, because their source input functions are very different (Plummer et al., 1993). The effect of matrix diffusion is, in part, to reduce the sharp peak of the tritium input function. Diffusion has less impact on the concentrations of CFC's, because CFC atmospheric concentrations have increased gradually in time. Shapiro's (1996) approach was to treat all ground-water samples as if they are drawn from a one-dimensional flow system, but the sample location along the flowpath is unknown. By adjusting diffusion coefficients in the bedrock and glacial drift, the general pattern of tritium and CFC-12 concentrations was matched.

C.R. Tiedeman (personal commun., 1994) modeled advective travel time using the large-scale flow model of Tiedeman and others (1997). A match could be obtained between the range in advective travel time to a bedrock well, and the ground-water ages determined from CFC-12. However, the calibrated effective porosity was considered too high to be representative of the bedrock at the Mirror Lake site.

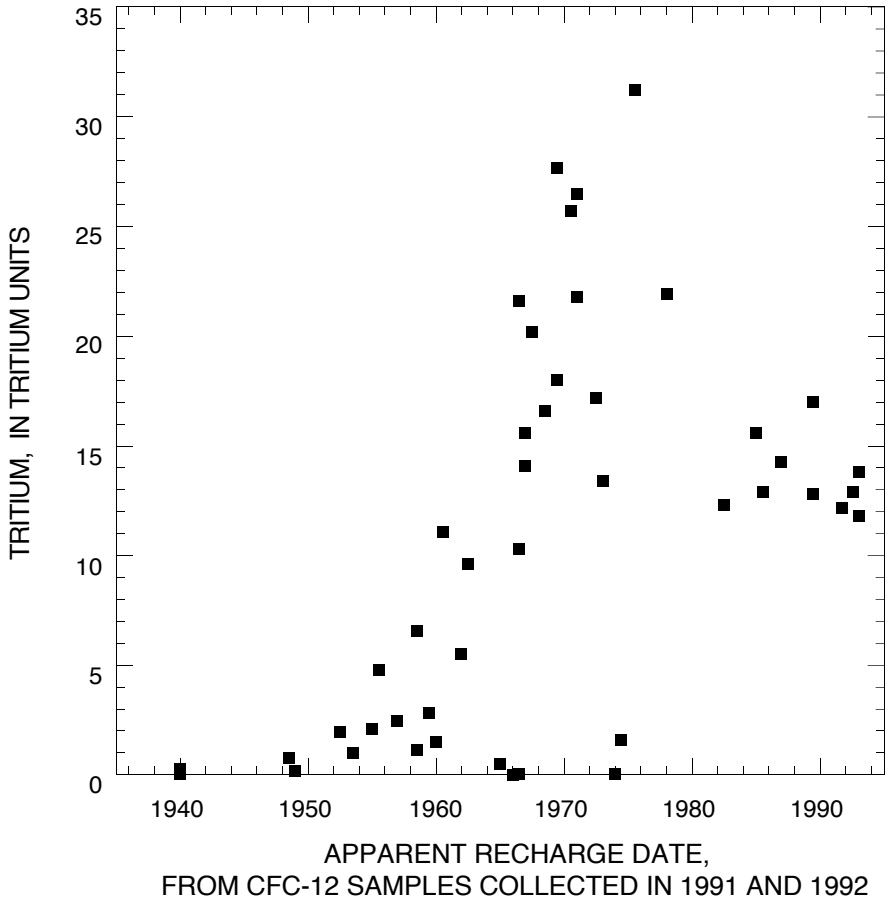

Figure 5-3 Tritium concentrations versus apparent recharge dates from CFC-12 concentrations in ground-water samples from drift piezometers and bedrock wells at Mirror Lake site (Busenberg and Plummer, 1996).

5.2.3 Scope of this study

The goal of this investigation is to illustrate the application of the methods developed in Chapter Two to simulation of ground-water age at the Mirror Lake site. The impact of matrix diffusion on ground-water age is investigated directly by including this process in the age transport model. The results of ground-water age simulation are compared to simulations of CFC-11 transport with and without matrix diffusion.

5.3 Model Construction

The flow and transport model used here is derived from that of Tiedeman and others (1997) in two main steps. The original nonlinear model is converted to a linear flow model by computing horizontal transmissivities from the calibrated model heads. The model structure and calibration results used here correspond to Parameterization D of Tiedeman and others (1997). Secondly, the model is re-gridded by subdividing larger model cells into square cells having the same dimensions as the smallest cells in the full model. Uniform horizontal gridding is required for the transport model modified and used here (Konikow et al., 1996).

First, the calibrated full model heads are used to compute saturated thicknesses of each model cell. The transmissivity of each model cell is then computed as the product of the saturated thickness and the calibrated hydraulic conductivity. Cells in which the hydraulic head is below the bottom of the cell are removed from the model domain (fig. 5-4). Recharge is applied to the top active cell at each location.

Ground water flows into streams in the model depending on the difference between the hydraulic head and a prescribed stream hydraulic head, estimated from topography. The streambed conductance is large, hence where streamflow is active, the difference between the head in the aquifer and in the stream is small. Because the transport model used here (Konikow and others, 1996) is not compatible with the stream simulation package used by Tiedeman and others (1997), the flux in each stream cell is computed for the calibrated model and used as a prescribed well flux (fig. 5-4). This procedure yields computed hydraulic heads and fluxes in the model that are essentially identical to the nonlinear model version, but only for this particular parameterization. If any of the hydraulic properties were changed, such as hydraulic conductivity, recharge or stream head, then the original nonlinear model with stream cells would have to be rerun and the conversion process described here repeated.

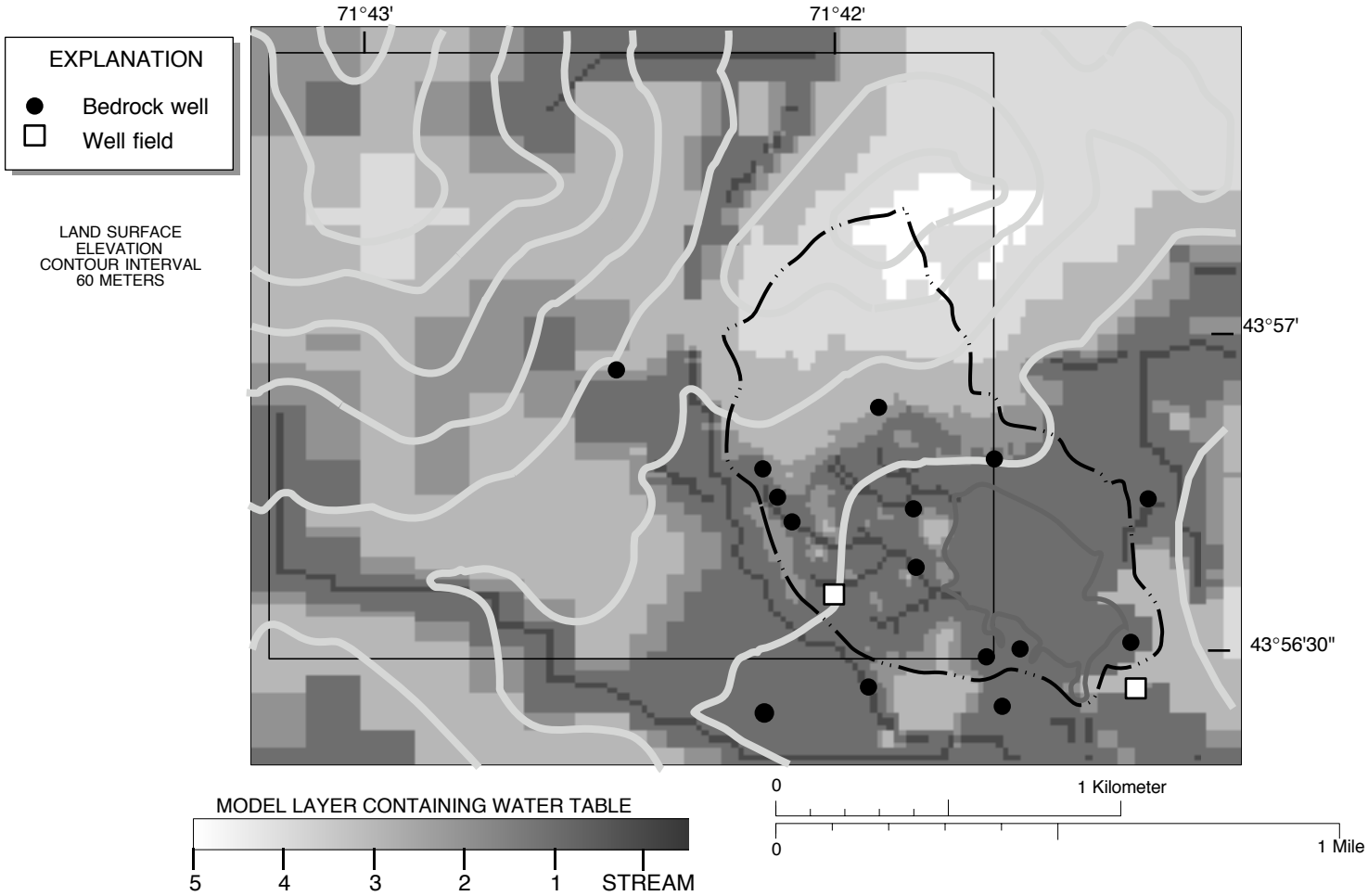

Figure 5-4. Stream cells and shading of uppermost active model layer containing water table in flow subgrid using model structure and calibrated parameters of Tiedeman and others (1997).

A uniform discretization subgrid is constructed for application of the transport model of Konikow and others (1996). The subgrid uses the smallest model cell size shown in figure 5-1 for all cells; the horizontal discretization is 16.67 by 16.67 m. Within the finest gridded portion of the full model there is a one-to-one correspondence between cells of the full grid and cells of the subgrid. Outside this area, larger cells are divided in thirds or ninths in each direction, depending on the cell size. A nearest neighbor procedure is used to assign the subgrid cells parameters from the full grid parameters.

Only a portion of the flow subgrid is used for solute transport simulations. One reason for choosing this transport subgrid is that an area of very high transport velocities in the sand and gravel unit south of Mirror Lake can be excluded. Inclusion of this area in a transport model imposes severe time-step restrictions. The primary goal of these simulations is to characterize the transport conditions in the glacial drift and bedrock in the Mirror Lake watershed to the northwest of the lake, and the sand and gravel unit to the south of Mirror Lake has essentially no effect on transport through the higher portions of the flow system.

The model structure used here is that of Tiedeman and others (1997). The thickness of the glacial drift is assumed to be 9 m, except in the vicinity of Mirror Lake where the thickness varies from 0 m to over 40 m based on drilling and seismic survey data (Winter, 1984; Tiedeman et al., 1997). The glacial drift is divided vertically into two model layers of equal thickness. The bedrock is divided vertically into three model layers having thicknesses of 30, 60, and 60 m, from top to bottom, respectively.

Tiedeman and others (1997) prescribed no-flow boundaries on all sides and on the bottom of the model domain. Here, computed heads in the model of Tiedeman and others (1997) at the flow subgrid boundary are used as prescribed heads for the smaller region. Uniform recharge is applied on the top of the saturated zone, except on Mirror

Lake itself. Mirror Lake is modeled as a zone of prescribed hydraulic head in the top saturated model layer.

In addition to geometric properties, some of the parameters of the model were not calibrated by Tiedeman and others (1997) because the model parameters were not sufficiently sensitive to the observed head and streamflow measurements. The hydraulic conductivity of a region of sand and gravel south of Mirror Lake is assumed to have a hydraulic conductivity of 5×10^{-5} m/s (T.C. Winter, personal commun., 1994). The lacustrine lake sediments underlying much of Mirror Lake are prescribed a hydraulic conductivity of 1×10^{-9} m/s (Rosenberry and Winter, 1993).

Estimated parameters of the flow model of Tiedeman and others (1997) for their Parameterization D include recharge, 280 mm/yr, glacial drift hydraulic conductivity, 1.74×10^{-6} m/s, bedrock hydraulic conductivity in the lower part of the basin, 3.21×10^{-7} m/s, and bedrock hydraulic conductivity in the upper part of the basin, 6.26×10^{-8} m/s.

5.3.1 Flow model results

The flow model results are essentially as described by Tiedeman and others (1997). The water table (fig. 5-5) occurs in the glacial drift model layers in the lower elevations of the watershed, and near flowing streams. At higher elevations, the water table is simulated in bedrock, and in a small part of the basin the water table is more than 90 m below the top of the bedrock surface. The water-table gradients are steepest in higher elevations of the watershed where the glacial drift is unsaturated and the bedrock has lower hydraulic conductivity than at lower elevations.

The simulated hydraulic head in the deepest model layer (fig. 5-6) is somewhat smoother than the water table configuration. Ground water generally flows from the northwest to the southeast, as indicated by the three-dimensional ground-water basin (fig. 5-2). Discharge to larger streams is evident in hydraulic head contours, even at depth in the bedrock.

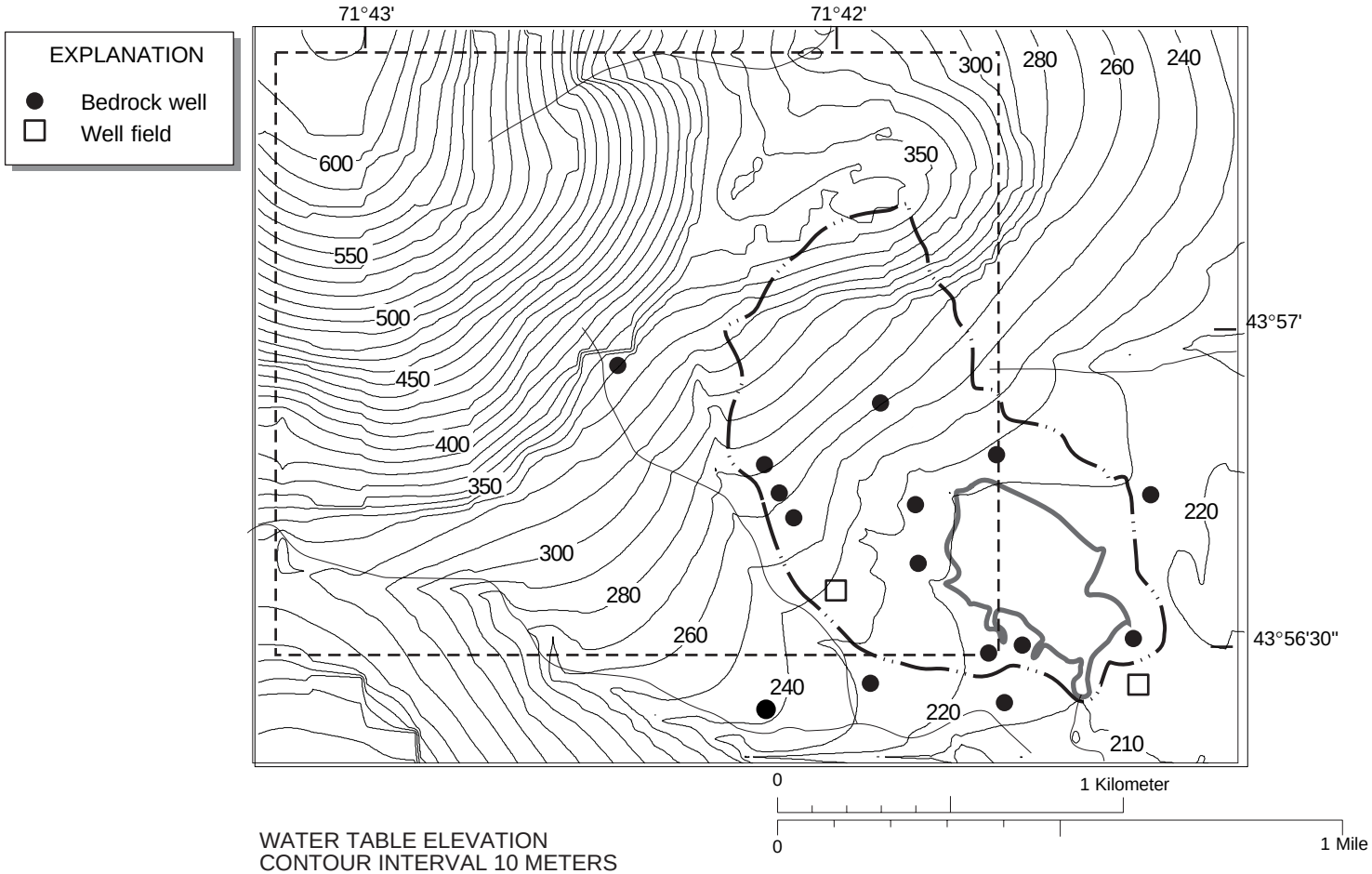

Figure 5-5 Simulated water-table elevation in flow subgrid using model structure and calibrated parameters of Tiedeman and others (1997).

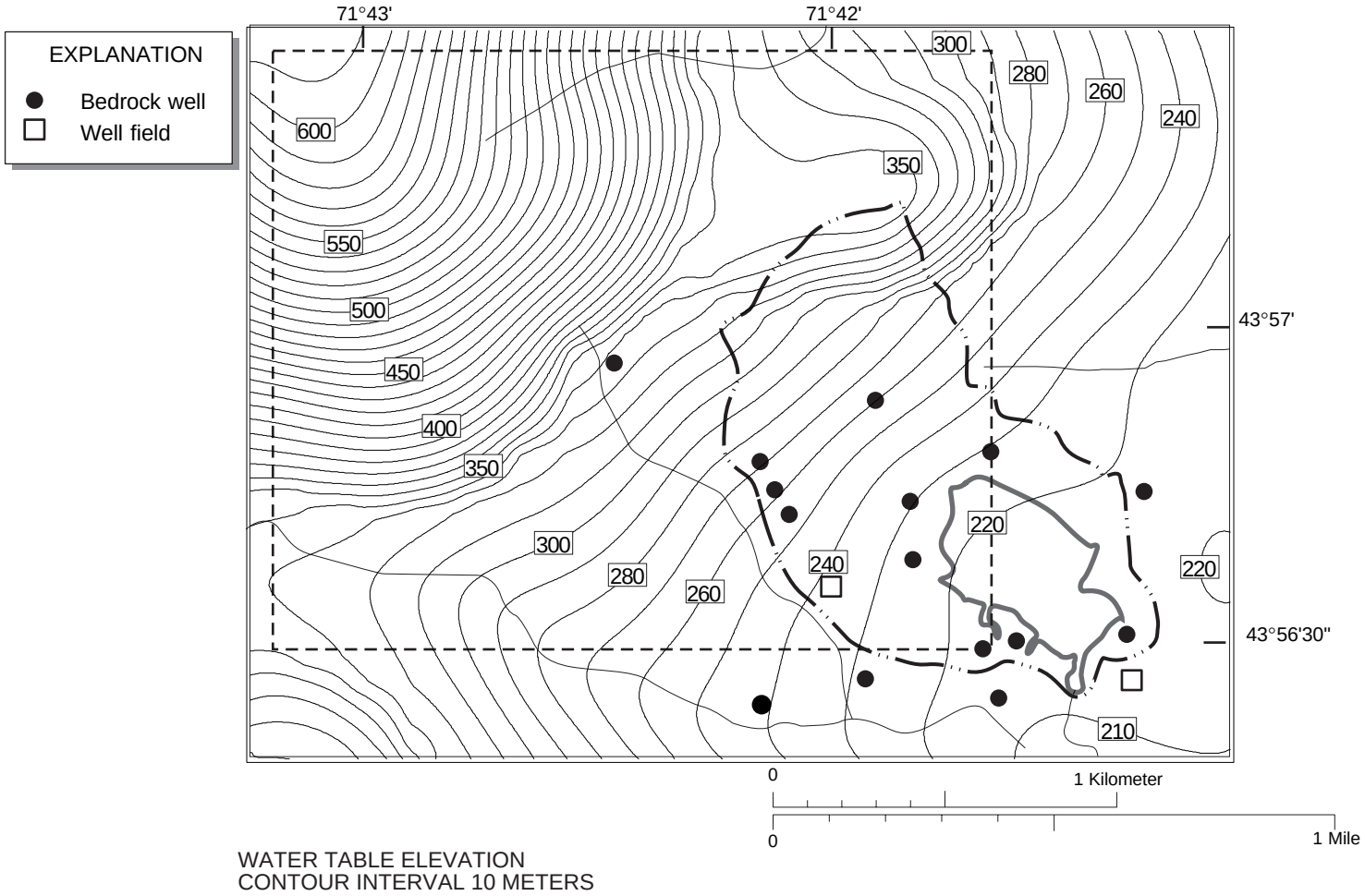

Figure 5-6 Hydraulic head in bottom model layer (5) representing bedrock between 90 and 150 m below bedrock surface.

5.4 Ground-Water Age

Ground-water age is simulated using the transport model developed in Chapter Two. Boundary conditions for the age simulation are incoming age of zero in recharge and in streamflow entering the aquifer. Only advective transport is considered in these simulations. The porosity of the glacial drift is assumed to be 0.2 for all simulations. Simulations are conducted for bedrock effective porosities of 0.05 and 0.005. For comparison, the low porosity value is representative of transport in the fractures alone, while the higher porosity value is assumed to represent the steady-state age as affected by matrix diffusion, where the rock matrix is assumed to have porosity of 0.045. Both of these values, 0.005 for effective porosity in fractures, and 0.05 for total porosity, may be too high for the fractured crystalline rock at the Mirror Lake site (Hsieh et al., 1993, Wood et al., 1996), but are used here for illustrative purposes.

Recharge water entering the saturated zone at the water table has an age of zero, by definition. In lower parts of the watershed, the water table occurs in the glacial drift, hence water must flow vertically downward before entering the bedrock. This leads to older ages in the upper bedrock in the lower parts of the watershed (fig. 5-7). At higher elevations, the glacial drift is unsaturated, and the water table, where recharge occurs, is in the bedrock. Hence, the age of water in the upper part of the bedrock in these areas is low (fig. 5-7). The oldest ages in the upper bedrock occur at discharge areas in the lower parts of the basin. Old water also occur in the upper bedrock beneath ground-water divides, where the head gradients and velocities are low.

The factors affecting age in the deep bedrock are similar to those for the upper bedrock, but ages are generally older (fig. 5-8) because of the additional time required to move down through 90 meters of bedrock. Youngest ages occur at higher elevation where the upper bedrock is unsaturated. Ages greater than 50 years occur in much of the area near Mirror Lake.

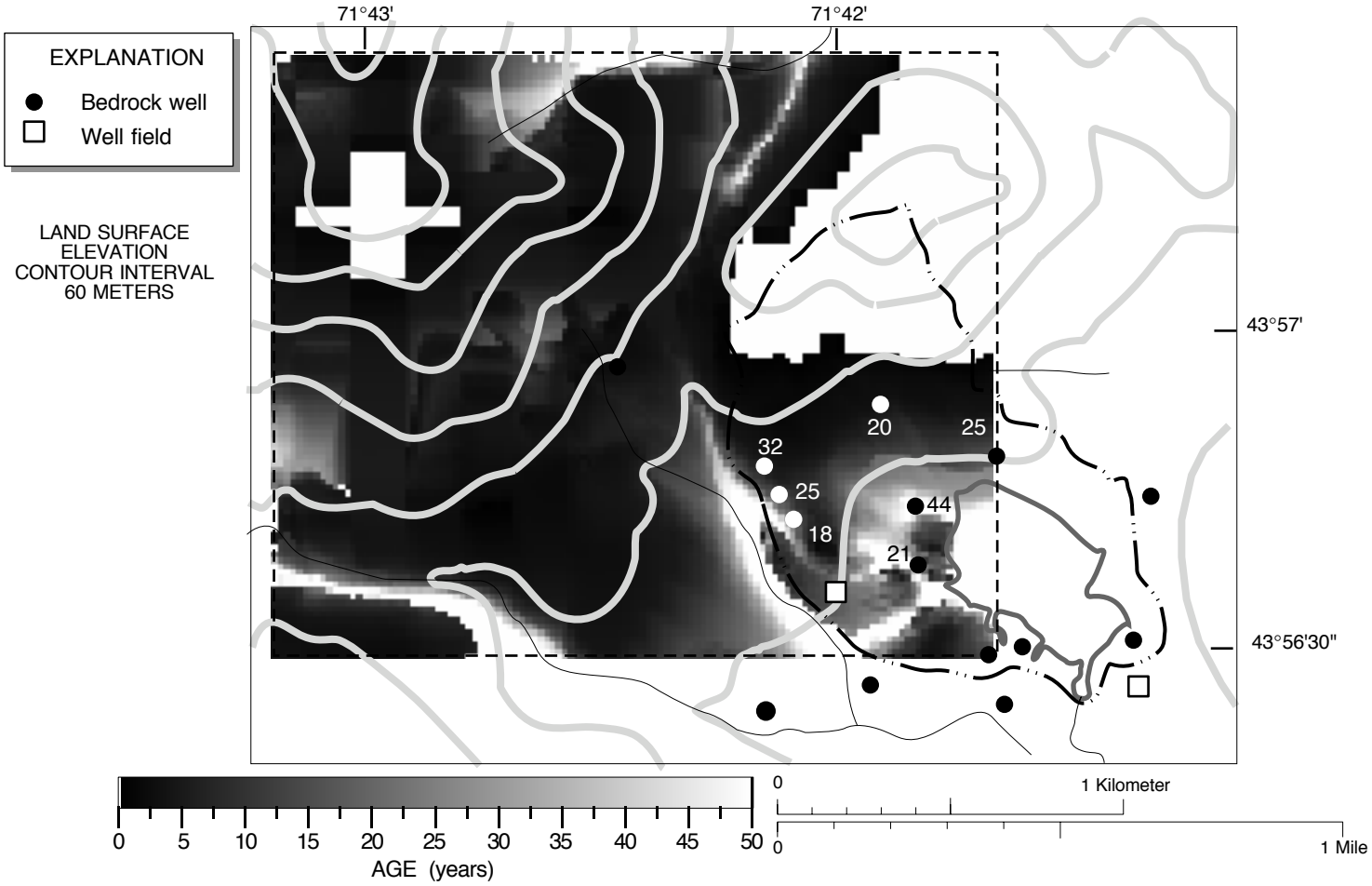

Figure 5-7 Simulated ground-water age in upper bedrock from bedrock surface to 30 meters below bedrock surface for advection only using bedrock effective porosity of 0.05. Numbers are apparent ages in shallowest sampled fracture zone from CFC-12 (Busenberg and Plummer, 1996).

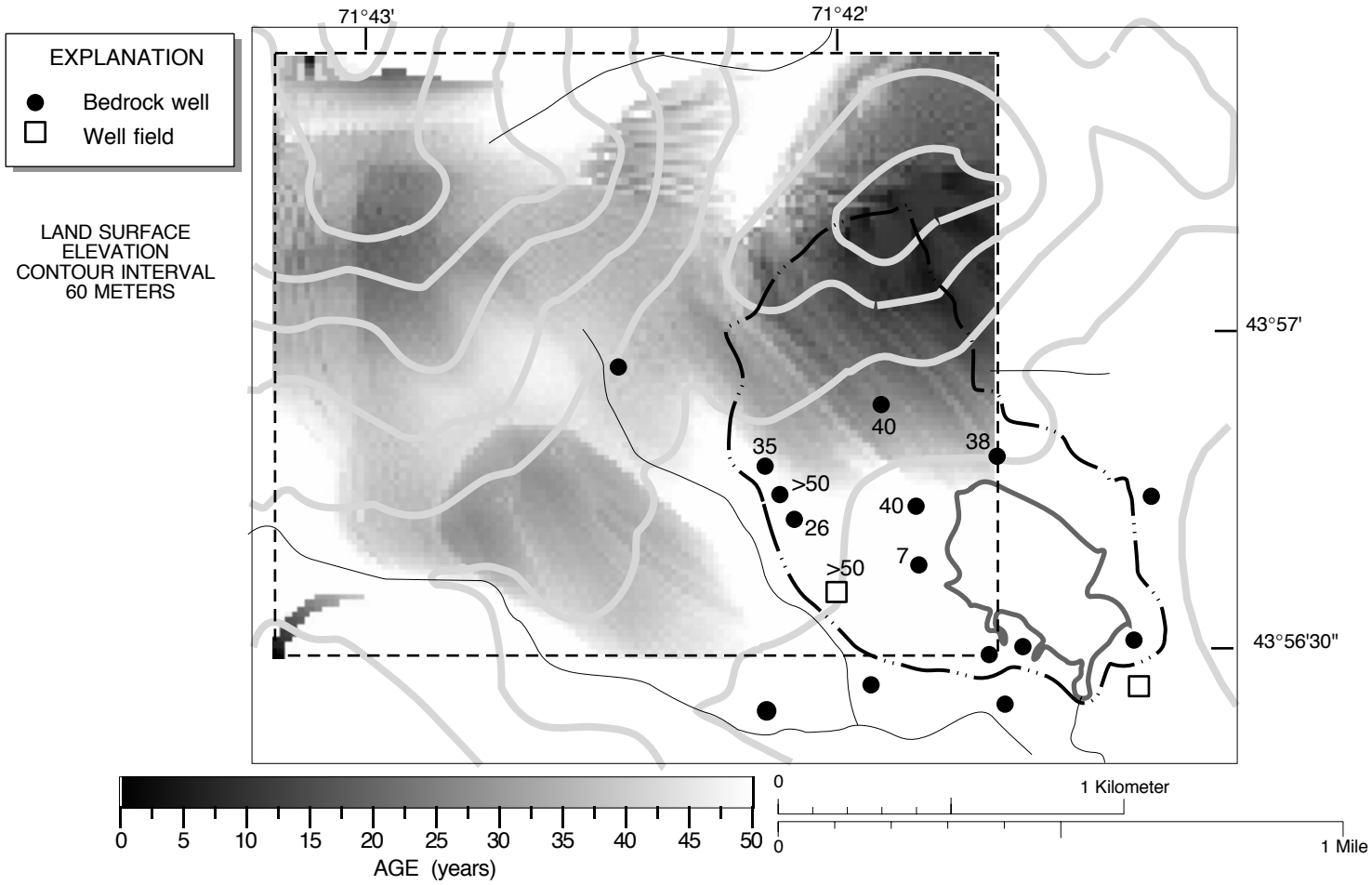

Figure 5-8 Simulated ground-water age in deep bedrock from 90 meters below bedrock surface to 150 meters below bedrock surface for advection only using bedrock effective porosity 0.05. Numbers are apparent ages in deepest sampled fracture zone from CFC-12 (Busenberg and Plummer, 1996).

With a factor of ten reduction in bedrock porosity to 0.005, ages are generally younger in bedrock layers, as expected. The spatial pattern of ages in the upper bedrock (fig. 5-9) is similar to the higher porosity case. Ages are generally less than a couple of years throughout the upper bedrock, and do not exceed 30 years in any locations. Similarly, ages are younger in the deep bedrock (fig. 5-10), although the spatial pattern is similar to the high porosity case.

Ideally, apparent ages from CFC-12 concentrations (Busenberg and Plummer, 1996) could be used to calibrate the flow and transport model. This model has not been calibrated, but preliminary comparisons can be made between observed apparent ages and simulated ages. The apparent ages are generally higher than the simulated ages for the low porosity case, even though this porosity is probably too high to represent the effective porosity for transport in the fractures. These results are consistent with travel time calibrations (C.R. Tiedeman, personal commun., 1994). The high porosity value, which may represent steady-state age as affected by matrix diffusion, yields ages more similar to the apparent ages. However, the porosity of 0.05 is higher than the measured 0.01 to 0.02 values on rock cores (Wood et al., 1996).

For the deep bedrock, several of the old waters are located in the portion of the basin where simulated ages for the high porosity case exceed 40 years. However, other nearby wells exhibit much younger ages. The young age observed in well T1 (7 years on the figs. 5-8 and 5-10) is in an area where the simulated ages in the upper bedrock are quite variable. T1 is located near Mirror Lake, but on a topographic high. This configuration leads to spatially variable ages; young water in the bedrock under the topographic high where the saturated glacial drift is thin, and old water in the lower parts where deep groundwater is discharging upward. Given the heterogeneous nature of the fracture flow system, these complex flow patterns would be expected to lead to highly variable ages in fractures intersecting bedrock wells.

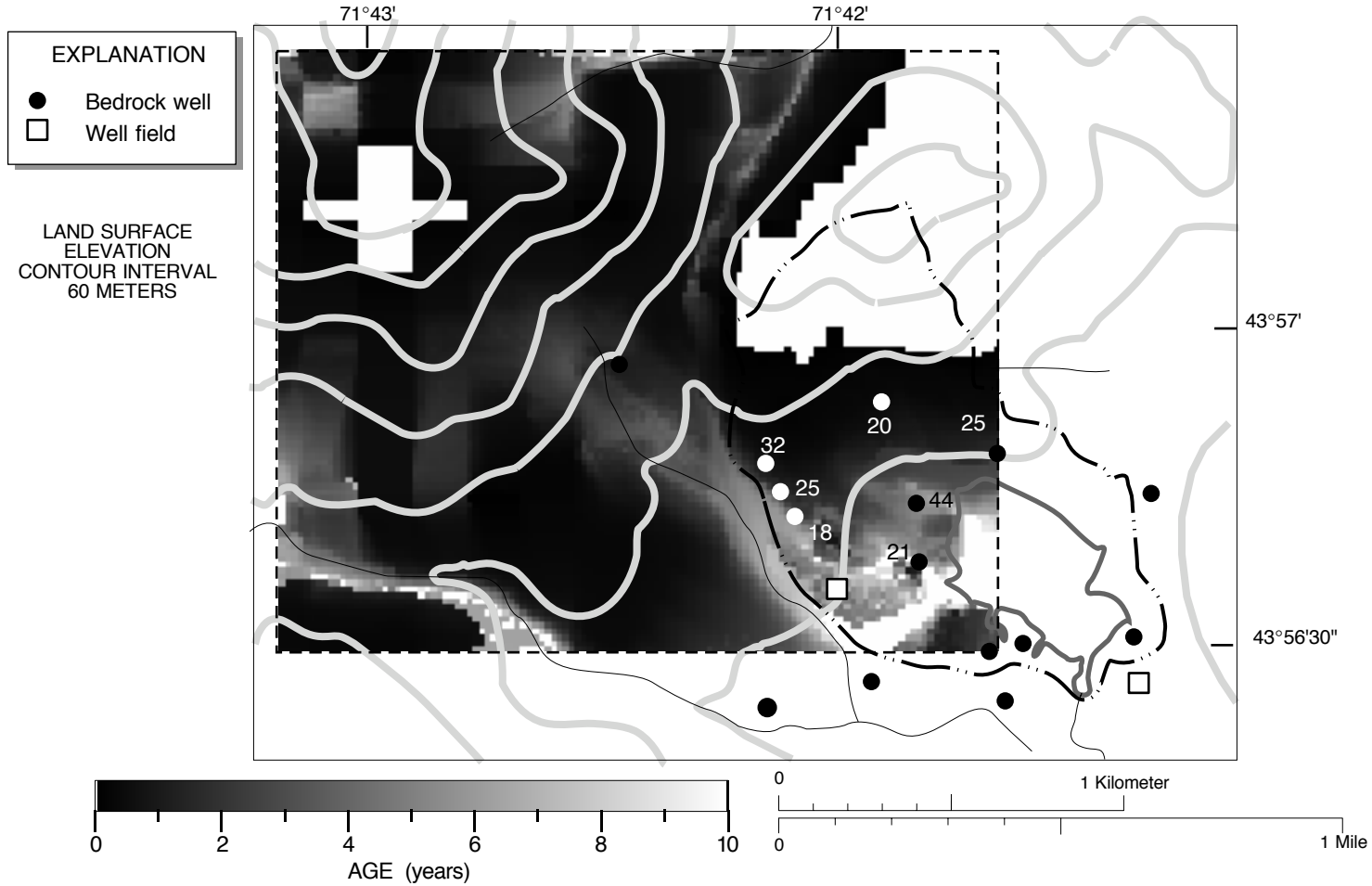

Figure 5-9 Simulated ground-water age in upper bedrock from bedrock surface to 30 meters below bedrock surface for advection only using bedrock effective porosity of 0.005. Numbers are apparent ages in shallowest sampled fracture zone from CFC-12 (Busenberg and Plummer, 1996). The age grayscale ranges from 0 to 10 years.

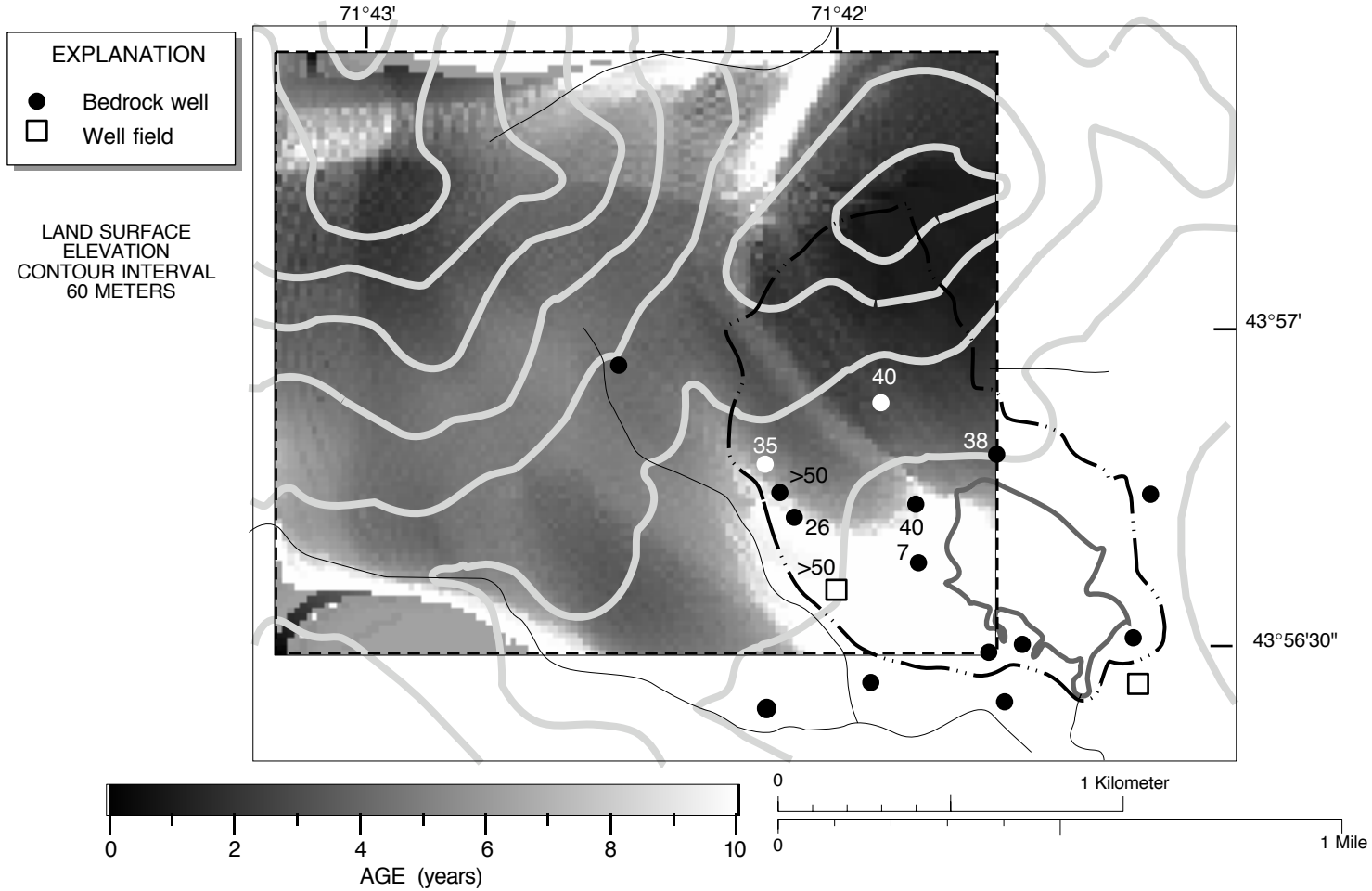

Figure 5-10 Simulated ground-water age in deep bedrock from 90 meters below bedrock surface to 150 meters below bedrock surface for advection only using bedrock effective porosity of 0.005. Numbers are apparent ages in deepest sampled fracture zone from CFC-12 (Busenberg and Plummer, 1996). The age grayscale ranges from 0 to 10 years.

5.5 CFC-11 Transport

Fifty years of CFC-11 transport is simulated to compare with the age transport results. The CFC-11 input function in recharge is based on global atmospheric levels and an assumed recharge temperature of about 6 °C. Based on observed CFC-11 degradation near an area of streamflow loss to the aquifer (Chapter Four), the CFC-11 concentration in streamflow to the aquifer is assumed to be zero.

5.5.1 Advective Transport

For advective transport alone, the CFC-11 concentration generally corresponds directly to the age, although the correspondence is not exactly linear. The atmospheric levels of CFC-11 (fig. 4-1) have been increasing almost linearly since the early 1960's, but before 1960 concentrations were increasing at a much slower rate. Thus, a linear relation is represented between CFC-11 and ages for waters younger than about 35 years, whereas very low, but nonzero, concentrations occur in older waters up to about 45 years old.

High CFC-11 concentrations are simulated in the upper bedrock (fig. 5-11) in parts of the basin where the glacial drift is unsaturated. As with the simulated ages, the CFC-11 concentrations in the upper bedrock are spatially variable in the area near a topographic high adjacent to Mirror Lake. The zero-CFC water discharging from stream to the glacial drift does not have a widespread impact on concentrations in the bedrock. If this impact were significant, areas of low CFC-11 concentrations would be observed in areas with very young ages.

The deep bedrock also exhibits high CFC-11 concentrations (fig. 5-12) beneath the topographic high where the water table is simulated deep in the system. However, CFC-11 concentrations are low in most of the deep bedrock for the high-porosity case.

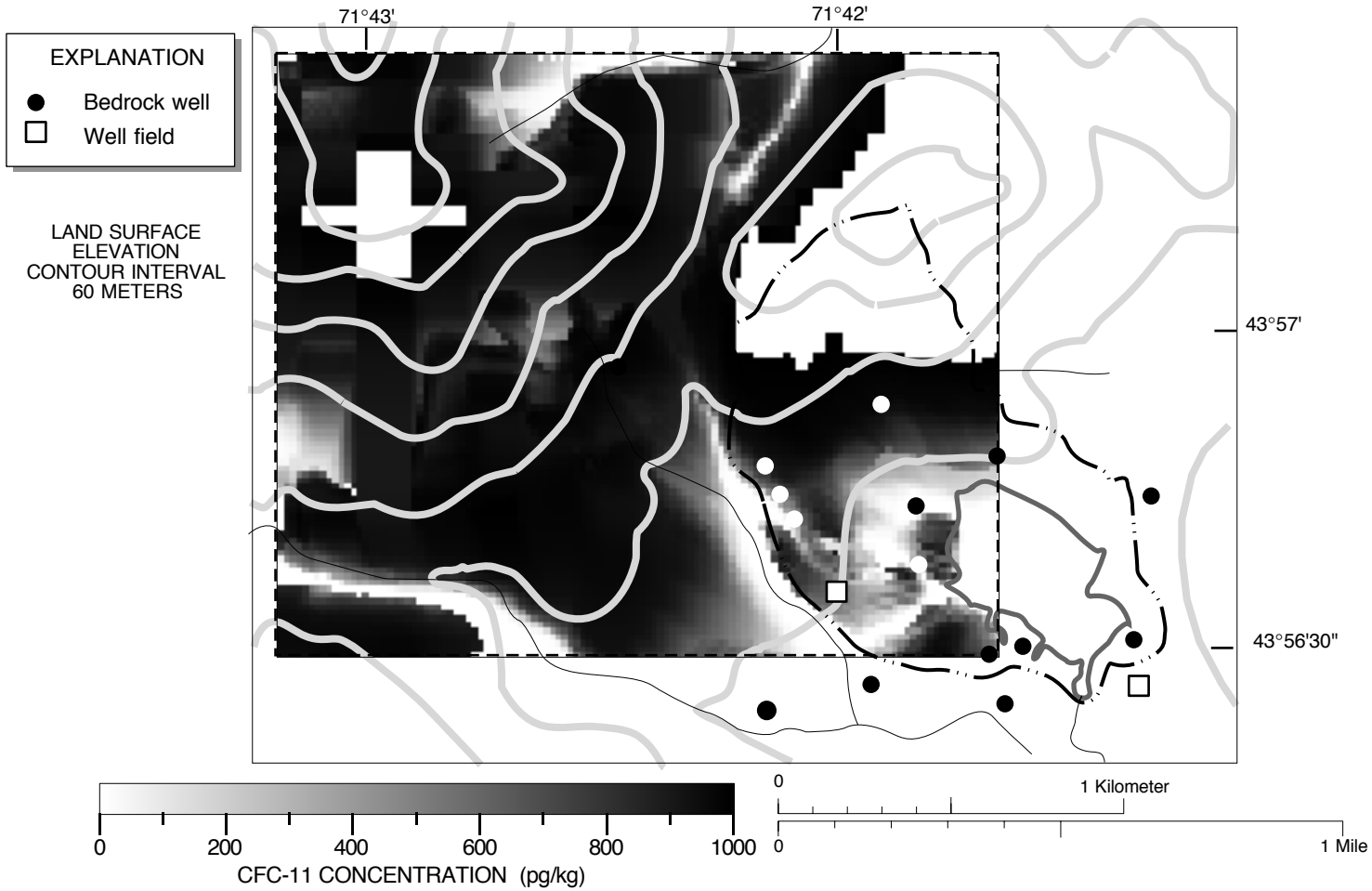

Figure 5-11 Simulated CFC-11 concentrations in upper bedrock from bedrock surface to 30 meters below bedrock surface for advection only using bedrock effective porosity of 0.05.

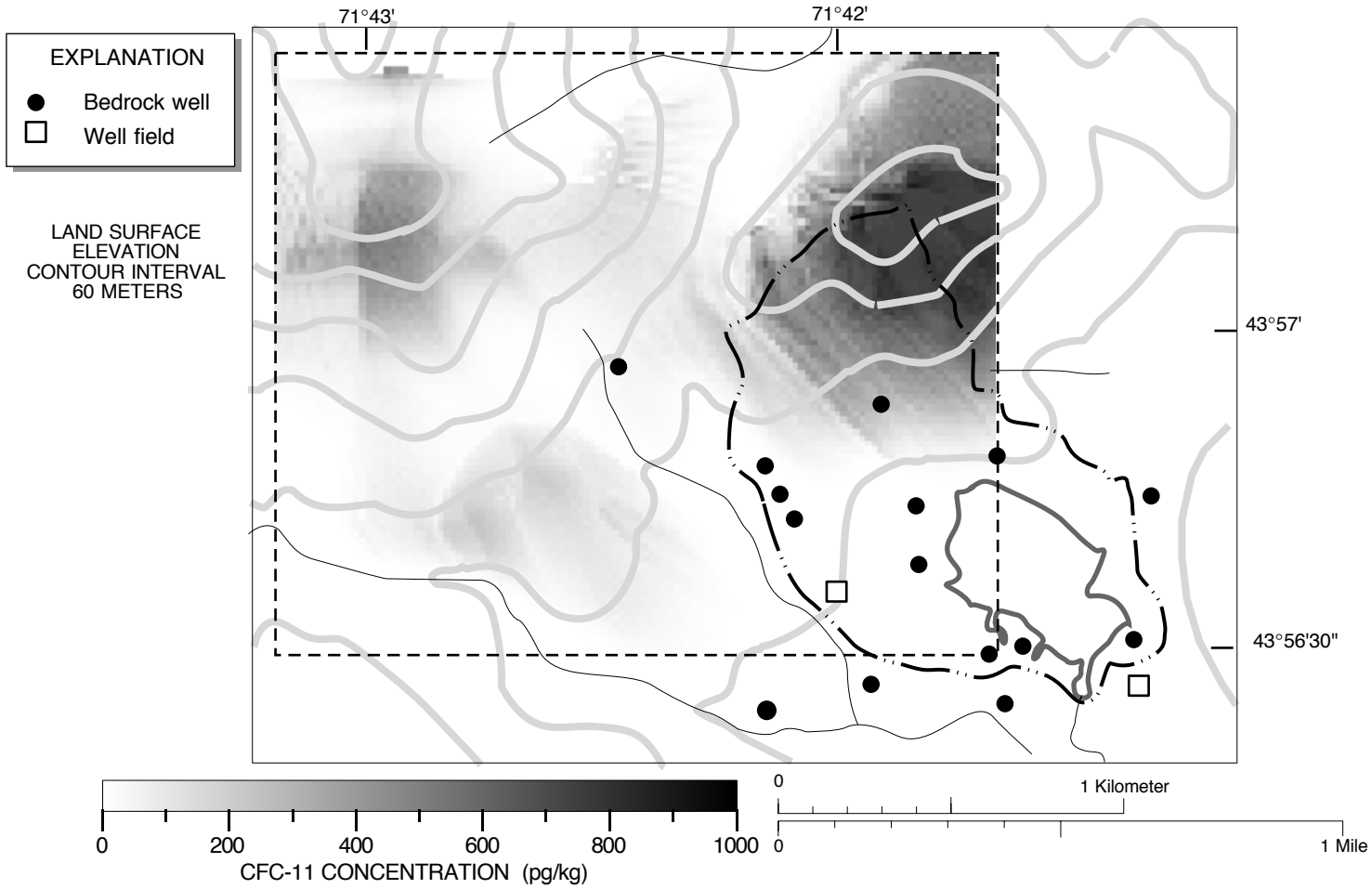

Figure 5-12 Simulated CFC-11 concentrations in deep bedrock from 90 meters below bedrock surface to 150 meters below bedrock surface for advection only using bedrock effective porosity of 0.05.

CFC-11 concentrations are higher in bedrock for the lower porosity simulation, under advection alone. These results are similar to those for the age simulations: the ground-water ages are younger in the bedrock using bedrock effective porosity of 0.005. Lowest concentrations occurring in the Mirror Lake basin are less than 25 pg/kg beneath the western shore of the lake where ground water is discharging upward through the low-permeability lake-bed sediments.

One difference between the age and CFC-11 simulations is in an area of streamflow loss to ground water. This occurs just to the southeast (down and to the right in the figure) of the lowest of the three wells along the western boundary of the Mirror Lake drainage basin. The upper bedrock concentrations here reflect, in part, stream loss which is assumed to have zero CFC-11 because of degradation in the stream bottom. This water has young age, but also has low CFC-11 concentrations, opposite the general relation where degradation is not present. However, this streamloss water apparently does not flow downward to the deep bedrock; there concentrations are higher reflecting rapid velocity of recent recharge through the system. This pattern is also shown in the higher porosity case (fig. 5-11), but is not as distinct because the upper bedrock has low CFC-11 concentrations in several locations in that case. This occurrence of streamloss water in the upper bedrock would lead to apparent ages of old water in the upper bedrock and young water in the deep bedrock, which is observed in some bedrock wells at Mirror Lake (fig. 4-3).

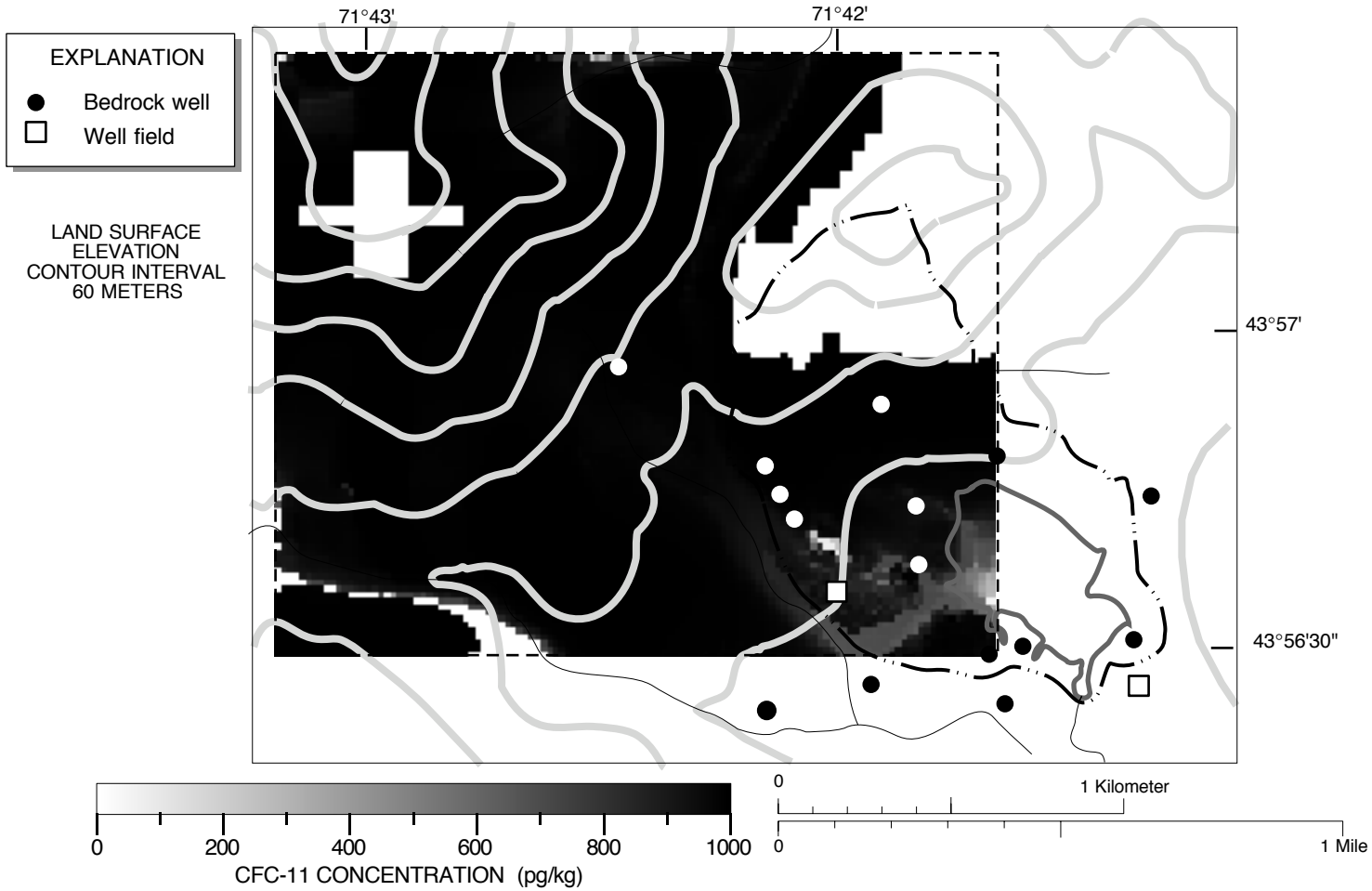

Figure 5-13 Simulated CFC-11 concentrations in upper bedrock from bedrock surface to 30 meters below bedrock surface for advection only using bedrock effective porosity of 0.005.

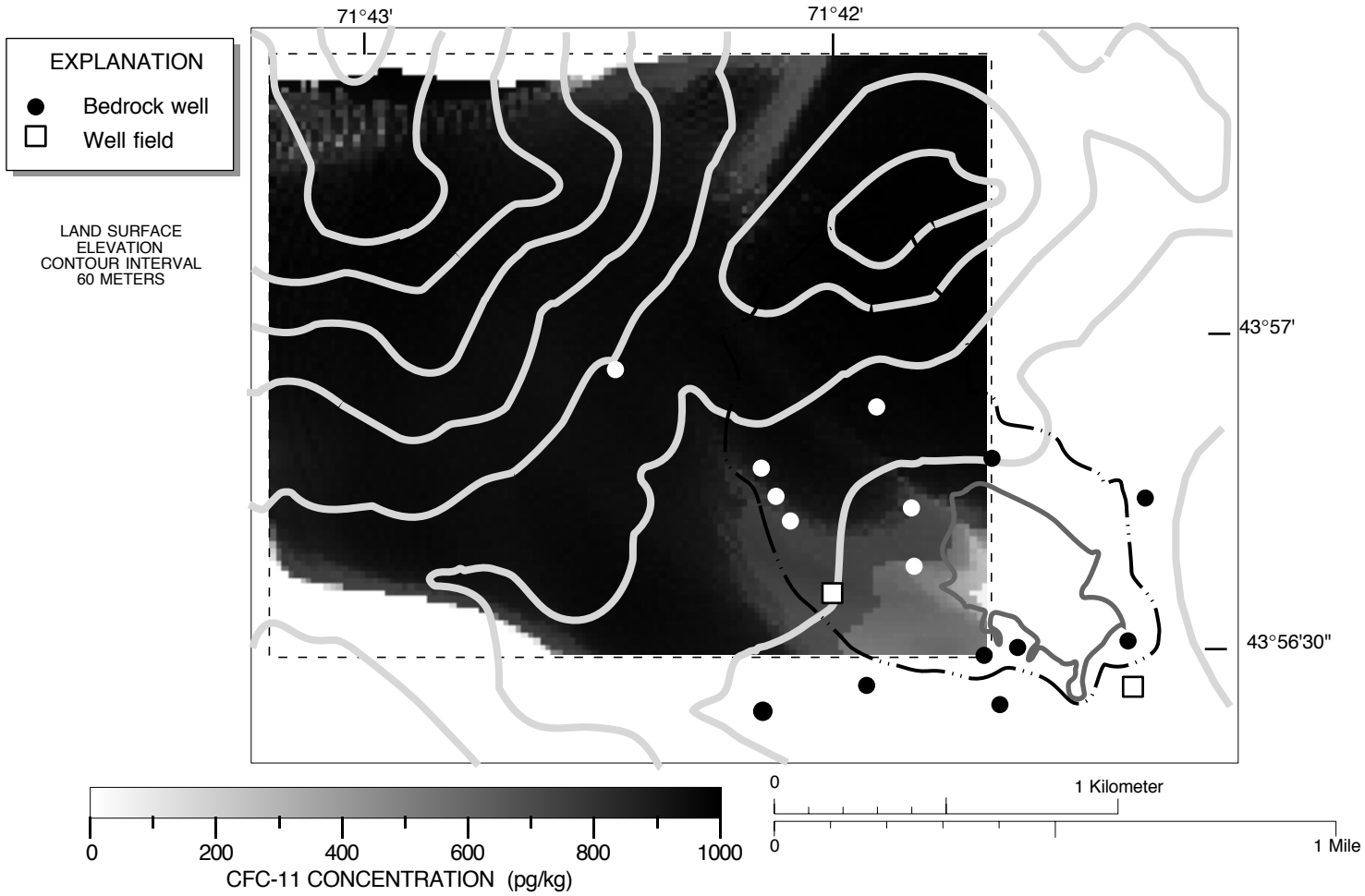

Figure 5-14 Simulated CFC-11 concentrations in deep bedrock from 90 meters below bedrock surface to 150 meters below the bedrock surface for advection only using bedrock effective porosity of 0.005.

The CFC-11 concentrations in ground water reflect the atmospheric source function (fig. 5-15). Near the water table, the ground-water concentration is essentially coincident with the atmospheric equilibrium level. A lag between the atmospheric level and the ground-water concentration occurs in deeper parts of the aquifer, depending on the advective travel times. For this case having low porosity, the lag between the water table and deeper concentrations is small, where the water table occurs in bedrock.

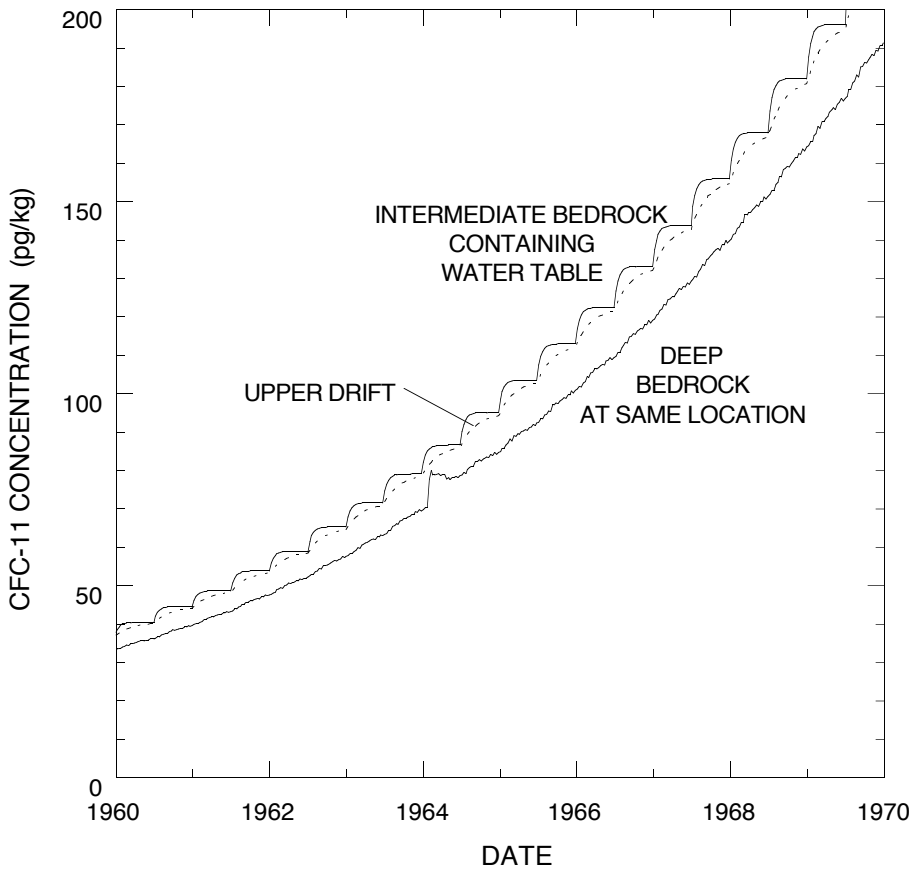

Figure 5-15 CFC-11 concentrations versus time in recharge areas for transport by advection only using bedrock effective porosity of 0.005.

The perturbation in the simulated concentrations for the deep bedrock are associated with particle regeneration in the method-of-characteristics numerical model

(Konikow et al., 1996). Particles are added to the domain as they leave fluid sources. When the maximum number of particles is reached, the initial uniform distribution of particles is regenerated, but with the current concentrations from the model nodes. As shown, this causes a temporary perturbation in computed concentrations that dissipates as particles redistribute themselves along flow lines. Konikow and Bredehoeft (1978) discuss fluctuations in computed concentrations associated with this discrete numerical method. Concentrations in the upper bedrock closely mirror the atmospheric levels when the water table is within the bedrock. The input source function has step changes in concentration every 6 months, and the bedrock water-table concentrations respond quickly to this step change because of the low storage in the rock.

5.5.2 Matrix Diffusion

The impact of matrix diffusion on CFC-11 concentrations depends on the relative porosity of the rock matrix and the fracture system, and the rate of diffusion in the rock matrix. Here, the simple double porosity model (Chapter Two) is used to approximate the effects of matrix diffusion. For these simulations, the bedrock effective porosity is 0.005, and the porosity of the immobile water zone in the rock matrix is 0.045. Hence, the total aquifer porosity is the same as the high-porosity case, 0.05. The limiting cases of exchange rate coefficient correspond to the advection-only cases. If the exchange coefficient is very high, then CFC-11 exchanges very quickly between the flowing fractures and the immobile zone. In this case, the effect is that the apparent solute velocity corresponds to the total porosity, 0.05, not just that of the fractures. At the other extreme, the rate of exchange between the rock matrix and the fractures is so slow that transport of CFC-11 is not significantly affected, and the aquifer's apparent effective porosity corresponds to that of the fractures alone, in this case 0.005. The exchange coefficient used here, 10^{-4} day^{-1}, yields transport results intermediate between these extremes (figs. 5-16 and 5-17).

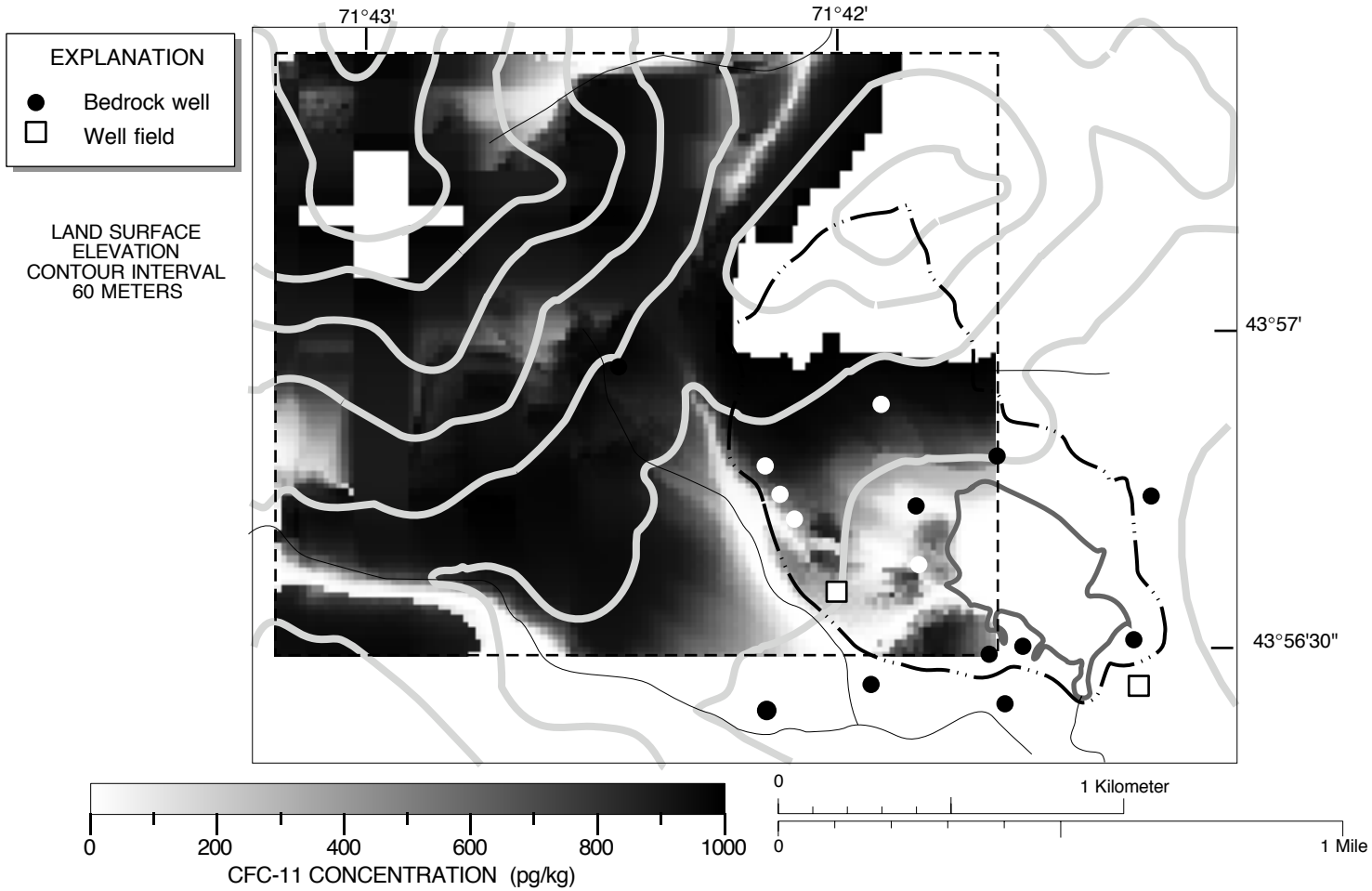

Figure 5-16 Simulated CFC-11 concentrations in upper bedrock from bedrock surface to 30 meters below bedrock surface for advection and matrix diffusion using bedrock effective porosity of 0.005, rock matrix porosity of 0.045 and exchange rate coefficient of 10^{-4} day^{-1}.

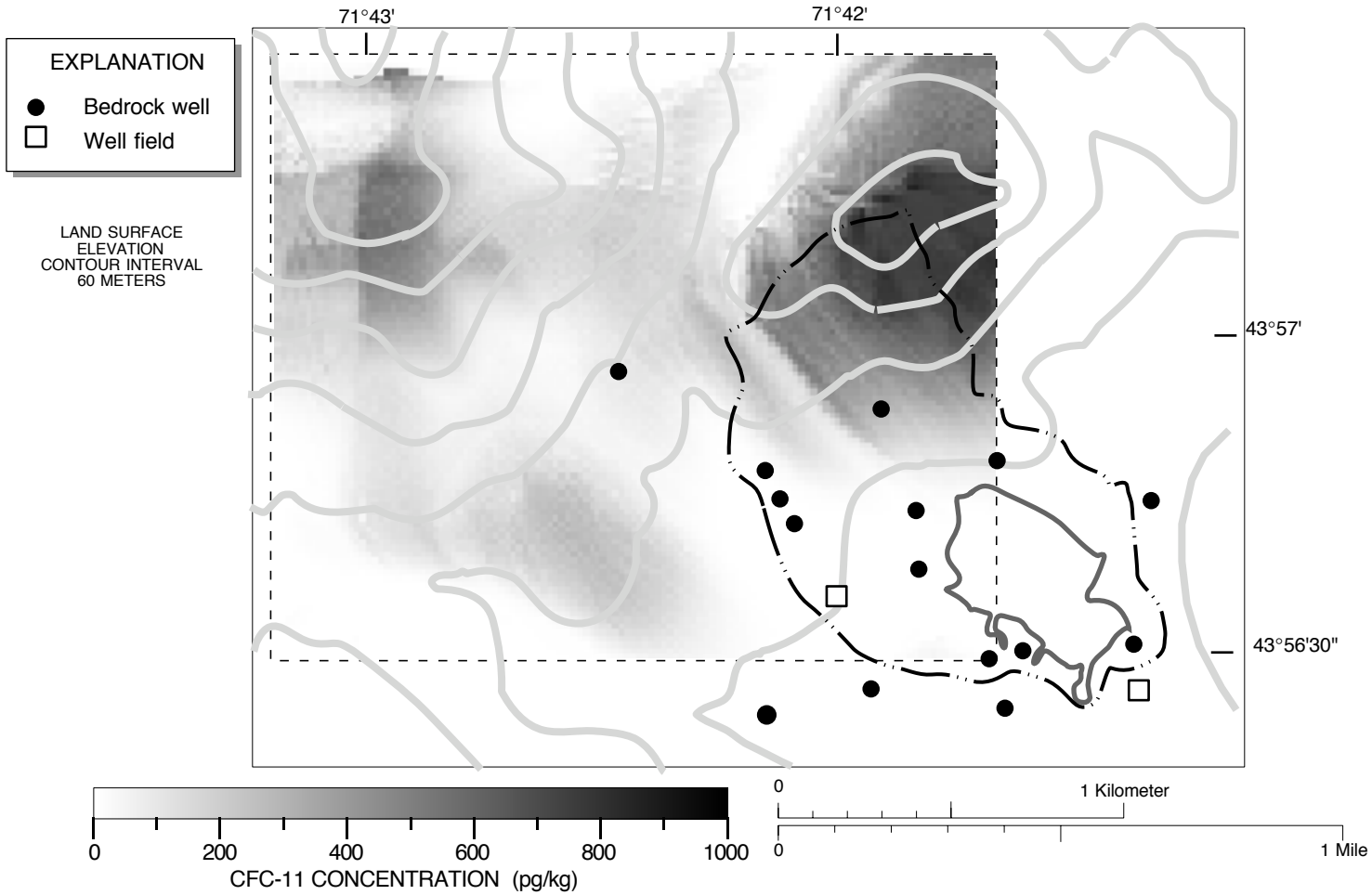

Figure 5-17 Simulated CFC-11 concentrations in deep bedrock from 90 meters below bedrock surface to 150 meters below bedrock surface for advection and matrix diffusion using bedrock effective porosity of 0.005, rock matrix porosity of 0.045 and exchange rate coefficient of 10^{-4} day^{-1}.

The effect of matrix diffusion is most apparent for the deep bedrock concentrations (fig. 5-17). Concentrations in deep bedrock are much lower than those for the case with the same effective porosity, but without matrix diffusion (fig. 5-14). This apparent increase in travel time is due to the retarding effect of rapid exchange between the flowing water in the fractures and the immobile water within the rock matrix. These results are more similar to the advective transport simulation with the high porosity value (fig. 5-12). One difference is that for the matrix diffusion case CFC-11 is present, albeit at low concentrations, throughout a larger part of the deep bedrock. This reflects the kinetics of the exchange process: most, but not all, of the CFC-11 is removed by diffusion into the rock matrix, but low concentrations persist in the flowing water zone because the exchange is not instantaneous.

The apparent increase in travel time through bedrock caused by matrix diffusion is also shown in the concentration histogram (fig. 5-18). Bedrock concentrations are lower and the lag between the water table in bedrock and underlying deep bedrock is substantially increased. The previously noted perturbation due to particle regeneration in the numerical method occurs at a little earlier in this simulation. Although the particle motion in the numerical model is identical for the cases with and without matrix diffusion, fewer particles were used in this case because of the additional computer storage required for the matrix-diffusion terms.

Matrix diffusion changes CFC-11 concentrations significantly only for certain values of the exchange-rate coefficient (β) (fig. 5-19). If β is greater than about 10^{-4} day^{-1}, then exchange is so rapid that concentrations in the fractures are essentially the same as if the effective porosity is equal to the total porosity. If β is less than about 10^{-6} day^{-1}, then matrix diffusion does not significantly impact CFC-11 concentrations during the time scale of this simulation. If the exchange-rate coefficient is within this range at the site, then this additional parameter will have to be incorporated in models to accurately estimate effective porosity from CFC-11 concentrations in bedrock.

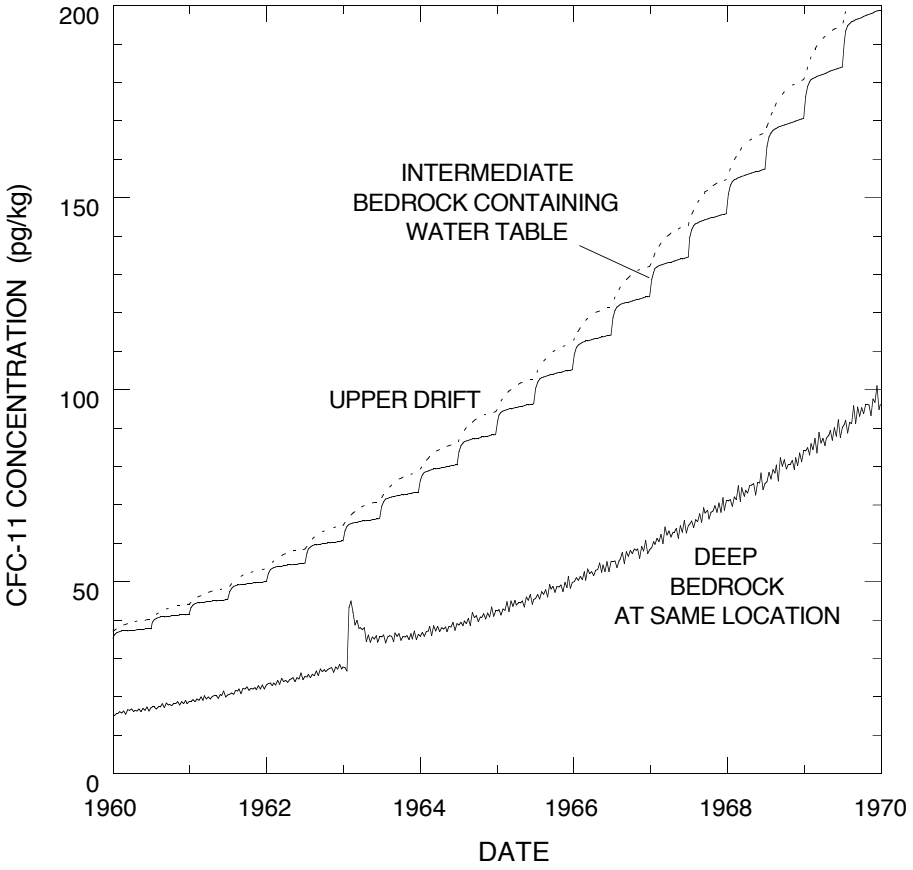

Figure 5-18 CFC-11 concentrations versus time in recharge areas for transport by advection and matrix diffusion using bedrock effective porosity of 0.005, rock matrix porosity of 0.045 and exchange rate coefficient of 10^{-4} day^{-1}.

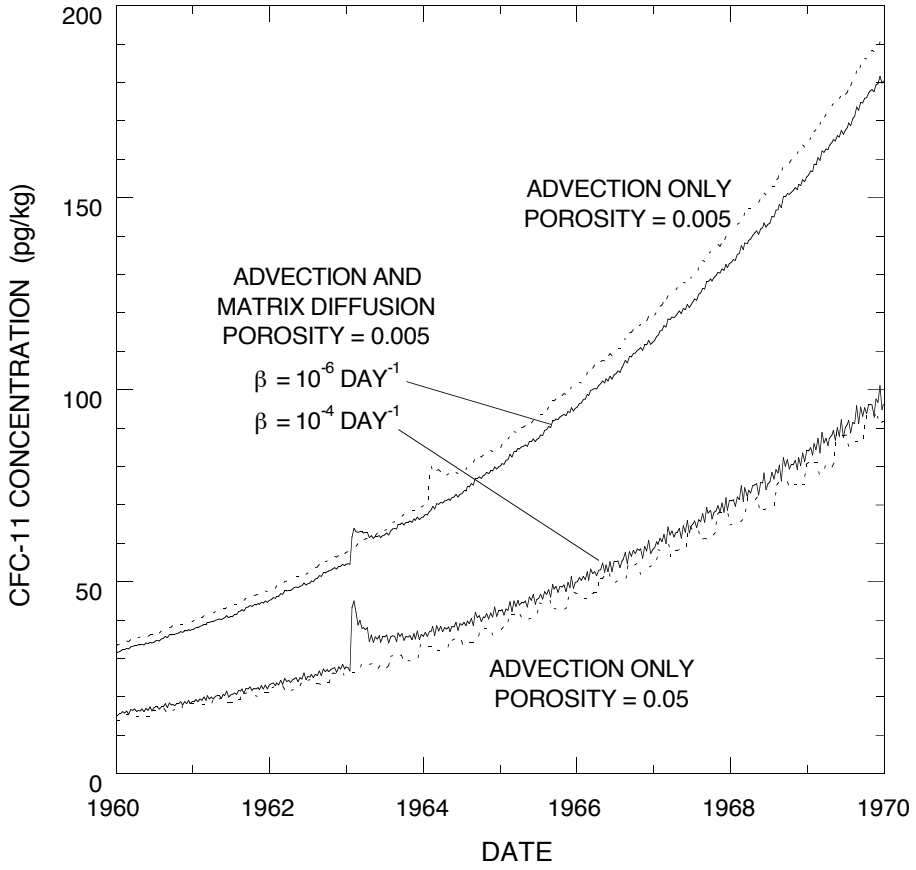

Figure 5-19 CFC-11 concentrations versus time for deep bedrock in recharge area for cases of transport by advection using bedrock effective porosities of 0.05 and 0.005, and transport by advection and matrix diffusion using bedrock effective porosity of 0.005, rock matrix porosity of 0.045 and exchange rate coefficients of 10^{-6} and 10^{-4} day^{-1}.

5.6 Summary

Preliminary simulations are conducted of age and CFC-11 transport in ground water at the Mirror Lake site, New Hampshire. The underlying connection between CFC concentrations and ground-water age is illustrated by the correspondence between simulated age and CFC-11 concentrations. CFC-depleted streamflow discharge to the glacial drift has a local impact on simulated CFC concentrations in the upper bedrock. Spatially variable age and CFC concentrations are simulated in the lower parts of the basin where local topographic highs occur next to discharge zones.

Steady-state age is insensitive to the diffusion rate for cases with matrix diffusion, but the CFC-11 concentrations are significantly different for different rates. Generally, the porosities required in the transport model to match age and CFC concentrations at the Mirror Lake site are higher than values measured on rock cores.

5.7 References

Busenberg, E., and Plummer, L.N., 1996, Concentrations of chlorofluorocarbons and other gases in ground water at Mirror Lake, New Hampshire: in Morganwalp, D.W., and Aronson, D.A., eds., U.S. Geological Survey Toxics Program Meeting, Colorado Springs, Colo., September 20-24, 1993: U.S. Geological Survey WRIR 94-4015.

Drenkard, S., Torgersen, T., Weppernig, R., Stute, M., Farley, K., and Schlosser, P., 1993, Helium isotopes and tritium-helium age dating: Mirror Lake, New Hampshire (abs.): GSA Abstracts with Programs, v. 25, no. 6, p. A-364.

Harte, P.T., 1992, Regional ground-water flow in crystalline bedrock and interaction with glacial drift in the New England uplands: M. S. Thesis, University of New Hampshire, Durham, 147 p.

Harte, P.T. and Winter, T.C., 1995, Simulations of flow in fractured crystalline rock in a hypothetical New England setting: Ground Water, v. 33, no. 3, p. 953-964.

Hill, M.C., 1992, A computer program (MODFLOWP) for estimating parameters of a transient, three-dimensional, ground-water flow model using nonlinear regression: U.S. Geological Survey Open-File Report 91-484, 358 p.

Hsieh, P. A., Shapiro, A. M., Barton, C. C., Haeni, F. P., Johnson, C. D., Martin, C. W., Paillet, F. L., Winter, T. C., and Wright, D. L., 1993, Methods of characterizing fluid movement and chemical transport in fractured rock: in Chaney, J. T., and Hepburn, C., (eds.) Field Trip Guidebook for northeastern United States, Geological Society of America, annual Meeting, October 25-28, 1993, Boston, Mass., v. 2, chap. R, p. R1-R23.

Konikow, L.F., D.J. Goode and G.Z. Hornberger, A three-dimensional method-of-characteristics solute-transport model (MOC3D): U.S. Geological Survey Water-Resources Investigations Report 96-4267, 87 p.

McDonald, M.G., and Harbaugh, A.W., 1988, A modular three-dimensional finite-difference ground-water flow model: U.S. Geological Survey Techniques of Water-Resources Investigations, book 6, chap. A1, 586 p.

Plummer, L. N., R.L. Michel, E.M. Thurman, and P.D. Glynn, 1993,. Environmental tracers for age dating young ground water, in *Regional Ground-Water Quality* , edited by W. M. Alley, pp. 255-294, Van Nostrand Reinhold, New York.

Rosenberry, D.O., and Winter, T.C., 1993, The significance of fracture flow to the water balance of a lake situated in fractured crystalline rock terrain, in Banks, Sheila, and Banks, David, eds., IAH Memoires of the 24th Congress, Hydrogeology of Hard Rock, As, Norway, June 28 to July 2, 1993: International Association of Hydrogeologists, p. 967-977.

Shapiro, A.M., 1996, Using environmental tracers to estimate matrix diffusion in fractured rock over distances of kilometers: Results from the Mirror Lake site, New Hampshire: Eos, Trans. AGU, v. 77, no. 17, p. S107.

Shapiro, A. M., and P. A. Hsieh, 1991, Research in fractured-rock hydrogeology: Characterizing fluid movement and chemical transport in fractured rock at the Mirror Lake drainage basin, New Hampshire: p. 155-161 in Mallard, G.E., and D. A. Aronson (eds.), U.S. Geol. Survey Toxic Substances Hydrology Program--Proc. Technical Meeting, Monterey, California, March 11-15, 1991: U.S. Geol. Survey Water-Resources Invest. Rep. 91-4034.

Shapiro, A.M., Wood, W.W., Busenberg, E., Drenkard, S., Plummer, L.N., Torgersen, T., and Schlosser, P., 1996, Conceptual model for estimating regional fluid velocity in the bedrock of the Mirror Lake area, Grafton County, New Hampshire, *in* Toxics Program Meeting, Colorado Springs, U.S. Geological Survey WRIR 94-4015.

Tiedeman, C.R., Goode, D.J., and Hsieh, P.A., 1997, Numerical simulation of ground-water flow through glacial deposits and crystalline bedrock in the Mirror Lake area, Grafton County, New Hampshire: U.S. Geological Survey Professional Paper 1572, 50 p.

Winter, T. C., 1984, Geohydrologic setting of Mirror Lake, West Thornton, New Hampshire: U.S. Geological Survey Water-Resources Investigations Report 84-4266, 61 p.

Winter, T. C., 1985, Physiographic setting and geologic origin of Mirror Lake: in Likens, G. E., ed., *An ecosystem approach to aquatic ecology: Mirror Lake and it Environment*: Springer-Verlag, New York, p. 40-53.

Winter, T. C., Eaton, J. S., and Likens, G. E., 1989, Evaluation of inflow to Mirror Lake, New Hampshire: Water Resources Bulletin, vol. 25, no. 5, p. 991-1008.

Wood, W.W., Shapiro, A.M., and Councell, Terry, 1996, Observational experimental and inferred evidence for solute diffusion in fractured granite aquifers: Examples from Mirror Lake Watershed, Grafton County, New Hampshire: in Morganwalp, D.W., and Aronson, D.A., eds., U.S. Geological Survey Toxics Program Meeting, Colorado Springs, Colo., September 20-24, 1993: U.S. Geological Survey WRIR 94-4015.

Chapter 6 Summary and Conclusions

This thesis addresses several issues associated with environmental tracers in ground water. Topics include mathematical and numerical modeling of age in complex ground-water systems, effects of temperature on atmospheric tracer transport to the water table, and a field study of CFC's at the water table. Specific examples and applications are drawn from the USGS fractured-rock research site at Mirror Lake, New Hampshire.

Chapter Two presents a theoretical model of ground-water age transport that can be used to characterize systems influenced by advection as well as matrix diffusion and dispersion. This approach bridges the gap between current approaches of treating transport as piston flow, or advection alone, focusing on ground-water age, and of simulating advective-dispersive transport, focusing on tracer concentrations. The theory presented is general and accounts directly for the effects of dispersion, matrix diffusion, and other processes on ground-water age. Simulation results using this method can be compared to apparent ages from tracer concentrations, and can be used to illustrate ground-water transport conditions in an intuitive age framework. However, this method does not supplant simulation of tracer transport as the best approach to estimating transport properties from observed concentrations because all processes that affect measured concentrations of a particular tracer, such as decay and sorption, can be explicitly included in the simulation. Errors in apparent age from tracer data, for example due to mixing, cannot be rectified by the proposed method.

In Chapter Three, the effects of temperature fluctuations on CFC-11 transport from the land surface to the water table in humid areas are examined by simulation. Generally, air-phase diffusion is sufficient to maintain water-table concentrations close to those in equilibrium with the atmosphere. A determining factor is the extent of temperature fluctuations at the highest location above the water table where moisture

contents are nearly saturated. Air-phase diffusion below this point will be unable to rapidly transport CFC's from the atmosphere to the underlying water table and a lag will occur due to water-phase transport in the unsaturated zone. If temperature fluctuations are large at this point, then concentration of CFC's in the water column will be elevated compared to the equilibrium partitioning at the mean temperature. This is caused by the nonlinear relation between temperature and Henry's Law coefficient, and will affect all dissolved gases, depending on the curvature of their temperature relation. Fine-grained porous media generally hold more moisture than coarse-grained materials and can restrict vertical CFC transport by limiting air-phase diffusion.

A three-year field study of the unsaturated zone and water table at the Mirror Lake site, New Hampshire, is presented in Chapter Four. Field data collected included water levels and unsaturated-zone pressure head, moisture content by TDR, and soil temperature. Water samples were collected from shallow piezometers and analyzed at USGS labs for general chemistry as well as dissolved gases, including CFC's, tritium, and other constituents. Results indicate that in some areas of the watershed CFC concentrations at the water table are significantly degraded by anaerobic biodegradation. CFC-11 and CFC-113 are completely absent at several locations, while CFC-12 is degraded to about one-third of modern levels. Independent evidence of anaerobic degradation includes methane concentrations and hydrogen gas concentrations. The latter suggest that methanogenesis and sulfate reduction are active terminal electron-accepting processes. Oxygen and CFC gas transport to the water table is presumed to be limited by normally high moisture content in the fine-grained glacial drift at the site. An area of observed streamflow loss corresponds to an area of active degradation, suggesting a link between the supply of organic carbon from the stream bottom and degradation in the aquifer. Where dissolved oxygen concentrations are above 4-5 mg/L, CFC concentrations are in equilibrium with the modern atmosphere, assuming equilibration temperatures ranging between 4 and 8 °C.

Chapter Five extends some of the general results of Chapter Two to a particular case of ground-water flow in glacial drift and bedrock at the Mirror Lake site, New Hampshire. Results from the age transport model indicate that ground-water ages in the bedrock are not markedly different than those of the glacial drift. As expected for a relatively homogeneous parameterization of hydraulic and transport properties, oldest ground-water ages exist beneath discharge locations where older water from deep in the aquifer rises to the land surface. CFC-11 transport simulation results can account for degradation of CFC-11 in streamflow entering the aquifer, a process that cannot be included in the general age model. This leads to low CFC-11 concentration beneath a losing stream reach, while the ground-water age is very young. Low CFC-11 concentrations are also observed where old water rises from deep in the aquifer to discharge at lower parts of the Mirror Lake watershed. CFC-11 concentrations are not related to age for waters older than about 50 years, because the atmospheric concentration before that time was essentially zero. The impact of matrix diffusion depends on the rate coefficient for exchange between the flowing water and the immobile water within the rock. If this exchange rate is small, then matrix diffusion has a minor retardation effect on ages and CFC-11 concentrations. However, in the case of age, the steady-state age distribution (after many, many years) is independent of the rate coefficient. CFC-11 concentrations in the bedrock can be significantly decreased by matrix diffusion, given the small porosity of the active flow fractures.

Future Work

Theoretical work on the effect of mixing on ground-water ages estimated from tracer data, and methods to account for this during interpretation of field data, are much needed. The theory presented here for ground-water age is developed only for the mass-weighted average age. Because the input functions of environmental tracers are not purely linear, the age associated with the concentration of a mixture is not equivalent to the average age of the mixture. Ground-water samples, especially from large pumping wells and springs, represent mixtures of water having different sources, pathways, and travel times. The ground-water age modeling framework presented here may provide a basis for methods to simulate the distribution of ages within a given volume, and the age distribution could then be directly related to corrsponding concentrations through convolution.

One of the aspects of seasonal temperature that is not considered here is the interaction between changing temperature and variable recharge. Here only steady-flow conditions are considered. There may be important effects of changing temperature that will be manifest only when a variable recharge function, such as that due to snowmelt in the early spring and evapotranspiration during summer, is coupled with the temperature fluctuation. Such studies would probably require more sophisticated coupled flow and heat transport models, in contrast to the methods here in which the temperature is independent of flow. However, preliminary simulations using isothermal flow hydraulic properties could be made using the numerical tools developed here.

A remaining question about the field results from the Mirror Lake site is the extent to which the observed CFC degradation at the water table affects CFC concentration in the bedrock. Additional spatial coverage of the watershed would help clarify this issue, although drilling is difficult in much of the area due to the steepness of the watershed, and boulders in the glacial drift. Loss of CFC's from bedrock samples

would yield apparent ages older than actual ages, but comparison of CFC-12 age dates and tritium concentrations suggests the opposite result, that the CFC-12 age dates are too young. More detailed study of transport processes between the glacial drift and bedrock, and within the bedrock, particularly the role of matrix diffusion and spatial variability, would be required to interpret CFC concentrations in bedrock at this site.

The large-scale transport model used here for illustration of age and CFC-11 transport does not incorporate smaller-scale spatial variability which exists, but can not be accurately quantified for the entire watershed. Some of the features evident in these simulations are not apparent in the measured CFC concentrations in bedrock at the site. This is similar to the lack of match between simulated vertical head gradients and observed vertical head gradients in the large-scale flow model. The large-scale model does not include these small-scale features, and these small-scale features may control CFC concentration. Given this inconsistency, it may be necessary to use stochastic modeling, perhaps in a conditional simulation framework, to generate plausible realizations of hydraulic and transport properties in the basin that yield simulation results consistent with observed field data.